

**TUmour Suppression  
and Subdual of Cancer  
(TUSSC) in elephants:  
*An in vitro* study to shed  
light on Peto's paradox**

Amèlia Jansen van Vuuren

**TUmour Suppression and Subdual of Cancer (TUSSC) in  
elephants: An *in vitro* Study to Shed Light on Peto's  
Paradox**

by

Amèlia Jansen van Vuuren

3731393

A thesis submitted in partial fulfilment of the requirements  
for the degree of Magister Scientiae

Faculty of Natural Science  
Department of Medial Bioscience  
University of the Western Cape  
Bellville, South Africa



Supervisor: Prof. M. de Kock

Co-Supervisors: Dr C Vandevoorde

Dr M Engelbrecht

Submitted: November 2022

# DECLARATION

---

I, Amèlia Jansen van Vuuren, declare that this thesis, titled: *TUmour Suppression and Subdual in Cancer (TUSSC) in elephants: An in vitro study to shed light on Petos's paradox* is my own work, that it has not been submitted for any degree or examination in any other university, and that all the sources I have used or quoted have been indicated and acknowledged by complete references.

*A. Jansen van Vuuren*

---

A Jansen van Vuuren

November 2022

Date



# ABSTRACT

---

Logic would suggest that cancer incidence is related to body mass and longevity. Gigantic animals such as elephants with a longer lifespan (more lifetime of cell divisions) and a larger body size (more cells) will have more time during their lifetime to accumulate a cancer-causing mutation in comparison to small-bodied, short-lived animals, such as mice. However, several studies and the mere existence of large-bodied, long-lived mammals such as elephants and whales, suggest that there is no correlation between body mass, lifespan and cancer incidence across different mammalian species. This is a phenomenon known as Peto's paradox. As there is a selection for large body size in evolution, there is likely also a selection for cancer suppression mechanisms that allow an organism to grow large and reproduce successfully. One of the rationales in the African savanna elephant (*Loxodonta africana*) is the duplication of a crucial tumour suppressor gene (TP53) encoding the tumour protein 53 (p53). The African elephant contain 20 copies of TP53 (40 alleles), while humans contain only 1 copy of TP53 with 2 functional TP53 alleles. Both alleles are required to function normally to prevent cancer. Within the Proboscidean lineage, the copies of TP53, called retrogenes (RTGs), expand quite rapidly within evolution when compared to close living family members of the African elephant. These TP53 RTGs could be one of the reasons why elephants who live up to 65 years in the wild and with over 3.72 quadrillion cells, have a higher probability to suppress cancer within their genome in comparison to humans.

Studies resolving the genomic mechanisms responsible for cancer suppression in gigantic species have not yet deciphered the working mechanism of how the TP53 RTGs may suppress cancer in elephants. The Tumour Suppression and Subdual on Cancer (TUSSC) in elephants research project investigates how the DNA damage response differs between elephants (20 copies of TP53) and humans (1 copy of TP53). This was conducted in an in vitro study, where the cells of both species were exposed to ionising radiation (IR) (250 kVp X-rays), a well-known radiation-induced DNA damaging agent to investigate the working mechanisms of TP53.

This study presented here was divided into 2 sections: (A) Primary elephant dermal fibroblast (EDF) cell line characterisation which included the establishment of a novel African savanna elephant cell line from small skin punch biopsies, growth curve, doubling time (Td), metaphase chromosome spread and cell cycle kinetics. (B) The comparison of primary normal human dermal fibroblast (NHDF) and primary EDF cell lines post X-ray irradiation to investigate biological endpoints which included clonogenic survival-(CSA), cell proliferation-, apoptosis assay and cell cycle progression.

(A) The first primary EDF radial explant of fibroblasts was visible after 8 – 25 days with a biopsy success rate of 83.33% among 6 elephants and a Td of  $62.13 \pm 7.15$  h (average  $\pm$  SD) for 3 elephants at passage 1. The metaphase chromosome spread confirms the diploid number of 56 chromosomes in the *L. africana*. Preliminary results concerning cell cycle kinetics indicate a length of the G0/G1 phase of 20 – 22 h, the S phase 10 h, the G2/M phase 5 h and M phase 1 h for primary EDFs at passage 9.

(B) CSA revealed a decrease in survival fraction (SF) with higher doses however, no significant difference in the SF was observed between the NHDFs and EDFs. However, based on the  $\alpha/\beta$  ratio, the EDFs showed to be more radiosensitive when compared to the NHDFs. A significant decrease in the cell proliferation assay was observed with higher doses, while in contrast, the EDFs had a remarkable recovery in cell growth with the cell proliferation assay after 120 h for 1 and 2 Gy and a slight recovery after 4, 8 and 16 Gy. Both the NHDFs and EDFs had no significant apoptosis-mediated cell death after irradiation. However, a non-statistically significant increase in early and late apoptosis was observed in EDFs compared to the NHDF cells, pointing to an elevated apoptosis level in EDF cells after irradiation exposure. The NHDFs remained in G0/G1 phase throughout all the conditions and no shift in the cell cycle was observed with different irradiation doses. The EDFs showed a decrease in G0/G1 phase and an increase in the G2/M phase with higher doses implicating cell cycle arrest. The possible G2/M cell cycle block allowed the damaged DNA to be repaired post-irradiation or to allow apoptosis induction. Moreover, an increase in cell proliferation was observed for lower doses at 120 h post-irradiated in EDFs, indicating that the G2/M block was potentially overcome. The latter is in line with the cell proliferation observations at 120 h for EDFs.

It could be speculated that the presence of TP53 RTGs in the elephant fibroblasts could possibly allow for a faster response to DNA damage to prevent the accumulation of cancer-causing mutation within their genome in comparison to human fibroblasts containing no extracellular

surveillance mechanisms. The data generated from the current MSc study is a steppingstone for future work on the TUSSC project to understand the molecular underpinnings of TP53/TP53 RTG and other mechanisms which could play a role in the elephants' cancer resistance.



# ACKNOWLEDGMENTS

---

Will it ever sink in that I completed my Master's? In addition, I had the best topic a girl can ask for. I mean, who in the world can say they investigated an African elephant? This is truly the best project ever! There were many curve balls, trust me, however all the teams involved helped me to overcome it and I am immensely grateful for each and everyone.

I want to start by thanking one of my supervisors, Dr Charlot Vandevoorde, for choosing me to be the student of the elephant project. Thank you for believing in me and giving me the greatest responsibility to produce data for such a unique and incredible project. All the opportunities that have come with this project. Wow, it is really mind blowing! My gratification can't even be described, I am lost for words and still feel like it is all a dream. I look into the mirror and think "why me"? The memories made during the last 2 years will never be forgotten. I am truly grateful for you and all your advice, guidance, patience and everything else I was not able to think of when I wrote this. You're such an inspiration to me and a terrific role model. Your passion for your work shines within and is highly contagious, (not like Covid and in a bad way).

To my other supervisors: Prof Maryna de Kock and Dr Monique Engelbrecht. Prof you are such an inspiration, and I am eternally grateful for everything you have done for me. Without you, I would NEVER have been able to be in this research field. You truly gave me a sense of purpose and belonging. You were so happy about the results; it gave me the energy I needed to finish writing. To Monique, thank you, thank you, thank you. All the road trips, late lab nights and many conversations.

This thesis wouldn't be a reality if it was not for my supervisors. All the corrections, all the long talks, all the motivation and more. The dictionary doesn't have enough words to describe how I feel. I am truly grateful to have you in my life. Your dedication towards this project is appreciated.

My iThemba family... From the first day when I walked in, I felt that I belong. Thank you for all the quick chats in the corridor and all the friendships that will never be forgotten. I am grateful and appreciate all the assistance with the elephant project when samples were obtained,

all the late nights, the arrangements and documentations with shipments, ethics and the list continue. I admire all of you! A special thank you to Dr Randall Fisher, for travelling to GSI, teaching me new techniques and just being an awesome person. You never cease to amaze me.

To my other work family in the northern hemisphere. Dr Walter Tinganelli and all the staff members and students from the Clinical Radiobiology group. Thank you for making this experience truly a great one. I am thankful for all the assistance, guidance, advice, friendship, food offerings and so much more. I have not only gained knowledge but also weight however, will redo everything in a heartbeat. I treasured every moment and the 5 months spent in Germany went by so fast that I feel we must turn back the clock. Furthermore, I would like to thank Dr Pradeep Gosh and the entire GET\_INVolved team for all the arrangements and support pertaining to my stay at GSI.

NRF iThemba LABS and GSI/FAIR infrastructure: Thank you for building, upgrading and maintaining such unique facilities. Research would not be possible without facilities like this. The measure of support, safety and security is immensely appreciated.

A special shoutout to Dr Willem Burger and the owners and staff members of the premises where elephant samples were collected. The elephant veterinarian safari is truly one of a kind and is something I will cherish forever. Moreover, to The African Wildlife Conservation Foundation (AWCF), thank you for all the work towards saving, maintaining and protecting African wildlife. Your dedication towards wildlife is an inspiration. I am going through life with a different perspective.

Dr Frazana Rahiman and the Animal Research Ethic Committee (AREC), thank you for making the elephant project a reality. All the work is immensely appreciated and will never be forgotten.

To the University of the Western Cape (UWC), thank you for all the teaching, learning, adapting and embracing moments. Coming from a small town and walking on such a big and beautiful campus made me feel there is so much more to life. Life is not only what you think and what you see but so much more.

To all my bursaries: In 2021, I was awarded the Southern African Institute for Nuclear Technology and Sciences (SAINTS) scholarship and I am proud to say this was the first scholarship awarded to me. To top it off in 2022, I was awarded a second scholarship from the



International Atomic Energy Agency (IAEA), Marie Skłodowska-Curie Fellowship Programme (MSCFP). Thank you for all the financial support.

To my dad, mom, sister, soon to be brother-in-law and “my ouma”. Words can’t even begin to describe how I feel. You guys kept me strong throughout this period. All of you had more confidence in me than I had in myself. It shone through like the sun would shine through on a cloudy day. Sometimes I don’t even remember how I got to this point, but I know for sure I would not have been able to do it by myself. Thank you for always staying positive for me, even when it feels like the world is ending on my side. You encouraged me to be the strong, independent woman I know I can be. Sometimes we were separated more than 10 000 km, but in my heart, I never felt there was any distance. I know it has been a tough time, but tough times don’t last forever, however tough people do! I am sure the future will have many ups and downs. But with a family like you, I will climb Mount Everest tomorrow. Maybe not tomorrow, but you get my point.

To my family and friends. Your support and motivation throughout this project are really valued and I couldn’t ask for a better support system. All the conversations and trying to understand what I am doing is appreciated. Your love and encouragement kept me going.

And lastly to the elephants... You know who you are, or maybe you don’t since you were under general anaesthesia when we collected the samples. However, this project wouldn’t be possible without you. Thank you for evolving!

“For I know the plans I have for you,” declares the Lord, “plans to prosper you and not to harm you, plans to give you hope and a future.”

Jeremiah 29:11

# DEDICATION

---

I am dedicating my dissertation work to my mom and dad.

“Tough times never last, but tough people do.” – Robert H. Schuller



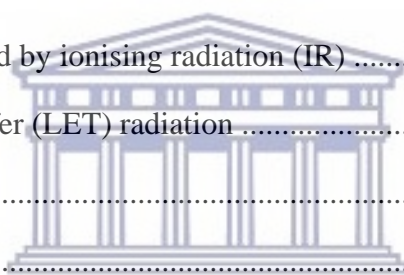
# TABLE OF CONTENT

---

DECLARATION .....	iii
ABSTRACT.....	iv
ACKNOWLEDGMENTS .....	vii
DEDICATION.....	x
TABLE OF CONTENT .....	xi
ABBREVIATIONS .....	xvii
LIST OF FIGURES .....	xxiii
LIST OF TABLES.....	xxxv
CHAPTER 1: .....	1
INTRODUCTION .....	1
1.1. Introduction.....	1
1.2. Cancer in elephants.....	5
1.2.1. Peto’s paradox .....	7
1.2.2. Redundancy of tumour suppressor gene in elephants .....	12
1.2.3. TP53 and aging effects .....	19
1.3. Tumour suppressor gene (TP53).....	21
1.3.1. TP53 history .....	21
1.3.2. TP53 mutation and TP53 in cancer .....	22
1.3.3. TP53 activation.....	24
1.4. Overview of the cell cycle .....	26
1.4.1. The G1 phase.....	28
1.4.2. The S phase.....	29

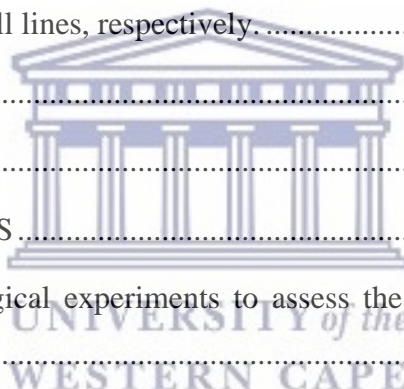


1.4.3.	The G2- and M phases .....	30
1.4.4.	Cell cycle checkpoints .....	30
1.4.4.1.	G1/S checkpoint .....	31
1.4.4.2.	G2/M checkpoint.....	32
1.4.4.3.	Mitotic checkpoint.....	34
1.5.	Mechanisms of cell death.....	35
1.5.1.	Extrinsic apoptotic pathway .....	36
1.5.2.	Intrinsic apoptotic pathway .....	37
1.5.3.	Caspase dependent apoptosis.....	39
1.5.4.	Caspase independent apoptosis .....	40
1.6.	Radiation .....	42
1.6.1.	DNA damage caused by ionising radiation (IR) .....	45
1.6.2.	Linear energy transfer (LET) radiation .....	47
1.6.3.	X-rays .....	48
1.7.	Aims and objectives.....	51
CHAPTER 2:	MATERIALS AND METHODS .....	53
Section A:	Primary elephant dermal fibroblast (EDF) cell line characterisation .....	53
2.1.	Primary EDF cell culture .....	53
2.1.1.	African elephant sample collection procedure .....	53
2.1.2.	African elephant biopsy preparation, outgrowth and culturing .....	56
2.1.2.1.	Biopsy preparation .....	56
2.1.2.2.	Primary EDF explant outgrowth and culturing .....	58
2.1.2.3.	Primary EDF cryopreservation.....	59
2.1.2.4.	Primary EDF life span.....	60
2.2.	Primary EDF growth curve and doubling time (Td).....	61
2.3.	Metaphase chromosome spread .....	63



UNIVERSITY of the  
WESTERN CAPE

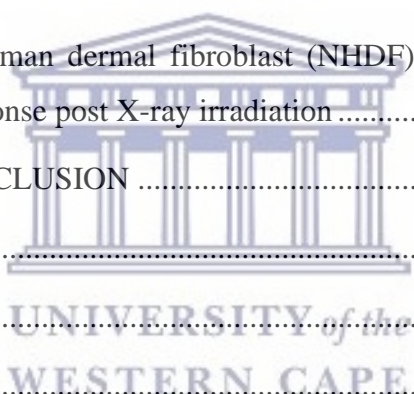
2.4. Cell synchronisation and mitotic index (MI) .....	66
CHAPTER 2: MATERIALS AND METHODS .....	68
Section B: Primary normal human dermal fibroblast (NHDF) vs primary elephant dermal fibroblast (EDF) radiation response post X-ray irradiation .....	68
2.5. Cell culture.....	69
2.5.1. Primary NHDF cell culture.....	69
2.5.1.1. Primary NHDF cell line establishment .....	69
2.5.1.2. Primary NHDF cryopreservation .....	70
2.5.1.3. Primary NHDF life span .....	70
2.5.2. Primary EDF cell culture .....	71
2.6. To assess the biological endpoints, post X-ray IR at GSI and NRF iThemba LABS for the primary NHDF and EDF cell lines, respectively. ....	72
2.7. X-ray irradiation setup .....	73
2.7.1. GSI.....	73
2.7.2. NRF iThemba LABS .....	75
2.8. Cell counting for biological experiments to assess the radiation damage post X-ray irradiation.....	77
2.8.1. Primary NHDF .....	77
2.8.2. Primary EDF.....	78
2.9. X-ray standardisation .....	79
2.10. Clonogenic survival assay (CSA) .....	81
2.10.1. Plating efficiency determination of NHDFs .....	81
2.10.2. Seeding density for IR of NHDFs.....	82
2.10.3. Clonogenic survival assay (CSA) dose response curve.....	84
2.10.3.1. Primary NHDF .....	84
2.10.3.2. Primary EDF .....	85
2.11. Proliferation assay .....	85



2.11.1.	Primary NHDFs .....	85
2.11.2.	Primary EDFs.....	88
2.12.	MTS assay .....	88
2.12.1.	Primary NHDF.....	88
2.12.2.	Primary EDF .....	89
2.13.	Flow cytometry .....	90
2.13.1.	Apoptosis assay.....	91
2.13.1.1.	Primary NHDF .....	92
2.13.1.2.	Primary EDF .....	93
2.13.2.	Cell cycle assay.....	94
2.13.2.1.	Primary NHDF .....	95
2.13.2.2.	Primary EDF .....	95
2.14.	Statistical analysis .....	96
CHAPTER 3:	RESULTS .....	97
Section A:	Primary elephant dermal fibroblast (EDF) cell line characterisation .....	97
3.1.	Primary EDF cell culture .....	97
3.1.1.	Primary EDF sample collection and outgrowth of fibroblasts .....	97
3.1.2.	Primary EDF growth curve.....	102
3.1.3.	Primary EDF doubling time (Td) .....	103
3.2.	Metaphase chromosome spread .....	104
3.3.	Cell synchronisation and mitotic index (MI) .....	107
CHAPTER 3:	RESULTS .....	110
Section B:	Primary normal human dermal fibroblast (NHDF) vs primary elephant dermal fibroblast (EDF) radiation response post X-ray irradiation .....	110
3.4.	X-ray standardisation .....	111
3.5.	Clonogenic survival assay (CSA) .....	112



3.5.1.	Plating efficiency determination of NHDFs .....	112
3.5.2.	Seeding density for IR for the NHDF cells .....	113
3.5.3.	Clonogenic survival assay (CSA) dose response curve.....	115
3.6.	Proliferation assay .....	119
3.7.	MTS assay.....	124
3.8.	Flow cytometry .....	126
3.8.1.	Apoptosis assay .....	126
3.8.2.	Cell cycle assay .....	129
CHAPTER 4:	DISCUSSION.....	137
Section A:	Primary elephant dermal fibroblast (EDF) cell line characterisation .....	137
CHAPTER 4:	DISCUSSION.....	143
Section B:	Primary normal human dermal fibroblast (NHDF) vs primary elephant dermal fibroblast (EDF) radiation response post X-ray irradiation .....	143
CHAPTER 5:	CONCLUSION .....	153
FUTURE PERSPECTIVES	.....	155
LIST OF REFERENCES	.....	159
APPENDIX	.....	199
Appendix I:	Reagents and consumables for primary EDF cell culture. ....	199
Appendix II:	Reagents and consumables for primary NHDF cell culture.....	203
Appendix III:	Reagents and consumables for biological assays at GSI for the NHDF cell line. ....	204
Appendix IV:	Reagents and consumables for biological assays at NRF iThemba LABS for the EDF cell line. ....	206
ANNEXURE	.....	208
Annexure I	.....	209
Annexure II	.....	211
Annexure III	.....	217



Annexure IV.....219  
Annexure V.....220  
Annexure VI.....221  
Annexure VII .....222





# ABBREVIATIONS

---

$\alpha$	Alpha
$\beta$	Beta
$\gamma$	Gamma
$\mu\text{g}$	Microgram(s)
$\mu\text{L}$	Microliter(s)
$\mu\text{m}$	Micrometer(s)
$^{\circ}$	Degree
$^{\circ}\text{C}$	Degree Celsius
14-3-3 $\sigma$	14-3-3 sigma
7-AAD	7-Amino-Actinomycin
AIF	Apoptosis inducing factor
Al	Aluminium
ANOVA	Two-way analysis of variance
Apaf-1	Apoptotic activating factor 1
APC/C	Anaphase-promoting complex/cyclosome
AREC	Animal Research Ethics Committee
ARF	Adenosine diphosphate-ribosylation factor
ATM	Ataxia telangiectasia mutated
ATR	Ataxia telangiectasia and Rad3-related
Bax	Bcl-2-like protein 4
Bcl-2	B-cell lymphoma 2
Be	Beryllium
BER	Base excision repair
BMR	Basal metabolic rate
C	Carboxy
$\text{CaCl}_2$	Calcium Chloride
CAK	Cyclin dependent kinase activating kinase
CARDs	Caspase recruitment domains

CDC	Cell division cycle
CDK	Cyclin dependent kinase
cEMEM	Complete Eagle's Minimum Essential Medium
cFGM	Complete Fibroblast Growth Medium
CHK	Checkpoint kinase
CHO-K1	Chinese hamster ovary
CIP/KIP	CDK interacting protein/Kinase inhibitory protein
CKI	Cyclin dependent kinases inhibitors
cm <sub>2</sub>	Square centimeter(s)
CO <sub>2</sub>	Carbon dioxide
CSA	Clonogenic survival assay
Cu	Copper
DAFF	Department of Agriculture, Forestry and Fisheries
DALRRD	Department of Agriculture, Land Reform and Rural Development
DD	Death domain
DED	Death effector domain
DFFE	The Department of Forestry Fisheries and The Environment
dH <sub>2</sub> O	Distilled water
DIABLO	Direct IAP binding protein with low pI
DISC	Death-inducing signalling complex
DMSO	Dimethyl Sulfoxide
DNA	Deoxyribonucleic acid
DSB(s)	Double strand break(s)
E 1 – 6	Elephant code
E2F	Transcription factor
ECD	Energy coupled dye
EDF(s)	Elephant dermal fibroblast(s)
EDTA	Ethylenediaminetetraacetic acid
EMEM	Eagle's Minimum Essential Medium
ENDOG	Endonuclease G
ER	Endoplasmic reticulum
EtOH	Ethanol

FACS	Fluorescence-activated single cell sorting
FADD	Fas-associated death domain
FasL	Fatty acid synthetase ligand
FasR	Fatty acid synthetase receptor
FBS	Fetal Bovine Serum
FGM	Fibroblast Growth Medium
FITC	Fluorescein isothiocyanate
FL	Fluorescence channel
FSC	Forward scatter
g	Gram(s)
g/mol	Gram(s) per mol
G0 phase	Quiescent phase
G1 phase	First growth phase
G2 phase	Second growth phase
GAAD	Granzyme A-activated deoxyribonuclease
GADD45 $\alpha$	DNA-damage inducible 45 alpha
Gy	Gray
H & E	Haemotoxylin and eosin
HBSS	Hanks Buffered Saline Solution
HEPES	2-[4-(2-hydroxyethyl) piperazin-1-yl]ethanesulfonic acid
HR	Homologous recombination
hr	Hour(s)
HRAT	Harvey Rat sarcoma virus
HtrA2	Omi/high temperature requirement protein A
HU	Hydroxyurea
IAP	Inhibitor of apoptosis
IARC	International Agency for Research on Cancer
INK4	Inhibitors of CDK4
IR	Ionising radiation
IS	Immune system
iThemba LABS	iThemba Laboratories for Accelerator Based Sciences
KCl	Potassium Chloride
kDa	Kilodalton

kGy	Kilogray
KOH	Potassium Hydroxide
kVp	Kilovoltage peak
L	Liter(s)
LET	Linear energy transfer
LFS	Li-Fraumeni Syndrome
LIF	Leukaemia inhibitory factor
LINAC	Linear accelerator
M	Molar
M phase	Mitotic phase
mA	Milliamp
MAT1	Menage a trois 1
MCM 2 – 7	Minichromosomal maintenance subunits 2 – 7
MDM2	Minute 2 homolog
mg	Milligram(s)
MgCl <sub>2</sub>	Magnesium Chloride
MI	Mitotic index
min	Minute(s)
mL	Milliliter(s)
mm	Millimeter(s)
mM	Millimolar
MMR	Mismatch repair
MOMP	Mitochondrial outer membrane permeabilisation
MTS	3-[4,5-dimethylthiazol-2-yl]-5-[3-carboxymethoxyphenyl]- 2-[4-sulfophenyl]-2H-tetrazolium
N	Amino
N/A	Not applicable
n	Number of experiment(s)
NaCl	Sodium Chloride
NCI	National Cancer Institute
NER	Nucleotide excision repair
ng	Nanogram(s)
NHDF(s)	Normal human dermal fibroblast(s)

NHEJ	Non-homologous end joining
NIR	Non-ionising radiation
nm	Nanometer(s)
NRF	Nasional Research Foundation
NuMA	Nuclear mitotic apparatus protein
OD	Optical densities
ORC	Origin recognition complex
p	Probability
P/S	Penicillin/Streptomycin
P/S/A	Penicillin/Streptomycin/Amphotericin B
p53	Tumour protein 53
PARP	Poly-ADP ribose polymerase
PBS	Phosphate Buffered Saline
PC5.5	Phycoerythrin-Cy <sup>TM</sup> 5.5 tandem dye
PCD	Program cell death
PCR	Polymerase chain reaction
PE	Phycoerythrin
pH	Potential of Hydrogen
PI	Propidium iodide
pRB	Protein retinoblastoma
pre-RCs	Pre-replicative complexes
PS	phosphatidylserine
PUMA	P53 upregulated modulator of apoptosis
PVC	Polyvinyl chloride polymer
Q	Quadrants
RBE	Relative biological effectiveness
RING	Really interesting new gene
RNA	Ribonucleic acid
RNase A	Ribonuclease A
ROS	Reactive oxygen species
RPMI	Roswell Park Memorial Institute 1640
RT	Radiation therapy
rt	Room temperature

RTG(s)	Retrogene(s)
s	Second(s)
S phase	Synthesis phase
SA- $\beta$ -GAL	Senescence-associated beta-galactosidase (SA- $\beta$ -GAL)
SAC	Spindle assembly checkpoint
SCF	Skp1p-CDC53p/cullin-F-box protein
SD	Standard deviation
SF	Survival fraction
Smac	Second mitochondrial activator of caspases
SOBP	Spread-out Bragg peak
SSB(s)	Single strand break(s)
SSC	Side scatter
SSD	Source-to-surface distance
Td	Doubling time
Thr <sup>160</sup>	Threonine 160
TNF	Tumour necrosis factor
TNF $\alpha$	Tumour necrosis factor alpha
TNF-R	Tumour necrosis factor receptor
TNFR1	Death receptor type 1 tumour necrosis factor
TNFR1	Tumour necrosis factor receptor -death receptor type 1
TP53	Tumour suppression gene
TRADD	Tumour necrosis factor receptor-associated death domain
TRP53	Transformation-related protein 53
TUSSC	TUMour Suppression and Subdual of Cancer
UK	United Kingdom
USA	United States of America
UV	Ultraviolet
UWC	University of the Western Cape
vs	Versus
WGS	Whole genome sequence
WHO	World Health Organisation

# LIST OF FIGURES

---

**Figure 1: Multistep carcinogenesis.** Step by step process of the transformation of a normal cell into a malignant tumour (LibreTexts, 2020). ..... 1

**Figure 2: IARC estimation of new cancer cases in 2020, worldwide, both sexes, all ages.** The top 3 new cancer cases in 2020 were breast, lung, colorectum with 11.7%, 11.4% and 10%, respectively (International Agency for Research on Cancer, 2022). ..... 2

**Figure 3: Estimated cancer deaths globally in 2002 compared to projected cancer deaths in 2030.** Deaths per million schematically projected with age from 2002 to 2030 (Mathers & Loncar, 2006). ..... 3

**Figure 4: Schematic representation of the burden of lifestyle diseases.** Examples of species that are of interest in finding novel targets for burden of lifestyle diseases that accumulate with age (Stenvinkel *et al.*, 2020). ..... 6

**Figure 5: A schematic presentation of Peto's paradox.** An illustration of Peto's paradox, where the solid red line demonstrates a linear relationship between cancer prevalence and body mass  $\times$  longevity. The dashed red line demonstrates an estimate of cancer prevalence assuming a model describing the probability of an individual developing colorectal cancer after a given number of cell divisions. The solid blue demonstrates the observation that there is no relationship between cancer risk and body mass  $\times$  longevity (Tollis *et al.*, 2019). ..... 8

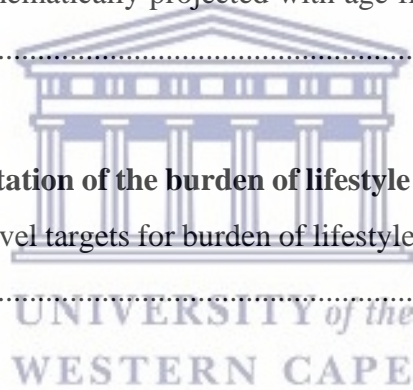


**Figure 6: A schematic comparison of humans and elephants.** Humans and elephants have an average lifespan of 71 and 65 years, weight up to 62 kg and 4 800 kg, contain 37.2 trillion and 3.72 quadrillion number of cells, have a cancer mortality of 11 – 25% and 4.81% and lastly have 1 and 20 copies, respectively. Adapted from (Leslie, 2015). Image created in BioRender.com. .... 13

**Figure 7: Schematic representation of TP53 and/or TP53 RTG numbers within different animals.** **A)** The number of TP53 and/or TP53 RTG in 61 Sarcopterygians (Lobe-finned fishes) with draft or completed genomes, including the African elephant indicated by the pink arrow. Clade names are shown for lineages in which the genome encodes more than 1 TP53 gene or pseudogene. **B)** Comparison of the Proboscidean lineage TP53 and/or TP53 RTG copy numbers inferred from complete genome sequencing data (WGS, purple), 1:1 orthology (green), gene tree reconciliation (blue) and normalised read depth from genome sequencing data (red). Whiskers on normalized read depth copy number estimated show the 95% confidence interval of the estimate (Sulak *et al.*, 2016). .... 15

**Figure 8: The LIF6 gene proposed mechanism in elephants.** Schematic presentation of elephant-specific LIF6 duplicate that is upregulated by TP53 (or p53 protein abbreviated in image) in response to DNA damage and movement of LIF6 to the mitochondria resulting in apoptosis (Vazquez *et al.*, 2018). .... 17

**Figure 9: Schematic presentation of the TP53 theory on lifespan.** Reactive oxygen species (ROS), DNA damage, telomere shortening results in cell damage and TP53 (or p53 protein abbreviated in image) activation which enable DNA repair and/or apoptosis. It is hypothesised that in long-lived animals the “improved” TP53 causes less activation than in their short-lived counterparts but still may sufficiently contribute to DNA damage repair and apoptosis. While in short-lived animals it causes a high activity of TP53 which promotes organismal aging, thus shortening the lifespan (Bartas *et al.*, 2021). .... 20

**Figure 10: Structure of TP53.** Schematic presentation of TP53 gene encoding 393 amino acids residues with its N-terminal transcriptional activation domain, central sequence-specific DNA-binding domain and C-terminal negative regulation domains (Mohammed, 2018). .... 21



**Figure 11: Germline vs somatic mutations.** Comparison of germline mutations such as LFS which is inherited from previous generations, while a somatic mutation is a point mutation (Positive Bioscience, 2019). .....23

**Figure 12: TP53-mediated tumour suppression.** TP53 (or p53 abbreviated in image) in an unstressed state and is maintained at a very low-level by promoting the ubiquitin-proteasome degradation pathway. TP53 in a stressed state due to DNA lesions or activation of oncogenes causing TP53 post-translational modification resulting in stabilization and transcriptional activity (Ub: ubiquitin; P: phosphorylation; Ac: acetylation) (Aubrey *et al.*, 2018).....25

**Figure 13: Schematic representation of the cell cycle with cyclin-CDK complexes.** The cell cycle begins at the G1 phase with an increase in the synthesis of cyclin D and partner with CDK4/6 which promotes cell cycle entry and its progression through G1 phase and G1/S phase transition. During S phase, cyclin A/CDK2 controls the phosphorylation of targets involved in the DNA replication. Cyclin A is highly expressed in the S phase until late G2 phase, where the primary regulator is CDK1. Thereafter, it is replaced with cyclin B/CDK1 to ensure M phase and 2 resulting daughter cells (García-Reyes *et al.*, 2018). .....27

**Figure 14: Control of cell cycle regulation when arresting G2 phase.** Transcriptional activation of p53 protein results in the induction of p21 that binds to and inhibits cyclin-CDK complexes. Induction of GADD45 and 14-3-3 and repression of cyclin B1 cause cell cycle arrest in the G2 phase (Capuzzo *et al.*, 2022). .....33

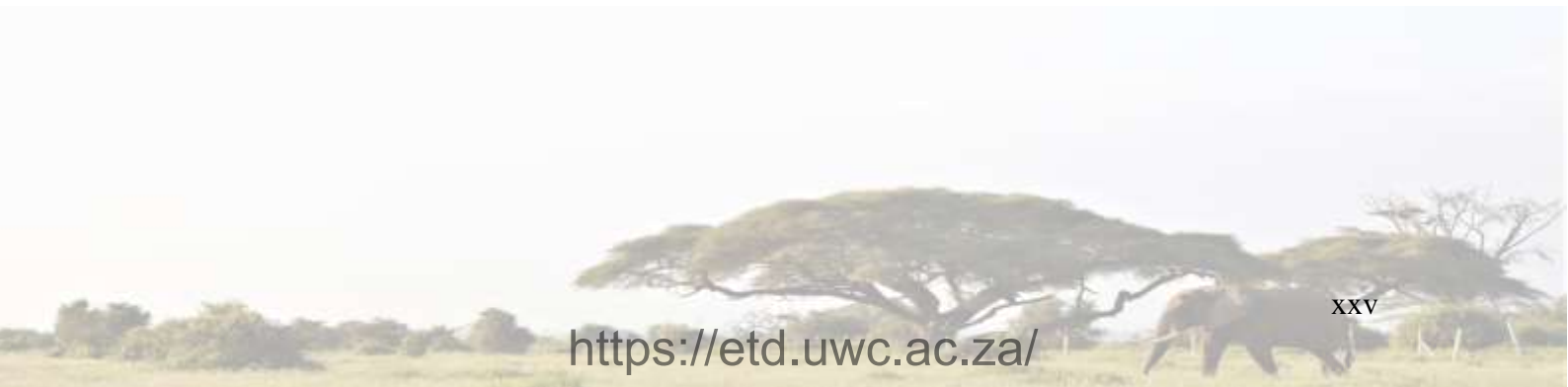
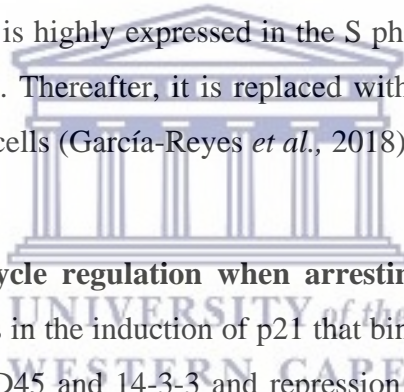


**Figure 15: Schematic diagram of apoptosis induction via the extrinsic or intrinsic apoptotic pathway.** Apoptosis induction can be executed through the extrinsic apoptotic pathway by signalling through death signals (TNF and FasL). The DD transmits the death signal from the cell membrane to the intracellular signalling pathway, whereby clusters of the DD recruit adaptors (TRADD and FADD) forming a complex namely DISC. Thereafter procaspase 9 is cleaved to its active form of caspase 9 followed by caspase 3 and the induction of apoptosis. Intracellular stress such as genetic damage, hypoxia and more causes an intrinsic apoptotic pathway. Pro-apoptotic molecules such as cytochrome c, Smac, DIABLO and Omi/HtrA2 are released from the mitochondria. Cytochrome c binds to Apaf-1 and forms an apoptosome, while Smac, DIABLO and Omi/HtrA2 inhibits the IAP family and aids in the process of caspase of cascades (Wong, 2011). .....38

**Figure 16: Induction of intracellular stress causing a caspase dependent and independent apoptosis pathway.** Caspase dependent apoptosis causes the release of cytochrome c from the mitochondria which binds to Apaf-1 forming an apoptosome. DIABLO and Omi/HtrA2 facilitate caspase activation by inhibiting several members of the inhibitor of apoptosis protein inhibits IAPs. On the contrary, AIF, ENDOG function in a caspase independent manner by which DNA fragmentation occur. In addition, HtrA2 can also cleave the cytoskeleton independently of caspases (Galluzzi *et al.*, 2011). .....41

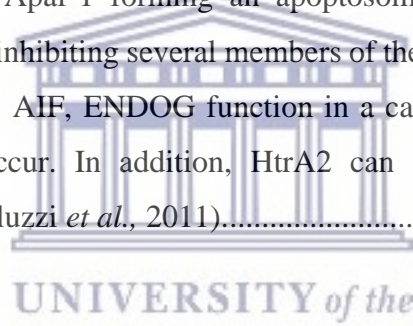


**Figure 17: Types of IR.** Different types of IR have different penetrating powers through different material.  $\alpha$ - and  $\beta$ - rays are stopped with paper and a thin aluminium plate, respectively, while X- and  $\gamma$ -rays are stopped by a lead plate. Water and paraffin stops neutrons from penetrating (Chen, 2015). .....42

**Figure 18: Direct and indirect actions of IR.** Direct action of IR is a secondary electron resulting from absorption of an X-ray photon interacts with the DNA to produce an damaging effect, while indirect action is for example a water molecule to produce a hydroxyl radical (OH $\cdot$ ) which results in DNA damage (S: sugar; P: phosphorus; A: adenine; T: thymine; G: guanine; C: cytosine) (Hall & Giaccia, 2012). .....44



**Figure 19: IR causes direct and indirect DNA damage inflicted by HR and NHEJ.** IR causes DNA damage either directly or through the generation of free radical formation. Both types of damage lead to an increase activity of p53 protein and cell cycle arrest allowing repair of DNA DSBs by activating the HR or NHEJ pathway. If the repair is successful, the cell cycle will resume its proliferation, in the case of major DNA damage, induction of a cell death pathway via up-regulation of p53 protein, carcinogenesis or teratogenesis can occur (Smith *et al.*, 2017b).....46

**Figure 20: Low vs high LET radiation.** Schematic representation of the energy disruption of low (left) and high (right) LET radiation. Low LET radiation contains several radiation tracks, while high LET radiation have a single fatal radiation track with a dense pattern of ionizations along this track (Scalliet & Gueulette, 2017).....47

**Figure 21: The classical view of TP53 activation and response post-irradiation.** DNA damage trigger the activation of ATM/ATR signalling pathway by phosphorylating CHK1/2 resulting in the stabilization of the p53 protein within the cell by breaking free from its inhibitor, MDM2. ARF activation enhances p53 protein stability and activation. The stabilisation of the p53 protein allows for the activation of target genes which causes cell cycle arrest, DNA repair, apoptosis and senescence based on the DNA damage present (Biegging, Mello & Attardi, 2014). .....49

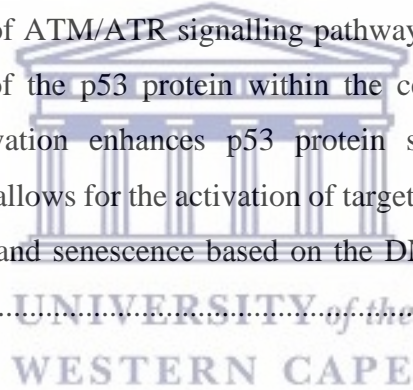


**Figure 22: Skin punch biopsy procedure.** A) Skin biopsies were collected behind the ear of an elephant. B – C) The skin of the elephants was washed and cleaned with 70% EtOH. D) Surgical draped behind the ear of the elephant to maintain sterility.....55

**Figure 23: Skin punch biopsy preparation.** A – C) Skin punch biopsy in transport medium containing and was transferred to a glass petri-dish followed by washing thrice in washing PBS. D) The epidermis was removed and discarded. E – F) Initial culturing medium was added to prevent dehydration of the tissue and was cut into smaller fragments. G) The tissue fragments were transferred with a glass Pasteur pipette and spread across the surface in the T25 tissue culture treated flask. H – I) FBS was added to cover the fragments and the T25 flask was incubated under standard conditions.....57

**Figure 24: Morphological depiction of EDFs (E1) in culture (10× magnification) at different passages with a different seeding density. Scale 200 μm.** No morphological changes were observed at 10× magnification. **A)** E1 at passage 3. **B)** E1 at passage 14.....60

**Figure 25: EDF growth curve of E3 – E5 establishment procedure to determine the Td.** **A)** The confluency was determined on 6 different regions on a T25 flask. **B)** The T25 flask in an incubator on the Cytosmart, Lonza® system. ....62

**Figure 26: Morphological depiction of NHDFs in culture at 10× magnification at different passages with a different seeding density. Scale 100 μm.** No morphological changes were observed at 10× magnification. **A)** NHDFs at passage 3. **B)** NHDFs at passage 14. ....71

**Figure 27: Primary NHDF and EDF experimental procedure.** Graphical depiction of the NHDF and EDF cell line initiation and biological endpoints which will be evaluated after radiation exposure. Created with BioRender.com. ....72

**Figure 28: X-ray machine at GSL.** **A)** The overview of the X-ray tube. The red arrow indicates the distance between the X-ray tube and the grey sample holder. **B)** T25 flask in the field view indicated with the blue arrow, the farmer ionisation chamber, in place of the grey sample holder. **C)** The control panel. The green button indicated by the green arrow was to execute the initiation of the X-ray radiation and the yellow button indicated that the X-ray machine was on. **D)** The PTW-UNIDOS dosimeter indicate the doses delivered to the sample and the dose rate/min. ....74

**Figure 29: PXi Precision X-ray machine at NRF iThemba LABS.** **A)** The overview of the X-ray machine. **B)** The control panel. The green arrow indicates the start button of the X-ray and the yellow button indicated the emergency stop button for the X-ray. **C)** T25 flask in the field view indicated by the purple arrow and the red arrow indicate the SSD. ....76

**Figure 30: Bio-Rad, TC 20™ Automated Cell Counter.** A) Cell suspension mixed with trypan blue and loaded on a counting slide. B) A range of 4 – 25 µm was set to count the cells. C) A graphic display of cells counted.....77

**Figure 31: Seeding densities of NHDF cells and respective IR doses.** Graphical depiction of the NHDF cell line to obtain 200, 400, 2 000, 5 000 and 10 000 NHDF cells/T25 flask for 0, 2, 4, 6 and 8 Gy, respectively. Image created with BioRender.com.....82

**Figure 32: Schematic representation of a 96 well plate.** Column 1, row A – H served as the black for all experimentations. The remaining wells were used for the samples (Templates, no date).....86

**Figure 33: The 96-well plates for 72 h post IR after crystal violet stain.** A) 0 Gy, B) 2 Gy, C) 4 Gy, D) 6 Gy, E) 8 Gy and F) 16 Gy. ....87

**Figure 34: The 96-well plates for 120 h post IR with MTS reagent colour observed before (A – B) and after the 2 h incubation period (C – D).** A) 0 Gy, 120 h, and MTS reagent colour observation before incubation, B) 16 Gy, 120 h, and MTS reagent colour observation before incubation, C) 0 Gy, 120 h, and MTS reagent colour observation after 2 h incubation, and D) 16 Gy, 120 h, and MTS reagent colour observation after 2 h incubation. ....89

**Figure 35: Light scattering via flow cytometer.** FSC is relative to cell size, while SSC is relative to cell granularity of internal complexity (Abraham & Staffurth, 2016).....90

**Figure 36: Graphically representation of apoptosis analysis done in FlowJo™.** A) FSC- vs SSC-Area dot plot graph to obtain a cell gate and exclude cell debris. B) FSC-Area vs FSC-Height dot plot graph to obtain a single cell gate and exclude doublets. C) PE-Annexin V/Annexin V FITC vs 7-AAD/PI graph divided into 4 quadrants. Q1: Live cells, Q2: Early apoptosis, Q3: Late apoptosis and Q4: Necrosis. ....92

**Figure 37: Graphical representation of cell cycle analysis done in FlowJo™.** A) FSC- vs SSC-Area dot plot graph to obtain a cell gate and exclude cell debris. B) FSC-Area vs FSC-Height dot plot graph to obtain a single cell gate and exclude doublets. C) Histogram representing G0/G1, S and G2/M phase. ....94

**Figure 38: First radial explant outgrowth of E1 after biopsy fragmentation.** A) The first images were taken of the cells in T25 flasks by the CytoSmart, Lonza® live cell imaging system (scale 200 µm) after the first visual confirmation of explant outgrowth of fibroblast cells. The green arrow illustrates the elephant biopsy fragment and the yellow arrow illustrates fibroblast cells. B) 15 h, C) 36 h and D) 67 h post initial EDFs confirmation..... 101

**Figure 39: Growth curve of E3, E4 and E5 determined with CytoSmart, Lonza® live cell imaging system for 11 consecutive days.** The percentage confluency captured over 6 regions of a T25 flask over 11 consecutive days was plotted for E3, E4 and E5. The average confluency for the 3 elephants was  $76.45\% \pm 26.56\%$  (average  $\pm$  SD) on the final day of imaging. The error bars represent the SD (n = 3)..... 102

**Figure 40: EDF Td over 6 days captured with a CytoSmart, Lonza® live cell imaging system.** E3, E4 and E5 at passage 1 with a Td of 53.90, 65.61 and 66.86, respectively and an average Td of  $62.13 \pm 7$  h (average  $\pm$  SD). The error bars represent the SD (n = 3). ..... 103

**Figure 41: Metaphase chromosome spread of E1.** A and B) Images were captured using a Metafer 4 platform with immersion oil lens objective (63×) showing a diploid chromosome number of 56 chromosomes obtained from E1 after 3 h of KaryoMAX™ Colcemid™. .... 106

**Figure 42: E6 fluctuation of MI after the release of G1/S block by HU.** Duplicate coverslips were removed every 2<sup>nd</sup> h for the first 6 h and thereafter removed hourly for 24 h. A peak in MI was observed 36 – 39 h after release of the HU..... 108

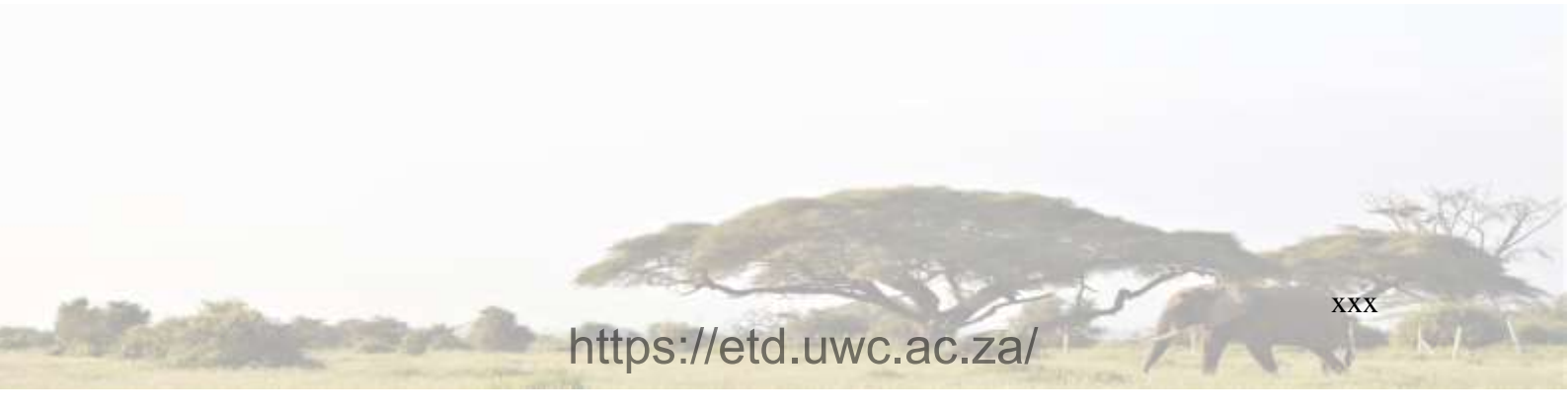
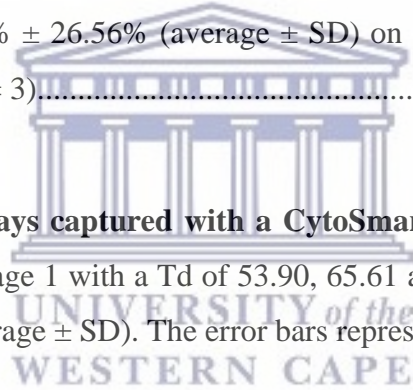


**Figure 43: Mitotic phases of E6 at 39 h after block release.** Viewed with Zeiss Primovert light microscope and images were captured with a Axio 208 colour, scale 50  $\mu\text{m}$ . Fibroblast indicated by a yellow arrow, prophase indicated by an orange arrow, metaphase showed by a blue arrow, purple arrow indicating anaphase and telophase showed by a pink arrow. **A – B)** At 20  $\times$  magnification. **C – D)** At 40  $\times$  magnification. .... 109

**Figure 44: Standardisation of the X-ray machine at both research facilities by using CHO-K1 cells.** A decrease in SF with higher doses for the CHO-K1 at both GSI (shown in blue) and NRF iThemba LABS (shown in pink). No statistical significance with a paired t test was observed in SF. Error bars represent the SD of the biological triplicates..... 111

**Figure 45: Plating efficiency determination of the NHDF flask with no IR exposure.** **A)** 200 cells seeded. **B)** 400 cells seeded. **C)** 600 cells seeded. **D)** 800 cells seeded. .... 112

**Figure 46: NHDF flasks post staining to determine seeding densities with IR exposure for CSA dose response curve.** **A)** 200 cells seeded, 0 Gy. **B)** 400 cells seeded, 2 Gy. **C)** 2 000 cells seeded, 4 Gy. **D)** 5 000 cells seeded, 6 Gy. **E)** 10 000 cells seeded, 8 Gy..... 114

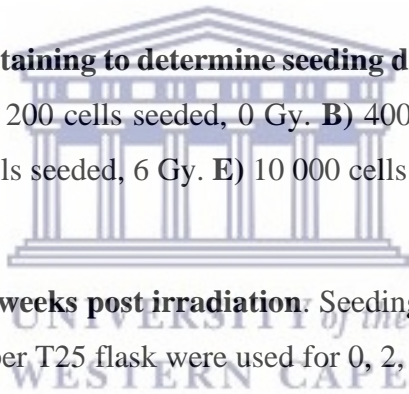


**Figure 47: SF of NHDFs at 2 weeks post irradiation.** Seeding densities of 200, 400, 2 000, 5 000 and 10 000 NHDF cells per T25 flask were used for 0, 2, 4, 6 and 8 Gy, respectively. A decrease in SF was noted with an increase in radiation doses. Error bars represent the SD of the biological triplicates. .... 114

**Figure 48: NHDF T25 flasks post staining to determine CSA dose response curve.** **A)** 200 cells seeded, 0Gy. **B)** 400 cells seeded, 1 Gy. **C)** 400 cells seeded, 2 Gy. **D)** 2 000 cells seeded, 4 Gy. **E)** 5 000 cells seeded, 5 Gy. **E)** 8 000 cells seeded, 6 Gy. **E)** 10 000 cells seeded, 7 Gy. **E)** 20 000 cells seeded, 8 Gy. .... 116

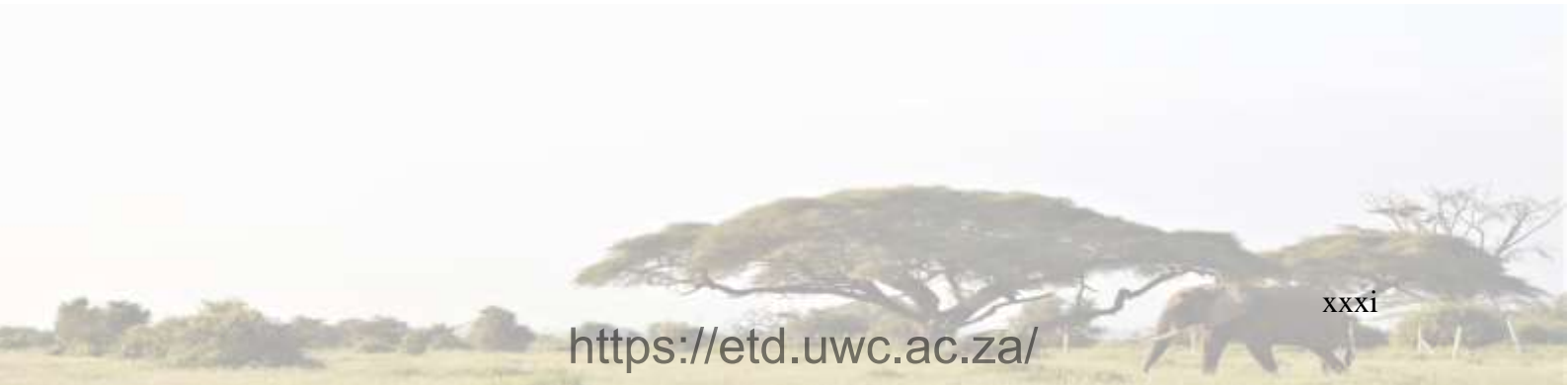


**Figure 49: EDF T25 flasks post staining to determine CSA dose response curve.** A) 200 cells seeded, 0 Gy. B) 400 cells seeded, 1 Gy. C) 400 cells seeded, 2 Gy. D) 2 000 cells seeded, 4 Gy. E) 5 000 cells seeded, 5 Gy. E) 8 000 cells seeded, 6 Gy. E) 10 000 cells seeded, 7 Gy. E) 20 000 cells seeded, 8 Gy. .... 117

**Figure 50: NHDFs and EDFs CSA dose response curve.** Seeding densities of 200, 400, 400, 2 000, 4 000, 8 000, 10 000 and 20 000 NHDF/EDF cells per T25 flask for 0, 1, 2, 4, 5, 6, 7 and 8 Gy, respectively. Both NHDFs and EDFs display a decrease in SF with higher doses. No statistical significance with a paired t test was observed in SF. However, the EDFs appear to be more radiosensitive based on the  $\alpha/\beta$  ratio. The SD of the biological triplicates represents the error bars. .... 118

**Figure 51: NHDF cell proliferation after 24, 48, 72, 96, 120 and 144 h of X-ray irradiation.** The NHDF cell proliferation capacity was dose-dependent and not time-dependent. The error bars represent the SD of the biological repeats. The statistically significant comparison between the irradiated and unirradiated was shown as follow: \* represents  $p < 0.05$ , \*\* represents  $p < 0.01$  and \*\*\* represents  $p < 0.0001$ . .... 120

**Figure 52: EDF cell proliferation after 72 and 120 h of X-ray irradiation.** The EDF cell proliferation capacity was dose-dependent and not time-dependent. A cell recovery was observed at 120 h for 1 and 2 Gy. The SD of the biological triplicates represented by the error bars. Significance indication of the irradiated and unirradiated sample was indicated as follow: \* represents  $p < 0.05$ , \*\* represents  $p < 0.01$  and \*\*\* represents  $p < 0.0001$ . .... 122

**Figure 53: NHDF cell viability when exposed to X-ray radiation after 72 and 120 h.** A significant decrease in cell viability was observed with higher doses. Significance indication: \*  $p < 0.05$ , \*\*  $p < 0.01$  and \*\*\*  $p < 0.0001$ . The SD of the biological triplicates represents the error bars. .... 125



**Figure 54: Apoptosis analysis 12 h post-irradiation for both NHDFs and EDFs.** No significant apoptosis induction was observed for both NHDF and EDF cell lines. A 10% increase from 0 to 8 Gy for the EDFs at early apoptosis was observed. Error bars represent the SD of the biological triplicates. .... 126

**Figure 55: Apoptosis analysis 24 h post-irradiation of both NHDFs and EDFs.** NHDFs showed a minimal change in apoptosis induction, whilst the EDFs showed a notable increase with 8 Gy in both early and late apoptotic response. However, both NHDF and EDF had no significant apoptosis induction after X-rays irradiations. The error bars indicate the SD..... 127

**Figure 56: Apoptosis analysis 48 h post-irradiation for both NHDFs and EDFs.** No significant change was observed with the NHDFs and EDFs. The EDFs had an increase in apoptotic response with late apoptosis having the highest indicator. The error bars show the SD of the biological triplicates..... 128

**Figure 57: NHDF and EDF flow cytometry cell cycle progression 24 h post-irradiation.** Example images obtained from 1 sample representing A) NDHF: 0 Gy, B) NHDF: 16 Gy, C) EDF: 0 Gy and D) EDF: 16 Gy. A significant increase was observed in EDF at 16 Gy, indicating a possible G2/M cell block. .... 135

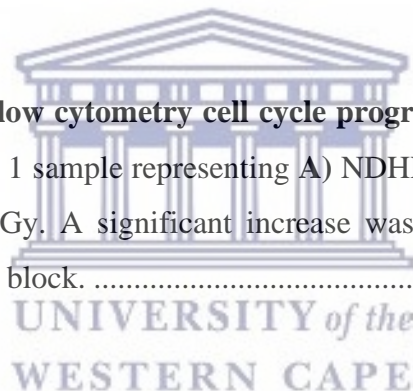


**Figure 58: Flow cytometry cell cycle progression for NHDF and EDF 48 h post-irradiation.** Example images obtained from 1 sample representing A) NDHF: 0 Gy, B) NHDF: 16 Gy, C) EDF: 0 Gy and D) EDF: 16 Gy with a significant cell cycle shift indicating a possible G2/M block. .... 136

**Figure 59: Cellular states and transitions into quiescence.** Quiescent cells can reversibly transition into an active state in which they enter the cell cycle and generate new differentiated cells to maintain tissue homeostasis. In contrasts to differentiation, cells can enter an irreversible senescent (G0) state, therefore hampering the regenerative potential (Urbain and Cheung, 2021)..... 148



**Figure 60: Contribution of the p53 protein to induce G2/M cell cycle arrest.** When DNA damage is present within the cell, the p53 protein triggers several parallel pathways that block the formation of the mitotic cyclin B-CDC2 complex and inhibit its activity to allow cell cycle continuation. The p53 protein targets the upregulation of p21 and causes an inhibition of the cyclin B-CDK complex acting as a cell cycle block. The upregulation of p53 acts on GADD45 and results in the binding to CDC2 and prevent the cyclin B complex activation. The p53 protein sequesters 14-3-3 $\sigma$  and inhibits the phosphorylated form of CDC25 isoform C which in turn dephosphorylate cyclin B-CDK complex. In addition, 14-3-3 $\sigma$  recruits CDC2 in the cytoplasm, preventing it from translocating into the nucleus in the late G2 phase. The p21 protein, GADD45, 14-3-3 $\sigma$  all are upregulated in the presence of TP53 in response to DNA damage inducing a G2/M cell cycle block (Sionov, Hayon & Haupt, 2013). ..... 150



# LIST OF TABLES

---

**Table 1: Metaphase chromosome spread conditions to determine a metaphase chromosome spreads and to confirm the presence of 56 chromosomes in the newly established EDF cell line.** E1 was tested under different cell densities and time points (h) with a working concentration of 0.05 µg/mL KaryoMAX™ Colcemid™ Solution in PBS.....64

**Table 2: CHO-K1 standardisation seeding density test.** CSA seeding density for CHO-K1. Cells were seeded in 3 T25 flasks for doses 2 – 8 Gy and in 4 T25 flasks for the control sample. ....80

**Table 3: Seeding densities of NHDFs and respective IR doses to plot a CSA dose response curve.** Cells were seeded in 3 T25 flasks for doses 1 – 8 Gy and in 4 T25 flasks for the control sample. ....84

**Table 4: Elephant sample collection with their respective age and sex.** Elephants' age ranged from 14 – 47 years. Sample collection occurred at 2 locations: Botlierskop Private Game Reserves and Sanbona Wildlife Reserve. ....98

**Table 5: Elephant sample collection and radial explant outgrowth of fibroblasts.** The number of days after first radial explant outgrowth of EDFs. Where no outgrowth of fibroblasts was detected, culture flasks were discarded after 40 days.....99

**Table 6: The time and cell density conditions applied in obtaining metaphase chromosome spreads.** Cells from E1 were exposed to KaryoMAX™ Colcemid™ at and had a cell density of 70 – 80%, 60 – 70% and 90 – 95%, respectively. A working concentration of 0.05 µg/mL KaryoMAX™ Colcemid™ was added for 3 – 28 h to prevent the EDFs from proceeding to anaphase. .... 105

**Table 7: Plating efficiency determination of NHDF cells after 2 weeks of incubation without IR exposure.** The highest plating efficiency was obtained with seeding 200 cells per T25 flask. A decrease in plating efficiency was observed in the samples with a higher seeding density (SD based on the biological triplicates). ..... 113

**Table 8: Statistical comparison between 72 and 120 h for the cell proliferation assay.** A significant difference for the NHDFs comparing 72 and 120 h were only observed at 16 Gy. In contrasts, the EDFs showed a significant difference at 1, 2 and 16 Gy. Significance indication: \*  $p < 0.05$ , \*\*  $p < 0.01$ , \*\*\*  $p < 0.0001$  and ns indicates no significance. .... 123

**Table 9: Cell cycle assay of NHDF and EDF cells before X-rays.** The NHDFs were in the G0/G1 phase with 84.50%, whilst 61.80% of the EDFs were in G0/G1 phase and 24.08% was in G2/M phase. NHDF results were displayed in green and EDF results shown in purple. Significant indication of comparison between the NHDF and EDF cell line was shown in orange with \*  $p < 0.05$  and \*\*\*  $p < 0.0001$ . ..... 129

**Table 10: NHDF and EDF cell cycle assay to reveal the cell cycle progression post 24 h X-ray irradiation.** More than 80% of the NHDFs were in the G0/G1 phase for all the doses. For the EDFs a decrease was observed in G0/G1 phase with an increase in the doses and a notable increase in the G2/M phase, shown in bold. Green indicates NHDF results while purple indicates EDF results. The statistically significant comparison between the irradiated and unirradiated sample shown in the colour of the cell line and \*\*\* indicate  $p < 0.0001$ . The significant comparison between the NHDF and EDF cell lines are presented in orange and \*\* represents  $p < 0.01$  and \*\*\* represents  $p < 0.0001$ . ..... 131

**Table 11: Cell cycle progression of NHDF and EDF cells post 48 h X-ray irradiation.** The NHDFs showed no clear shift in cell cycle progression in response to the IR. The EDFs showed a decreased number of cells in the G0/G1 phase with an increase of cells in the G2/M phase after irradiation with 4, 8, 12 and 16 Gy (bold). NHDF results showed in green and EDF results in purple and both cell line significance of the control and IR was shown in the respective colours. The NHDF and EDF significance comparison is presented in orange. Significance indication: \*  $p < 0.05$ , \*\*  $p < 0.01$  and \*\*\*  $p < 0.0001$ . ..... 133

# CHAPTER 1:

## INTRODUCTION

---

### 1.1. Introduction

Cancer is a multifactorial disease and is defined by uncontrolled cell proliferation. The carcinogenesis process finds its origin in the activation of oncogenes and/or inactivation of tumour suppressor genes, which ultimately lead to uncontrolled cell cycle progression and inhibition of cell death (**Figure 1**) (Hanahan & Weinberg, 2000; Padma, 2015; Sarkar *et al.*, 2013).



**Figure 1: Multistep carcinogenesis.** Step by step process of the transformation of a normal cell into a malignant tumour (LibreTexts, 2020).

In the latest report, the International Agency for Research on Cancer (IARC) estimated that the number of new cases worldwide in 2020 was 19.3 million with 10.1 and 9.2 million in men and women (all ages), respectively (**Figure 2**) (International Agency for Research on Cancer, 2022). With this growing global burden, cancer prevention is one of the most significant public health challenges of the 21<sup>st</sup> century (World Cancer Research Fund, 2020).

Estimated number of new cases in 2020, World, both sexes, all ages

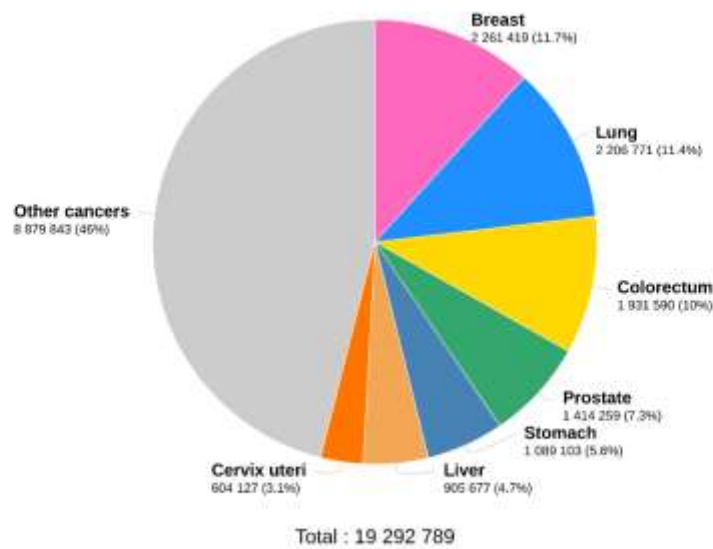


**Figure 2: IARC estimation of new cancer cases in 2020, worldwide, both sexes, all ages.** The top 3 new cancer cases in 2020 were breast, lung, colorectum with 11.7%, 11.4% and 10%, respectively (International Agency for Research on Cancer, 2022).

The World Health Organisation (WHO) identified cancer as the leading cause of death worldwide with 10 million deaths in 2020, or approximately 1 in 6 deaths (World Health Organisation, 2022). Lung, colon and rectum and liver are the top 3 cancer-related deaths in 2020 responsible for a total of approximately 1.8 million cancer deaths, of which 916 000 in men and 830 000 deaths in women (World Health Organisation, 2022). Also in Africa, cancer is an emerging health problem that needs to be addressed appropriately in order to control the increased cancer occurrence and mortality rates (Hamdi *et al.*, 2021). In 2020, a 110 000 new cancer cases were diagnosed, and 56 000 cancer-related deaths were reported in South Africa alone (Cairncross *et al.*, 2021).

It is predicted that the annual cancer occurrence and mortality rate is likely to increase by approximately 70% in 2030 (Figure 3) (Parkin *et al.*, 2014). The National Cancer Institute (NCI) (2021) stated that the number of cancer cases per 100 000 people in 3 different age groups will be as follows: i) Less than 25 people in the age group under 20 years of age, ii) 350 people in the age group of 45 – 49 and iii) more than 1 000 people in the age group above 60 years of age (National Cancer Institute, 2021). With the escalating effect of cancer occurrence,

it is of great significance to comprehend cancer preventative measures, improve diagnosis and treatments and prevent mortality. Much progress has been made in the oncology field, however, is still insufficient evidence to cope with the growing cancer burden and further research is needed (Pucci, Martinelli & Ciofani, 2019).

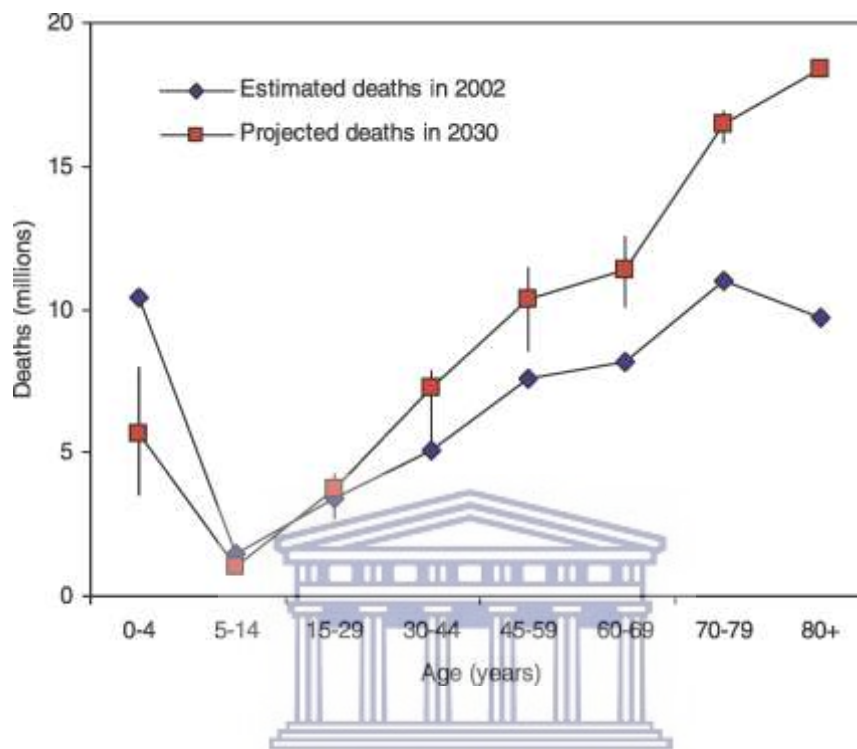


**Figure 3: Estimated cancer deaths globally in 2002 compared to projected cancer deaths in 2030.** Deaths per million schematically projected with age from 2002 to 2030 (Mathers and Loncar, 2006).

Despite all the technical advances in the field of cancer diagnostics, early detection and imaging of cancer remains challenging, not only in African countries but across the world (Frangioni, Fran-Gioni & Deaconess, 2008). Systems such as X-ray radiography, computed tomography, optical imaging, ultrasound, magnetic resonance imaging, single-photon emission computed tomography and positron emission tomography are all imaging modalities used by clinicians who diagnose, define the stage and treat cancers (Frangioni, Fran-Gioni & Deaconess, 2008; Grodzinski, Silver & Molnar, 2006; Higgins & Pomper, 2011). However, challenges related to limitations in sensitivity and spatial resolution remain roadblocks for early cancer detection and diagnosis (Frangioni, Fran-Gioni & Deaconess, 2008; Grodzinski, Silver & Molnar, 2006).

The appropriate cancer treatment is determined based on the type, location and the stage of cancer (Chu *et al.*, 2020). Treatment options comprise surgery to remove tumour(s), chemotherapy and radiation therapy (RT); either alone or in a combination of therapies (Debela *et al.*, 2021; Huang *et al.*, 2017; Kim *et al.*, 2018). Surgery is considered to be one of the most effective treatment options since it brings loco-regional control, however, only at an early stage of disease progression and often in combination with other therapies at later stages (Dare *et al.*, 2015; Debela *et al.*, 2021). Combination therapies have been at the forefront of treating cancer though the adverse impact on a person's ability to function and their quality of life remains a challenge (Waldman, Fritz & Lenardo, 2020).

Approximately 50% of cancer patients receive RT during their course of illness which contributes to 40% of curative treatment for cancer (Barton, Frommer & Shafiq, 2006; Baskar *et al.*, 2012a). RT aims to deprive the tumour cells of their multiplication potential by damaging the deoxyribonucleic acid (DNA) via high doses of ionizing radiation (see Section 1.6) (Kim *et al.*, 2015). Increased levels of radiation are required to eradicate cancer cells however, it is limited to the tolerance of surrounding healthy tissue (Barnett *et al.*, 2009; Kim *et al.*, 2015). RT is not an invasive procedure and has a faster recovery rate when compared to surgery (Babaei and Ganjalikhani, 2014). However, a large portion of cancer patients still experience radiation resistance and recurrence of cancers (Kim *et al.*, 2015). High-energy photons (X- and gamma ( $\gamma$ )-rays) are the most commonly used radiation qualities in external beam RT, but charged particles such as protons and carbon ions, provide dosimetry and radiobiological advantages and are rapidly gaining momentum as modern RT techniques (Durante & Loeffler, 2010).



## 1.2. Cancer in elephants

Traditionally rats (*Rattus rattus*) and mice (*Mus musculus*) are used to investigate the development of cancer, due to their short life span, rapid reproduction and their vulnerability towards cancer (Stenvinkel *et al.*, 2020). However, these traits imply that rats and mice have fewer anticancer mechanisms and novel tumour resistance mechanisms are less likely to be discovered using these models (Tian *et al.*, 2013). Despite these disadvantages, mouse models have become very popular due to the development of gene targeting. The latter enables cancer biologists to study tumour biology *in vivo*, which is more realistic in a dynamic physiological system when compared to *in vitro* studies (Zhang, Moore & Ji, 2011). However, biologists are currently looking beyond the traditional rodent models, by investigating non-standard mammalian species providing novel comprehensions into cancer resistance, (Seluanov *et al.*, 2018).

Species such as elephants (Loxodonta), the naked mole rats (*Heterocephalus glaber*) and the Tasmanian devil (*Sarcophilus harrisii*) show remarkable resistance against cancer (**Figure 4**) (Seluanov *et al.*, 2018; Stenvinkel *et al.*, 2020). The rate of cancer development differs in animals, for example, ferrets (*Mustela putorius furo*) and dogs (*Canis lupus familiaris*) show a very high cancer incidence rate (Callier, 2019). Researchers concluded that cancer occurrence and resistance could be shaped by natural selection (Albuquerque *et al.*, 2018; Athena Aktipis *et al.*, 2015). In this way, nature can direct oncology research to study pathways that have been naturally selected to allow survival in challenging environments with different resources. Changing from the traditional approach with standard cell culture lines and mouse models, new preventative mechanisms as well as therapeutic strategies can be discovered with this novel bio-inspired approach, known as biomimetics (Stenvinkel *et al.*, 2020).

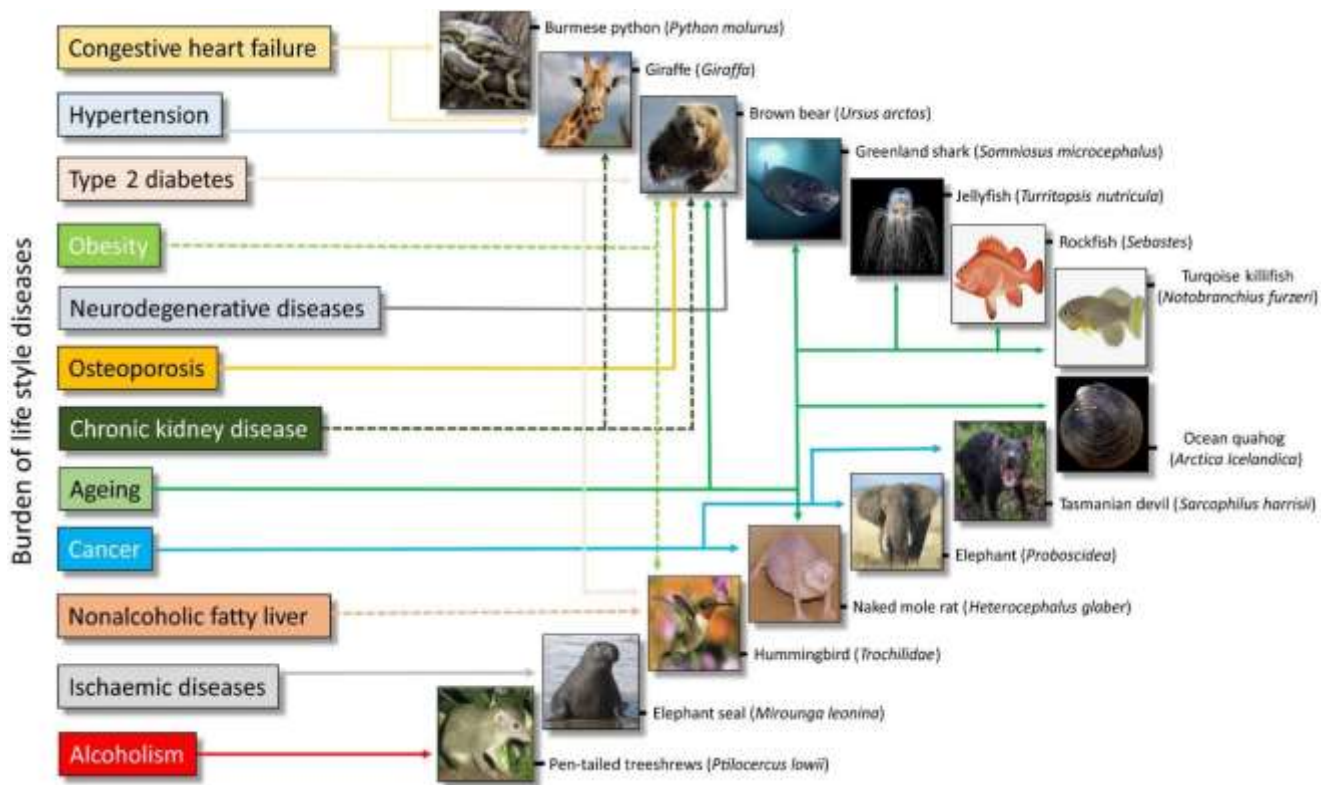
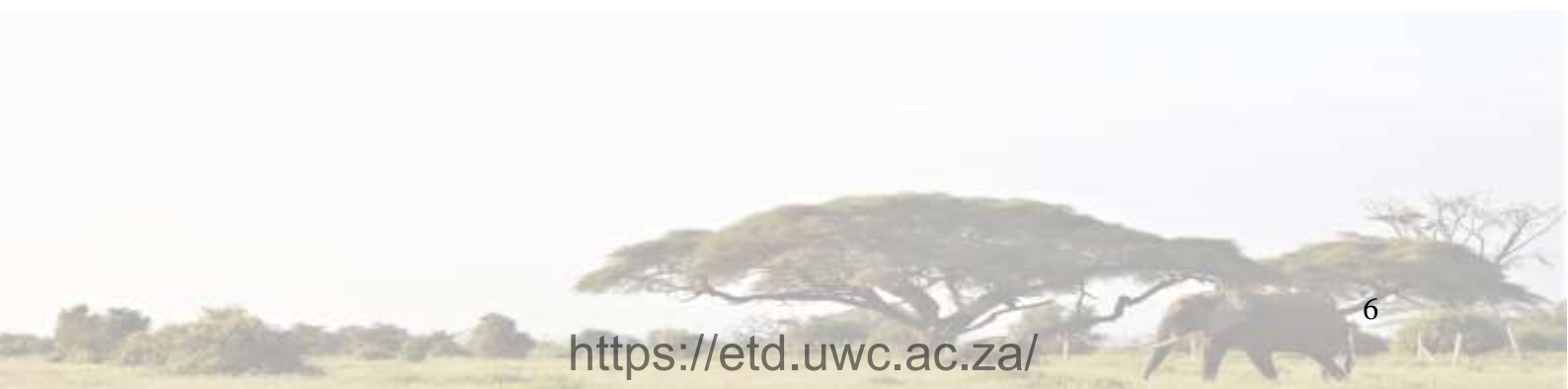
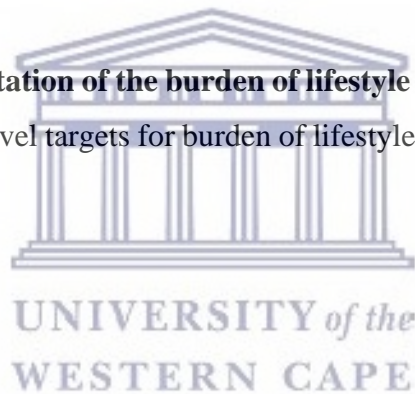
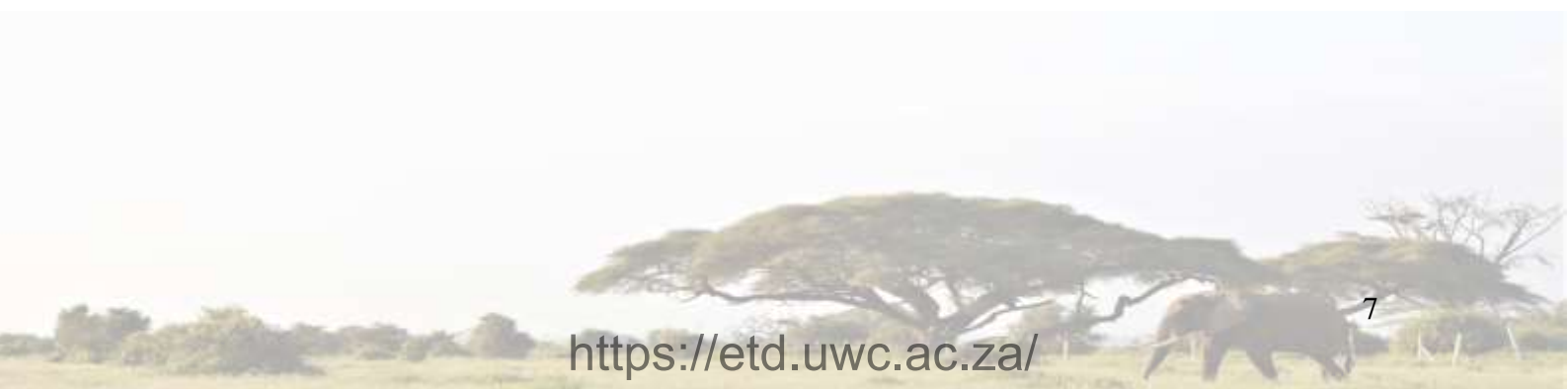


**Figure 4: Schematic representation of the burden of lifestyle diseases.** Examples of species that are of interest in finding novel targets for burden of lifestyle diseases that accumulate with age (Stenvinkel *et al.*, 2020).



### 1.2.1. Peto's paradox

In 1975, a British epidemiologist called Richard Peto, observed that cancer risk does not correlate with body size and species lifespan. He postulated a question: why humans who contain 1 000 times more cells and live 30 times longer than mice, do not suffer from much higher probabilities of developing cancer (Peto *et al.*, 1975)? The paradox is that animals with a longer lifespan (more lifetime of cell divisions) and larger body size (more cells) have more time to accumulate cancer-causing mutations than animals with a shorter lifespan and smaller body size and therefore should be at an increased risk of developing cancer (**Figure 5**) (Abegglen *et al.*, 2015; Barkley, Song & Vaziri, 2009; Callier, 2019; Tollis, Boddy & Maley, 2017; Vincze *et al.*, 2022). However, cancer incidence across the animal kingdom does not appear to increase as theoretically expected when taking into account the number of cells and the cell divisions of the organisms (Tollis, Boddy & Maley, 2017). This seemingly counterintuitive occurrence is known in evolutionary biology as Peto's paradox.



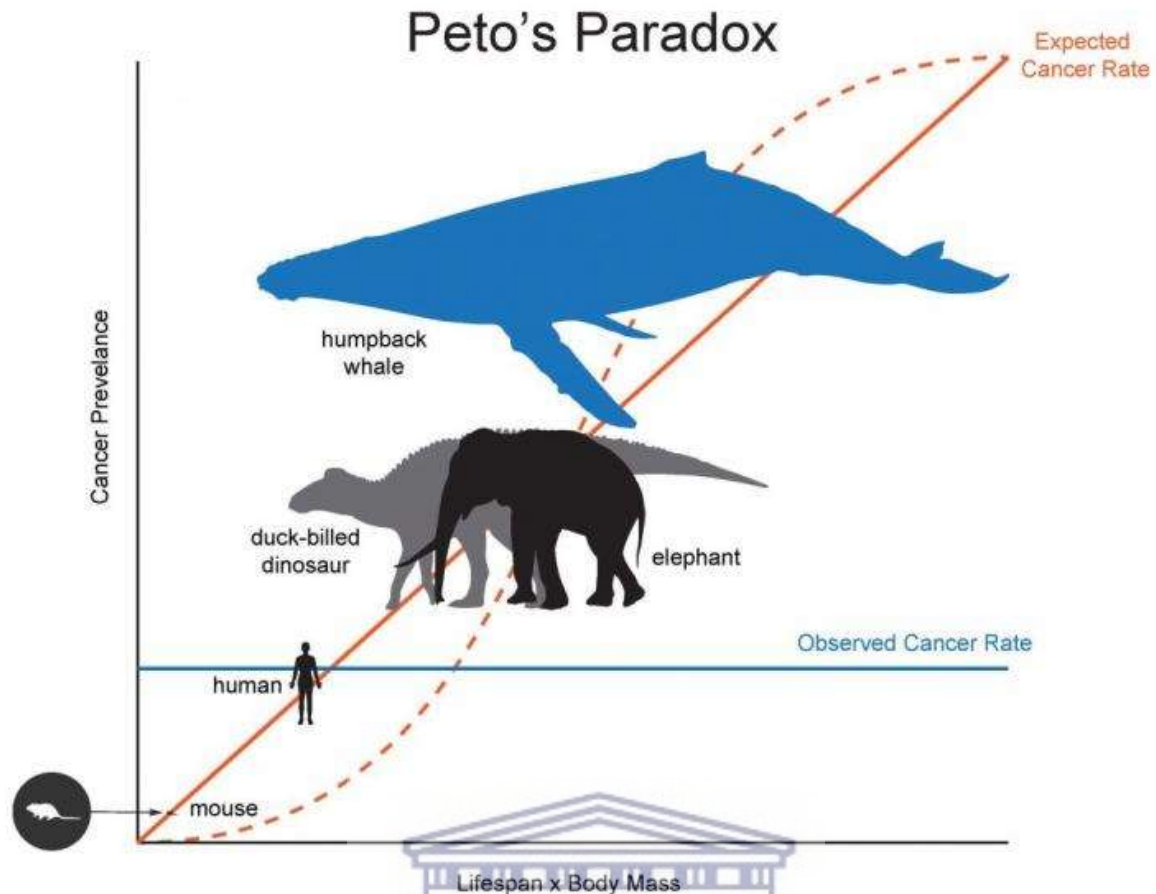


**Figure 5: A schematic presentation of Peto's paradox.** An illustration of Peto's paradox, where the solid red line demonstrates a linear relationship between cancer prevalence and body mass  $\times$  longevity. The dashed red line demonstrates an estimate of cancer prevalence assuming a model describing the probability of an individual developing colorectal cancer after a given number of cell divisions. The solid blue demonstrates the observation that there is no relationship between cancer risk and body mass  $\times$  longevity (Tollis *et al.*, 2019).

A counterargument could be that records on cancer incidence rates in wild and captive mammals might not be well documented for all species. However, the mere existence of large, long-living elephants suggest that they suppress cancer more efficiently than humans, since they would quickly become extinct if cancer incidence would scale with their body size (Abegglen *et al.*, 2015; Caulin & Maley, 2011; Lichtenstein, 2005). Whales (*Cetacea*) would most likely die before they could reproduce and would be extinct since they would have a theoretical 1 000 times greater chance of developing cancer compared to humans (Lichtenstein, 2005). Cancer rates across multicellular animals only vary by approximately 2-fold even though the difference of size among mammals alone can be in the order of a million-fold (Leroi, Koufopanou & Burt, 2003; Siegel *et al.*, 2021).

Within the same species, larger individuals have a greater probability to develop cancer than smaller individuals and the same theory is applicable for age, which is considered to be the most potent carcinogenic risk factor (Vincze *et al.*, 2022). When other risk factors are controlled, cancer risks seems to be associated with body size in humans; for every 10 cm in height there is a 10% increase in cancer occurrence (Green *et al.*, 2011; Nunney, 2018). Furthermore, domesticated dogs are diagnosed with many of the same cancers as humans (Merlo *et al.*, 2008), and osteosarcomas occur 200 times more in larger dogs in comparison to small and medium breeds (Caulin & Maley, 2011). Cancer is also the leading cause of death in dogs for over 10 years with 50% of older dogs developing cancer and approximately 1 in 4 dogs eventually die from cancer (Davis & Ostrander, 2014). In the United States of America only 1.7% of all cancer-related human deaths in both sexes occur before the age of 40 years, and 90% of cancers are diagnosed in those aged >50 years (Laconi, Marongiu & DeGregori, 2020; Siegel *et al.*, 2021).

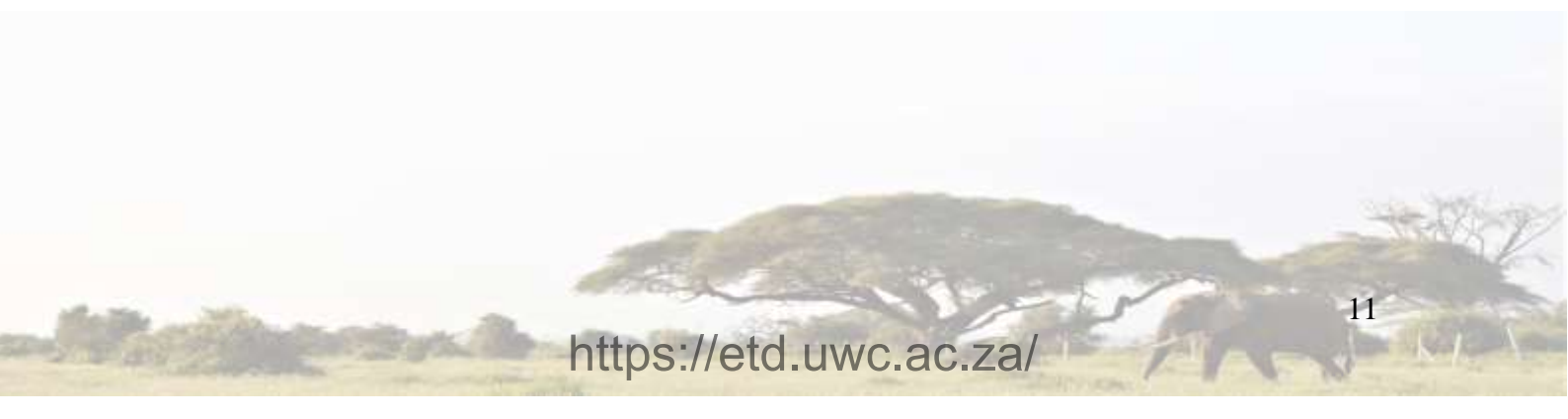
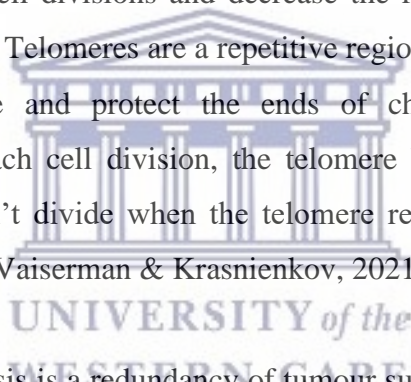
Smaller, long-lived animals such as the grey squirrels (*Sciurus carolinensis*), microbats (*Microchiroptera*), the blind mole rat (*Spalacinae*) and the naked mole rat (*Heterocephalus glaber*) also display cancer suppression (Sulak *et al.*, 2016). These mammals are a typical example of the fact that cancer mortality rates don't always correlate with an increase in longevity (Abegglen *et al.*, 2015). For example, the naked mole rat showed extreme sensitivity to contact inhibition, which likely acts as an anticancer mechanism in this species (Seluanov *et al.*, 2009; Tian *et al.*, 2013). Whereas, the blind mole rat evolved a unique anticancer mechanism mediated by strong induction of the necrotic cell-death response to hyperproliferation and other cell death mechanisms that are also likely prevent cancer (Avivi *et al.*, 2005; Gorbunova *et al.*, 2012). Both these animals adapted cancer suppression

mechanisms in different ways, allowing them to live underground for very long periods (Gorbunova *et al.*, 2012; Tian *et al.*, 2013). Naked mole rats live underground where the environmental conditions are harsh, yet can live for an estimated 30 years, almost 7 times longer than its close cousin house mouse which is particularly susceptible to cancer (Tian *et al.*, 2013). Furthermore, mole arts perform the heavy work of digging their tunnels under highly hypoxic/hypercapnic conditions and unlike most other mammals, these mole rats can achieve high levels of metabolic rate under these extreme conditions while their metabolic rate at low work rates is depressed (Gorbunova *et al.*, 2012; Tian *et al.*, 2013; Widmer *et al.*, 1997). Widmer and team concluded that in their study when investigating the respiratory adaptations in the blind mole rat that the structural adaptations in lung and muscle tissue improve the oxygen diffusion conditions and serve to maintain high metabolic rates in hypoxia but have no consequences for achieving the volume of oxygen the body uses while working ( $\dot{V}O_2$  max) under normoxic conditions (Widmer *et al.*, 1997). Thus, while some of the mechanisms that underlie cancer resistance in small, long-lived mammals have been identified, the mechanisms by which large-bodied animals evolved enhanced cancer resistance are yet to be discovered or need to be confirmed. Globally, over 5 400 different mammalian species exist and this adds to the challenge of solving Peto's paradox (Ferris *et al.*, 2018; Gewin, 2013).

Caulin and Maley formulated several potential hypotheses on how large-bodied, long-lived animals, such as elephants, don't have a higher probability to develop cancer when compared to small-bodied, short-lived animals, such as mice (Caulin and Maley, 2011). The authors proposed some potential tumour suppression mechanisms as follows:

- i. **Metabolism:** A slower metabolism works as a protective mechanism in larger animals with a decreased production of free radicals. With a lower basal metabolic rate (BMR) in larger animals, less endogenous damage is present and this contributes to a decrease in somatic mutation rate (Totter, 1980).
- ii. **Immune system (IS):** Large animals could potentially better suppress cancer due to a better immune surveillance, which provides them the opportunity to attack foreign objects such as neoplastic cells at an early stage (Tollis, Boddy & Maley, 2017). Since tumours are initially immunogenic, larger animals can better detect tumorigenesis compared to mice which show a delayed IS surveillance (Caulin & Maley, 2011).

- iii. Sensitivity to apoptosis: Cells from larger animals could be more sensitive to DNA damage and induce apoptosis more quickly compared to smaller animals. When human and mice cells were irradiated, results showed that mice cells had a higher percentage of cell proliferation despite the DNA damaged inflicted by the radiation compared to human cells, illustrating their reduced apoptosis response compared to humans (Huijbregts *et al.*, 2009).
- iv. Hypersensitive contact inhibition: As mentioned above, the naked mole rat shows hypersensitivity to contact inhibition which may contribute to cancer suppression and longevity (Tian *et al.*, 2013). In culture, naked mole-rat cells stop dividing at much lower cell densities than human and mouse cells due to the early activation of senescence (Seluanov *et al.*, 2009).
- v. Telomeres: Larger animals could potentially have a shorter telomere length that will limit their number of cell divisions and decrease the risk of carcinogenesis (Tollis, Boddy & Maley, 2017). Telomeres are a repetitive region on the DNA sequence at the end of a chromosome and protect the ends of chromosomes from becoming frayed/tangled. With each cell division, the telomere becomes slightly shorter and eventually, the cell can't divide when the telomere reaches its limit and goes into replicative senescence (Vaiserman & Krasnienkov, 2021).
- vi. Lastly, another hypothesis is a redundancy of tumour suppressor genes, which will be discussed in Section 1.2.2 and is the main focus of this research project.



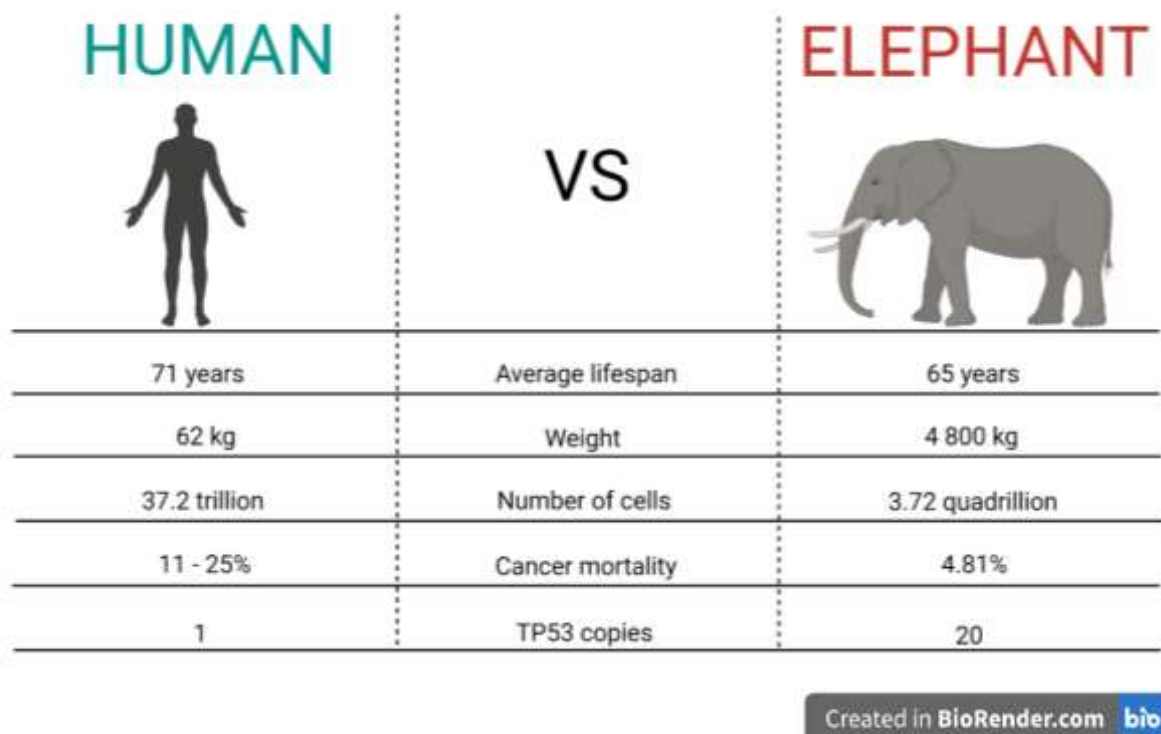
### 1.2.2. Redundancy of tumour suppressor gene in elephants

The first evidence to unravel Peto's paradox in elephants was only discovered in 2015. Necropsy data from the San Diego Zoo was examined for many different mammal species with different weights, from mice to elephants. The study found no relationship between body size and cancer incidence, providing empirical support to Peto's initial observation (Abegglen *et al.*, 2015). In addition, 2 independent research groups discovered that elephants harbour dozens of extra copies of the tumour suppressor gene TP53 (Abegglen *et al.*, 2015; Sulak *et al.*, 2016; Callier, 2019).

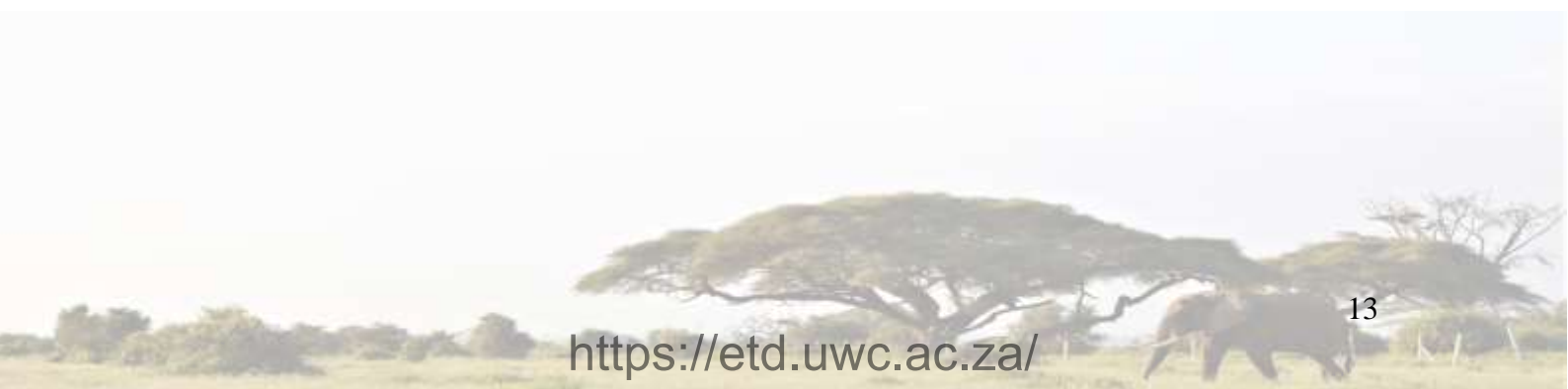
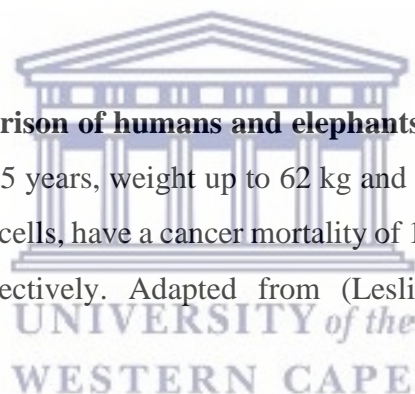
Sulak *et al.* used an evolutionary genomics approach and studied a crucial tumour suppressor gene or anti-cancer gene, called tumour protein 53 (p53). TP53 was studied in animals of various sizes and results revealed that all the animals had at least 1 copy of TP53, while elephants had multiple extra copies of TP53, called retrogenes (RTGs) (Sulak *et al.*, 2016). In particular the African savanna elephant (*Loxodonta africana*), known as the largest living land mammal, has at least 19 TP53 RTGs, which make it the animal with the most copies TP53 RTGs across the animal kingdom (Abegglen *et al.*, 2015; Bartas *et al.*, 2021; Ferris *et al.*, 2018; Sulak *et al.*, 2016).

RTGs, which are sometimes called pseudogenes, are generally regarded as “dead” genes and have limited transcriptional activity (Sulak *et al.*, 2016; Staszak & Makołowska, 2021). In the case of elephants, most of the additional copies of TP53 RTGs do not appear to be directly transcriptionally active and lack true introns. However, the elephant lineage seems to have maintained some functional active TP53 duplicates, but it is unlikely that they transcribe a fully functional p53 protein. However, even though the TP53 RTGs may be largely dysfunctional as transcription factors, they could nevertheless possess other functions. Firstly, to inhibit TP53 signalling in the absence of activating stimuli to prevent over secretion of TP53. Secondly to improve DNA damage sensitivity, by for instance enhancing the effectiveness of the single TP53 gene to detect early cell dysfunction (Haupt & Haupt, 2017). The TP53 RTGs could potentially act as a “pool of protected TP53” which results in a rapid response to DNA damage, but further research is needed to understand the underlying control mechanisms of the TP53 RTG activity (Haupt & Haupt, 2017; Nunney, 2018).

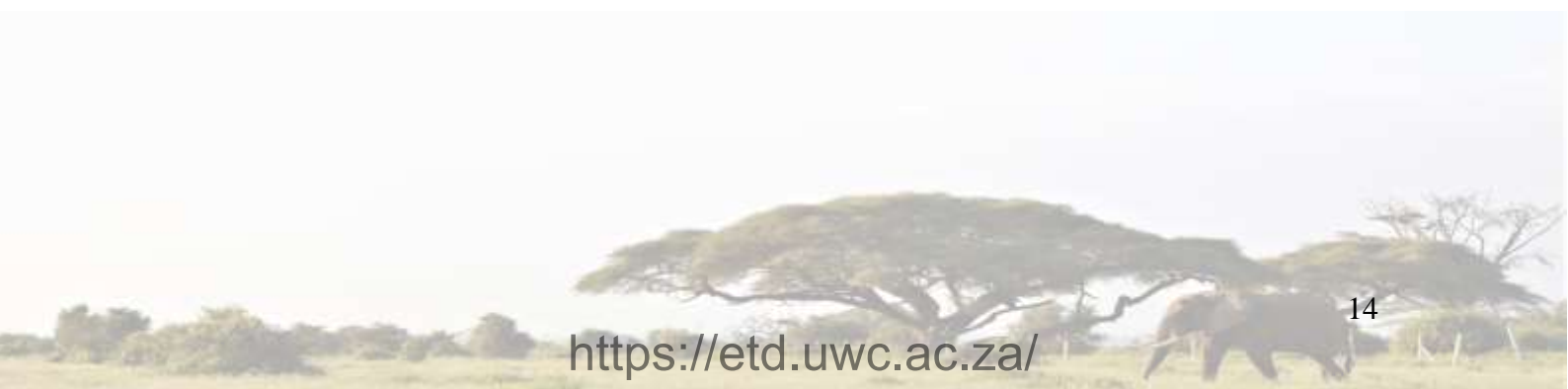
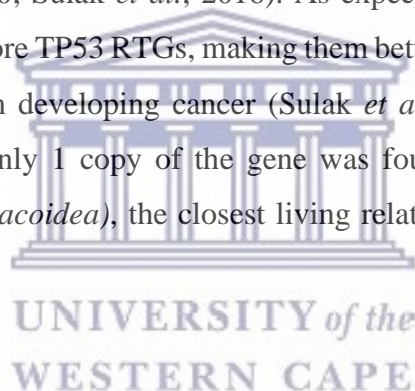


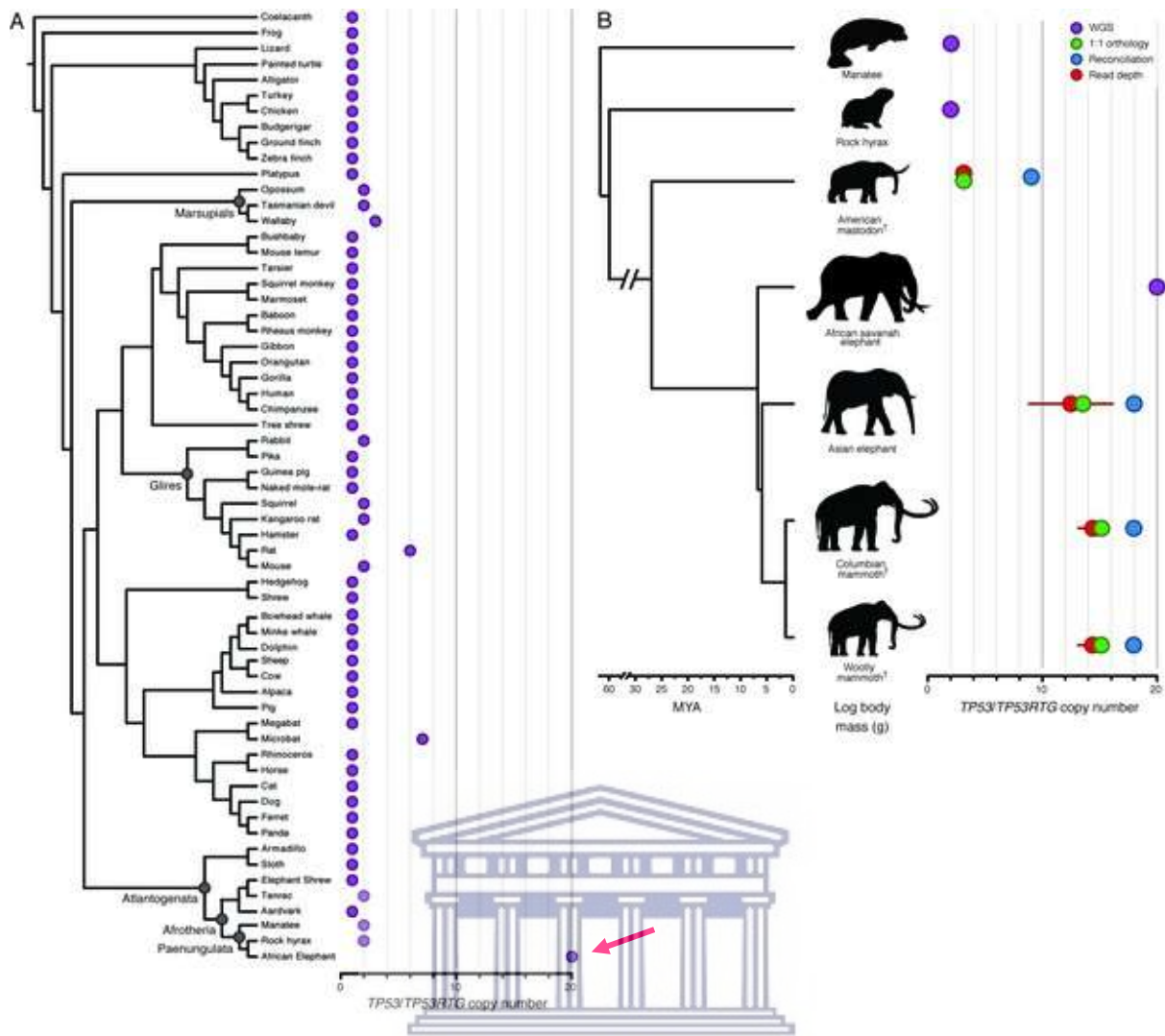


**Figure 6: A schematic comparison of humans and elephants.** Humans and elephants have an average lifespan of 71 and 65 years, weight up to 62 kg and 4 800 kg, contain 37.2 trillion and 3.72 quadrillion number of cells, have a cancer mortality of 11 – 25% and 4.81% and lastly have 1 and 20 copies, respectively. Adapted from (Leslie, 2015). Image created in BioRender.com.



To investigate why African elephants have so many more TP53 RTG copies, Sulak and team analysed the DNA of species related to the African elephant to trace the expansion of TP53 RTGs gene family in the Proboscidean lineage with greater phylogenetic resolution (**Figure 7**) (Sulak *et al.*, 2016). The study used 3 methods to estimate the minimum (1:1 orthology), average (normalized read depth) and maximum (gene tree reconciliation) TP53 RTG copy number in the Asian elephant (*Elephas maximus*), the extinct woolly mammoth (*Mammuthus primigenius*), the Columbian mammoth (*Mammuthus columbi*) and the extinct American mastodon (*Mammut americanum*) using existing whole genome sequences (WGS) data (Enk *et al.*, 2014; Rohland *et al.*, 2010). Sulak *et al.* identified a single canonical TP53 gene in the species mentioned above and estimated 12 – 17, 14 and 3 – 8 TP53 RTGs copies for the Asian elephant, both the Columbian and woolly mammoth and the American mastodon genome, respectively. They found within the Proboscidean lineage, the number of TP53 increased quite rapidly which coincides with the evolution of large-bodied, long-lived animals. There is a relatively low number of the TP53 RTGs in the extinct 50 000 – 130 000-year-old American mastodon (Rohland *et al.*, 2010; Sulak *et al.*, 2016). As expected, as species evolved larger body sizes they also evolved more TP53 RTGs, making them better equipped to deal with DNA damage and protect them from developing cancer (Sulak *et al.*, 2016; Smith *et al.*, 2017a; Callier, 2019). Furthermore, only 1 copy of the gene was found in the DNA of manatees (*Trichechus*) and hyraxes (*Hyracoidea*), the closest living relatives to the elephant (Sulak *et al.*, 2016; Smith *et al.*, 2017a).

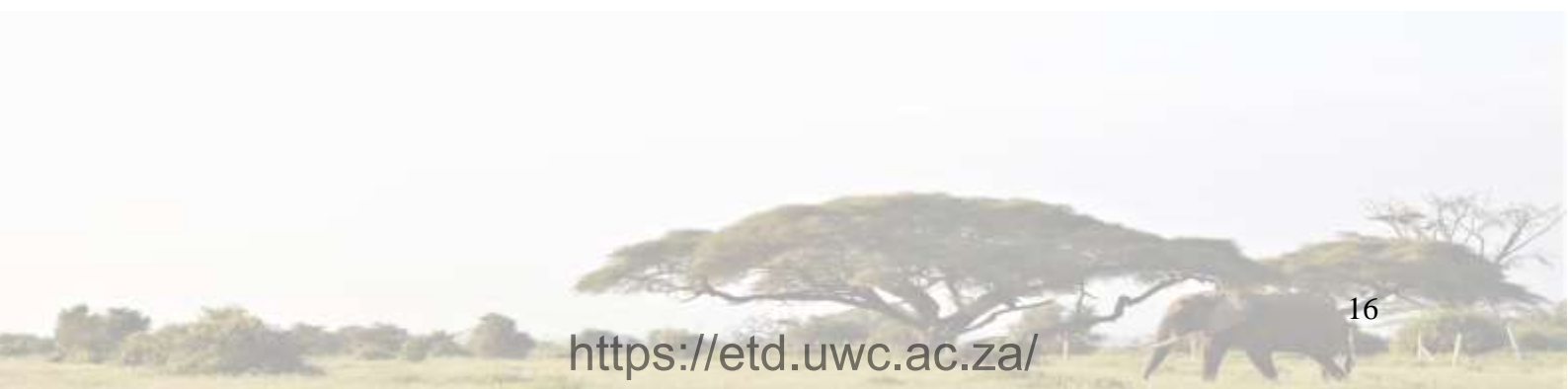
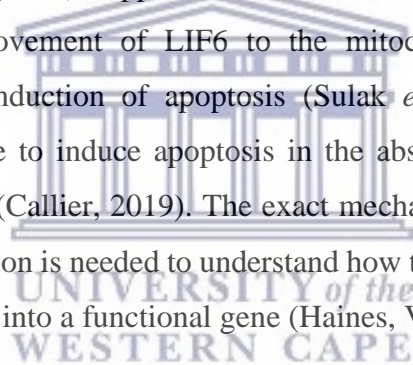




**Figure 7: Schematic representation of TP53 and/or TP53 RTG numbers within different animals. A)** The number of TP53 and/or TP53 RTG in 61 Sarcotrypania (Lobe-finned fishes) with draft or completed genomes, including the African elephant indicated by the pink arrow. Clade names are shown for lineages in which the genome encodes more than 1 TP53 gene or pseudogene. **B)** Comparison of the Proboscidean lineage TP53 and/or TP53 RTG copy numbers inferred from complete genome sequencing data (WGS, purple), 1:1 orthology (green), gene tree reconciliation (blue) and normalised read depth from genome sequencing data (red). Whiskers on normalized read depth copy number estimated show the 95% confidence interval of the estimate (Sulak *et al.*, 2016).

In 2015, peripheral blood lymphocytes from the African and Asian elephant genomes were exposed to ionising radiation (IR) and doxorubicin, both potent inducers of DNA damage. Abegglen *et al.* found that elephant lymphocytes showed a higher rate of TP53-mediated apoptosis compared to human lymphocytes, with no difference in DNA double-strand breaks (DSBs) at different time points post-irradiation (Abegglen *et al.*, 2015). This indicates that the increased apoptosis in elephants cannot be attributed to a higher rate of initial radiation-induced DNA damage. The study confirmed that elephant lymphocyte cells most likely have an increased apoptotic response and gives them the potential to eliminate (pre-) cancerous cells at a very early stage (Abegglen *et al.*, 2015).

Furthermore, Vazquez and team showed that elephants may have developed an additional mechanism to potentially explain Peto's paradox, namely via 11 copies of a leukaemia inhibitory factor (LIF) pseudogene. The LIF pseudogenes appeared transcriptionally inactive, but it seems like LIF6 evolved a new on-switch, and is a valuable working gene with transcriptional activity (Sulak *et al.*, 2016; Vazquez *et al.*, 2018). Most importantly, humans have a single copy of the LIF gene (as opposed to LIF6 in animals) (Ferris *et al.*, 2018). The activation of LIF6 causes movement of LIF6 to the mitochondria and opening of the mitochondrial pore and the induction of apoptosis (Sulak *et al.*, 2016). In addition, an overexpression of LIF6 is able to induce apoptosis in the absence of DNA damage or the activation of TP53 (**Figure 8**) (Callier, 2019). The exact mechanism is still to be determined and therefore further investigation is needed to understand how this former genetic supposedly "junk" DNA molecule evolved into a functional gene (Haines, Voyle & Rathjen, 2000).



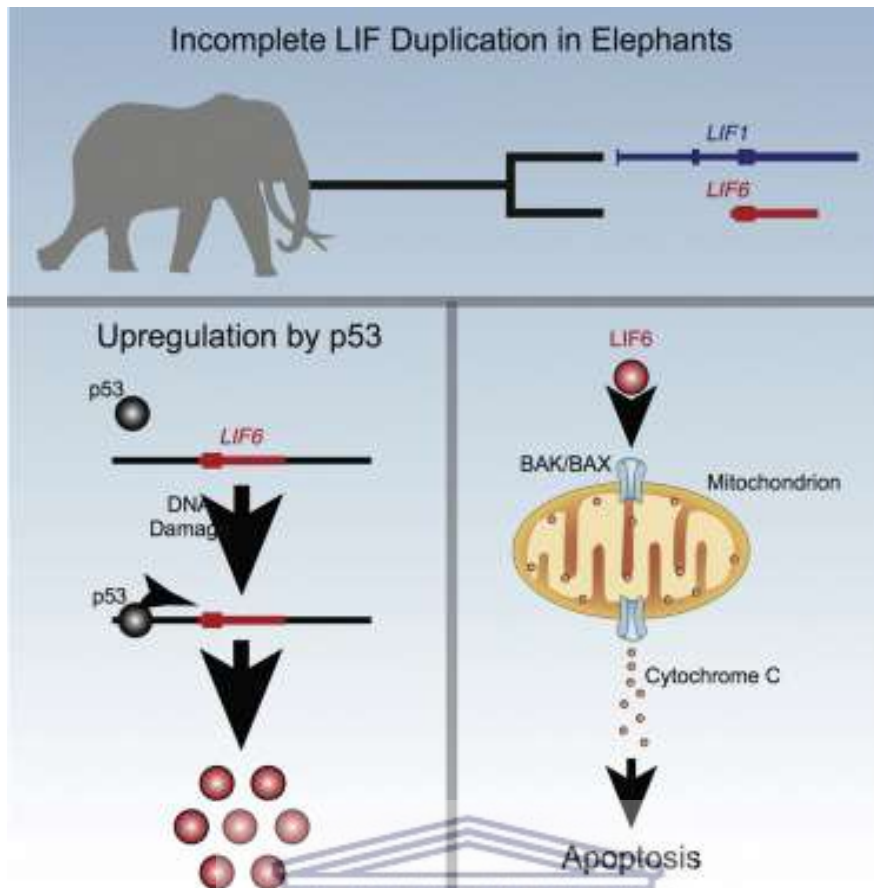
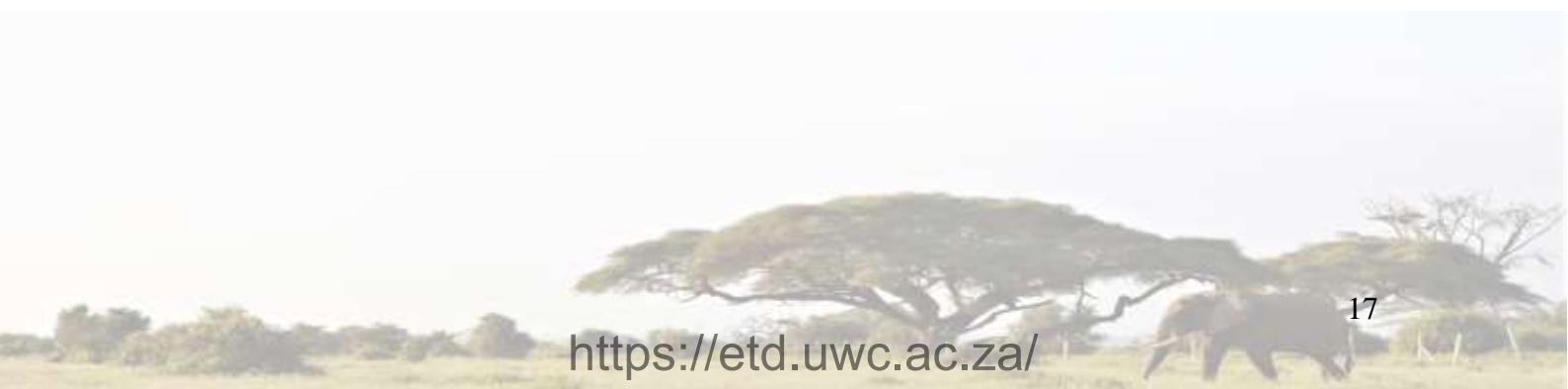


**Figure 8: The LIF6 gene proposed mechanism in elephants.** Schematic presentation of elephant-specific LIF6 duplicate that is upregulated by TP53 (or p53 protein abbreviated in image) in response to DNA damage and movement of LIF6 to the mitochondria resulting in apoptosis (Vazquez *et al.*, 2018).



TP53 is identified as one of the most important tumour suppressor genes and a key component of the cancer protection mechanisms (Hanahan & Weinberg, 2000). However, TP53 can also get damaged and/or mutated resulting in the inactivation and loss of function of TP53. This results in a suppression of apoptosis, increased proliferation and genomic instability (Abegglen *et al.*, 2015; Callier, 2019; Caulin & Maley, 2011; Hanahan and Weinberg, 2000; Seluanov *et al.*, 2009; Sulak *et al.*, 2016; Zhou *et al.*, 2014). The human genome contains only 1 copy of TP53 with 2 functional TP53 alleles, yet to suppress cancer, both alleles are required to function normally to prevent the formation of cancer (Abegglen *et al.*, 2015). An example of overactive TP53 has been proposed as an important pathophysiological factor for bone marrow failure syndromes, including Fanconi anaemia (Li *et al.*, 2018). Mammals could have a greater probability to suppress cancer if they harbour extra copies of TP53 or other genes (e.g., LIF6) that encode tumour suppresser genes, but the mechanisms of how these retrogenes function and alter DNA damage response/tumour suppression pathways remain unknown. See Section 1.3.2 for more information on TP53 mutation.

Interestingly, despite the TP53 RTGs, a 56-year-old nulliparous female Asian elephant (*Elephas maximus*) at the zoological garden of Naples, in Italy, died of cervical cancer (Laricchiuta *et al.*, 2018). In 2021, Landolfi reported a 80% occurrence of neoplasms in a sample size of 80 Asian elephants residing in a managed care facility in the United States from 1988 – 2019 (Landolfi *et al.*, 2021). Benign and malignant neoplasms affecting the uterus have the potential to impact fecundity and thus may represent obstacles to conservation in managed care facilities. Recently Abegglen *et al.* reported that as elephants age, both the Asian and African female elephants exhibit reproductive lesions that can impair conception, implantation, pregnancy or labour. This was more common in the Asian elephant and especially, in older, nulliparous females (Abegglen *et al.*, 2022). The higher prevalence was observed in the Asian elephant when compared to the African elephants could possibly be due to the smaller number of TP53 copies, which have been reported to be 12 – 17 in Asian elephants vs 20 copies of TP53 in African elephants (Sulak *et al.*, 2016). As far as we know, there are currently no studies on the link between the multiple TP53 copies and conception, pregnancy and implantation in elephants. Furthermore, the prevalence of any type of neoplasia is unknown in free-ranging elephants, but the high prevalence in Zoo elephants suggest that these benign or malignant tumours may also develop in free-ranging animals (Landolfi *et al.*, 2021; Parsa, 2012). Environmental factors could play a role since Zoo animals live in an artificial environment and

on average live longer than their wild counterparts. For example, pregnancy and reproduction in Zoo elephants are probably much lower than in wild elephants (Tidière *et al.*, 2016).

### 1.2.3. TP53 and aging effects

As the age of humans increases, the higher the probability of cancer occurrence, but this is not the case for most elephants in their natural habitat. During evolution, mammals developed the DNA damage response, which comprises potent tumour suppressor mechanisms which are crucial to prevent tumorigenesis (Tyner *et al.*, 2002). However, some of these suppressor mechanisms, such as reproductive senescence, are directly linked to aging.

In 2002, Tyner and team studied the biological effect of altered TP53 function by generating mice with a deletion mutation in the first 6 exons of the TP53 gene that express a truncated ribonucleic acid (RNA) capable of encoding a carboxy (C)-terminal TP53 fragment. They found that mice carrying supernumerary copies of TP53 in the form of large genomic transgenes had a resistance to spontaneous tumorigenesis compared to wild type TP53, but unfortunately premature ageing phenotypes, including a 23% reduction in medium lifespan, osteoporosis, generalized organ atrophy and a diminished stress tolerance were observed (Tyner *et al.*, 2002). An excess of TP53 function was potentially caused by a truncated p53 protein in the study of Tyner *et al.*, which could result in a constitutive activation of wild-type TP53

Garcia-Cao *et al.*, generated and characterised mice carrying an increased dosage of TP53. The results demonstrated that the mice carrying supernumerary copies of presumably functional TP53 were protected from cancer. These mice exhibited an enhanced response to DNA damage when compared with normal mice, but no premature aging was observed (García-Cao *et al.*, 2002) confirming that an excess of TP53 function in the study of Tyner *et al.*, potentially caused by a truncated TP53 protein, could result in a constitutive activation of wild type TP53 (Tyner *et al.*, 2002). In elephants, despite harbouring 20 copies of TP53, premature aging is not observed and elephant in the wild have a life expectancy of 60 – 70 years (Tyner *et al.*, 2002; Callier, 2019). It could be that elephants have an enhanced apoptotic response and their TP53 activity is closely controlled and balanced by alternative adaptations to prevent premature stem cell exhaustion (Abegglen *et al.*, 2015; Seluanov *et al.*, 2018). Further adaptations related to stem cells and tissue maintenance could be key in the longevity of elephants (Seluanov *et al.*, 2018).

Bartas *et al.*, 2021, discovered that the TP53 amino acid sequence is phylogenetically related to an organism that show a variation in their lifespan. They showed that lifespan variability correlates with TP53 amino acid variations. Specific substitutions in TP53 amino acid sequences were seen in long-lived animals and these changes enable TP53 to interact with different protein partners to induce gene expression programs that vary in species with a normal lifespan (Bartas *et al.*, 2021). Although augmented activity of TP53 promotes aging and a shortened lifespan, the longevity of elephants proves that there could be an advanced TP53 mechanism that prevents cancer formation without promoting aging (Bartas *et al.*, 2021).

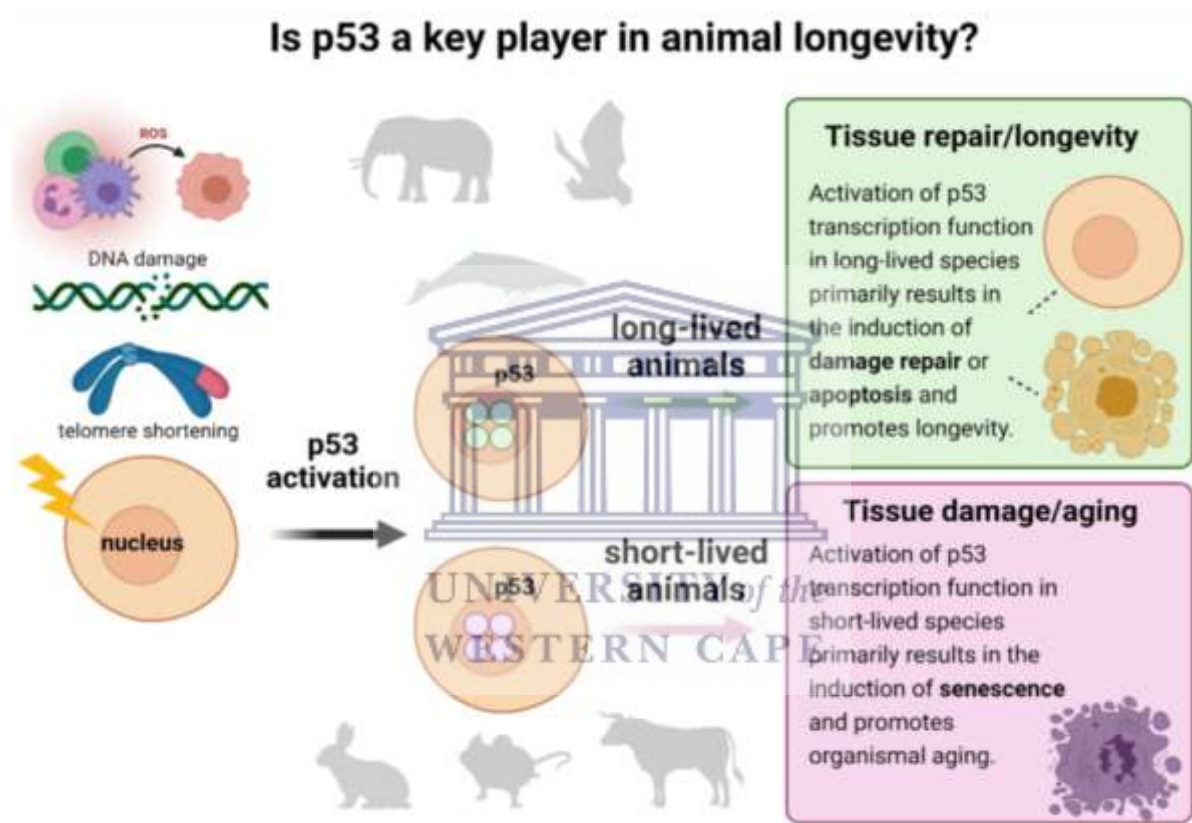


**Figure 9: Schematic presentation of the TP53 theory on lifespan.** Reactive oxygen species (ROS), DNA damage, telomere shortening results in cell damage and TP53 (or p53 protein abbreviated in image) activation which enable DNA repair and/or apoptosis. It is hypothesised that in long-lived animals the “improved” TP53 causes less activation than in their short-lived counterparts but still may sufficiently contribute to DNA damage repair and apoptosis. While in short-lived animals it causes a high activity of TP53 which promotes organismal aging, thus shortening the lifespan (Bartas *et al.*, 2021).



### 1.3. Tumour suppressor gene (TP53)

#### 1.3.1. TP53 history

The tumour suppressor gene was first discovered in oncology research in 1979 (Joerger & Fersht, 2010; Soussi, 2010). Soon after its discovery, the TP53 gene was named “guardian of the genome”, since it suppresses cancer and transcribes protein p53, the most extensively studied protein in cancer research (Haupt *et al.*, 2003). The p53 protein encodes 393 amino acid-long protein which can be found on the short arm of chromosome 17 in humans and the name is derived from the molecular mass of this protein, namely 53 kilodalton (kDa) (Monti *et al.*, 2020; Soussi, 2010). The p53 protein has a modular domain structure with folded central DNA binding- and tetramerization domains, flanked by intrinsically disordered regions at both the amino (N)- and C-termini (Joerger & Fersht, 2010). It is composed of  $\approx 100$  and  $\approx 90$  amino acids at the N- and C-terminal domains, respectively and is highly modified by post-translational modification (**Figure 10**) (Appella & Anderson, 2001). The tetrameric transcription factor can regulate the expression of many target genes in response to cell stress, including cell cycle arrest, cell death, DNA restoration, autophagy and metabolism regulation (Kim *et al.*, 2012; Monti *et al.*, 2020).

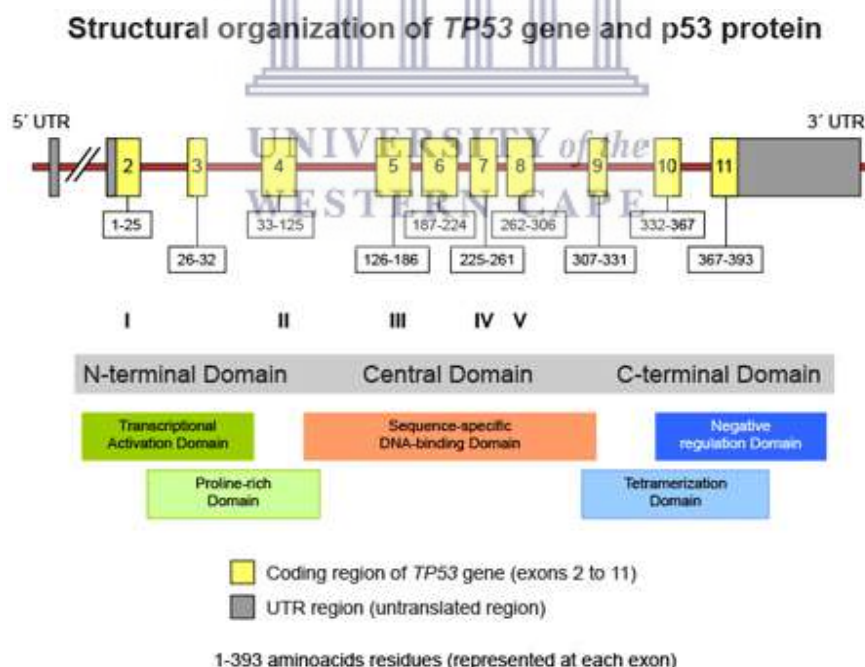


**Figure 10: Structure of TP53.** Schematic presentation of TP53 gene encoding 393 amino acids residues with its N-terminal transcriptional activation domain, central sequence-specific DNA-binding domain and C-terminal negative regulation domains (Mohammed, 2018).

### 1.3.2. TP53 mutation and TP53 in cancer

Mutated TP53 can present missense mutations which are single-based substitutions and loss of alleles, disturbed throughout the coding sequence. Mutations can happen in the central DNA binding domain of the protein and the tetramerisation domain (Monti *et al.*, 2022; Olivier, Hollstein & Hainaut, 2010; Pfister & Prives, 2017). Mutations in TP53 cause single amino acid changes at different positions, making identification patterns in relations with cancer type aetiologically possible (Monti *et al.*, 2020; Olivier, Hollstein & Hainaut, 2010).

More than 50% of human cancers carry a TP53 gene mutation. Sporadic human cancers can harbour somatic mutations in the TP53 gene locus, while germline mutations in TP53 are the underlying cause of Li-Fraumeni Syndrome (LFS) (**Figure 11**) (Meulmeester & Jochemsen, 2008; Monti *et al.*, 2020). Somatic mutations are either spontaneous, due to errors in DNA repair mechanism due to age or direct stress (Miles & Tadi, 2020). Sporadic human cancers usually have a point mutation in 1 allele that permits the expression of mutant p53 protein joined by a removal of the other allele, including neighbouring regions (Aubrey *et al.*, 2018). A germline mutation is a mutation inherited from previous generations and is a predisposition in individuals thereby increasing their susceptibility to develop cancer during their lifetime, even from an early age (Milanese *et al.*, 2019).



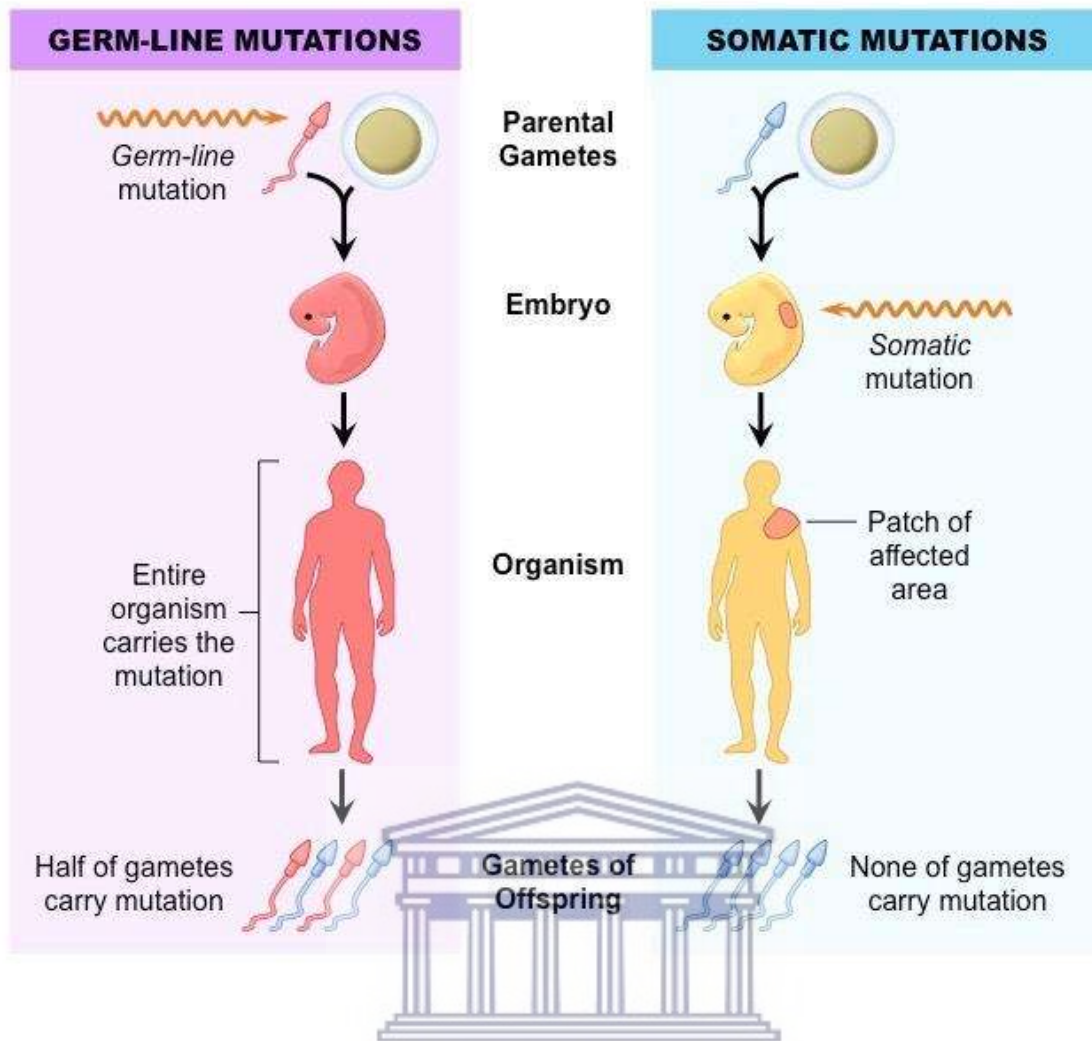


**Figure 11: Germline vs somatic mutations.** Comparison of germline mutations such as LFS which is inherited from previous generations, while a somatic mutation is a point mutation (Positive Bioscience, 2019).

### 1.3.3. TP53 activation

The TP53 gene transcribes a short-lived, multifunctional and highly regulated protein called p53. (Aubrey *et al.*, 2017; Haupt *et al.*, 2003). The TP53 is expressed ubiquitously in all cell types as an inactive, latent, transcription factor that becomes active only when the cells are subjected to a variety of cellular insults (García-Cao *et al.*, 2002). These can include internal and/or external cellular stress signals, DNA damage, expressing oncogenes, hypoxia, starvation, nucleotide depletion and several other genotoxic stressors (Appella & Anderson, 2001; Brooks & Gu, 2010; Giaccia & Kastan, 1998).

It is maintained at low activity levels during homeostasis and its stabilisation and activation is regulated by post-translational modifications (Brooks & Gu, 2010). TP53 is controlled by an autoregulatory negative feedback loop by its natural inhibitor minute 2 homolog (MDM2), through promoting the ubiquitin-proteasome degradation pathway (Bálint, Vousden & KH, 2001; Brooks & Gu, 2010; Haupt *et al.*, 2003). MDM2 binds to TP53 within the N-terminus, creating a direct blockage of TP53 for the transcriptional coactivators and inhibiting the activation of target genes (Bálint, Vousden & KH, 2001; Fang *et al.*, 2000; Momand *et al.*, 1992).

In cell stressed conditions, the initial disruption and stabilisation of TP53 occurs via the targeted disruption of TP53 at the C-terminus, followed by acetylation of protein activators that are required for transcriptional downstream regulatory factors (Brooks & Gu, 2006, 2010). In addition, acetylation of MDM2 happens within the RING (really interesting new gene) domain (Brooks & Gu, 2006). Adenosine diphosphate-ribosylation factor (ARF) inhibit the complete MDM2 and causes its relocation from the nucleoplasm to the nucleolus resulting in the final activation and stabilisation of TP53 (Bálint, Vousden & KH, 2001; Sharpless & DePinho, 2004).

TP53 plays a critical role in the DNA damage response following exposure to IR which causes a stressed state as shown in **Figure 12**. In a stressed state, DNA DSBs are sensed by Ataxia telangiectasia mutated (ATM), while DNA single strand breaks (SSBs) are registered by Ataxia telangiectasia and Rad3-related (ATR). Checkpoint kinase 1 and 2 (CHK1 and CHK2) pathways are then activated and induce either G1/S arrest (senescence or transient), S phase arrest or G2/M arrest (see Section 1.4. for more information) (Appella & Anderson, 2001; Kruse & Gu, 2009).

Activated TP53 induces or inhibits the expression of more than 150 genes resulting in cell cycle arrest for repairing damaged DNA at cell cycle checkpoints or an apoptotic pathway (Appella & Anderson, 2001; Aubrey *et al.*, 2017). This is accomplished by translocation of TP53 to the nucleus where it stimulates cyclin dependent kinases inhibitors (CKI) or activates any proapoptotic proteins for cell cycle arrest or apoptosis, respectively (Zilfou & Lowe, 2009). Wild type TP53 directly activates several genes that function in pathways of DNA repair which include the ribonucleotide reductase gene (Gasco, Shami & Crook, 2002). After the DNA repair, the cell can continue with the cell cycle or if the DNA damage is too severe apoptosis can be induced, TP53 is dephosphorylated and destroyed by the accumulation of MDM2 (Bálint, Vousden & KH, 2001; Massagué, 2004; Aubrey *et al.*, 2017).

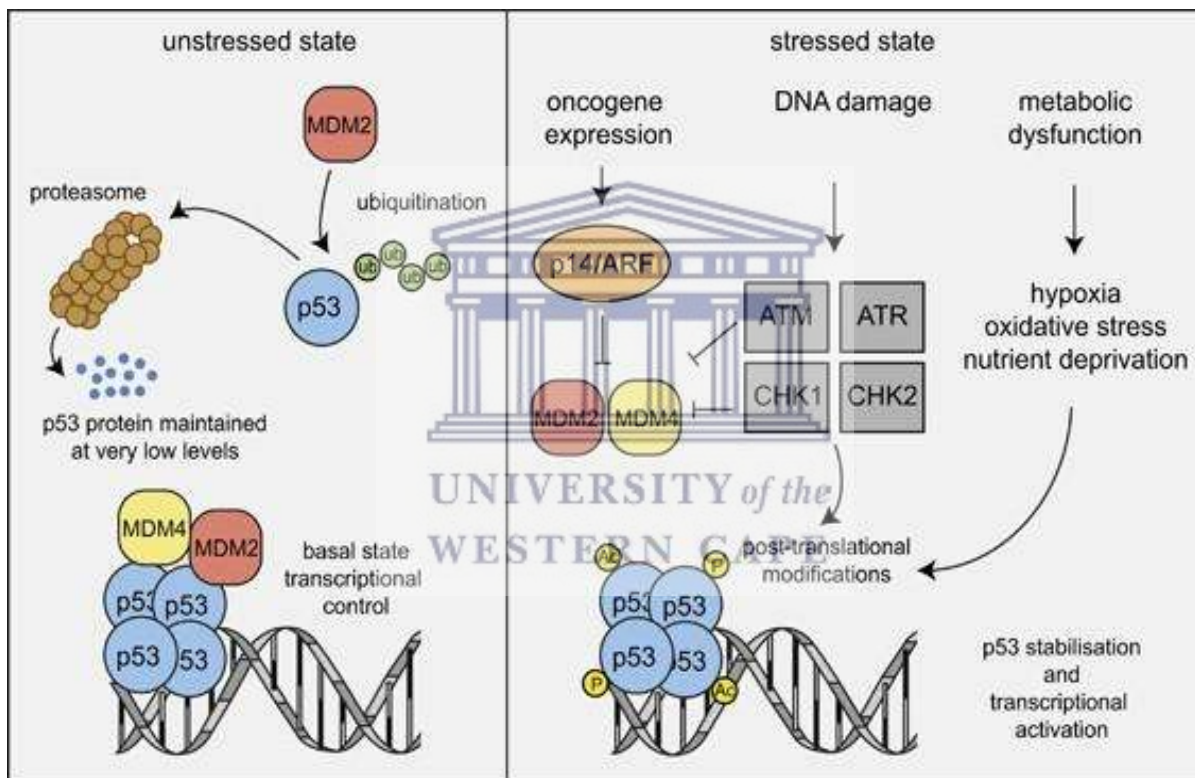


**Figure 12: TP53-mediated tumour suppression.** TP53 (or p53 abbreviated in image) in an unstressed state and is maintained at a very low-level by promoting the ubiquitin-proteasome degradation pathway. TP53 in a stressed state due to DNA lesions or activation of oncogenes causing TP53 post-translational modification resulting in stabilization and transcriptional activity (Ub: ubiquitin; P: phosphorylation; Ac: acetylation) (Aubrey *et al.*, 2018).

#### 1.4. Overview of the cell cycle

The cell cycle is a series of tightly controlled events that take place in a cell in order to allow for growth and division (Lai *et al.*, 2005). The cell cycle in a eukaryotic cell consists of 5 stages: quiescent phase (G<sub>0</sub>), synthesis (S) phase, mitotic (M) phase and 2 growth (G<sub>1</sub> and G<sub>2</sub>) phases (Ding *et al.*, 2020; Imoto *et al.*, 2011). The S phase involves DNA replication, the M phase consist of the segregation of 2 complete sets of chromosomes to 2 resulting daughter cells (Barberis *et al.*, 2007). The G<sub>1</sub> phase separate the M phase and the S phase and the G<sub>2</sub> phase separate the S phase and the M phase (Blow & Tanaka, 2005).

Cell cycle progression is regulated by cyclins and cyclin dependent kinases (CDK) which contains serine/threonine kinases that can phosphorylate multiple substrates (**Figure 13**) (Frouin *et al.*, 2002; Suryadinata, Sadowski & Sarcevic, 2010). There are 11 CDK family members. CDK 1, 2, 3, 4 and 6 play essential roles in the cell cycle and CDK7 activate the CDKs involved in the cell cycle while the rest mediate gene transcription (Ding *et al.*, 2020; Malumbres *et al.*, 2009). Cyclin A is important in the control of cells moving from the S phase to the M phase (Coverley, Laman & Laskey, 2002). Cyclin B is essential in the G<sub>2</sub>/M phase transition and the regulation of cells in the M phase (Lindqvist *et al.*, 2005). Cyclin H plays a role in the CDK activating kinases (CAK) process (Ding *et al.*, 2020). The monomeric, non-phosphorylated CDKs have no detectable kinase activity. Activation requires the association of a positive regulatory cyclin and activating phosphorylation of the kinase on a threonine residue (threonine 161 (Thr<sup>161</sup>) in the human CDK1) (Brown *et al.*, 1999; García-Reyes *et al.*, 2018; Gould *et al.*, 1991). The synthesis of cyclins is mostly controlled at the level of transcription, and they are degraded by ubiquitin-mediated proteolysis (Lim and Kaldis, 2013). Cyclins are recognized by the ubiquitin-protein ligases anaphase-promoting complex/cyclosome (APC/C) or Skp1p-CDC53p/cullin-F-box protein (SCF), polyubiquitinated and destroyed by the 26S proteasome (Ding *et al.*, 2020; Kaldis *et al.*, 2013). Phosphorylation or dephosphorylation of CDK and cyclins also play an important role in the cell cycle since it regulates kinases activity (Ding *et al.*, 2020). Phosphorylation is performed by means of CAK and dephosphorylation is mediated by members of the cell division cycle 25 (CDC25) family of dual specificity protein phosphatases (Shen & Huang, 2012). For example, in p34<sup>CDC25</sup> (CDK1), the phosphorylation of threonine 14 and tyrosine 15 results in inactivation of CDK1-cyclin B complexes for the regulation of cells entering the M phase. When cells are ready for the G<sub>2</sub>/M phase transition, CDC25 removes the phosphatases from the kinase (Ding *et al.*, 2020). CAK is the enzyme responsible for the activation by means of phosphorylation

of CDK1, 2, 4 and 6 and is composed of 3 subunits: CDK7, cyclin H and Menage a trois 1(MAT1) (Ding *et al.*, 2020; Garrett *et al.*, 2001).

Cyclin-CDK complexes are regulated by many CKIs resulting in blocking the complex interaction with its targets (Goel *et al.*, 2018). Based on the CDK structure and role of CKI, it is divided into 2 families: Inhibitors of CDK4 (INK4) and CDK interacting protein/Kinase inhibitory protein (CIP/KIP). The INK4 family includes p15, p16, p18 and p19, which inhibits CDK4 and CDK6 binding and the action of cyclin D, while the CIP/KIP family includes p21, p27 and p57, which are broad-spectrum CDKs inhibitors (Buck, Chiu & Saito, 2009).

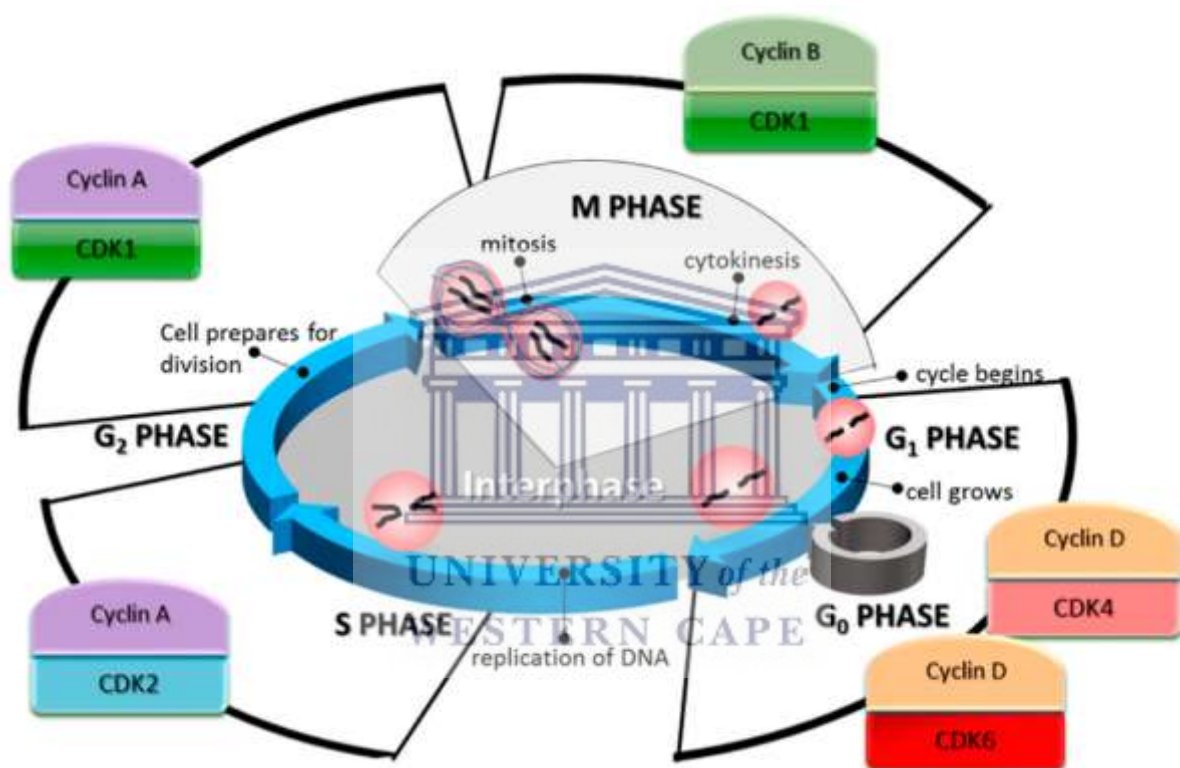
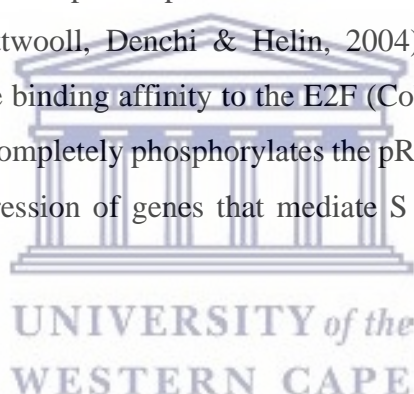


**Figure 13: Schematic representation of the cell cycle with cyclin-CDK complexes.** The cell cycle begins at the G1 phase with an increase in the synthesis in cyclin D and partner with CDK4/6 which promotes cell cycle entry and its progression through G1 phase and G1/S phase transition. During S phase, cyclin A/CDK2 controls the phosphorylation of targets involved in the DNA replication. Cyclin A is highly expressed in the S phase until late G2 phase, where the primary regulator is CDK1. Thereafter, it is replaced with cyclin B/CDK1 to ensure M phase and 2 resulting daughter cells (García-Reyes *et al.*, 2018).

### 1.4.1. The G1 phase

G1 is the first growth phase and assesses if a cell is prepared to enter the S phase based on nutrients and growth factors availability (Massagué, 2004). An increase in production in cyclin D causes an activation of the cyclin D-CDK4 complex which activates the tumour suppressor protein retinoblastoma (pRB)/transcription factor (E2F) pathway (Lim & Kaldis, 2013). The pRB is the product of retinoblastoma tumour suppressor gene. Cyclins of the D class (D1, D2 and D3) and their partners CDK4/CDK6 are involved in the initial pRB phosphorylation. pRB phosphorylation in the entry and exit of the S phase is mediated by cyclin E-CDK2. The E2F family regulates cell cycle components, apoptosis, differentiation, DNA damage repair, metabolism and angiogenesis (Berridge, 2014; Xie *et al.*, 2021).

The E2F family consist of 8 genes and E2F 1 – 3 preferentially bind to pRB (Attwooll, Denchi & Helin, 2004). Once E2Fs are bound to pocket proteins, their transactivating activity is inhibited and the overexpression of any of the pocket proteins leads to G1 arrest (Trimarchi and Lees, 2002). Phosphorylation of pocket proteins releases the E2Fs, which are then able to activate their target genes (Attwooll, Denchi & Helin, 2004). Therefore pRB is partially phosphorylated and reduces the binding affinity to the E2F (Cobrinik, 2005). Near the end of the G1 phase, cyclin E-CDK2 completely phosphorylates the pRB, leading to the release of the E2F and allowing for the expression of genes that mediate S phase entry (Cobrinik, 2005; Harbour & Dean, 2000).





### 1.4.2. The S phase

As the cell moves from G1 to S phase, cyclin E and is replaced with cyclin A in order for replication to occur where each identical copy segregates into duplicate daughter cells (Coverley, Laman & Laskey, 2002). Cyclin A-CDK2 has dual functions; (A) to ensure that the G1 ends before the DNA synthesis begins and (B) to ensure that DNA replication occur only once per cell cycle (Coverley, Laman & Laskey, 2002; Yam, Fung & Poon, 2002). The mini-chromosome maintenance subunits 2 – 7 (MCM 2 – 7) hexamer structure function as a replicative helicase and ensure that the replication only occur once-per-cell-cycle (Prasanth *et al.*, 2003).

The DNA replication is dependent on essential molecules and the origin recognition complex (ORC) marks the position of replication origins in the genome and serves as the landing pad for the assembly of a multiprotein, pre-replicative complex (pre-RC) at the origins, consisting of ORC, CDC6 and MCM 2 – 7 proteins (Prasanth *et al.*, 2003). ORC contains 6 subunits with ORC1 being the largest subunit (120 kDa) and ORC6 the smallest (50 kDa). Furthermore, the ORC promotes the initiation of DNA replication, by binding to CDC6 to form a complex which aids the replication factor for the loading of the MCM 2 – 7 DNA helicase onto the replication origins (Duncker, Chesnokov and McConkey, 2009). CDC6 expression is mainly controlled by the pRB/E2F factors that regulate S-phase promoting genes and plays a key role in the establishment and maintenance of the pre-RCs (Borlado & Méndez, 2008; Cocker *et al.*, 1996). The pre-RC formation is necessary during this phase to assemble the helicase machinery in order for the 2 DNA strands to separate (Labib, Tercero and Diffley, 2000). When the CDK activity ceases, an inhibition is placed on the pre-RC formation (Prasanth *et al.*, 2003). The ORC promotes the MCM 2 – 7 protein complexes for the initiation and elongation of DNA replication and the completion of the this phase (Labib, Tercero & Diffley, 2000).

### 1.4.3. The G2- and M phases

The S/G2 phase is driven by the activation of cyclin A-CDK1 and cyclin B-CDK1 and when several positive feedback loops can amplify cyclin B-CDK1 activation to ensure complete commitment to a mitotic state, the initiation of mitosis is reached (Lindqvist, Rodríguez-Bravo & Medema, 2009). CDC25 has 3 isoforms (A, B and C). It plays an important role in chromatin condensation, whereas isoform B specifically activates cyclin B-CDK1 at the centrosomes and the isoforms are specifically needed to activate the entry into mitosis (Lindqvist *et al.*, 2005).

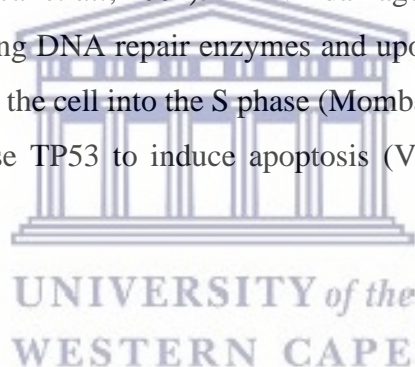
The M phase is the nuclear division of the cell cycle which contains 4 phases: prophase, metaphase, anaphase and telophase (Vermeulen, Van Bockstaele & Berneman, 2003). Cyclin B activity continues till late mitosis and is degraded in anaphase. The mitotic metaphase to anaphase is controlled by the spindle assembly checkpoints (SAC) and the anaphase is dependent on the decreased activity of CDK1 via the degradation of cyclin B by APC/C (Ding *et al.*, 2020). Therefore, anaphase initiation is caused by the APC/C ubiquitination and its activator CDC20 (APC/C<sup>CDC20</sup>). The loss of CDK1 activity activates the mitotic exit and the completion of the cell cycle (Parry and O'Farrell, 2001). Mitotic exits comprise of an organization series of events leading to the segregation of sister chromatids to completion of mitosis by means of cytokinesis (Mcintosh, 2016).

### 1.4.4. Cell cycle checkpoints

Cell cycle checkpoints are a type of surveillance mechanism that monitor the order, integrity and fidelity of the major events of the cell cycle (Barnum & O'Connell, 2014). The cells implement this safeguard mechanisms to correctly complete cell cycle phases, repair damage, commit suicide in case damage is too severe or enter a temporary/permanent quiescence state (Visconti, Della Monica & Grieco, 2016). The 3 main cell cycle checkpoints are: G1/S, G2/M and mitotic checkpoint (Kousholt, Menzel & Sørensen, 2012; Visconti, Della Monica & Grieco, 2016).

#### 1.4.4.1. G1/S checkpoint

G1/S checkpoint screens for damaged DNA in the form of DSBs and/or SSBs before and after DNA replication (Medema & MacŮrek, 2012). DSBs activate ATM and phosphorylate CHK2. CHK2 phosphorylates CDC25 isoform A, leading to its degradation. SSBs/DSBs activate ATR and phosphorylate CHK1 resulting in the degradation of CDC25A in response to ultraviolet (UV) radiation. CDC25 phosphatase degradation prevents dephosphorylation and activation of cyclin E-CDK2 that results in inhibition of the origin of fire (Mombach, Bugs & Chaouiya, 2014; Sancar *et al.*, 2004). The inhibition of CDK2 activity in the S phase blocks loading of CDC45 onto chromatin, a step that is that required for the recruitment of DNA polymerase  $\alpha$ , into assembled pre-RCs (Kastan & Bartek, 2004). (Bartek & Lukas, 2003). Release of TP53 from MDM2 results in stabilisation and activation of the p53 protein (Kastan & Bartek, 2004) mediating the maintenance of the G1/S arrest though the transcription and activation of p21. The p21 protein inhibits cyclin E-CDK2 and causes a G1 arrest (Haupt *et al.*, 2003; Kastan & Bartek, 2004) by preventing the phosphorylation of RB/E2F and thus the transcription of genes required for S phase entry (Sancar *et al.*, 2004). If DNA damage is repairable, TP53 promotes the expression of genes encoding DNA repair enzymes and upon DNA repair, a cyclin-CDK complex is activated and drives the cell into the S phase (Mombach, Bugs & Chaouiya, 2014). Major DNA damage will cause TP53 to induce apoptosis (Vermeulen, Van Bockstaele & Berneman, 2003).



#### 1.4.4.2. G2/M checkpoint

Inducing G2/M arrest have been suggested in 2 pathways. The first pathway involves the phosphorylation and activation of TP53 as described in Section 1.3.3. TP53 play a role in the regulation of the G2/M checkpoint by upregulation of cell cycle inhibitors such as p21, DNA-damage inducible 45 (GADD45) and 14-3-3 sigma ( $\sigma$ ) proteins (**Figure 14**) (Taylor & Stark, 2001; Kastan & Bartek, 2004). The activation of TP53 induces genes for the restoration or apoptosis (Taylor & Stark, 2001). A second pathway of G2/M arrest occurs due to the inhibition of CDC25B by the ATM/ATR and CHK1/CHK2 pathways (Baus Charrier-Savournin *et al.*, 2004). Activation of either of these pathways induce the G2/M checkpoint by phosphorylation and inhibition of CDC25B. CDC25B dephosphorylates CDK1, activating cyclin B-CDK1 that is responsible for mitosis entry (Lindqvist, Rodríguez-Bravo & Medema, 2009). Inappropriate cyclin B-CDK1 complex activation results in cell cycle progression, bypassing the G2/M checkpoint resulting in improper mitosis entry and formation of tetraploidy cells with damaged DNA.



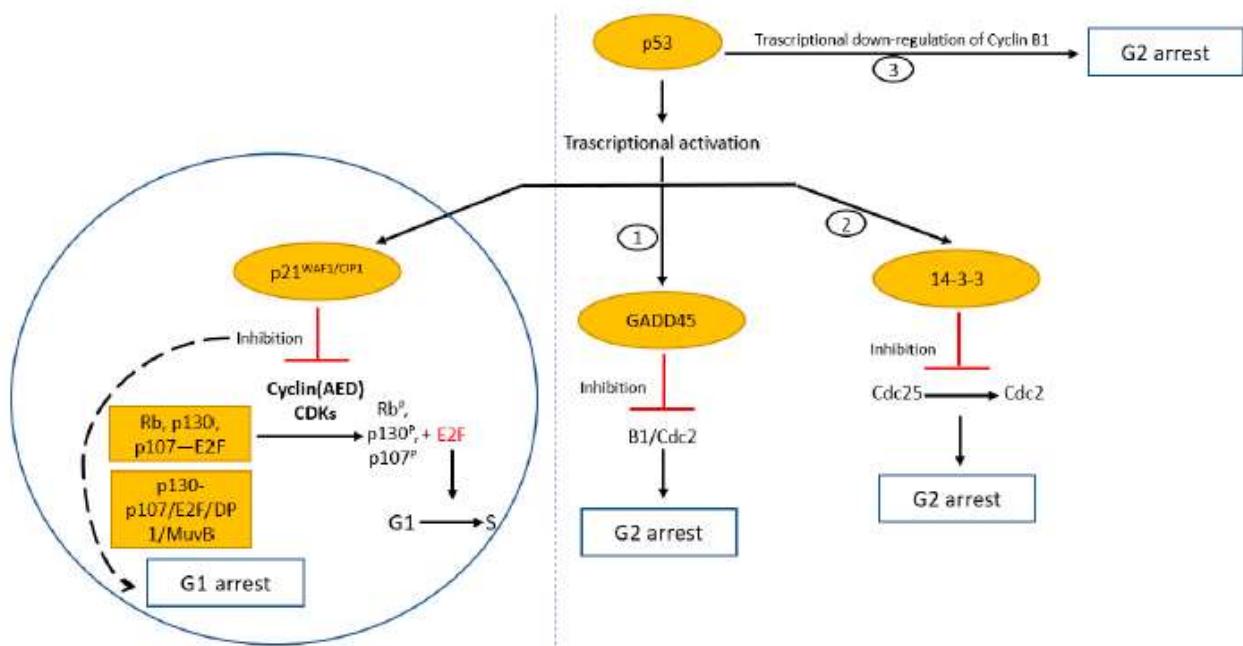
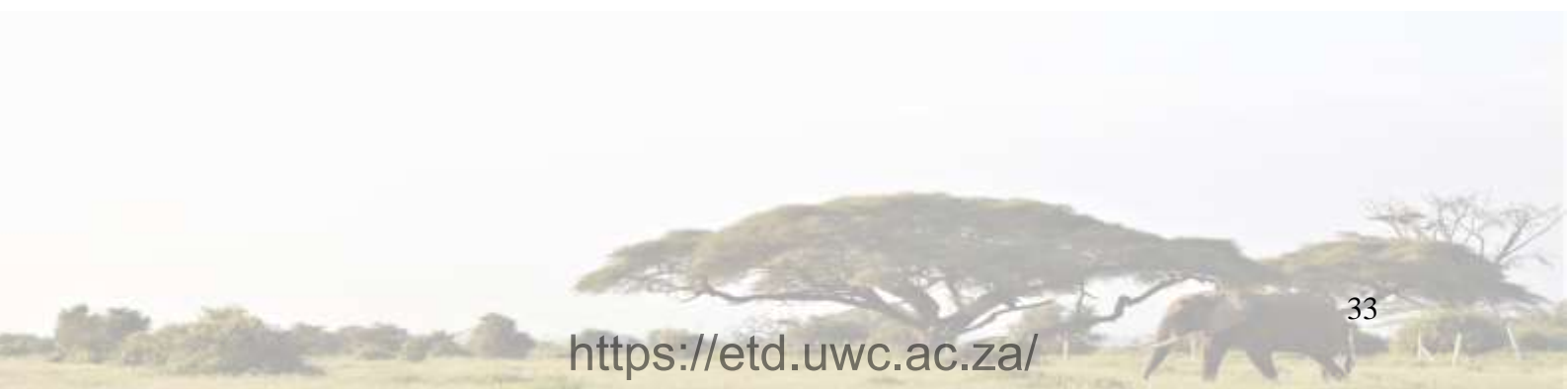
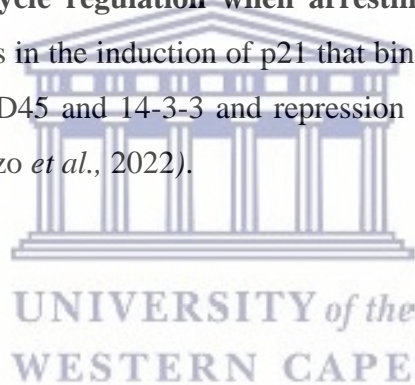
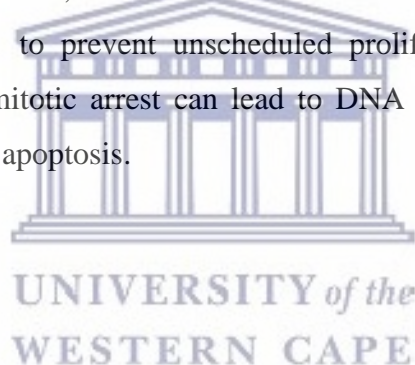


**Figure 14: Control of cell cycle regulation when arresting G2 phase.** Transcriptional activation of p53 protein results in the induction of p21 that binds to and inhibits cyclin-CDK complexes. Induction of GADD45 and 14-3-3 and repression of cyclin B1 cause cell cycle arrest in the G2 phase (Capuozzo *et al.*, 2022).



#### 1.4.4.3. Mitotic checkpoint

The checkpoint ensures for error free chromosome segregation and is dependent on a stable connection between spindle microtubules and kinetochores (Vermeulen, Van Bockstaele and Berneman, 2003). The kinetochores are attached and aligned at the equator plate thereby anaphase can proceed activating the E3 ubiquitin ligase activation system, also called the APC/C. If the alignment is incorrect, the SAC, will prevent the activation of APC/C polyubiquitin system and inhibit anaphase (McLean *et al.*, 2011; Sacristan & Kops, 2015). Once aligned, the metaphase to anaphase transition is caused by the APC/C ubiquitination and its activator CDC20 (APC/C<sup>CDC20</sup>) or CDH1 (APC/C<sup>CDH1</sup>) (Kernan, Bonacci & Emanuele, 2018). The attached sister kinetochores will result in a poleward force to opposite poles at metaphase and are counterbalanced by the sister chromatid cohesion forces which allows for chromosomes to stably align at the equator and move separately forming identical daughter cells with the aid of CDC20 (LeMaire-Adkins, Radke & Hunt, 1997). Furthermore, APC/C<sup>CDC20</sup> targets mitotic cyclins for degradation and CDK downregulation to promote mitotic progression. Later in mitosis, the CDH1 binds to APC/C and forms APC/C<sup>CDH1</sup> which remains active throughout G1 to prevent unscheduled proliferation (Kernan, Bonacci & Emanuele, 2018). Prolonged mitotic arrest can lead to DNA damage and TP53 induction, followed by cell cycle arrest or apoptosis.



### 1.5. Mechanisms of cell death

Various modes of cell death such as apoptosis, oncosis, autophagy, mitotic catastrophe, pyroptosis, ferroptosis, metabolic catastrophe and necrosis are currently recognised (Galluzzi *et al.*, 2018). Cell death can be classified according to its morphological appearance which may be apoptotic, necrotic, autophagic and/or enzymological criteria (the possible involvement of nucleases or proteases). Classification can also be based on functional aspects (programmed or accidental) or characteristics (immunogenic or non-immunogenic) (Melino, 2001). Programmed cell death (PCD) is crucial for the development, regulation and maintenance of multicellular organisms (Kroemer *et al.*, 2009).

Apoptosis, also known as PCD, is a mechanism of controlled cell deletion mediated by caspases and is a key component of several processes such as cell turnover, proper development, functioning of the immune system, hormone-dependent atrophy, embryonic development and chemical-induced cell death (Elmore, 2007; Monti *et al.*, 2020). Characteristics of apoptosis is cell shrinkage, chromatin condensation, nuclear compaction, DNA fragmentation, cytoplasmic condensation, reduction in cellular volume (pyknosis), mitochondrial permeabilisation, plasma membrane blebbing and the formation of apoptotic bodies/vesicles (Gerschenson & Rotello, 1992; Reed, 2000; Ziegler & Groscurth, 2004). Apoptosis is defined as an energy dependent irreversible systemic elimination of unnecessary or abnormal cells by a series of controlled molecular steps mediated by an intracellular program. (Elmore, 2007). The uniqueness of apoptosis is that the plasma membrane remains intact throughout the process without inciting an inflammatory response (Wong, 2011).

Apoptosis can be induced by various stimuli, including the binding of ligands to cell surface receptors of the tumour necrosis factor (TNF) family, damage to the DNA integrity caused by various stress factors or radiation and/or any major change in the cell homeostasis (Ziegler & Groscurth, 2004). Apoptosis in mammalian cells comprises 3 different classes, namely: intrinsic, extrinsic and the less familiar pathway, the intrinsic endoplasmic reticulum (ER) pathway (Wong, 2011). The ER pathway is caspase 12 dependent and mitochondria independent. Cellular stress for example hypoxia, free radical or starvation causes the ER to be injured resulting in the unfolding of proteins and reduction in protein synthesis and the initiation of PCD (Szegezdi, Fitzgerald & Samali, 2003).

### 1.5.1. Extrinsic apoptotic pathway

The extrinsic apoptotic pathway (**Figure 15**) involves a transmembrane receptor-mediated interaction which occurs via death receptors that form part of the tumour necrosis factor receptor (TNF-R) gene superfamily (Elmore, 2007; Haupt *et al.*, 2003). The TNF-R family have the similar cysteine-rich extracellular domains as well as a cytoplasmic domain called the death domain (DD) (Locksley, Killeen & Lenardo, 2001). Other death receptors include TNF-death receptor type 1 TNF (TNF-TNFR1), fatty acid synthetase ligand-fatty acid synthetase (FasL-Fas) and TNF-related apoptosis-inducing ligand death receptors 4 or 5 (Trail-DR4 or DR5) (Wong, 2011). The pathway is mediated by a lethal ligand which binds to a death receptor. Once bounded, a protein interaction exposes the DD (Holler *et al.*, 2003; Wong, 2011). For example, the lethal ligand TNF alpha (TNF $\alpha$ ) and FasL bind to the TNFR1 and Fas receptor (FasR), respectively (Reed, 2000; Wong, 2011). The DD transmits the death signal from the cell membrane to the intracellular signalling pathway (Elmore, 2007; Yanumula and Cusick, 2020). Clusters of the DD recruit adaptor proteins such as TNF receptor-associated death domain (TRADD) and Fas-associated death domain (FADD), respectively (Holler *et al.*, 2003; Wong, 2011). The binding of the death ligand to the death receptors in the formation of a binding site for an adaptor protein and the whole ligand-receptor-adaptor protein complex is known as the death-inducing signalling complex (DISC) (Holler *et al.*, 2003; Wong, 2011; Yanumula and Cusick, 2020). This subsequently forms a second protein interaction with the death effector domain (DED) and associates with the auto-catalytic activation of pro-caspase 8 (Holler *et al.*, 2003; Lindqvist *et al.*, 2005; Yanumula and Cusick, 2020).

Once caspase 8 is activated, it leads to the activation of effector caspases 3 and 7 which are responsible for degradation of more than 280 cellular protein identified so far (Elmore, 2007). These proteins are involved in scaffolding of the cytoplasm and nucleus, signalling transduction, regulation of cell cycles progression and DNA replication and repair (Haupt *et al.*, 2003; Holler *et al.*, 2003; Wong, 2011).



### 1.5.2. Intrinsic apoptotic pathway

The intrinsic pathway (**Figure 15**) refers to the mitochondrial mediated apoptotic pathway and is activated by intra-cellular stresses such as DNA damage, oxidative stress, irradiation and treatment with cytotoxic drugs (Jan & Chaudhry, 2019). Regardless of the internal stimulation, there will be an increase in mitochondrial permeability and a secretion of pro-apoptotic molecules which induce cytochrome c release into the cytoplasm (Danial & Korsmeyer, 2004; Wong, 2011). The pathway is regulated by the B-cell lymphoma 2 (Bcl-2) family and the 2 main protein groups are the pro-apoptotic and anti-apoptotic proteins which can promote or block cytochrome c release from the mitochondria, respectively (Reed, 2000; Wong, 2011).

Bcl-2-like protein 4 (Bax), is induced by TP53 and undergoes a conformational change in the cytoplasm and translocate to the outer membrane of the mitochondria in response to an apoptotic stimulus (Haupt *et al.*, 2003). Subsequently, Bax causes a disruption of the mitochondrial membrane barrier by the formation of ion-permeable pores and causes a release of cytochrome c (Nouraini *et al.*, 2000). On the other hand, Bcl-2 and other anti-apoptotic protein members act primarily against the function of Bax and prevent cytochrome c release (Jan & Chaudhry, 2019). However, the overexpression of Bax can overcome the inhibition (Nouraini *et al.*, 2000; Wong, 2011).

The overexpression of Bax and the formation of mitochondrial outer membrane permeabilization (MOMP) are caused by several factors namely: p53 upregulated modulator of apoptosis (PUMA) (Brooks & Gu, 2010), cathepsin in the lysosomal department (Jung *et al.*, 2015) and ER stress (Rao *et al.*, 2001). Other apoptotic factors are released from the mitochondria intermembrane space which include apoptosis inducing factor (AIF), second mitochondrial activator of caspases (Smac), direct inhibitor of apoptosis (IAP) binding protein with low pI (DIABLO) and Omi/high temperature requirement protein A (HtrA2) (Kroemer, Galluzzi & Brenner, 2007; Wong, 2011).

The release of cytochrome c in the cytoplasm allows for the binding to the apoptotic activating factor 1 (Apaf-1) and forms an apoptosome resulting in the counteraction of Smac/DIABLO and Omi/HtrA2 by inhibiting the IAP (Danial and Korsmeyer, 2004; Fan *et al.*, 2005). The Apoptosome complex cleaves and activates caspase 9 (Loreto *et al.*, 2014). Activated caspase 9 cleaves executioner caspases to induce apoptosis mainly through the activation of caspase 3 (Ghobrial, Witzig & Adjei, 2005).

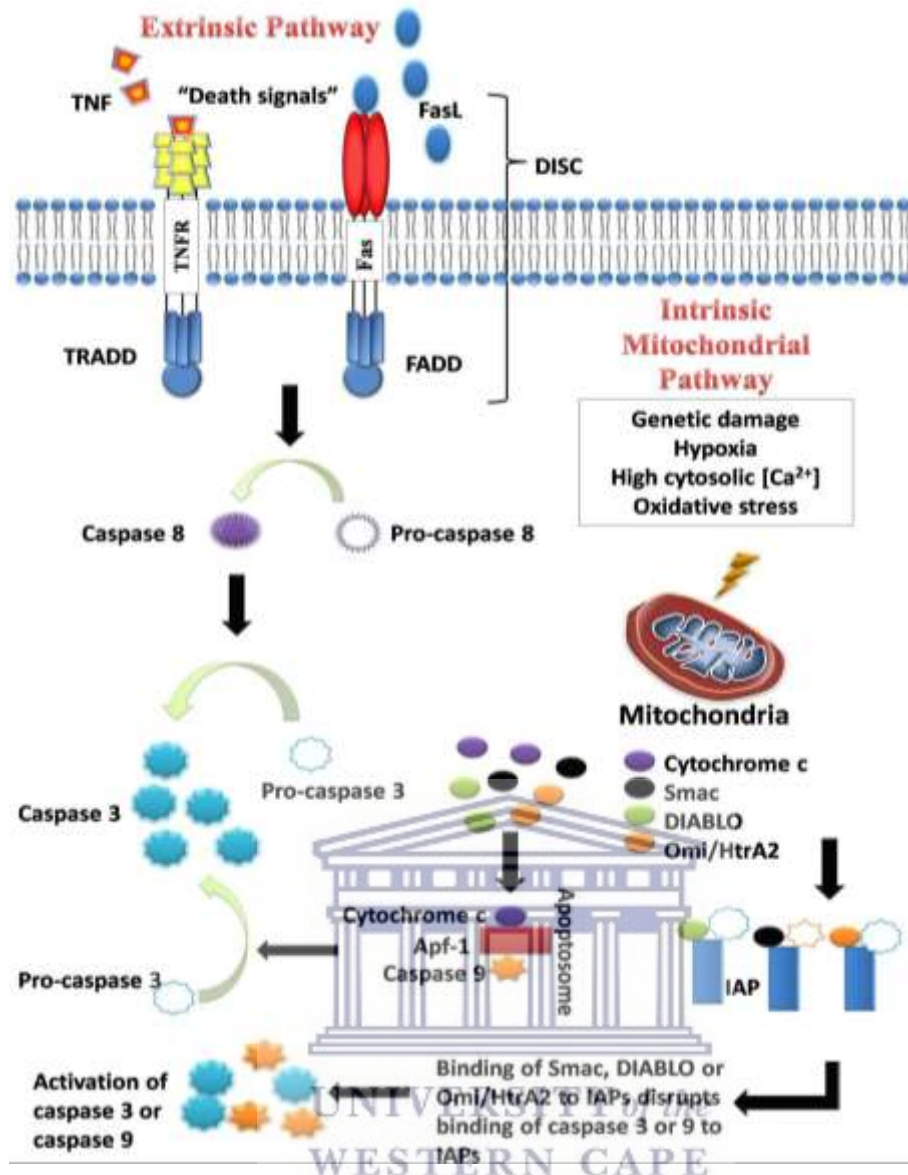


**Figure 15: Schematic diagram of apoptosis induction via the extrinsic or intrinsic apoptotic pathway.** Apoptosis induction can be executed through the extrinsic apoptotic pathway by signalling through death signals (TNF and FasL). The DD transmits the death signal from the cell membrane to the intracellular signalling pathway, whereby clusters of the DD recruit adaptors (TRADD and FADD) forming a complex namely DISC. Thereafter procaspase 9 is cleaved to its active form of caspase 9 followed by caspase 3 and the induction of apoptosis. Intracellular stress such as genetic damage, hypoxia and more causes an intrinsic apoptotic pathway. Pro-apoptotic molecules such as cytochrome c, Smac, DIABLO and Omi/HtrA2 are released from the mitochondria. Cytochrome c binds to Apaf-1 and forms an apoptosome, while Smac, DIABLO and Omi/HtrA2 inhibits the IAP family and aids in the process of caspase of cascades (Wong, 2011).

### 1.5.3. Caspase dependent apoptosis

As previously mentioned, caspases are a family of cysteinyl aspartate proteinases (cysteine proteases that cleave their substrates at specific aspartyl residues) and are instrumental to the exclusion of apoptosis (Seaman *et al.*, 2016). Apoptosis caspases belong to 1 of 2 categories: initiator (upstream) caspases or effector/executioner (downstream) caspases. Initiator caspases that trigger apoptosome include caspase 2, 4, 8, 9 and 10. Executioner caspases include 3, 6 and 7 (**Figure 16**) (Loreto *et al.*, 2014; Seaman *et al.*, 2016; Wong, 2011).

These initiators of caspases tend to have long N-terminal regions (pro-domains) with motifs, caspase recruitment domains (CARDs) and DEDs which promote their aggregation (Slee, Adrain & Martin, 2001). There are 3 caspase-dependent cell death pathways including the mitochondrial pathway (intrinsic), death receptor pathway (extrinsic) and the endoplasmic specific pathway. Although the extrinsic and intrinsic death pathways act independently to intrinsic cell death, in most tumourigenic cells there is cross talk between these 2 pathways which results in the activation of executioner caspases (Haupt *et al.*, 2003).

Caspases 3, 6 and 7 coordinate the execution phase of apoptosis by cleaving multiple structural and repair proteins; these caspases tend to have short or absent pro-domains (Slee, Adrain & Martin, 2001). Both caspase 9 and 8 converge to caspase 3, where caspase 3 then cleaves the inhibitor of the caspase-activated deoxyribonuclease, which is responsible for nuclear apoptosis (Ghobrial, Witzig & Adjei, 2005). In addition, caspase 6 and 7 cleave various substrates including cytokeratin, poly-ADP ribose polymerase (PARP), the plasma membrane cytoskeletal protein  $\alpha$  fodrin, the nuclear mitotic apparatus protein (NuMA) causing the morphological and biochemical changes seen in apoptotic cells (Elmore, 2007; Slee, Adrain & Martin, 2001). The effect on the cytoskeleton, cell cycle and signalling pathways are a hallmark for apoptosis induction and execution (Wong, 2011).

#### 1.5.4. Caspase independent apoptosis

During apoptosis, cytochrome c is released from the intermembrane space because of a significant increase in MOMP. Other apoptogenic signalling molecules, such as AIF, endonuclease G (ENDOG) and Omi/HtrA2 are also released (**Figure 16**) (Candé *et al.*, 2002; G. Liu *et al.*, 2016) and can trigger a caspase independent apoptosis pathway (Kögel & Prehn, 2013). Both AIF and ENDOG function independently of caspases by relocating to the nucleus and mediating a large-scale DNA fragmentation (Galluzzi *et al.*, 2011). HtrA2 are activated in both caspase dependent and independent pathway, however its role is dependent on its enzymatic activity (Kögel & Prehn, 2013). The extramitochondrial targeted overexpression of HtrA2 induces apoptosis independently of caspases via a serine protease-dependent manner (Suzuki *et al.*, 2001) where HtrA2 contributes by cleaving a wide array of cellular substrates including cytoskeletal proteins (Galluzzi *et al.*, 2011).

In addition to caspases, other proteases such as serine proteases, cathepsins, calpains and granzymes are also involved in PCD (Beresford *et al.*, 2001; Borner & Monney, 1999; Suzuki *et al.*, 2001; Wang *et al.*, 2001). Granzymes consist of 2 isoforms. Granzyme A triggers caspase-independent cell death by activating the endonuclease granzyme A-activated deoxyribonuclease (GAAD), leading to single-strand DNA nicking including membrane perturbation, chromatin condensation and loss of mitochondrial inner membrane potential (Beresford *et al.*, 2001). While granzyme B triggers the intrinsic cell death pathway via truncation of Bid in a caspase-independent cleavage event upstream of the mitochondria (Wang *et al.*, 2001). Similar to granzyme B, cathepsins have been implicated in cleavage and activation of Bid (Stoka *et al.*, 2001; Kögel & Prehn., 2018). The overexpression of cathepsin D by ectopic expression induces cell death in the absence of any external stimulus and makes it a positive mediators of apoptosis (Stoka *et al.*, 2001). Furthermore, another strong candidate for fragmentation in caspase independent apoptosis, are the calpains (Kögel & Prehn., 2018). These proteases participate in apoptosis in response to an increased cytoplasmic calcium level, for example due to mitochondrial damages. Calpains cleave the cytoskeletal protein fodrin upstream of caspases, which disrupts the cytoskeletal network and allows the persistent membrane blebbing seen in caspase independent apoptosis (Borner & Monney, 1999).

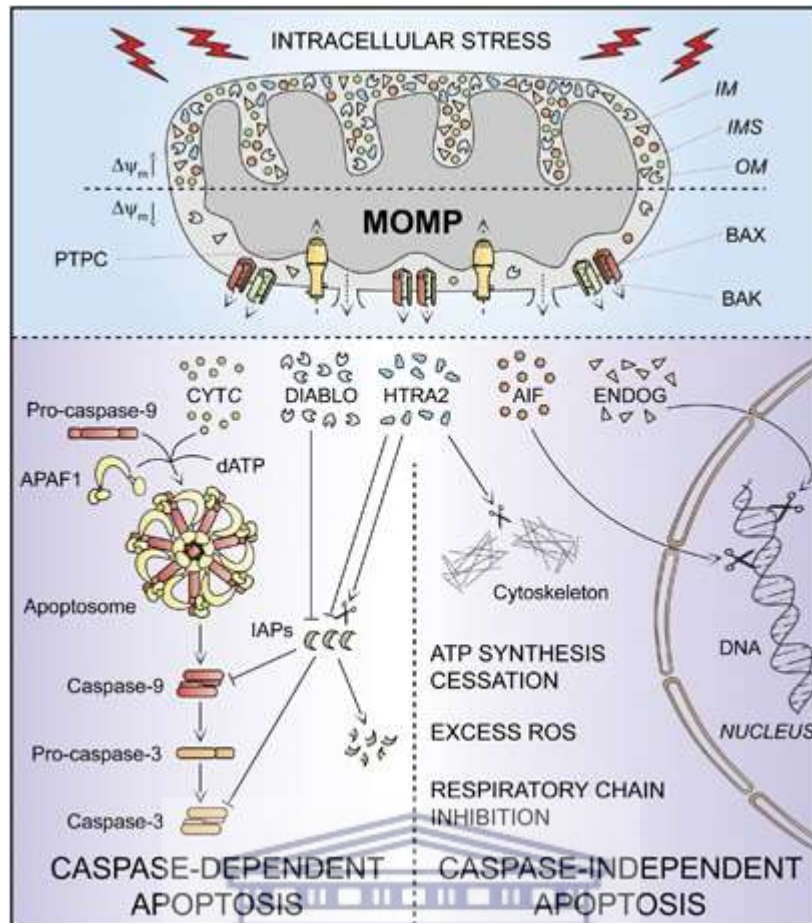


**Figure 16: Induction of intracellular stress causing a caspase dependent and independent apoptosis pathway.** Caspase dependent apoptosis causes the release of cytochrome c from the mitochondria which binds to Apaf-1 forming an apoptosome. DIABLO and Omi/HtrA2 facilitate caspase activation by inhibiting several members of the inhibitor of apoptosis protein inhibits IAPs. On the contrary, AIF, ENDOG function in a caspase independent manner by which DNA fragmentation occur. In addition, HtrA2 can also cleave the cytoskeleton independently of caspases (Galluzzi *et al.*, 2011).

## 1.6. Radiation

Radiation is the transmission of energy and is transmitted through space/matter in the form of particles or waves. IR is defined as radiation with sufficient energy to remove an electron from an atom or molecule, inducing a process which is called an ionisation (Babaei and Ganjalikhani, 2014). Radiation can be classified into 2 categories, namely: IR and non-ionising radiation (NIR) (Gerschenson & Rotello, 1992; Kottou, 2014; Tuieng *et al.*, 2021).

NIR is radiation with insufficient energy levels to cause ionisations, for example UV, visible light, infrared radiation, microwaves and radio waves (Gherardini *et al.*, 2014; Kottou, 2014; Sowa *et al.*, 2012). IR, on the contrary, consists of a stream of high energy particles or waves, which ionise molecules and atoms which may result in bond rearrangement and bond breakage of chemical bonds of the biological molecules and have the potential to destroy cells and genetic material (Sowa *et al.*, 2012; Tuieng *et al.*, 2021). IR is further categorised into 2 major categories namely: electromagnetic radiation such as photons (X- and  $\gamma$ -rays) and particle radiation such as electrons, protons, neutrons and  $\alpha$ -particles, to name a few (Cutler & Polycove, 2009; McColl *et al.*, 2015).

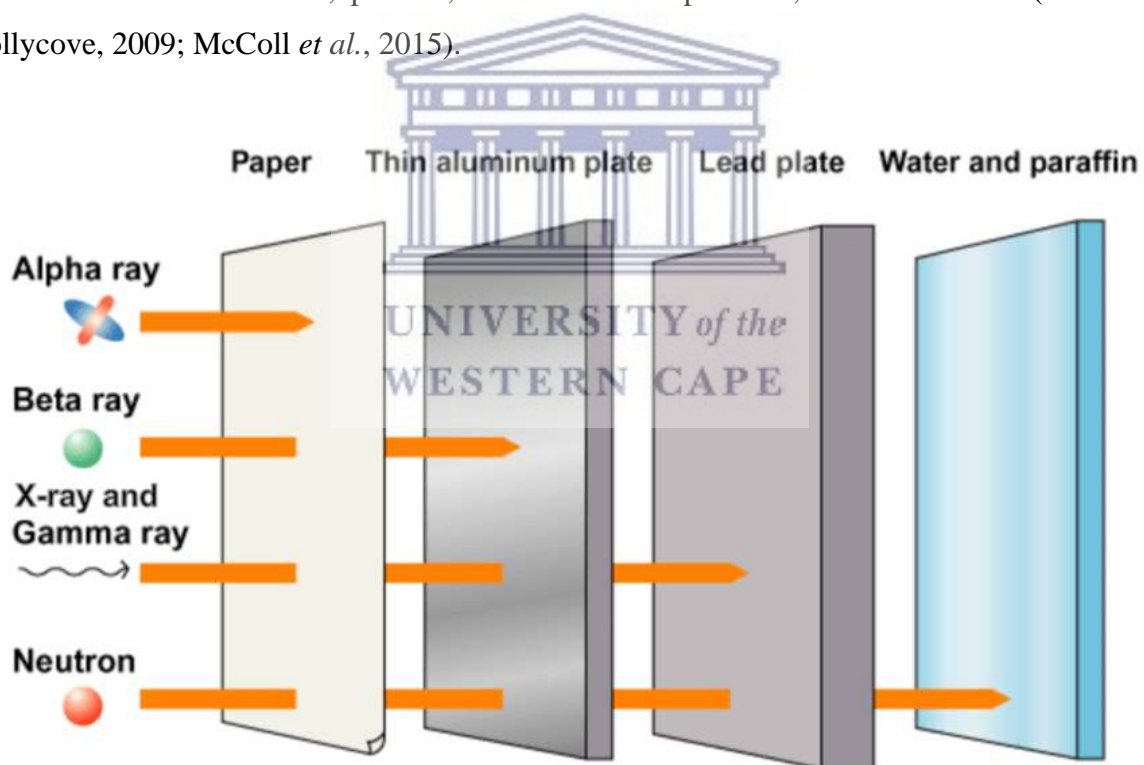


**Figure 17: Types of IR.** Different types of IR have different penetrating powers through different material.  $\alpha$ - and  $\beta$ - rays are stopped with paper and a thin aluminium plate, respectively, while X- and  $\gamma$ -rays are stopped by a lead plate. Water and paraffin stops neutrons from penetrating (Chen, 2015).

Electromagnetic radiation (X- and  $\gamma$ -rays) contains neither mass nor charge, however, travels through space at the speed of light in a packet of radiant energy called photons, whereas particle radiation has a mass component, a charge and travels slower than the speed of light (Percuoco, 2013; Roobol *et al.*, 2020). Furthermore, IR may be divided into directly and indirectly IR for the understanding of biological effects (Baskar, *et al.*, 2012b; Nikitaki *et al.*, 2016).

Most of the electromagnetic radiation (photons) are indirectly IR because they induce their damage through secondary electrons that are produced through the energy absorption of the material. The process of removing an electron from atoms by the occurrence of radiation leaves electrically charged particles behind, which may later produce significant biological effects in the irradiated material (International Atomic Energy Agency, 2010). For example, the secondary electron may either cause direct DNA damage or indirect damage through the radiation-associated formation of free radicals or return to the parent state (Smith *et al.*, 2017b). If the energy transferred by IR to the atom is insufficient to eject orbital electrons, the electrons may be raised from lower to higher orbitals (Tuieng *et al.*, 2021). This process is called excitation (Tuieng *et al.*, 2021).

In contrast to electromagnetic radiation, particle radiation subsisting of electron or particle beams, such as protons, carbon ions,  $\alpha$ - and  $\beta$ - particles, are mainly directly ionising because they directly disrupt the atomic structure and therefore the atoms of the target itself may be ionised, thus initiating the chain of events that leads to a biologic change (Hall & Giaccia, 2012). However, the main exception is neutron radiation, which is a form of particle radiation, but indirectly ionising (Hall & Giaccia, 2012). Proton beams consist of positively and charged particles, which cause less damage but are more effective at killing cells at the end of their path (Ishikawa *et al.*, 2019). Proton beams pass directly through cells and affect each cell as it passes and exits (Scalliet & Gueulette, 2017). An advantage of proton beam is to deliver radiation more conform to cancer tissue whilst causing fewer side effects to normal tissues based on the depth-dose distribution necessary to cover the target volume with the flat region along the Bragg Peak known as the spread-out Bragg Peak (SOBP) (Cunningham *et al.*, 2021; Durante & Loeffler, 2010). Radiation such as  $\alpha$ - particles,  $\beta$ -particles or electrons, protons or neutrons are also used in specific cases to target cancer tissue (Baskar, *et al.*, 2012a). The foremost common form of radiation used for cancer treatment during RT utilising photons (X- and  $\gamma$ -rays), which are derived from radioactive sources such as cobalt, caesium or a linear accelerator (LINAC) (Ravichandran, 2009).

Radiation damage to cells can be caused by the direct or indirect action on the DNA molecules (**Figure 18**) (Desouky, Ding & Zhou, 2015). In the case of direct action, IR causes structural changes to the DNA by hitting the DNA molecule directly, which disrupts the molecular structure and can eventually lead to DNA breaks or even cell death. The indirect action is based on the production of radicals, such as hydroxyl hydroxide and superoxide anion, caused by the interaction of IR with water molecules that surround cellular bio-macromolecules (Zhou *et al.*, 2014). These radicals have an unpaired electron in their structure, which makes them highly reactive and provides the ability to interact with the DNA and cause molecular structural damage. The number of free radicals that are produced will increase linearly with the radiation dose. In case of photon irradiation, which is the radiation quality used in this project, the majority of the radiation-induced DNA damage is caused by this indirect mode of action.

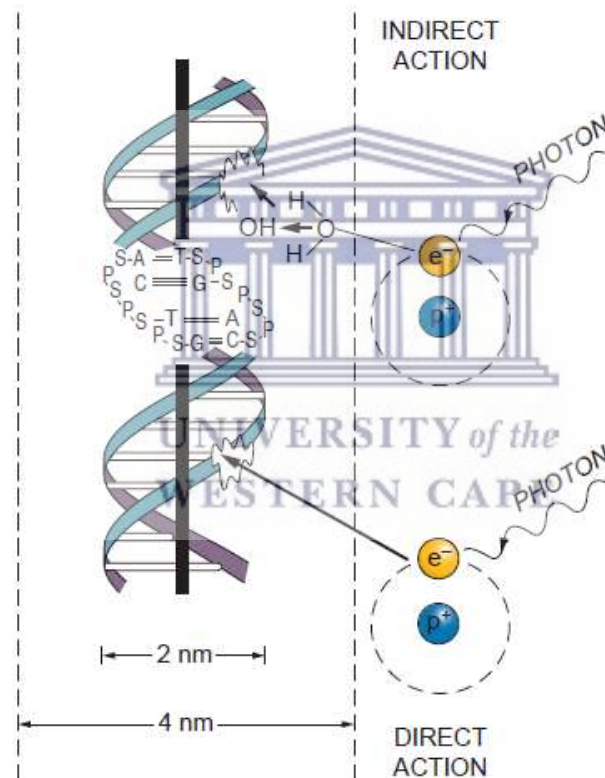


**Figure 18: Direct and indirect actions of IR.** Direct action of IR is a secondary electron resulting from absorption of an X-ray photon interacts with the DNA to produce a damaging effect, while indirect action is for example a water molecule to produce a hydroxyl radical ( $\text{OH}^\cdot$ ) which results in DNA damage (S: sugar; P: phosphorus; A: adenine; T: thymine; G: guanine; C: cytosine) (Hall & Giaccia, 2012).



### 1.6.1. DNA damage caused by ionising radiation (IR)

Radiation induces a large number of DNA lesions and the majority are able to undergo a successful repair process within the cell, while others result in cellular death, genetic mutations and potentially carcinogenesis (Smith *et al.*, 2017b). IR induces a plethora of DNA damage types and the identity of specific lesions responsible for the biological effects of radiation remains uncertain (Sutherland *et al.*, 2000). IR exposure to a cell can cause a wide range of lesions to the DNA, including SSBs, DSBs, base damage, cross-links and the destruction of sugars. While the number of lesions generated by IR is large, the percentage of lesions that causes cell death or mutations is relatively small, due to the existence of the DNA damage response mechanisms in mammalian cells (Hall & Giaccia, 2012).

SSBs cause little biological consequences based on cell killing since the opposite strand of the DNA helix is used as a template (Hossain, Lin & Yan, 2018). Repairing SSBs include the detection of SSBs, DNA end processing, DNA gap filling and DNA ligation (Caldecott, 2008). Furthermore, DSBs results in the cleavage of chromatin into 2 pieces and translocations, leading to severe genome instability which are considered the most cytotoxic, with lesions often irreparable (Atanassova and Grainge, 2008). IR inducing DBSs are approximately 0.04 times that of SSBs, and DBSs are induced linearly with dose, indicating that they are formed by single tracks of IR (Hall & Giaccia, 2012). Lastly, clustered DNA damages results in 2 or more closely spaced damages on opposing strands of the DNA helix and are critical lesions producing lethal and mutagenic effects of IR (Sutherland *et al.*, 2000). Clustered DNA damage is categorised as bi-stranded or tandem when the lesions are on opposing DNA strands, or when the lesions are on the same DNA strand, respectively (Eccles, O'Neill & Lomax, 2011). Mammalian cells have developed specialised pathways to sense, respond to and repair the DNA damage and include at least 5 major DNA damage repair pathways: base excision repair (BER), nucleotide excision repair (NER), mismatch repair (MMR), homologous recombination (HR) and non-homologous end joining (NHEJ) (Chatterjee & Walker, 2017; Hall & Giaccia, 2012; Martín-López & Fishel, 2013; Simonelli *et al.*, 2005). These pathways are active throughout the different stages of the cell cycle, allowing the cells to repair the DNA damage (Chatterjee & Walker, 2017).

BER of a single nucleotide is where the strands must be complementary: adenine pairs with thymine and guanine pairs with cytosine (Simonelli *et al.*, 2005). NER removes bulky adducts in the DNA such as pyrimidine dimers (Hall & Giaccia, 2012). The MMR pathway removes

base-base and small insertion mismatches that occur during replication and also removes base–base mismatches in HR intermediates (Martín-López & Fishel, 2013). Furthermore, DNA DSBs can be repaired by 2 basic processes namely HR and NHEJ (Li & Heyer, 2008). HR repair requires an undamaged DNA strand to participate in the repair process by acting as a template (Hall & Giaccia, 2012). The NHEJ repair pathway mediates an end-to-end joining and is considered the major pathway for the repair of radiation induced DSBs in mammalian cells (Asaithamby *et al.*, 2011; Li & Heyer, 2008). However, DSBs repair is dependent on the cell cycle phase. HR occurs in late S/G2 phase when undamaged sister chromatid is available to act as a template, while NHEJ can function in all the phases of the cell cycle (Burma, Chen & Chen, 2006; Hall & Giaccia, 2012).

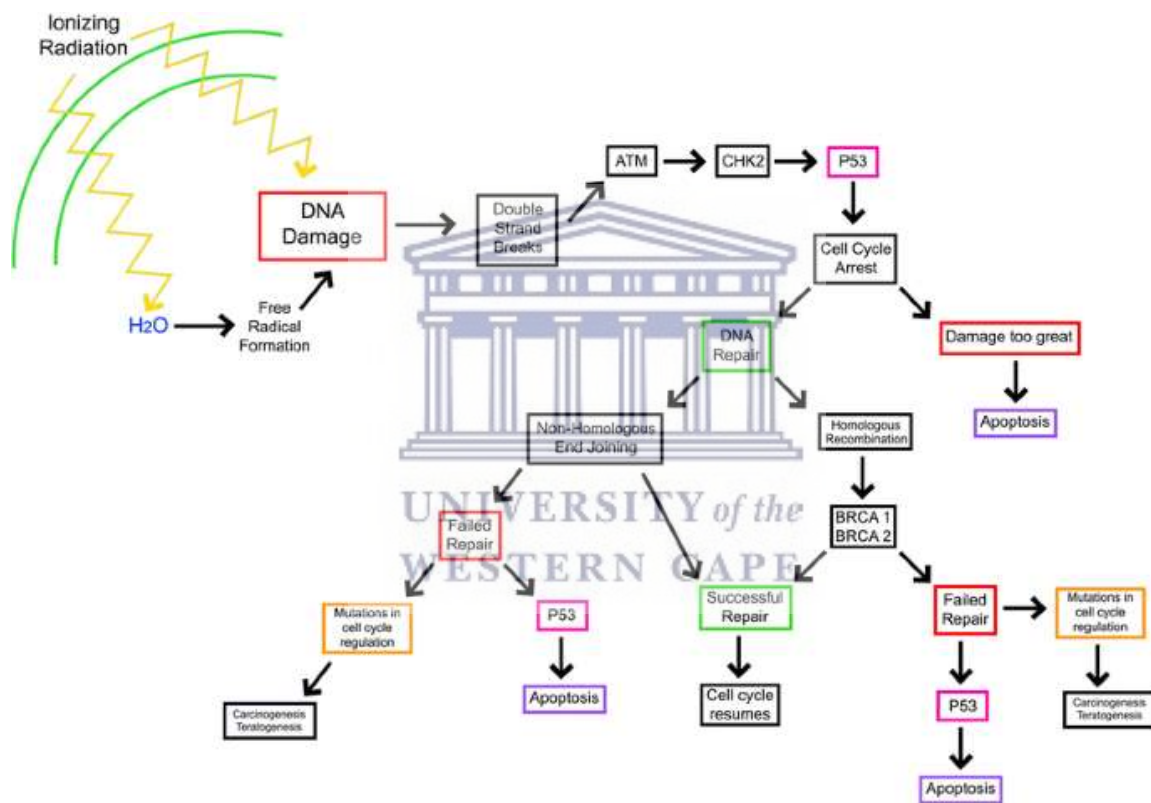


**Figure 19: IR causes direct and indirect DNA damage inflicted by HR and NHEJ.** IR causes DNA damage either directly or through the generation of free radical formation. Both types of damage lead to an increase activity of p53 protein and cell cycle arrest allowing repair of DNA DSBs by activating the HR or NHEJ pathway. If the repair is successful, the cell cycle will resume its proliferation, in the case of major DNA damage, induction of a cell death pathway via up-regulation of p53 protein, carcinogenesis or teratogenesis can occur (Smith *et al.*, 2017b).

### 1.6.2. Linear energy transfer (LET) radiation

Different types or qualities of IR can be classified as low- or high-LET radiation and the severity of the DNA damage is dependent on the LET and the path structure of the particle beam (Nikitaki *et al.*, 2016). The LET of radiation is the spatial distribution of energy absorption in a medium or the average energy deposited per unit path length along the track of an ionising particle, expressed as keV/ $\mu\text{m}$  (Bruce, Pearson & Freedhoff, 1963; Danzker, Kessarlis & Laughlin, 1959). There is a linear relationship between LET radiation and the complexity and lethality of the DNA damage, and thus the relative biological effectiveness (RBE) (Kirkby *et al.*, 2020). RBE is defined as the ratio of a dose of standard radiation to the dose of test radiation to produce the same level of biological effect (Neshasteh-Riz, Pashazadeh & Mahdavi, 2013). The radiation dose received by a tissue/organ is the absorbed dose and is defined as the energy deposition per unit mass with effect depending on the total mass (Babaei and Ganjalikhani, 2014). The absorbed dose is measured in Gray (Gy) wherein 1 Gy (100 rad) is equal to 1 J/Kg (McColl *et al.*, 2015). The cellular damage is dependent on many factors, such as the type of radiation and the sensitivity of the tissue/organ (Babaei and Ganjalikhani, 2014). Photon irradiation is classified as low LET radiation source, producing a randomly distributed pattern of DNA damage in the cell nucleus as presented in **Figure 20** (Percuoco, 2013; Roobol *et al.*, 2020).

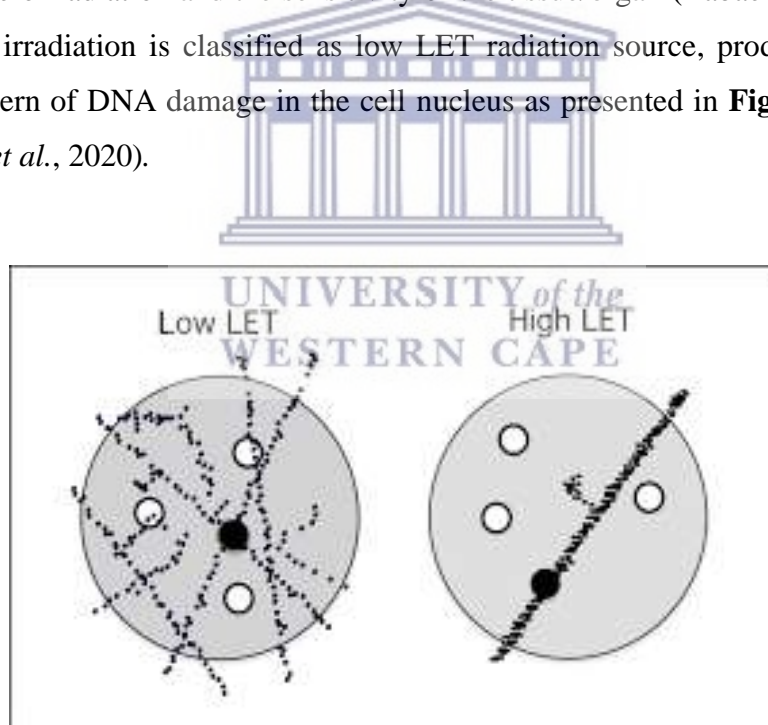


**Figure 20: Low vs high LET radiation.** Schematic representation of the energy disruption of low (left) and high (right) LET radiation. Low LET radiation contains several radiation tracks, while high LET radiation have a single fatal radiation track with a dense pattern of ionizations along this track (Scalliet & Gueulette, 2017).

### 1.6.3. X-rays

The discovery of X-rays in 1895 by Wilhelm Conrad Röntgen and the award of a second Nobel Prize to Marie Curie for her research into radium, helped spawn the medical application of IR, used to both diagnose and treat diseases (Frankel, 1995; Ngwa *et al.*, 2014)

Conventional X-ray production involves the excitation of tungsten metal to release photons (Sy, Samboju & Mukhdomi, 2021). The underlying basis for the diagnostic medical application of X-rays depends on the differential attenuation of X-ray when interacting with the human body (Fang Khoo & Foley, 2001). The photons can be completely absorbed into the tissue based on the tissue properties. This creates contrast among the different tissue within the body allowing for a separation of intensity values and evaluating potential pathology (Sy, Samboju & Mukhdomi, 2021). In other words, this process creates a superimposed “shadow” of the internal anatomy of interest and are converted into a visible projection image to provide anatomical information to a medical practitioner (Fang Khoo & Foley, 2001). As mentioned in Section 1.1, imaging systems such as X-rays is crucial for clinicians who diagnose, define stage and treat cancers (Frangioni, Fran-Gioni & Deaconess, 2008; Grodzinski, Silver & Molnar, 2006; Higgins & Pomper, 2011). However, a downside of imaging modalities is the fact that they use IR to generate the images. Even at low doses, IR can cause direct DNA damage and generate ROS and free radicals, leading to DNA, protein and lipid membrane damage (Smith *et al.*, 2017b).

The primary target of IR which is studied in radiobiology is the chromosomal DNA (Holley *et al.*, 2014). X-ray IR is a form of low LET radiation source and induces approximately 3 000 base damages, 1 000 SSBs and 40 DSBs for 1 and Gy (Hall and Giaccia, 2012). As a general rule of thumb, for every DSB at least 25 SSBs will be generated. As a response to the induction of SSBs and DSBs, a cascade of enzymatic processes is triggered to allow for damage DNA to be repaired or to induce a cell death pathway through activating TP53 and the induction of cell cycle arrest (**Figure 21**) (Smith *et al.*, 2017b). Most of the DNA damage caused by X-ray IR radiation is repairable (Porcel *et al.*, 2010), since the energy distribution is more randomly (**Figure 20**) (Löbrich, Cooper & Rydberg, 1996).

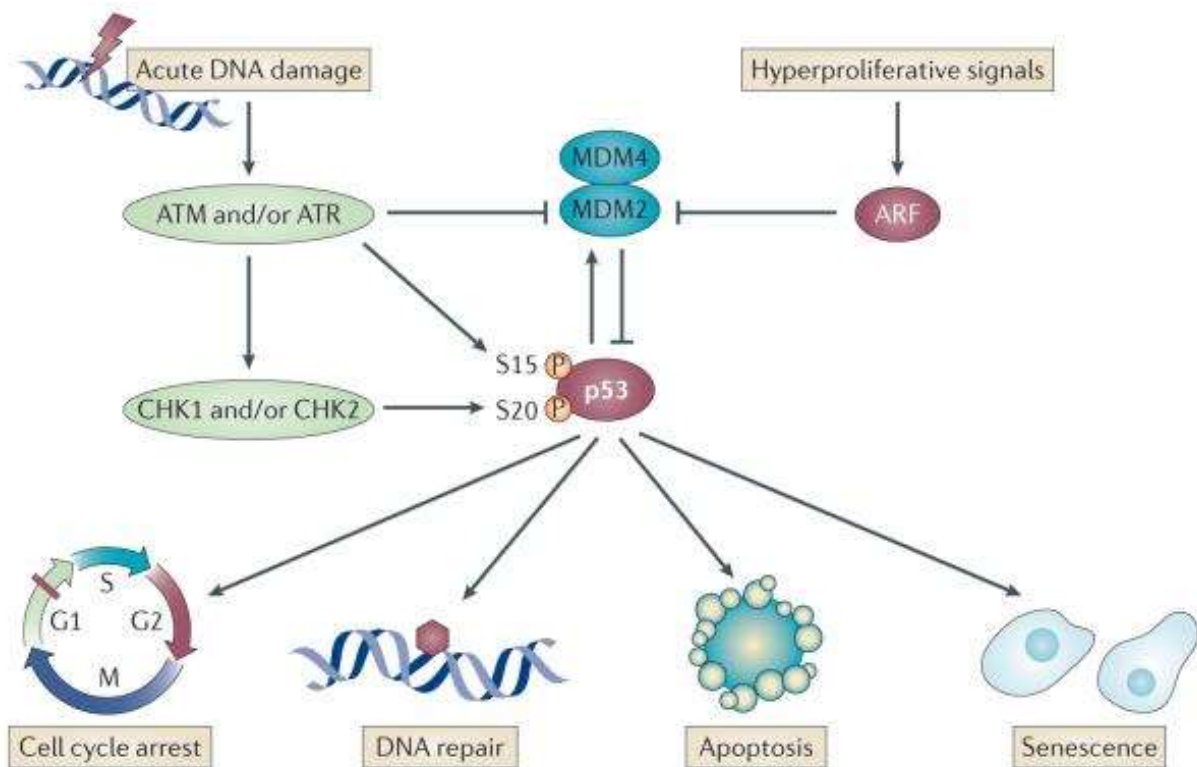


**Figure 21: The classical view of TP53 activation and response post-irradiation.** DNA damage trigger the activation of ATM/ATR signalling pathway by phosphorylating CHK1/2 resulting in the stabilization of the p53 protein within the cell by breaking free from its inhibitor, MDM2. ARF activation enhances p53 protein stability and activation. The stabilisation of the p53 protein allows for the activation of target genes which causes cell cycle arrest, DNA repair, apoptosis and senescence based on the DNA damage present (Biegging, Mello & Attardi, 2014).

X-rays irradiation deposits most of its energy as a single ionisation event, but ~30% of the ionisation events are formed closely together leading to the production of clusters of lesions, while high LET radiation produce an even higher density of DNA lesions within 10 – 20 base pair separation (Eccles, O'Neill & Lomax, 2011). Ward and team considered the potential importance of clustered DNA damage was ~103 SSB induced by 1 Gy IR which is equivalent to ~2.6 million SSB being induced by hydrogen peroxide and resulting in a similar level of cellular inactivation (Ward, Blakely & Joner, 1985). High levels of endogenous DNA damage are encountered on a daily basis as the result of metabolic, endogenous processes as well as exogenous DNA damage by exposure to exogenous factors such as chemicals, UV and IR. All of this together results in approximately 10 000 DNA damages/cell/day (Eccles, O'Neill & Lomax, 2011).



## 1.7. Aims and objectives

The aim of the **TU**mour **SU**ppression and **SU**bdual of **C**ancer (TUSSC) research project is to characterise a newly established primary elephant dermal fibroblast (EDF) cell line from African savanna elephants (*Loxodonta africana*) and to compare the radiation response of human (1 copy of TP53) vs elephant (20 copies of TP53) cells. Based on literature, it is anticipated that elephant cells have multiple copies of TP53, which might play a fundamental role in the induction and outcome of the DNA damage response. By using IR as a mean to induce DNA damage, we aim to investigate how the multiple copies of TP53 mediate the radiosensitivity of elephant fibroblast cells and how this affects the outcome of clonogenic survival-(CSA), cell proliferation-, apoptosis assay and cell cycle progression when compared to human fibroblast cells.

The TUSSC research project presented in this MSc thesis consist of 2 sections, namely: (A) Primary elephant dermal fibroblast (EDF) cell line characterisation and (B) primary normal human dermal fibroblast (NHDF) vs primary elephant dermal fibroblast (EDF) radiation response post X-ray irradiation. This is mainly a preliminary study to unravel the cancer suppression mechanisms of elephants.

### A. Primary elephant dermal fibroblast (EDF) cell line characterisation:

This part of the study focussed on the establishment and characterisation of the first primary EDF cell line of the African savannah elephant, which can be used for future studies to unravel the working mechanisms of the TP53 RTGs and to study their effect on the DNA damage response of elephants' vs humans. Objectives of Section A of the TUSSC research project were as follow:

- Obtain, establish and cultivate a primary EDF cell line from living, semi- and free-ranging African savanna elephants (*L. Africana*) naturally residing in the Western Cape, South Africa.
- Determine a primary EDF growth curve and the doubling time (Td) of the newly established EDF cell line.
- Confirm the known number of 56 chromosomes in the primary EDF cell line with a metaphase chromosome spread.
- Determine the duration of the cell cycle and the G0/G1, S and G2/M phase by cell synchronisation and quantification of the mitotic index (MI).

**B. Primary normal human dermal fibroblasts (NHDF) vs primary elephant dermal fibroblasts (EDF) radiation response post X-ray irradiation:**

Section B was to compare the radiation response post X-ray irradiation of the NHDF and EDF cell lines of the TUSSC research project. The objectives were as follow:

- Determining a survival curve from the primary NHDF and EDF cells post X-ray irradiation.
- Evaluating the cell proliferation capacity of the primary NHDF cells post X-ray irradiation, which would serve as a baseline for future comparisons with EDF cells.
- Based on the optimal time points determined on the primary NHDF cell proliferation results, a dose response curve will be determined for the primary NHDF and EDF cell line cells post X-ray irradiation by using the cell proliferation and MTS cell viability assay.
- Establish apoptosis pre- and post-irradiation in the primary NHDF and EDF cells by flow cytometry.
- Study the cell cycle progression of the primary NHDF and EDF cell lines pre- and post-X-ray irradiation by flow cytometry.





# CHAPTER 2:

## MATERIALS AND METHODS

---

### Section A: Primary elephant dermal fibroblast (EDF) cell line characterisation

#### 2.1. Primary EDF cell culture

Section A of the study was undertaken at the Radiation Biophysics Division of the National Research Foundation (NRF) iThemba Laboratory for Accelerator Based Sciences (LABS) and the Medical Bioscience Department of the University of the Western Cape (UWC) (both Cape Town, Western Cape, South Africa).

##### 2.1.1. African elephant sample collection procedure

The Animal Research Ethics Committee (AREC) of UWC approved this study on the 31<sup>st</sup> of August 2021, with ethics reference number AR21/6/4 (**Annexure I**). The Department of Forestry Fisheries and The Environment (DFFE) issued a standing permit for collection, receiving, transporting and temporary possession of specimens of the species with registration number 02307 in terms of the provision of the National Environmental Management: Biodiversity Act 2004, Act 10 of 2004 (permit number: S-65761) (**Annexure II**). Section 20 of the Animal Disease Act 1948 (Act number 35 of 19884). approval was granted by the South African Department of Agriculture, Land Reform and Rural Development (DALRRD) formerly the Department of Agriculture, Forestry and Fisheries (DAFF Section 20: 12/11/1/7) (**Annexure III**).

Biological samples were collected from 6 African savanna elephants (*Loxodonta Africana*). These include semi- and free-ranging elephants aged 14 – 47 years, residing in the natural habitat at Botlierskop Private Game Reserves (Gonnakraal Road, Little Brak River, 6503, Western Cape, South Africa) or Sanbona Wildlife Reserve (R62, Montagu, 6720, Western

Cape, South Africa). A hard copy of the landowner permission letter was obtained prior to sample collection (**Annexure IV** and **V**, respectively).

Samples were obtained from elephants who underwent a scheduled veterinary intervention requiring sedation. This was necessary for routine veterinary interventions, including testosterone vaccinations or the removal of tracking collar. The sample collection piggybacked on these interventions, which limited unnecessary sedation risks to the elephants and no animals were sedated for the sole purpose of this pilot study.

Wildlife veterinarian, Dr Willem Burger, darted the elephants with a specially formulated anaesthetic Thianil®. The anaesthetic substance was administered via a single intramuscular injection with a concentration of dosage vs body mass (**Appendix I**). During the period of sedation, oxygen levels and general body conditions of the elephant was closely monitored by Dr Burger and experienced field rangers. When the elephants were immobilised and secured, skin punch biopsy samples were collected. Approximately 4 – 6 skin punch biopsies of 5 mm in diameter were taken with a standard punch biopsy needle behind the ear of the elephant where the skin the thinnest is (**Figure 22 A**) (Smith, 1890). The number of biopsies was determined by Dr Burger based on the timing of the elephant being under general anaesthesia.

The following procedure was followed for the skin punch biopsy collection. Firstly, the skin was washed (**Figure 22 B**) and cleaned with 70% EtOH (**Figure 22 C**), dried and surgically draped (**Figure 22 D**). Once collected, biopsies were transferred to a sterile 15 mL conical tube containing 10 mL transport medium comprised of 90% Eagle's Minimum Essential Medium (EMEM) and 10% Penicillin/Streptomycin/Amphotericin B (P/S/A) to prevent dehydration and further contamination of the sample, respectively.

After the sample collection and veterinarian intervention, a reversal agent for the anaesthetic was administered which woke the elephant up within 5 min after which the elephant was monitored to ensure it got back on its feet and reunited with its herd.

Samples were transported at 0 – 4°C and monitored with a Temperature Data Logger M1 V1.3 (Tempmate®, GmbH, Heilbron, Baden-Württemberg, Germany), with indirect contact to ice to prevent freezing, to NRF iThemba LABS. Upon arrival in the Radiation Biophysics Division at NRF iThemba LABS, the skin biopsies samples were processed in a Biosafety Class II facility (Esco Airstream®, Esco technologies Pty. Ltd., Cape Town, Western Cape, South Africa) under sterile conditions within 24 h of collection.



**Figure 22: Skin punch biopsy procedure.** A) Skin biopsies were collected behind the ear of an elephant. B – C) The skin of the elephants was washed and cleaned with 70% EtOH. D) Surgical draped behind the ear of the elephant to maintain sterility.

## 2.1.2. African elephant biopsy preparation, outgrowth and culturing

### 2.1.2.1. Biopsy preparation

The samples were cultured using standard sterile cell culture procedures. All cell culture materials, solutions and equipment were sterile and culturing medium and reagents were pre-warmed in a water bath (37°C) before usage (see **Appendix I** for additional information and vendor). The skin punch biopsy was transferred from the transport medium conical tube to a glass petri-dish and washed thrice with washing phosphate buffered saline (PBS), containing 10% P/S/A and 2% gentamicin (**Figure 23 A – C**). The epidermis (the dark part of the elephant skin biopsy) containing keratinocytes, melanocytes, Merkel's cells and Langerhans cells (Yousef, Alhajj & Sharma, 2020), was removed by using 2 scalpels and dark tissue fragment was discarded as biological waste (**Figure 23 D**). Subsequently, the remaining biopsy was cut into smaller fragments, by holding the sharp parts of the scalpels firmly to the bottom of the petri-dish. While performing this task, a few drops initial culturing medium (EMEM with 20% Fetal Bovine Serum (FBS) and 1% P/S/A) was added to prevent dehydration of the tissue fragments (**Figure 23 E, F**). The small tissue fragments of the elephant biopsy were transferred into a T25 flask by the means of a glass sterile Pasteur pipet and spread out over the surface of the T25 flask (**Figure 23 G**). The small fragments in the T25 flask were covered with 0.5 mL FBS (**Figure 23 H**) and incubated under standard conditions that is 37°C in a humidified 5% carbon dioxide (CO<sub>2</sub>) incubator. The tissue fragments did not float but were covered with the FBS (**Figure 23 I**).

After 24 h, the T25 flasks were placed upside down for 24 h to allow cells to properly attach to the surface and to avoid the fragments floating in media. On every 3<sup>rd</sup> day thereafter, 1 mL initial culturing medium was added without detaching the small tissue fragments. Each day, the T25 flasks tissue fragments were monitored using a Zeiss Primovert inverted microscope (Carl Zeiss SMT GmbH, Roßdorf, Hessen, Germany), at 20× magnification to observe explant dislodging and the overall explant radial migration of the primary EDF cells around the tissue fragments. At 40× magnification, the T25 flasks were monitored for any microbial or fungal contamination.

A random selection of 1 elephant cell pellet was sent to Pathcare, Somerset West, Western Cape, South Africa for a 16S ribosomal RNA gene polymerase chain reaction (PCR) for detection of possible bacterial DNA. No bacterial DNA, including Mycoplasma species, were detected (**Annexure VI**).

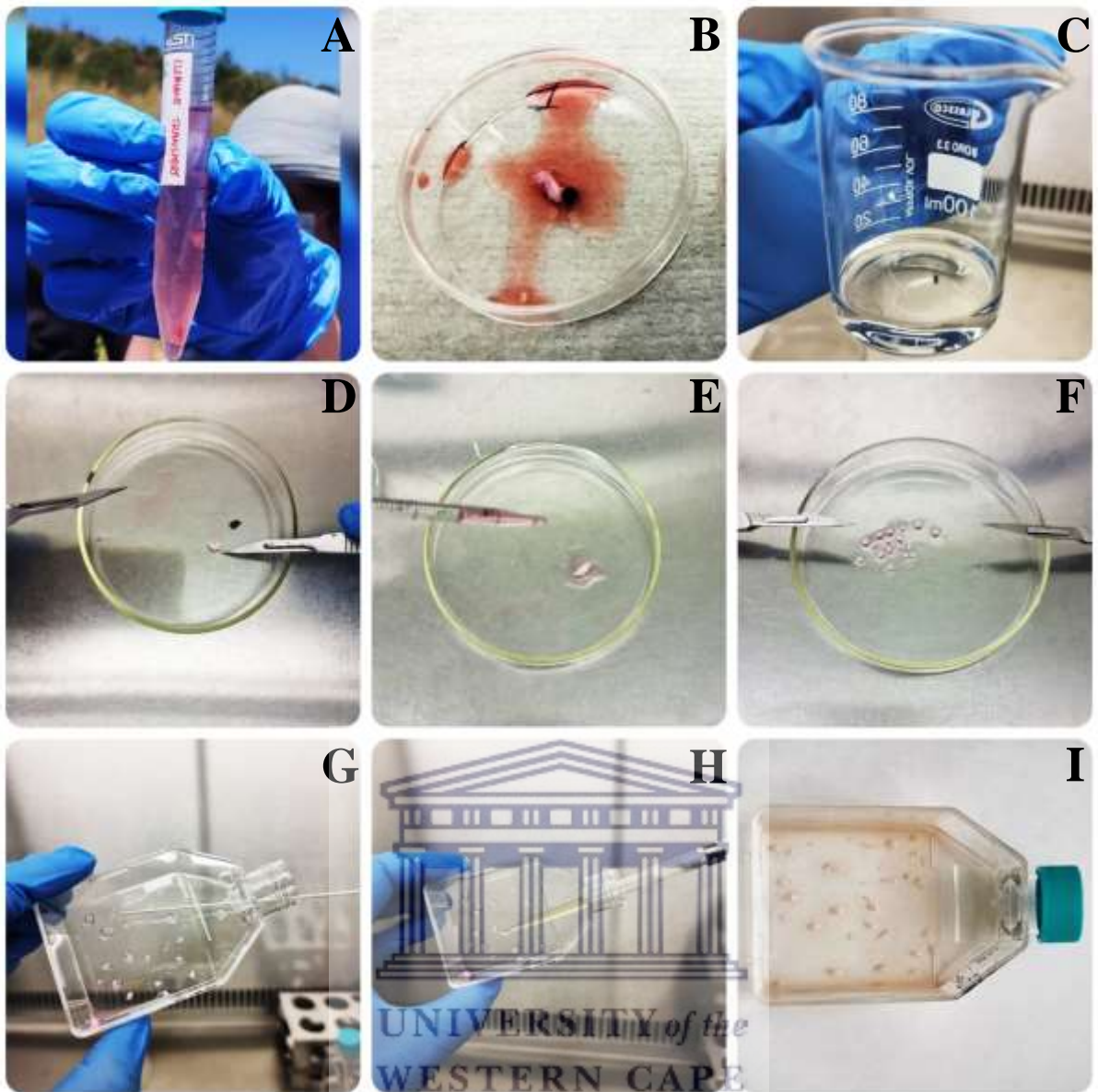


**Figure 23: Skin punch biopsy preparation.** A – C) Skin punch biopsy in transport medium containing and was transferred to a glass petri-dish followed by washing thrice in washing PBS. D) The epidermis was removed and discarded. E – F) Initial culturing medium was added to prevent dehydration of the tissue and was cut into smaller fragments. G) The tissue fragments were transferred with a glass Pasteur pipette and spread across the surface in the T25 tissue culture treated flask. H – I) FBS was added to cover the fragments and the T25 flask was incubated under standard conditions.

### 2.1.2.2. Primary EDF explant outgrowth and culturing

When the explant outgrowth of EDF cells from the tissue fragments reached 70% confluency, the T25 flask was sub-cultured. The medium was aspirated and the EDFs were washed twice with 2 mL PBS and 1 mL of trypsin ethylenediaminetetraacetic acid (EDTA) solution 1× was added. The trypsin EDTA solution 1× was gently swirled around to cover the monolayer of the T25 flask and incubated for 2 – 4 min.

After 75% of cells detached, 2 mL complete EMEM (cEMEM: EMEM, 20% FBS and 1% Penicillin/Streptomycin (P/S)) was added to inactivate the enzyme activity. The cell suspension was transferred to a 15 mL conical tube. The T25 flask was washed again with 1 mL PBS, which was transferred to the 15 mL conical tube, followed by an additional 1 mL trypsin EDTA solution 1× repeated incubation to ensure 95% of cell detached from the initial T25 flask. Once the remaining cells in the flasks were detached, 2 mL cEMEM was added and dispersed by pipetting over the cell layer surface several times followed by transferring the cell solution to the same 15 mL conical tube.

The 15 mL conical tube was centrifuged at 200 g-force for 8 min. The supernatant was discarded, and the cell pellet was gently resuspended in 2 mL cEMEM with a P1000 pipette and transferred to a new a tissue culture treated flask.

From passage 1 and onwards, EDFs were cultured with cEMEM without amphotericin B to prevent effects of the cell proliferation. In addition, from passage 2 and onwards, EDFs were either subcultured, directly used for experiments or frozen for long-term storage.

A 90 – 95% confluent T25 flask contained 500 000 – 700 000 cells. A seeding density of 3 500 – 7 000 cells/cm<sup>2</sup> was followed for subculturing. The media of the subcultured T25 flasks was changed every 2<sup>nd</sup> – 3<sup>rd</sup> day. The T25 flask monolayer was first washed with 2× 2 mL PBS and refreshed with 2 mL cEMEM. When confluent, the cells were subcultured as previously described in this section.

### 2.1.2.3. Primary EDF cryopreservation

When a T25 flask reached confluency, the adherent EDFs were detached as mentioned above (Section 2.1.2.2). After centrifugation the cell pellet was resuspended with freezing medium (90% FBS + 10% Dimethyl Sulfoxide (DMSO)).

The cells from 1 confluent T25 flasks were aliquoted into 4 cryovials and transferred to a freezing container containing isopropyl alcohol acclimated to  $-80^{\circ}\text{C}$  overnight. Thereafter cryopreserved EDFs were stored in a  $-80^{\circ}\text{C}$  freezer (NuAire Laboratory Equipment, Plymouth, Minnesota, USA) at NRF iThemba LABS. The freezing container ensures that the cooling rate is slow enough to allow the cells time to dehydrate, but fast enough to prevent excessive dehydration damage (Jang *et al.*, 2017).

To resuscitate the EDFs, a cryovial was placed in a warm water bath ( $37^{\circ}\text{C}$ ) and agitated gently to allow rapid thawing. The cell suspension from the cryovial was added to a 15 mL conical tube containing 6 mL of cEMEM and centrifuged. The supernatant was discarded and the pellet was resuspended in 2 mL cEMEM and transferred to a T25 flask. Attachment was observed approximately 4 h after seeding and a media change occurred every 2<sup>nd</sup> – 3<sup>rd</sup> day.



#### 2.1.2.4. Primary EDF life span

There is no defined maximum number of passages for the primary EDF cell line yet. The morphology of the cells was closely monitored by eye throughout passages with a Zeiss Primovert, light microscope and a live cell imaging system CytoSmart, Lonza® (CytoSmart Technologies B.V., Eindhoven, North Brabant, Netherlands). **Figure 24** represents the cell morphology at passages 3 and 14 throughout the EDF cell culture over a period of approximately 3 months.

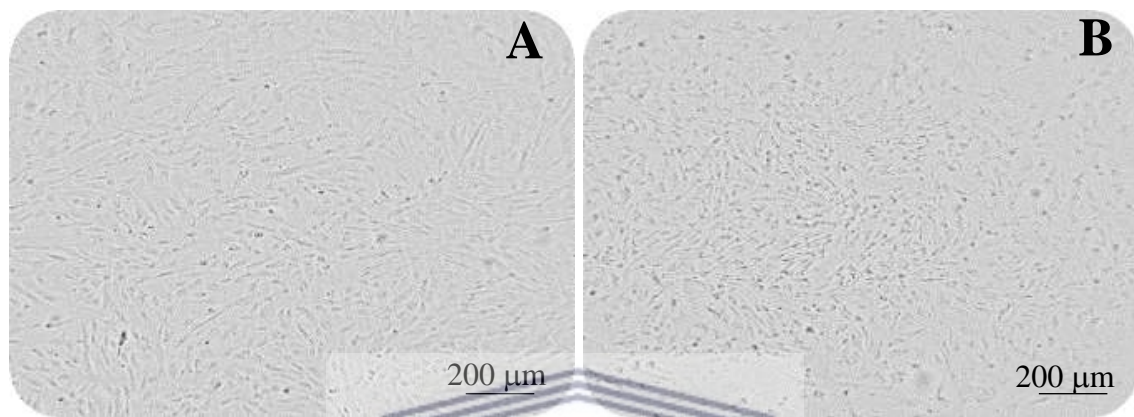


**Figure 24: Morphological depiction of EDFs (E1) in culture (10× magnification) at different passages with a different seeding density. Scale 200 μm. No morphological changes were observed at 10× magnification. A) E1 at passage 3. B) E1 at passage 14.**

UNIVERSITY of the  
WESTERN CAPE



## 2.2. Primary EDF growth curve and doubling time (Td)

A growth curve comparison was established based on confluency measurements of EDF cultures from 3 different elephants (E3 – E5) after sub-culturing at passage 2. Post seeding, the cells were incubated for 2 days and from day 3 onwards, 6 images were taken daily in 6 different regions (**Figure 25 A**) of the T25 flask until a confluent monolayer was reached (field of view  $2.40 \times 1.40$  mm). During this period, the T25 flasks were washed with PBS and refreshed every 2<sup>nd</sup> – 3<sup>rd</sup> day with cEMEM. The confluency was defined using a live cell imaging system CytoSmart, Lonza® (**Figure 25 B**) using the confluency algorithm (<https://cytosmart.com/applications/cell-confluence>). Results were standardised as a percentage as shown below:

$$\frac{y}{\text{maximum confluency}} \times 100$$

In addition, primary EDF Td was determined based on the confluency algorithm and plotted on a histogram. The following equation was used to calculate the Td, where t represents time.


$$\text{Doubling time (Td)} = \frac{t_2 - t_1}{x}$$

UNIVERSITY of the  
WESTERN CAPE

$$x = \frac{\log\left(\frac{\text{end cell coverage}}{\text{start cell coverage}}\right)}{\log(2)}$$

All results were graphically plotted in GraphPad Prism®.

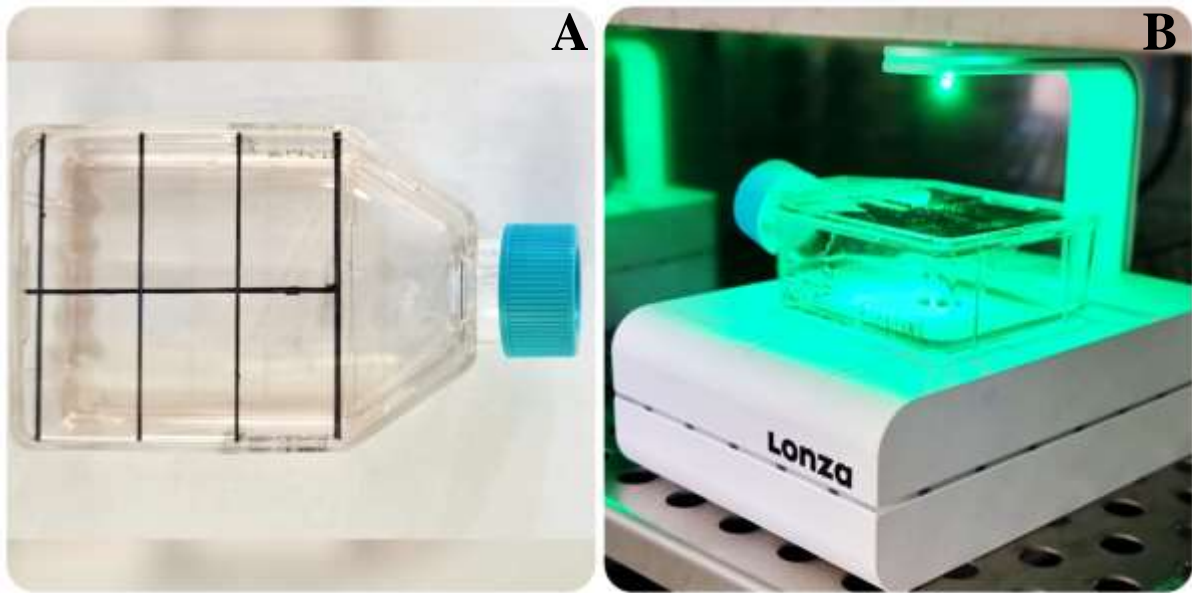


**Figure 25: EDF growth curve of E3 – E5 establishment procedure to determine the Td.**  
A) The confluency was determined on 6 different regions on a T25 flask. B) The T25 flask in an incubator on the Cytosmart, Lonza® system.



### 2.3. Metaphase chromosome spread

Chromosome analysis is widely used for the detection of chromosome instability. Chromosomes are analysed at the metaphase stage of mitosis, when they are most condensed and more clearly visible (Howe, Umrigar & Tsien, 2014). Well-spread metaphase chromosomes are fundamental for cytogenetic studies (Deng *et al.*, 2003). While these type of studies will be part of future experiments, the scope of the MSc project was to optimize the methodology and to confirm the presence of 56 chromosomes in these newly established EDF cell lines as described in previous studies on the Elephantidae family (Frönicke *et al.*, 2003; Hungerford *et al.*, 1966; Yang *et al.*, 2003). Therefore, the purpose of this experiment was to obtain an optimal number of metaphase chromosome spreads (Uttamatinin *et al.*, 2013). This is especially important for any future experimentation on the EDF cell line, for example the dicentric chromosome assays (Lee *et al.*, 2019).

For the optimization of the metaphase chromosome spread presented here, the EDF cells of E1 were used. The selection was primarily based on the timeline of sample collection and experimentation. The EDFs of E1 were sub-cultured and seeded in a concentration of 35 000 cells/petri dish followed by incubation under standard conditions. Exponentially growing cells were treated with 5  $\mu$ L/mL KaryoMAX™ Colcemid™ Solution in PBS at different percentage of confluency. In addition, different KaryoMAX™ Colcemid™ incubation times (listed in **Table 1**) were tested in order to determine the optimal exposure time to achieve a sufficient number of metaphase chromosome spreads. Colcemid is a mitotic inhibitor that binds to the protein tubulin and prevents the spindle fibre formation and therefore causes metaphase arrest (Rodman, Flehinger & Rohlf, 1980). This incubation inactivated spindle fibre formation.

**Table 1: Metaphase chromosome spread conditions to determine a metaphase chromosome spreads and to confirm the presence of 56 chromosomes in the newly established EDF cell line.** E1 was tested under different cell densities and time points (h) with a working concentration of 0.05 µg/mL KaryoMAX™ Colcemid™ Solution in PBS.

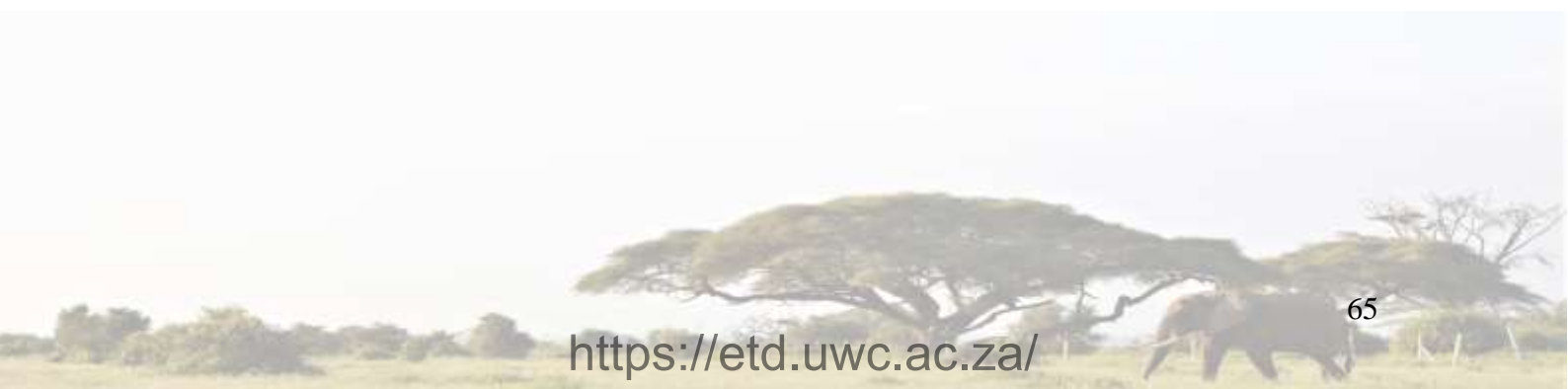
Density of EDFs in culture	Time points (h)
70 – 80%	3
	6
60 – 70%	6
	15
	24
	28
90 – 95%	3
	6
	12
	24

After the incubation periods, the cells were harvested and the supernatant discarded. Thereafter 5 mL prewarmed 0.075 M Potassium Chloride (KCl) was added to the 15 mL conical tube in a dropwise manner while stirring vigorously. The cell suspension was left for 10 min in the hypotonic solution at room temperature (rt), followed by 1.5 mL of methanol - acetic acid fixative solution (3:1 ratio, freshly prepared at rt). The fixative solution was slowly added at the bottom of the 15 mL conical tube and then centrifuged at 200 g-force for 8 min. The supernatant was discarded and 2× 5 mL fixative was added dropwise until the fixative was clear, while stirring vigorously and centrifuged. The cell pellet was resuspended in 200 µL of the left-over supernatant and 50 µL of the cell suspension was dropped from 30 cm height on wet slides (stored in dH<sub>2</sub>O with 10% methanol, at 4°C) to allow a good quality metaphase spread on the slide (Deng *et al.*, 2003).

Once the slides were air dried, the staining solution was prepared. HEPES (2-[4-(2-hydroxyethyl) piperazin-1-yl] ethanesulfonic acid) buffer stock solution was made by adding 900 mL HEPES solution A with 100 mL HEPES solution B (0.1 M, pH 6.5) and HEPES buffer working solution was made by adding 300 mL HEPES buffer stock solution to 700 mL dH<sub>2</sub>O (0.03 M, pH 6.5).

A 1:25 Giemsa's Azur Eosin Methylene Blue Solution with HEPES buffer working solution was made in a Hellendahl jar just before use. The metaphase slides were added to the jar for 3 min and protected from light. Thereafter, the slides were rinsed 3 times in dH<sub>2</sub>O and left to dry.

Once dried, the stained slides were covered with a drop of DPX followed by a 24 × 50 mm glass coverslip by placing the coverslip at a 45° angle to avoid air bubbles and baked overnight at 37°C till the slides were dry. The metaphase chromosome spread of the EDFs were enumerated manually at 10× magnification with a Zeiss Primovert and images were captured using the metaphase finder algorithm of Metafer (MetaSystems, Heidelberg, Hessen, Germany) and subsequently captured with an immersion oil lens objective (63× magnification).



#### 2.4. Cell synchronisation and mitotic index (MI)

The durations of the S phase, G<sub>2</sub>/M transition period and mitosis were determined with the aid of mitotic indices after removal of hydroxyurea (HU) (Loitering *et al.*, 1996). E6 cells were seeded (passage 9) with a cell seeding density of 40 000/petri dish on autoclaved sterile coverslips (20 × 20 mm). The cells were allowed to attach (4 h). Pre-confluent monolayers of E6 cells were exposed to 2 mM HU in cEMEM for 36 h which effectively block the cells at the G<sub>1</sub>/S boundary. HU is commonly used to inhibit ongoing DNA replication by causing a depletion of ribonucleotide reductase resulting a nucleotide depletion and S phase stalling (Sabatinos & Forsburg, 2010).

After the 36 h, the HU was washed out with 3 cEMEM media changes over 5 min intervals and the cells were left for 24 h. After these 24 h, duplicate petri dishes were removed every 2<sup>nd</sup> h for 6 h and then removed hourly for 24 h, followed by fixation in Bouins fixative for 20 min and stained with haematoxylin and eosin (H & E) for 30 and 5 min, respectively (Gurina & Simms, 2022). This is a widely employed staining technique in histopathology to enhance contrast and discern between nuclei and cytoplasm in tissues/cells by staining them in different colours (Hristu *et al.*, 2021). Haematoxylin is a basic, deep blue-purple dye and stains basophilic structures such as nucleic acids by applying hemalum which is a complex formed from aluminium (Al) ions and oxidized haematoxylin (Fischer *et al.*, 2008; Kuru, 2014; Gurina & Simms, 2022). On the other hand, eosin is an acidic pink dye and stains acidophilic proteins non-specifically, for example the cytoplasm, by applying an aqueous or alcoholic eosin solution (Fischer *et al.*, 2008; Kuru, 2014; Gurina & Simms, 2022).

After fixation, the cells were placed in 70% EtOH for 20 min (or stored for longer periods) then washed in H<sub>2</sub>O till the H<sub>2</sub>O was colourless. The coverslips were then stained with haematoxylin for 30 min followed by washing in H<sub>2</sub>O for 1 min. Next, the coverslips were stained with eosin staining solution for 5 min. The cells were then dehydrated by placing the coverslips through increasing concentration of alcoholic baths: 2× in 70%, 80% and 90% EtOH for 2 min, 1× in 95% EtOH for 2 min, 2× in 100% for 2 min and lastly cleared 2× in Xylene where after the coverslips were fixed onto EtOH cleaned glass microscopic slides with DPX.

The MI were calculated in H & E stained cells and the morphology of the EDFs cells were studied using a light microscopy (Zeiss Primovert) at 10× and 40× magnification. A total of 1 000 cells/slide were counted which include all normal phases of the dividing cells.

The MI was scored and calculated using the following calculation:

$$\frac{\textit{Cells observed with visible chromosomes}}{1000} \times 100$$

Prophase, metaphase, anaphase and telophase at 39 h after block was released was viewed with a Zeiss Primovert light microscope. Images were captured with an Axio 208 colour (Carl Zeiss SMT GmbH, Roßdorf, Hessen, Germany) and imaging software of Zen 3.6 (blue edition) (Carl Zeiss SMT GmbH, Roßdorf, Hessen, Germany).



# CHAPTER 2:

## MATERIALS AND METHODS

---

### Section B: Primary normal human dermal fibroblast (NHDF) vs primary elephant dermal fibroblast (EDF) radiation response post X-ray irradiation

For the comparison of the primary NHDF and EDF cell line in Section B, the TUSSC research project consists of 2 phases based on the location of the experimentation:

- i. The first phase of the experimentation was on a commercial primary NHDF cell line from an adult donor. The NHDF cell line acts as the baseline for the TUSSC research project to allow future comparisons between primary human and elephant fibroblast cells. The NHDF cells were irradiated at GSI Helmholtzzentrum für Schwerionenforschung GmbH (Darmstadt, Hessen, Germany) under the GET\_INvolved internship and training program.
- ii. The second phase involves the culturing and experimentation on primary EDFs (E6) that occurred at Radiation Biophysics Division of the NRF iThemba LABS and the Medical Bioscience Department of the UWC (both Cape Town, Western Cape, South Africa). See Section A of Chapter 2 for the collection of the elephant fibroblasts from an African savanna elephant (*L. africana*) at private game reserves and the establishment of a primary EDF cell line.



## 2.5. Cell culture

### 2.5.1. Primary NHDF cell culture

#### 2.5.1.1. Primary NHDF cell line establishment

The NHDF cell line was commercially purchased and cultured in Fibroblast Growth Medium (FGM) supplemented with FBS, basic fibroblast growth factor and insulin (**Appendix II**). The complete FGM (cFGM) did not contain antibiotics or antimycotics.

Upon receiving the cryovial from PromoCell (500 000 cryopreserved cells at passage 2), the cryovial was placed in liquid nitrogen (Locator™ JR Plus, Thermo Scientific™, Chart Inc, Ball Ground, Georgia, USA) for storage until thawing. All cell culture materials, solutions and equipment were sterile and culturing medium and reagents were pre-warmed in a water bath (37°C) before usage (see **Appendix II** for additional information and vendor). Upon thawing, the cryovial was removed from the liquid nitrogen and placed in a Thermo Scientific™ Maxisafe 2020 Class II Biological Safety Cabinet, (Thermo Electron LED GmbH, Langenselbold, Hessen, Germany). The cryovial was placed in a water bath (37°C) up to a height of the cap for 2 min. The cryovial was cleaned with 70% ethanol (EtOH) and placed in the biological safety cabinet. A 1:4 ratio was followed to seed the recommended seeding density of 3 500 – 7 000 cells/cm<sup>2</sup>. To achieve this, 250 µL cell suspension of a total volume of 1 mL, was transferred to a T25 tissue culture treated flask which contained 5 mL prewarmed cFGM. The T25 flasks were seeded and incubated under standard conditions.

After 24 h, the T25 flask underwent medium replenishment. Every 2<sup>nd</sup> – 3<sup>rd</sup> day thereafter, the medium was aspirated, and 2 mL Hanks Buffered Saline Solution (HBSS) was added to wash the monolayer of the cells and discarded, thereafter replaced with 2 mL cFGM. When the T25 flask reach 90 – 95% confluency (20 000 cells/cm<sup>2</sup>), the medium was aspirated, washed with 2 mL HBSS and 1 mL trypsin EDTA 1× was added to cover the monolayer of the cells. The T25 flask was incubated for 5 – 8 min. If approximately 75% of cells were detached, 2 mL complete cFGM was added to inactivate the enzyme activity. The cell solution was transferred to a 15 mL conical tube. The T25 flask was washed again with 1 mL HBSS and transferred to the same 15 mL conical tube, followed by 1 mL trypsin EDTA solution 1× and the incubation was repeated to ensure 95% recovery of cells. The incubation time was kept at a minimum to avoid overexposure to trypsin. When the remaining cells were detached, 2 mL cFGM was added and dispersed by pipetting over the cell layer surface several times followed by

transferring the cell solution to the same 15 mL conical tube. The 15 mL conical tube was centrifuged at 200 g-force for 4 min. After centrifugation, the supernatant was discarded, and the cell pellet was resuspended gently in 2 mL cFGM with a P1000 pipette and transferred to a new tissue culture treated flask.

NHDF cells were either subcultured, used for experiments or frozen for long-term storage. The NHDFs were subcultured/frozen in tissue culture flask/cryovials, respectively, applying above mentioned seeding densities.

### **2.5.1.2. Primary NHDF cryopreservation**

NHDFs cryopreservation occurred following the same steps mentioned in Section 2.1.2.3. The cryopreserved NHDFs were stored for long term storage in liquid nitrogen.

### **2.5.1.3. Primary NHDF life span**

PromoCell quality control procedure included the cultivation of the fibroblasts up to passage 15. This ensures that the NHDF cells can be grown for a minimum of 15 passages, however, it does not mean that the cells immediately reach senescence after 15 passages. The maximum passages were not determined and most NHDFs can be subcultured until passage 20 based on PromoCell quality control procedures.

NHDFs were monitored for any morphological changes (no experimental analysis was done to confirm this) throughout passaging (**Figure 26**). Cell cultures were monitored with the naked eye by the means of a AE31 series Motic® inverted light microscope (Motic Deutschland GmbH, Wetzlar, Hessen, Germany). Cell culture images were obtained with the MotiCam 3, Motic Deutschland GmbH, Wetzlar, Hessen, Germany and imaging software Motic Images Plus 3.0 (×64) (Motic Deutschland GmbH, Wetzlar, Hessen, Germany).

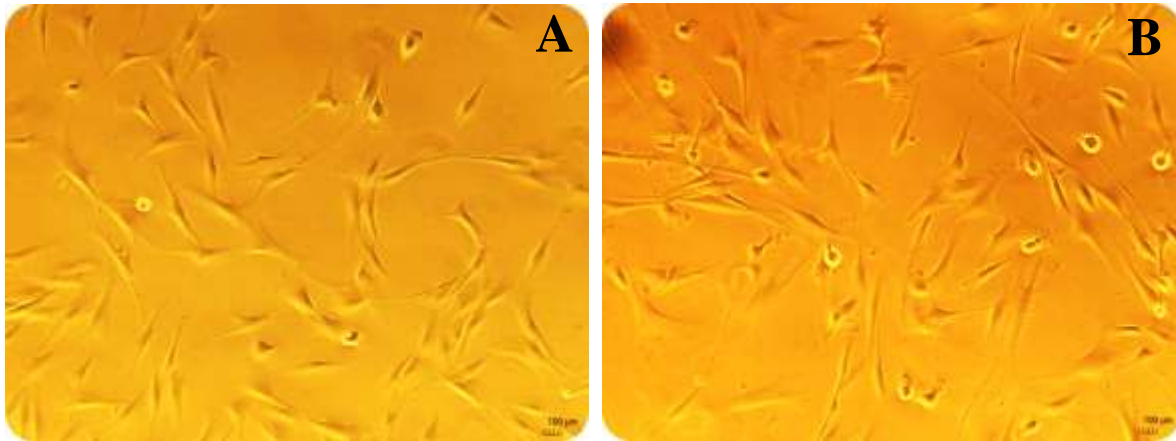
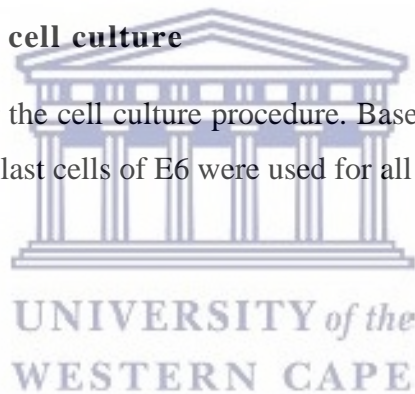


**Figure 26: Morphological depiction of NHDFs in culture at 10× magnification at different passages with a different seeding density. Scale 100 µm. No morphological changes were observed at 10× magnification. A) NHDFs at passage 3. B) NHDFs at passage 14.**

### 2.5.2. Primary EDF cell culture

See Section A of Chapter 2 for the cell culture procedure. Based on the timeline of culturing and experimentation, the fibroblast cells of E6 were used for all experiments in Section B.



**2.6. To assess the biological endpoints, post X-ray IR at GSI and NRF iThemba LABS for the primary NHDF and EDF cell lines, respectively.**

Primary NHDFs and EDFs were cultured according to standard tissue culture procedures (Chapter 2 Section A) and irradiated with X-rays at GSI and NRF iThemba LABS to investigate the radiation sensitivity of human and elephant fibroblast cells, respectively. The following assays were performed on both cell lines: clonogenic survival- (CSA), cell proliferation-, MTS-, as well as apoptosis- and cell cycle assay with flow cytometry (**Figure 27**).

The NHDF cell line was used to optimise the techniques for the above-mentioned biological endpoints. Based on the results for the NHDF experiments, the same principle was applied with the EDF cells at NRF iThemba LABS. All cell culture materials, solutions and equipment were sterile and reagents were used according to standard procedure (see **Appendix III** and **IV** for additional information and vendor).

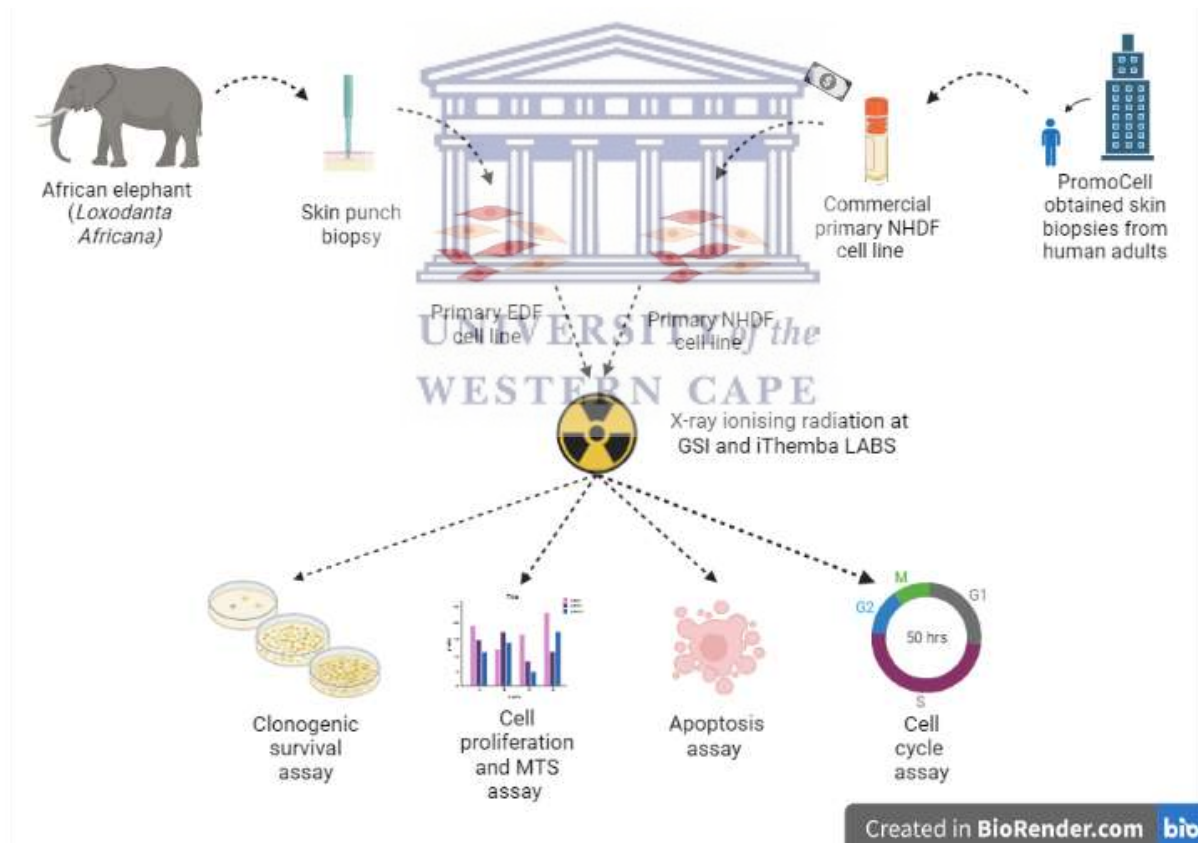


**Figure 27: Primary NHDF and EDF experimental procedure.** Graphical depiction of the NHDF and EDF cell line initiation and biological endpoints which will be evaluated after radiation exposure. Created with BioRender.com.

## 2.7. X-ray irradiation setup

### 2.7.1. GSI

X-ray irradiation was performed using an Isovolt DSI (Seifert, Ahrensberg) X-ray generator with a vertical downwards beam. A source-to-surface distance (SSD) of 30 cm from the filter edge to the sample was selected for the irradiations, resulting in a dose rate of 2 – 3 Gy/min (**Figure 28 A**). A plastic sample holder was placed inside a marked field with lines on the specimen table, which guarantees a central position of the sample in the radiation beam (not present in **Figure 28**). Samples in T25 flasks and 96-well tissue culture plates were placed in the plastic sample holder manufactured of polyvinyl chloride polymer (PVC). The plastic sample holder houses the farmer ionisation chamber within a groove and was present during the irradiations to confirm the delivery of the radiation dose (SNA4, PTW Freiburg, Baden-Württemberg, Germany) (blue arrow, **Figure 28 B**). The build-up cap of the ionisation chamber was removed before irradiation and placed back on after irradiations. The standard values for voltage and current for the X-ray machine are 250 kVp and 16 mA, respectively and a filter consisting of 7 mm Beryllium (Be), 1 mm Al and 1 mm Copper (Cu) was used for the irradiations. Furthermore, the samples were irradiated from the top, where the beam is traversing first the air plus the medium before reaching the cells. However, these circumstances have been taken into consideration by the medical physicists who performed the dose calibrations for the irradiation set-up at GSI. Unfortunately, this calibration is based on an in-house protocol and not published, therefore no reference can be given for the in-house irradiation set-up at GSI.

Before each run, the system was calibrated by inducing a 2 Gy trial run (**Figure 28 C**). When the PTW-UNIDOS dosimeter reached 2 Gy as indicated on the screen and this correlated with the computer (**Figure 28 D**), the actual experimental samples were irradiated. The desired doses were set by the computer and initiated as shown in **Figure 28 C**. The X-ray tube was set up according to standard procedure with all the necessary safety protocols in place to comply with GSI's radiation protection regulations.

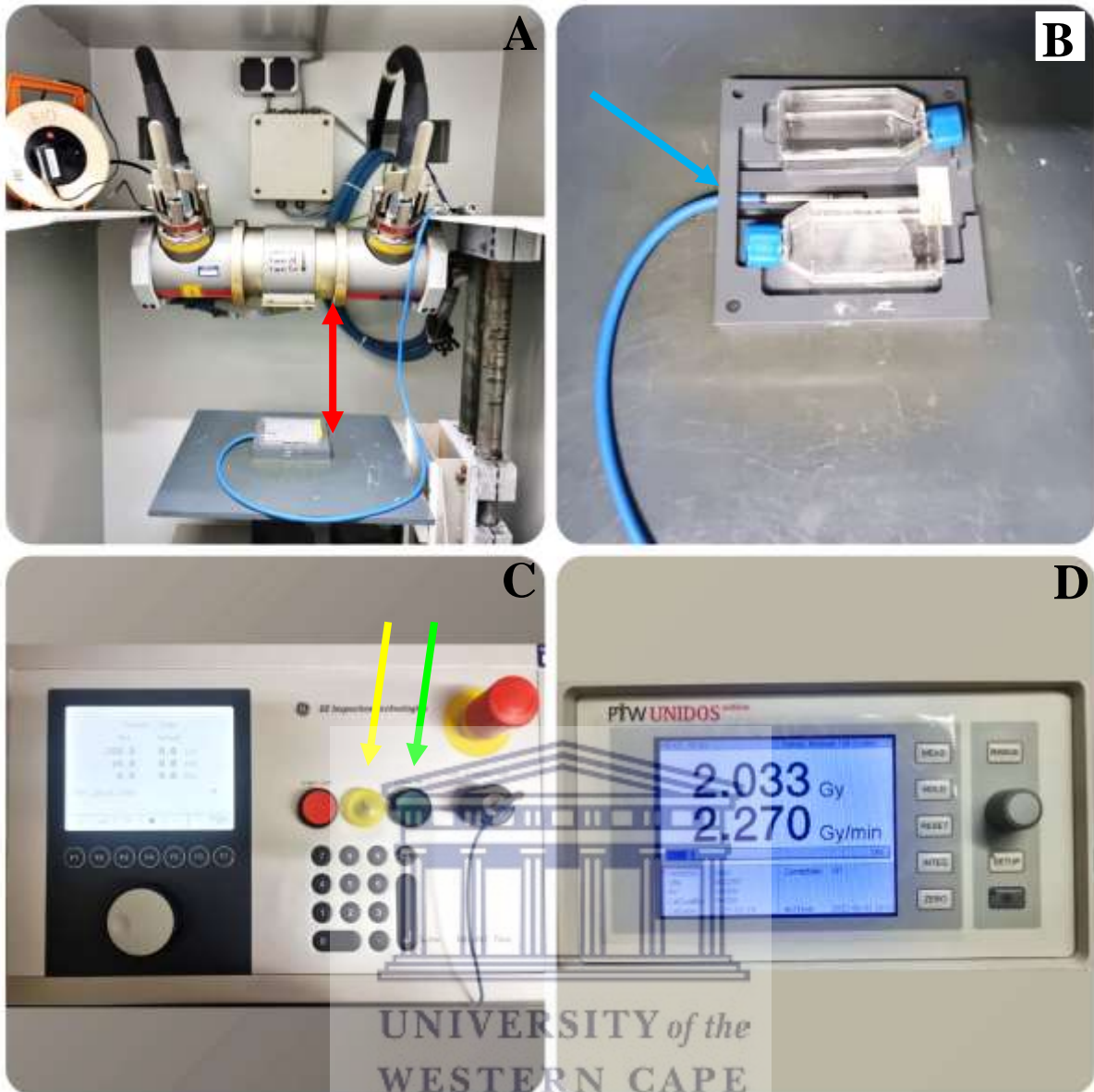


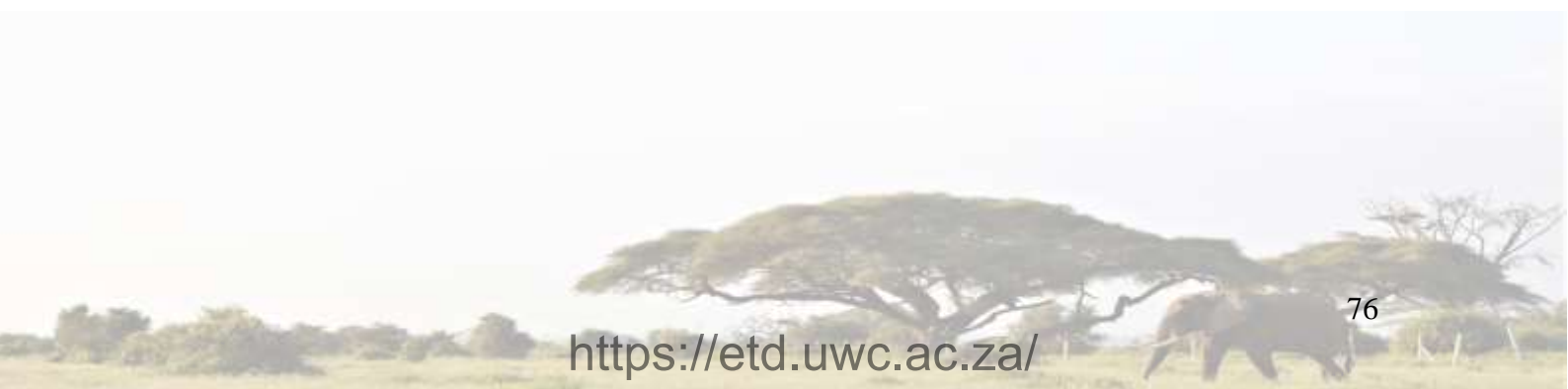
**Figure 28: X-ray machine at GSL.** **A)** The overview of the X-ray tube. The red arrow indicates the distance between the X-ray tube and the grey sample holder. **B)** T25 flask in the field view indicated with the blue arrow, the farmer ionisation chamber, in place of the grey sample holder. **C)** The control panel. The green button indicated by the green arrow was to execute the initiation of the X-ray radiation and the yellow button indicated that the X-ray machine was on. **D)** The PTW-UNIDOS dosimeter indicate the doses delivered to the sample and the dose rate/min.

### 2.7.2. NRF iThemba LABS

An X-RAD 320 X-ray irradiator unit, manufactured by Precision X-ray (North Branford, Connecticut, United States), was used at NRF iThemba LABS to perform all X-ray irradiation experiments. Similar to the set-up at GSI, the X-ray beam is directed vertical downwards towards the specimen shelf. All irradiations were done with the tube voltage set at 250 kVp and with the field size set as 15 cm × 15 cm at an SSD of 50 cm (**Figure 29 C** indicated by the red arrow). A custom filter consisting of 3.271 mm Al and 1.519 mm Cu were used. The inherent filtration is 3 mm Be. This, together with the added filtration of the Perpex protective plates (shown by the purple arrow in **Figure 29 C**) and glass mirrors of the adjustable collimator, gives a beam (at 250 kVp) having a first half-value layer of 2.529 mm Cu and a homogeneity factor of 0.74 (the second half-value layer is 3.343 mm Cu). The dose output at the surface of a solid dosimetry phantom was determined using the AAPM TG-61 dosimetry protocol (Ma *et al.*, 2001). This water-equivalent dosimetry phantom (Hill, Kuncic and Baldock, 2010) is made from 30 cm x 30 cm Virtual Water slabs (Virtual Water: Med-Cal, Verona, WI) with a total thickness of 7 cm that are placed on a stack of 30 cm x 30 cm Perspex blocks with total thickness 12 cm, thereby ensuring full backscatter as required by the TG-61 protocol. The in-air kerma measurements were performed with a PTW TN30013 Farmer-type ionisation chamber connected to a PTW UNIDOS-E T10010 electrometer. Based on individual output factor measurements for each of the different sample holders, a simple program was provided to compute the tube current and exposure time to use in order to deliver a given dose to the samples. The overall dose uncertainty for the T25 flask is less than 2.1% for exposure times greater than 12 s. The average dose rate for the T25 flask (for the standard setup in the 250 kVp beam) is 0.685 Gy/min for a tube current of 16 mA. The X-ray tube was set up according to standard procedure with all the necessary safety protocols in place to comply with NRF iThemba LABS radiation protection regulations.



**Figure 29: PXi Precision X-ray machine at NRF iThemba LABS.** A) The overview of the X-ray machine. B) The control panel. The green arrow indicates the start button of the X-ray and the yellow button indicated the emergency stop button for the X-ray. C) T25 flask in the field view indicated by the purple arrow and the red arrow indicate the SSD.





## 2.8. Cell counting for biological experiments to assess the radiation damage post X-ray irradiation

### 2.8.1. Primary NHDF

The number of NHDF cells were quantified with a TC 20™ Automated Cell Counter, Bio-Rad Laboratories, Inc, Hercules, California, United States. Trypan blue dye is a water soluble, azo dye, and differentiates between viable and non-viable cells. In principle, the viable cells possess an intact cell membrane and are impermeable to the dye, while on the other hand, non-viable cells are permeable to the dye so the cytoplasm is stained blue (Strober, 2001). According to standard procedure, the cell pellet was resuspended in cFGM and 10 µL cell suspension with 10 µL trypan blue was mixed gently but thoroughly by pipetting. Thereafter, 10 µL/chamber was loaded onto the counting slide by placing the pipet tip at a 45° angle at the loading area of the slide and the sample was loaded through capillary action (**Figure 30 A**). Samples were measured in a range of 4 – 25 µm to ensure all cell sizes were recorded since fibroblasts have a variable morphology description (**Figure 30 B**). A slide was used per sample to obtain 2 recordings and an average of live counted cells based on the trypan blue assessment/final volume of cell suspension (**Figure 30 C**) was used to seed the desired number of cells based on the assay requirement.



**Figure 30: Bio-Rad, TC 20™ Automated Cell Counter.** A) Cell suspension mixed with trypan blue and loaded on a counting slide. B) A range of 4 – 25 µm was set to count the cells. C) A graphic display of cells counted.

### 2.8.2. Primary EDF

The EDF cell numbers for seeding were determined by using a haemocytometer and counted with a light microscope (Zeiss Primovert), to seed the desired number of cells based on the assay requirement since no automated cell counter is available at NRF iThemba LABS. The EDFs were re-suspended with cEMEM after centrifugation and thereafter mixed with trypan blue dye in a 1:1 ratio and loaded onto the counting chamber. All 4 quadrants (upper left quadrant: Q1, upper right quadrant: Q2, lower left quadrant: Q3 and lower right quadrant: Q4) of the haemocytometer were counted and an average of live counted cells was used to seed the desired number of cells as per assay requirement. The hemacytometer counting grid is 3 mm × 3 mm in size. The grid contains 9 squares with a subdivision width of 1 mm for each quadrant. The following calculations were completed in order to achieve seeding densities:

$$\left(\frac{Q1 + Q2 + Q3 + Q4}{4}\right) \times 20\,000 = \text{average live cells}/1\text{ mL}$$

$$\begin{aligned} \text{average live cells}/1\text{ mL} \times \text{final volume of cell suspension} \\ = \text{average live cells}/\text{final volume} \end{aligned}$$



## 2.9. X-ray standardisation

A standardisation test was done with the different X-ray machines at GSI and NRF iThemba LABS to compare the radiation qualities with one another to ensure a reliable comparison on the investigation of the DNA damage response between the NHDFs irradiated by GSI and the EDFs irradiated by iThemba LABS. A Chinese Hamster Ovary (CHO-K1) cell line was used to carry out this test. CHO-K1 is an epithelial cell line derived from the sub clone from the original biopsy of an adult's Chinese hamster ovary. CHO-K1 cells are widely used in toxicology studies and they are immortalised cells but not neoplastic (Wang *et al.*, 2018).

The CHO-K1 cells were cultured under standard conditions with Roswell Park Memorial Institute (RPMI) 1640 media supplemented with 10% FBS and 1% P/S. A CSA was carried out with the CHO-K1 cells for the comparison between the X-ray machines at the different institutions.

A CSA is a colony survival assay which is widely used in radiobiology studies. The *in vitro* assay determines the ability of a single cell to form a colony which consists of at least 50 or more cells per colony (Franken *et al.*, 2006). The CSA is used to assess the differences in reproductive viability. In other words, the capacity of cells to produce progeny, between control untreated cells and cells that have undergone treatments such as exposure to IR (Rafehi *et al.*, 2011). Only a fraction of seeded cells retains the capacity to produce colonies. Before treatment, cells were seeded out in appropriate dilutions to form colonies in 2 weeks and dose-survival curves depicted on GraphPad were obtained by using the linear quadratic cell death model.

The CHO-K1 cells were sub-cultured (passage 27 and 24 at GSI and NRF iThemba LABS, respectively), counted and seeded as listed in **Table 2** based on previous experiments (Cunningham *et al.*, 2021). The T25 flasks were seeded in 3 T25 flasks for IR exposure and in 4 T25 flasks for the control sample. The T25 flasks were incubated under standard conditions for 4 h to allow single cell attachment. After 4 h, T25 flasks were irradiated (**Table 2**) and incubated for 5 days. After 5 days, the media was removed and the T25 flasks were stained with 3 mL 3× methylene blue for 20 min. Thereafter, the stain was removed and the T25 flasks were washed gently with dH<sub>2</sub>O. The T25 flasks were set to air dry and once dry, the colonies were counted/scored.

Methylene blue 3× consists of 300 mL methylene blue solution, 90 mL 0.1% Potassium Hydroxide (KOH) and 50 mL methanol adjusted to 1 L dH<sub>2</sub>O. The solution was mixed in a glass beaker and filter with paper filter.

**Table 2: CHO-K1 standardisation seeding density test.** CSA seeding density for CHO-K1. Cells were seeded in 3 T25 flasks for doses 2 – 8 Gy and in 4 T25 flasks for the control sample.

Seeding density (cells/T25 flask)	Dose (Gy)
250	0
250	2
500	4
5 000	6
10 000	8



## 2.10. Clonogenic survival assay (CSA)

The same method applies as described in Section 2.9

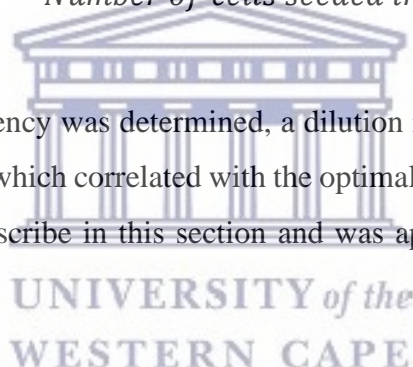
### 2.10.1. Plating efficiency determination of NHDFs

Initially the plating efficiency of the NHDF cells (passage 4) was determined by harvesting the cells according to standard procedure and counting (Section 2.8.1). The NHDFs were seeded as follow: 200-, 400-, 600- and 800 cells/T25 flask in 4 T25 flasks. The flasks were incubated for 14 days with no IR exposure and then stained with 3× methylene blue for 20 min. The same method was applied as described in Section 2.9.

The plating efficiency was determined by the following formula:

$$\text{Plating efficiency} = \frac{\text{Average colonies counted/flask}}{\text{Number of cells seeded in T25 flask}} \times 100$$

Once the optimal plating efficiency was determined, a dilution route was calculated to obtain 200 cells in the control sample which correlated with the optimal plating efficiency determined by the initial experiment as describe in this section and was applied for all experimentation thereafter.



### 2.10.2. Seeding density for IR of NHDFs

To determine the effect of IR exposure on the cells, the NHDF cells were harvested from 1 confluent T25 flask (passage 10) according to standard procedure and counted (Section 2.8.1). Once the average cells numbers were obtained, the sample was diluted to 200 000 cells/tube followed by a dilution route to obtain cell seeded densities as describe in **Figure 31**.

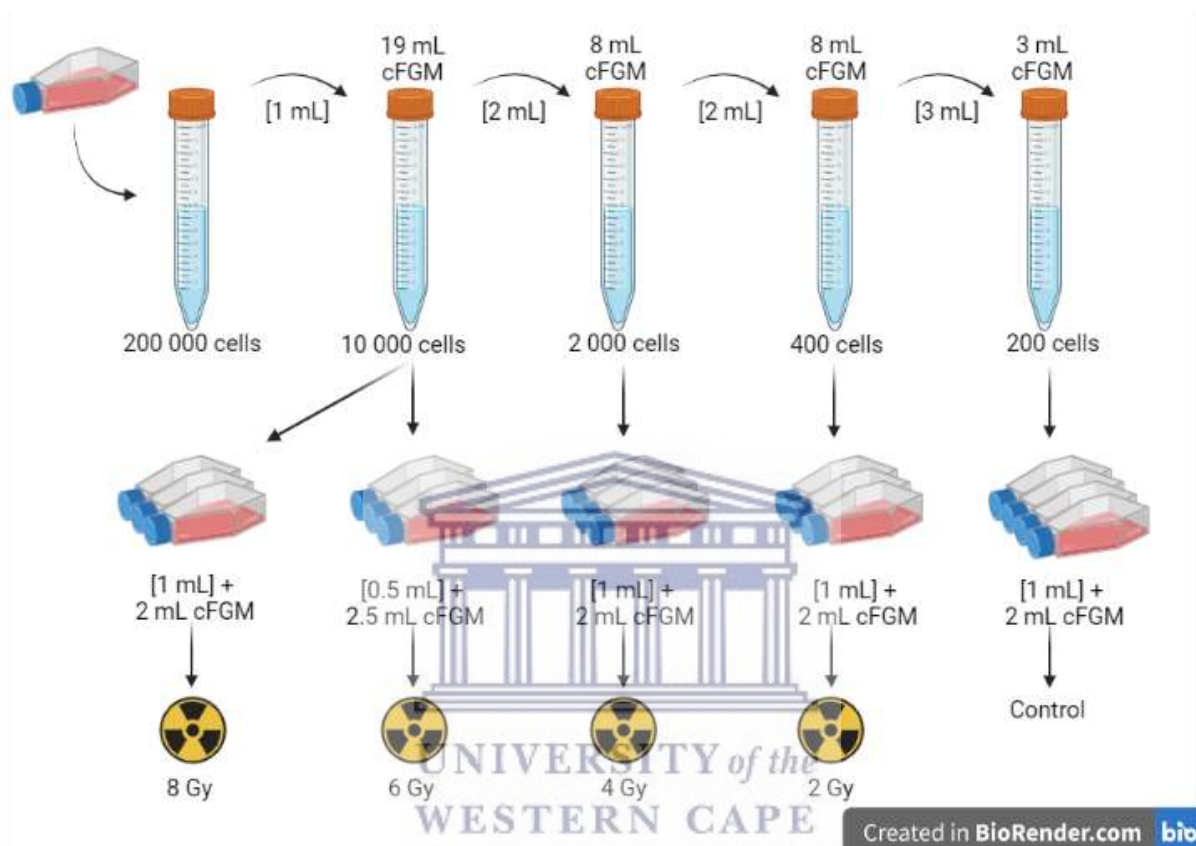


**Figure 31: Seeding densities of NHDF cells and respective IR doses.** Graphical depiction of the NHDF cell line to obtain 200, 400, 2 000, 5 000 and 10 000 NHDF cells/T25 flask for 0, 2, 4, 6 and 8 Gy, respectively. Image created with BioRender.com.

The NHDFs were seeded in 3 T25 flasks for IR exposure and the control was seeded in 4 T25 flasks. The T25 flasks were incubated under standard conditions for 4 h to allow cell attachment. After 4 h, the T25 flask were irradiated for 0, 2, 4, 6 and 8 Gy. The T25 flasks were incubated for 14 days. Thereafter, the cFGM was removed and T25 flasks were stained with 3× methylene blue as describe in Section 2.9.

The survival fraction (SF) was determined by the following formulas:

$$\text{Adjusted cell number with plating efficiency} = \text{Number of cells seeded in T25 flask} \times \text{plating efficiency of the control sample}$$

$$\text{Survival fraction (SF)} = \frac{\text{Average colonies counted}}{\text{Adjusted cell number with PE}}$$

Final analyses were plotted on a dose response curve with GraphPad Prism®.



### 2.10.3. Clonogenic survival assay (CSA) dose response curve

#### 2.10.3.1. Primary NHDF

NHDF cells were harvested (passage 12) according to standard procedure and counted (Section 2.8.1). Once the average live numbers of cells were obtained, the sample was diluted to 200 000 cells/tube followed by a dilution route to obtain cell seeded densities as describe in **Table 3** based on the same principle as in **Figure 31**.

**Table 3: Seeding densities of NHDFs and respective IR doses to plot a CSA dose response curve.** Cells were seeded in 3 T25 flasks for doses 1 – 8 Gy and in 4 T25 flasks for the control sample.

Seeding density (cells/T25 flask)	Dose (Gy)
200	0
400	1
400	2
2 000	4
4 000	5
8 000	6
10 000	7
20 000	8

UNIVERSITY of the  
WESTERN CAPE

The NHDFs were seeded in 3 T25 flasks and 4 T25 flasks for IR exposure and no IR exposure, respectively. The T25 flasks were incubated under standard conditions for 4 h to allow cell attachment.

After 4 h, T25 flask were irradiated and incubated for 14 days. After 14 days, the cFGM was removed and T25 flasks were stained with 3× methylene blue as describe in Section 2.9. Results were plotted with GraphPad Prism® to obtain a NHDF CSA dose response curve.

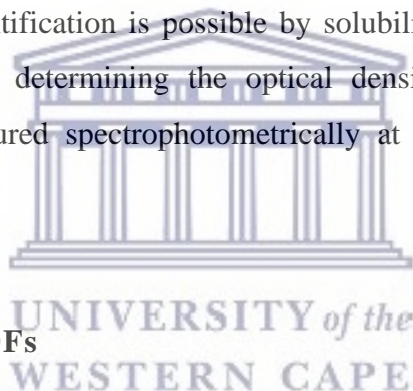


### 2.10.3.2. Primary EDF

The EDFs were harvested (passage 10) according to standard procedure and counted (Section 2.8.2). The same dilution route and seeding density was followed as indicated in **Table 3** for NHDF cells and experiment termination and staining were followed as mentioned above in Section 2.9. to obtain an EDF CSA dose response curve.

## 2.11. Proliferation assay

Quantification of the difference between cell proliferation and cell death can be determined by using the crystal violet assay. Crystal violet is a triarylmethane dye that binds to, and stain proteins and DNA of viable cells, to quantify the number of monolayer cells within a sample. For the crystal violet assay the absorbance of the solution containing the dye incorporated into the DNA of the cells is used to quantify the number of cells allowing for rapid, accurate and reproducible quantification of cell numbers grown in 96-well plates (Aslantürk, 2017; Vega-Avila & Pugsley, 2011). Quantification is possible by solubilising the absorbed dye into a solution of triton X-100 and determining the optical density using spectrophotometry. Absorbance of the dye measured spectrophotometrically at 570 nm corresponds to cell numbers.



### 2.11.1. Primary NHDFs

The NHDF cells were sub-cultured (passage 12), counted (Section 2.8.1) and seeded according to standard procedures in a 96-well tissue culture plate in triplicate. A 1 000 cells/well were seeded with 200  $\mu$ L cFGM/well under sterile conditions. The plates were incubated for 4 h to allow cell attachment and irradiated with 0, 2, 4, 6, 8 and 16 Gy. After IR, the plates were incubated under standard conditions for 24, 48, 72, 96, 120 and 144 h.

The experiment was terminated by aspirating the cFGM from the 96-well plates. The cells were fixed with 100  $\mu$ L/well of 1% glutaraldehyde in PBS and incubated for 15 min at rt. A 100  $\mu$ L/well of 0.1% crystal violet dye was added and the plates were incubated for 30 min at rt. Afterwards, the stained cells were rinsed with running H<sub>2</sub>O for 15 min and set aside to air dry (**Figure 33**).

Once dry, the plates were treated with 200  $\mu\text{L}$ /well of 0.1% Triton-X 100 in PBS and incubated for 30 min at rt. Triton-X 100 is used to solubilise the crystal violet and lyse the cells to extract proteins and other cellular organelles. Each 96-well plate contained 0.1% Triton-X 100 in column 1, which primarily served as the blank (**Figure 32**). From the crystal violet stained 96-well plate, a 100  $\mu\text{L}$  of the 0.1% Triton-X 100 solution was transferred, using reverse pipetting, to a new 96-well flat bottom plate. The plates were read with a UV-visible spectrophotometer, BioTek®, Winooski, Vermont, USA. The wavelength was set at 570 nm and optical densities (OD) were recorded via the Gen5™ microplate reader and imager software (version 1.11).

The observed OD were standardised and expressed as percentage as indicated below:

$$\frac{x}{\text{average of control}} \times 100$$

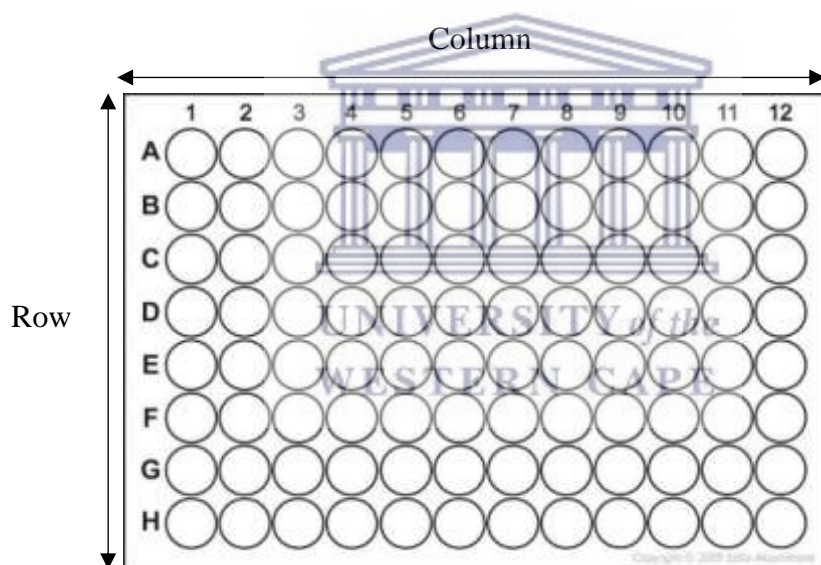


**Figure 32: Schematic representation of a 96 well plate.** Column 1, row A – H served as the blank for all experimentations. The remaining wells were used for the samples (Templates, no date).

Results display the comparison of the control (expressed as 100%) with the proliferation capacity of cells exposed to IR. The amount of crystal violet staining in the assay is directly

proportional to the cell biomass that is attached to the plate, meaning the live cells who remained attached during staining.

Results were used to obtain the best optimal time point/s to carry out with the EDF cell proliferation assay and the MTS assay.

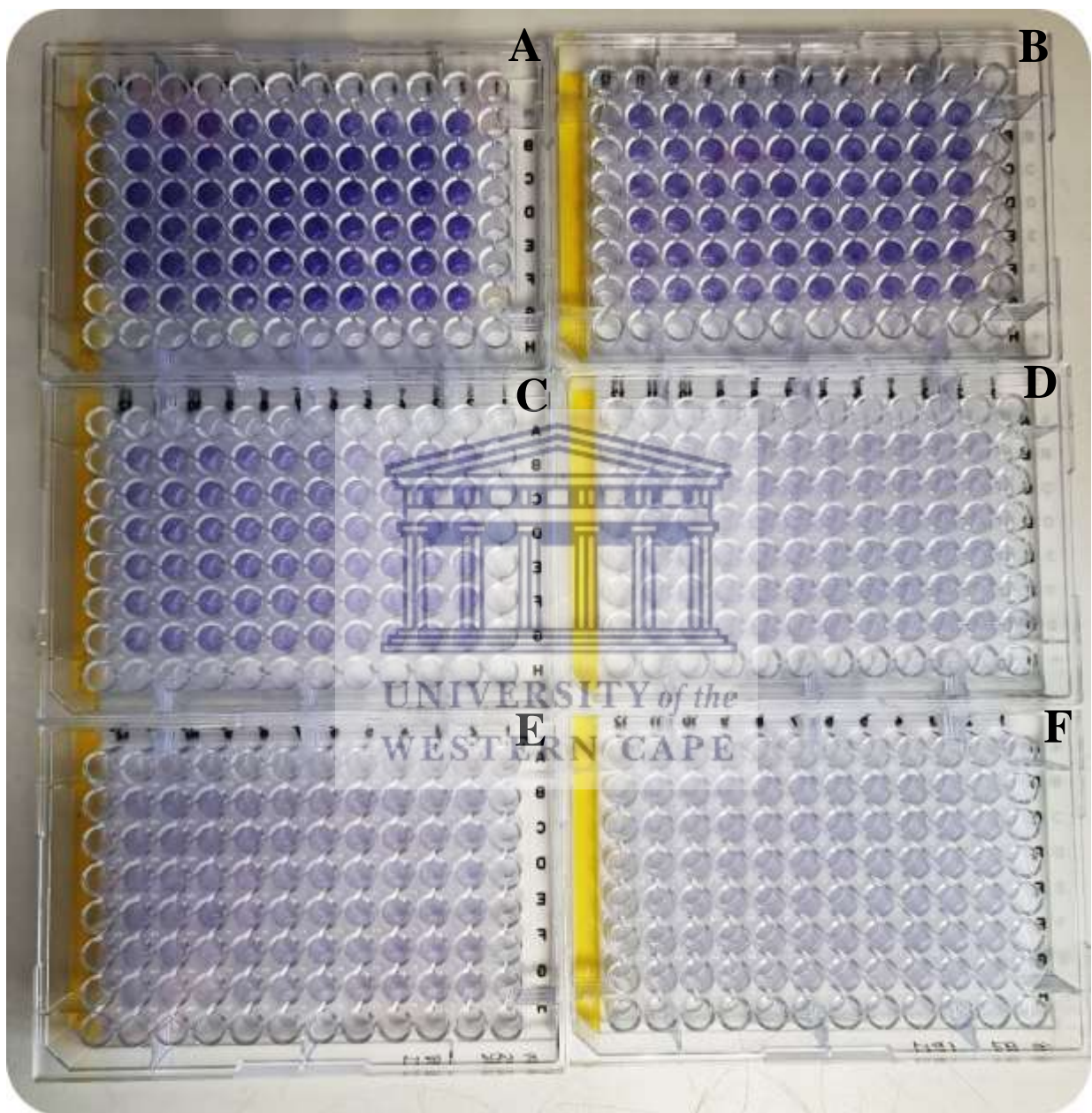


**Figure 33: The 96-well plates for 72 h post IR after crystal violet stain. A) 0 Gy, B) 2 Gy, C) 4 Gy, D) 6 Gy, E) 8 Gy and F) 16 Gy.**

### 2.11.2. Primary EDFs

The EDFs were treated the same as mentioned above in Section 2.11.1. (passage 13). EDFs were irradiated with 0, 2, 4, 6, 8 and 16 Gy irradiations and incubated under standard conditions for 72 and 120 h. OD at NRF iThemba LABS were obtained with a UV-visible spectrophotometer plate reader Apollo 11 and Apollo 11 PhotoRead software (Berthold Technologies, Bad Wildbad, Baden-Württemberg, Germany).

### 2.12. MTS assay

The MTS assay uses a colorimetric method for the sensitive quantifications of viable cells. The protocol is based on the reduction of the MTS (3-[4,5-dimethylthiazol-2-yl]-5-[3-carboxymethoxyphenyl]-2-[4-sulfophenyl]-2H-tetrazolium) tetrazolium compound by viable mammalian cells to generate a coloured formazan dye that is soluble in cell culture media. This conversion is carried out by nicotinamide adenine dinucleotide phosphate dependent dehydrogenase enzymes in metabolically active cells. The MTS reagent is negatively charged and does not readily penetrate the cells, but rather uses an intermediate electron acceptor that can transfer electrons from the cytoplasm or plasma membrane to facilitate the reduction of the tetrazolium into a coloured formazan product. The formazan dye is quantified by measuring the absorbance (Riss, Niles & Minor, 2004; Wang *et al.*, 2021a).

#### 2.12.1. Primary NHDF

The NHDF cells were seeded (passage 14) according to standard procedures, in a 96-well tissue culture plate in triplicate. A total of 1 000 cells/well was seeded in 200  $\mu$ L cFGM/well under sterile conditions. The plates were incubated for 4 h to allow cell attachment and subsequently irradiated with 0, 2, 4, 6, 8 and 16 Gy. After IR, the plates were incubated under standard conditions for 72 and 120 h, respectively. The selection of these 2 time points was based on the results obtained with the cell proliferation assay described in Section 2.11.

After 72 and 120 h, 20  $\mu$ L MTS reagent/well was added and the plates again incubated for 2 h under sterile conditions (**Figure 34**). The plates were briefly shaken and the absorbance was measured at 490 nm. The plates were read with a UV-visible spectrophotometer, BioTek®, and OD were recorded accordingly via the Gen5™ microplate reader and imager software (version

1.11). The observed OD were converted and expressed as percentage. The control sample was expressed as a 100% and compared with the cell viability with IR exposers.

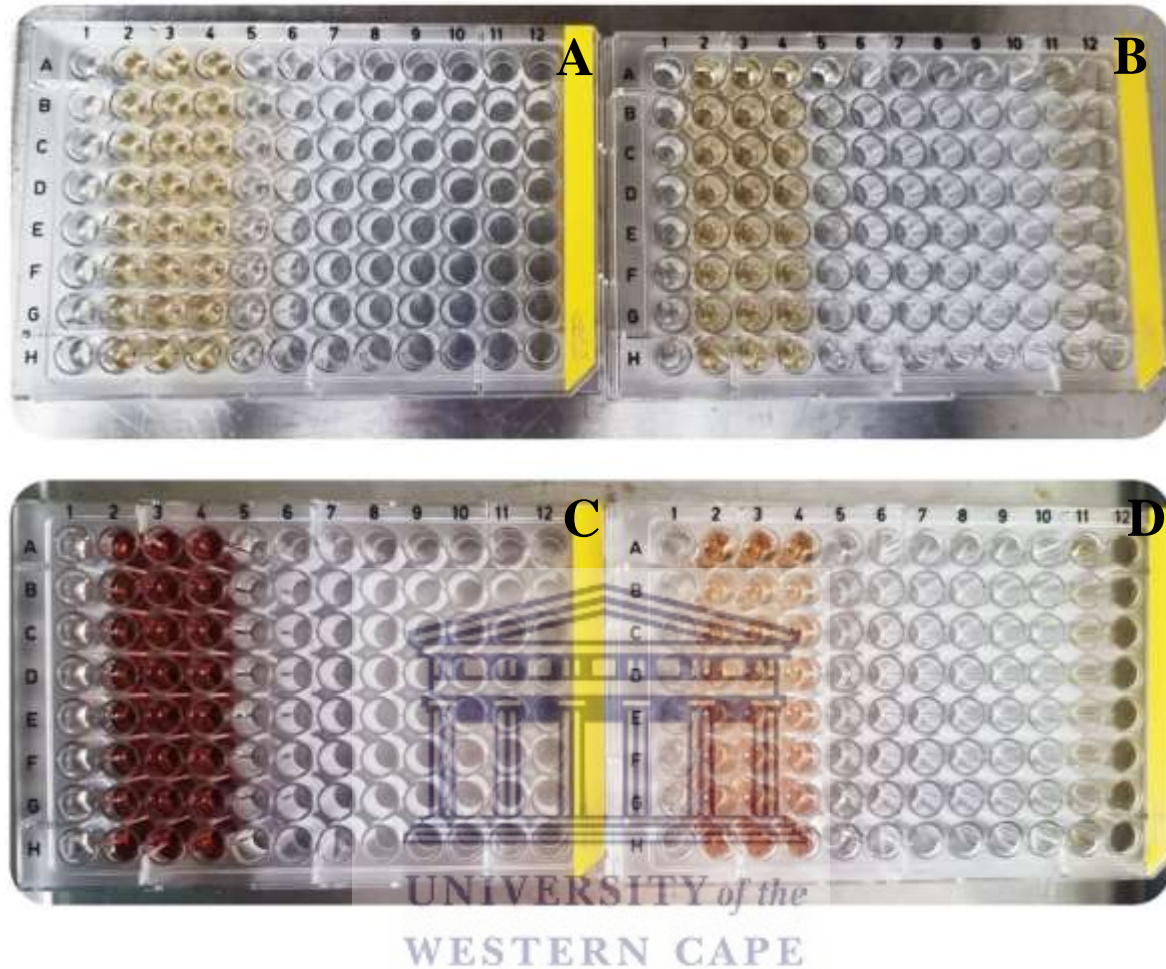


**Figure 34:** The 96-well plates for 120 h post IR with MTS reagent colour observed before (A – B) and after the 2 h incubation period (C – D). A) 0 Gy, 120 h, and MTS reagent colour observation before incubation, B) 16 Gy, 120 h, and MTS reagent colour observation before incubation, C) 0 Gy, 120 h, and MTS reagent colour observation after 2 h incubation, and D) 16 Gy, 120 h, and MTS reagent colour observation after 2 h incubation.

### 2.12.2. Primary EDF

The MTS assay was not performed with the EDFs due to shipment delays of consumables to South Africa.

### 2.13. Flow cytometry

The principle of flow cytometry is based on the analysis of single cells as they flow past a single/multiple laser(s) while suspended in a buffered salt-based solution. The cells are analysed for visible light scatter and one/multiple fluorescence parameters. The visible light scatter is measured in 2 different directions, namely: the Forward Scatter (FSC) and the Side Scatter (SSC) (**Figure 35**). FSC indicate the relative size of the cell, whereas SSC at 90° indicated the internal complexity or granularity of the cell. The intensity of the light scatter is dependent on the fluorescence. The underlying principle of flow cytometry is related to light scattering and fluorescence emission, which occurs as light from the excitation source (a laser beam) that strikes the moving particles (Abraham & Staffurth, 2016; McKinnon, 2018).

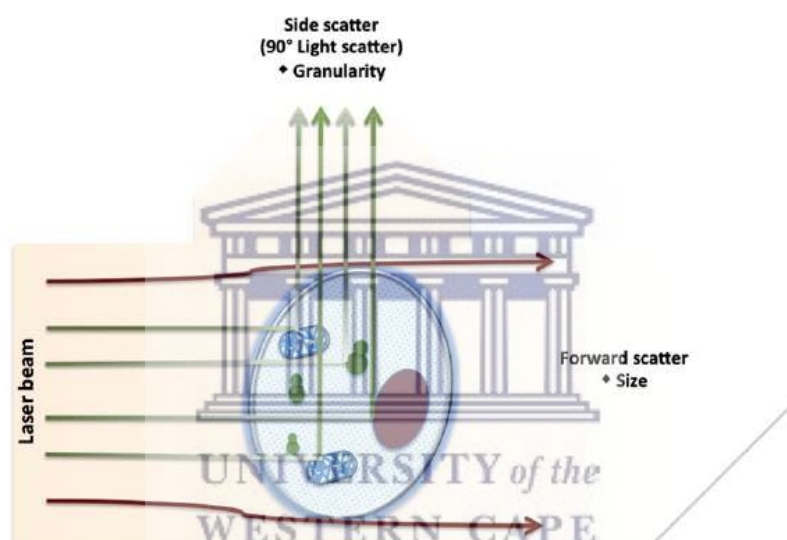


**Figure 35: Light scattering via flow cytometer.** FSC is relative to cell size, while SSC is relative to cell granularity of internal complexity (Abraham & Staffurth, 2016).

Both apoptosis and cell cycle analysis were done via flow cytometry at GSI with a CytoFlex S system (Beckman Coulter, Inc, Life Science, Brea, California, USA) and at NRF iThemba LABS with a BD Accuri™ C6 (BD Biosciences, San Jose, California, USA). The fluorescence counts were captured and graphically depicted in a dot graph representing the respective amounts of scattering cells.

### 2.13.1. Apoptosis assay

In apoptotic cells, the membrane phospholipid phosphatidylserine (PS) is translocated from the inner to the outer leaflet of the plasma membrane thereby exposing PS to the external cellular environment. Annexin V is a 35 – 36 kDa calcium ion dependent phospholipid-binding protein that has high affinity for PS and binds to cells exposed to PS. Annexin V may be conjugated with fluorochromes including phycoerythrin (PE). This format remains its high affinity for PS and serves as a sensitive probe for flow cytometric analysis of the cells that are undergoing apoptosis (Demchenko, 2013; Lakshmanan & Batra, 2013). Annexin V-PE and 7-AAD were used at GSI, while Annexin V-FITC (fluorescein isothiocyanate) and propidium iodide (PI) were used at NRF iThemba LABS to evaluate early and late apoptosis.

PE-Annexin V/Annexin V fluorescein isothiocyanate (FITC) staining leads up to the loss of membrane integrity which accompanies the latest stages of cells death resulting from either apoptotic or necrotic processes. PE-Annexin V is used in conjunction with a vital dye, 7-Amino-Actinomycin (7-AAD), or with PI to identify early apoptotic cells. Both 7-AAD and PI are a plasma membrane permeability markers used in conjunction with PE-Annexin V/Annexin V FITC (Wlodkowic *et al.*, 2011). Viable cells with intact membrane exclude 7-AAD/PI. For example, cells are considered viable when both PE Annexin V/Annexin V FITC and 7-AAD/PI are negative while cells that are in early apoptosis are PE-Annexin V/Annexin V FITC positive and 7-AAD/PI negative, while cells that are in late apoptosis or already dead are both PE-Annexin V/Annexin V FITC and 7-AAD/PI positive. This assay does not distinguish between cells that have undergone apoptotic death vs those that have died as a result of a necrotic pathway because in either case, the dead cells will stain with both PE-Annexin V/Annexin V FITC and 7-AAD/PI. When apoptosis is measured over time, cells can be tracked from PE-Annexin V/Annexin V FITC and 7-AAD/PI negative (viable, or no measurable apoptosis), to PE Annexin V/Annexin V FITC and 7-AAD/PI positive (end stage apoptosis and death). The movement of cells through these 3 stages suggest apoptosis (Rieger *et al.*, 2011).

The gating strategy was done using FlowJo™ and all the cell debris and doublets were excluded by means of cell gating. A cell gate was placed on the FSC- vs SSC-Area dot plot graph (**Figure 36 A**) followed by placing a single cell gate on the FSC-Area vs FSC-Height dot plot graph (**Figure 36 B**). The single cell gate was plotted on 7-AAD/PI vs PE-Annexin V/Annexin V FITC graph and was divided into 4 quadrants (**Figure 36 C**) representing live cells, early

apoptosis, late apoptosis and necrosis. Q1: PE-Annexin V/Annexin V FITC and 7-AAD/PI negative representing the live cells, Q2: PE-Annexin V/Annexin V FITC positive and 7-AAD/PI negative representing the early apoptosis, Q3: PE-Annexin V/Annexin V FITC and 7-AAD/PI positive representing late apoptosis and Q4: PE-Annexin V/Annexin V FITC and 7-AAD/PI negative representing necrotic cells.

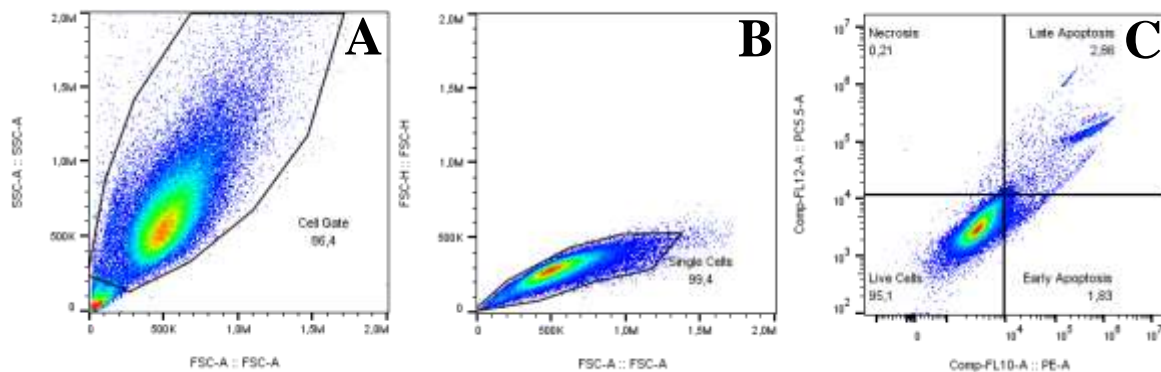
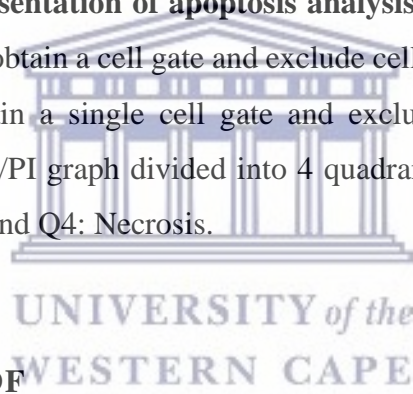


**Figure 36: Graphically representation of apoptosis analysis done in FlowJo™.** A) FSC- vs SSC-Area dot plot graph to obtain a cell gate and exclude cell debris. B) FSC-Area vs FSC-Height dot plot graph to obtain a single cell gate and exclude doublets. C) PE-Annexin V/Annexin V FITC vs 7-AAD/PI graph divided into 4 quadrants. Q1: Live cells, Q2: Early apoptosis, Q3: Late apoptosis and Q4: Necrosis.



### 2.13.1.1. Primary NHDF

Exponentially growing NHDF cells were sub-cultured (passage10) and seeded into T25 flask (500 000 cells) in duplicates according to standard procedures. The NHDFs were incubated for 48 h and thereafter exposed to 0 and 8 Gy irradiation. The T25 flasks were incubated after IR for 12, 24 and 48 h.

After the appropriate time periods, the old cFGM was transferred from the T25 flask under sterile conditions to a 15 mL conical tube. The T25 flasks were sub-cultured, and the cell solution was transferred to the same 15 mL conical tube and centrifuged for 200 g-force for 5 min at 4°C. The NHDF cells were washed twice with 1 mL PBS, centrifuged and stained. The cell pellet was resuspended in 200 µL 1× annexin binding buffer and a 100 µL was transferred to Eppendorf tubes. Stock solution of 10× annexin binding buffer was made with 0.1 M HEPES (pH7.4), 1.4M Sodium Chloride (NaCl) and 25 mM Calcium Chloride (CaCl<sub>2</sub>).



Subsequently, a working solution was made to obtain a 1× Annexin binding buffer with dH<sub>2</sub>O. Thereafter 3 µl PE-Annexin V and 3 µl 7-AAD were added to the samples. Samples were mixed carefully and incubated for 20 min at rt in the dark. After the incubation period, 200 µL of 1× annexin binding buffer was added to each sample. Fluorescence-activated single cell sorting (FACS) measurements were done within 1 h on a CytoFlex S system. The samples were read with a laser at a wavelength of 488 and 561 nm via the fluorescence channel (FL) of 690/50 band pass for PC5.5 (Phycoerythrin-Cy<sup>TM</sup>5.5 tandem dye) which represents 7-AAD. PE-Annexin V, was read at 561 nm via the FL of 585/42 band pass. The FACS analysis were done at a flow rate of 60 µL/min.

#### **2.13.1.2. Primary EDF**

EDFs (passage 7) were treated the same as mentioned above in Section 2.13.1.1. The EDF cells were stained with Annexin V-FITC and PI. The FACS measurements were done within 1 h on the BD Accuri<sup>TM</sup> C6 flow cytometry with a flow rate of 66 µl/min. The samples were read with a laser at a wavelength of 488 nm via filters 670 long pass, 610/20 (detector FL3) for PI. Annexin V-FITC was read at 488 nm via filters 533/30 (detector FL1).



### 2.13.2. Cell cycle assay

Flow cytometry was used for cell cycle analysis to show possible changes in the distribution of cells in G0/G1, S and G2/M cell cycle phase after IR. The flow cytometric quantification of the different phases of the cell cycle is mainly based on the DNA content by staining with a DNA binding fluorochrome, namely PI (Whaley *et al.*, 2021). There is a direct correlation to the amount of DNA within a specific cell population and different quantities of the DNA is expressed during different phases of the cell cycle, making the various phases distinguishable and provides quantitative data (McKinnon, 2018).

In FlowJo™ the cell debris and doublets were excluded by using cell gating. First the cell gate was placed on the FSC- vs SSC-Area dot plot graph (**Figure 37 A**) and secondly a single cell gate was placed on the FSC-Area vs FSC-Height dot plot graph (**Figure 37 B**). Thereafter a histogram was plotted to distinguish the different cell cycle phases (**Figure 37 C**).

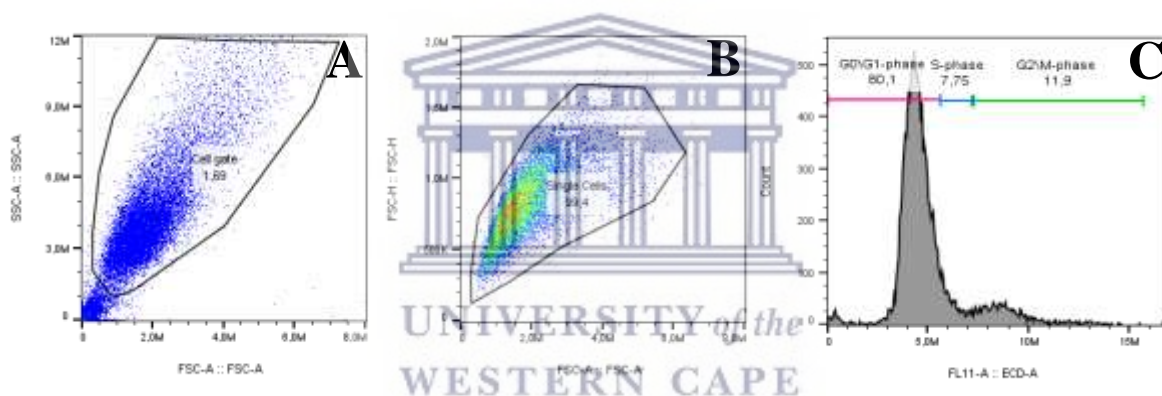


**Figure 37: Graphically representation of cell cycle analysis done in FlowJo™.** A) FSC- vs SSC-Area dot plot graph to obtain a cell gate and exclude cell debris. B) FSC-Area vs FSC-Height dot plot graph to obtain a single cell gate and exclude doublets. C) Histogram representing G0/G1, S and G2/M phase.

### 2.13.2.1. Primary NHDF

Exponentially growing NHDF cells were sub-cultured at passage 14 and seeded into T25 flask (200 000 cells/T25 flask) according to standard procedure. The NHDFs were incubated for 48 h and thereafter exposed to 0, 4, 8, 12 and 16 Gy irradiation. The T25 flasks were incubated after IR for 0, 24 and 48 h.

After the appropriate time periods, the cFGM were transferred from the T25 flask under sterile conditions to a 15 mL conical tube. The T25 flasks were sub-cultured according to standard procedure and the cell solution was transferred to the same 15 mL conical tube. Subsequently, centrifuge at 200 g-force for 5 min at 4°C. The supernatant was aspirated and the NHDFs were washed with 2 mL PBS and centrifuged. The supernatant was aspirated and the cells were fixed with 2 mL ice cold 80% EtOH in a drop wise manner while vigorously stirring to form a single cell suspension. The samples were incubated on ice for 10 min. Thereafter, the fixed EtOH cells were centrifuged at 400 g-force for 5 min at 4°C. The supernatant was aspirated, and the cell pellet was resuspended in 50 µL cold PBS and transferred to an Eppendorf tube. Both Ribonuclease A (Rnase A) and PI were diluted in PBS, a 1:1 000 and 1:10, respectively. Next the cells were stained with a 100 µL of both Rnase A and PI and were incubated for 30 min at 37°C in the dark.

The fixed cell FACS measurements were carried out with a CytoFlex S system within 1 h. FACS measurements was done at a flow rate of 60 µL/min at a wavelength of 561 nm via the 610/20 band pass FL for ECD (Energy Coupled Dye) representing PI.

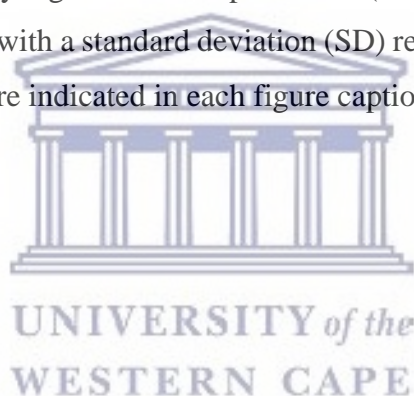
### 2.13.2.2. Primary EDF

EDFs at passage 7 were treated in the same way as mentioned above in Section 2.13.2.1. The EDF cells were stained with 0.5 mL FxCycle™PI/Rnase Staining Solution and incubated for 30 min in the dark at rt. FACS measurements were done with a BD Accuri™ C6 flow cytometry within 1 h with a flow rate of 66 µL/min. PI was measured at a wavelength of 488 nm via filters 670 long pass, 610/20 (detector FL3).

## 2.14. Statistical analysis

All statistical analysis was performed using Microsoft Office Excel 2020 (Microsoft Corporation, Washington DC, USA) and GraphPad Prism® (version 5.01) (GraphPad Software, San Diego, California, USA). The primary EDF growth curve, Td determination, cell proliferation- and MTS assay were standardised before graphically plotted and the 2 latter non-irradiated samples were expressed as 100%. Two-way analysis of variance (ANOVA) with Bonferroni post-test was used for statistical comparison. CSA survival curves were depicted using a linear quadratic cell death model and statistical analysis was performed by way of paired t-test. Apoptosis- and cell cycle assay results were analysed by flow cytometry data by using FlowJo™ version 10.7 (BD Bioscience, USA). Kruskal Wallis test was performed for statistical analysis for the apoptosis assay, while for the cell cycle assay Bonferroni post-tests was used.

A significance level of 0.05 was used in all tests, hence  $p < 0.05$  (\*) were considered statistically significant,  $p < 0.01$  (\*\*) highly significant and  $p < 0.001$  (\*\*\*) extremely significant. Data was reported as average values with a standard deviation (SD) represented by an error bar. The numbers of experiments (n) were indicated in each figure caption were applicable.



# CHAPTER 3:

## RESULTS

---

### Section A: Primary elephant dermal fibroblast (EDF) cell line characterisation

#### 3.1. Primary EDF cell culture

##### 3.1.1. Primary EDF sample collection and outgrowth of fibroblasts

A range of 4 – 6 skin punch biopsies were collected from 6 elephants with a punch biopsy needle. The samples were named as E1, E2, E3, E4, E5 and E6, where each code refers to the specific elephant as listed in **Table 4**.



**Table 4: Elephant sample collection with their respective age and sex.** Elephants' age ranged from 14 – 47 years. Sample collection occurred at 2 locations: Botlierskop Private Game Reserves and Sanbona Wildlife Reserve.

Elephant (E)	Location	Date of sample collection	Age	Sex
E1	Botlierskop Private Game Reserves	25.09.2021	25	Male
E2	Botlierskop Private Game Reserves	19.11.2021	14	Male
E3	Sanbona Wildlife Reserve	16.12.2021	35	Female
E4	Sanbona Wildlife Reserve	16.12.2022	25	Male
E5	Botlierskop Private Game Reserves	15.01.2022	26	Male
E6	Botlierskop Private Game Reserves	16.04.2022	47	Male

The first radial explant outgrowth of the primary EDFs (**Figure 38 A**, yellow arrow) from the biopsy fragment (**Figure 38 A**, green arrow) was visible after 8 – 25 days with an average of  $15.25 \pm 1.48$  days (mean  $\pm$  SD) (**Table 5**). E6 exhibited the fastest explant outgrowth of fibroblasts 8 days after the initial culturing date; followed by sample E5 at 11 days; E1 at 13.25 days; E3 at 19 days and lastly 25 days for E4. The outgrowth of EDFs from the explant source resulted initially in a dense area with high cell numbers, which gradually migrated and spread outward over time.

An overall EDFs explant culture outgrowth success rate of 83.33% was obtained among the 6 elephants. E1 had an overall biopsy success rate of 80%, while E3, E4 and E5 had lower biopsy success rates of 33.33%, and E6 was 25% (**Table 5**). Not all skin punch biopsies of the same elephant resulted in successful cultures and the underlying reason for this variability remains unclear. Unfortunately, E2 exhibited no outgrowth of the biopsy fragment and culture flasks were discarded 40 days after the initial culturing date.

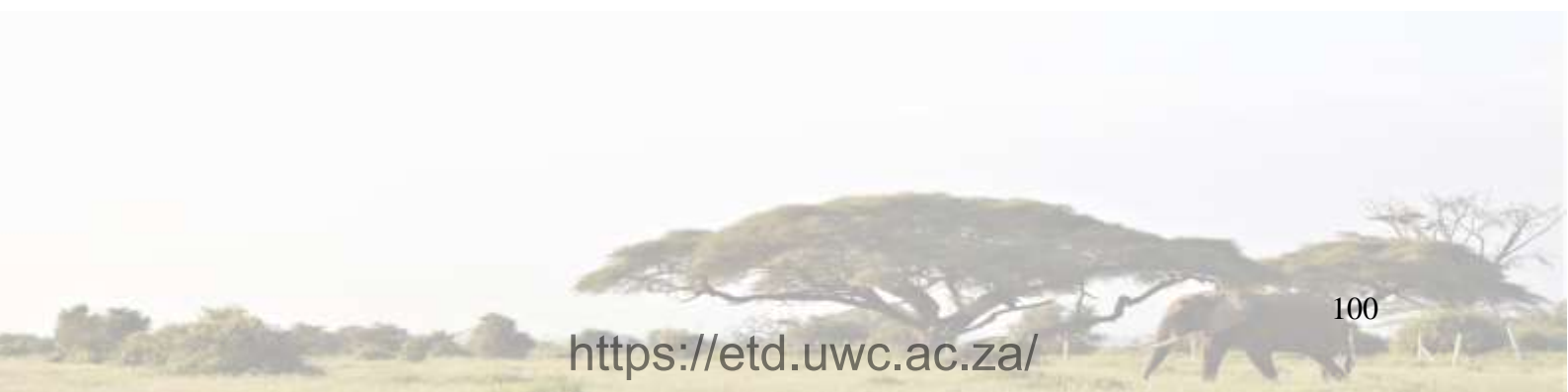
**Table 5: Elephant sample collection and radial explant outgrowth of fibroblasts.** The number of days after first radial explant outgrowth of EDFs. Where no outgrowth of fibroblasts was detected, culture flasks were discarded after 40 days.

<b>Elephant (E)</b>	<b>Biopsy</b>	<b># Number of days after explant outgrowth</b>	<b>Biopsy success (Successful fibroblast visualisation/Total number of biopsies)</b>	<b>Average days until explant outgrowth of EDFs (Average <math>\pm</math> SD)</b>
E1	1	16	4/5	13.25 $\pm$ 3.40
	2	9		
	3	-		
	4	12		
E2	1 - 5	-	0/5	N/A
E3	1	18	2/6	19. $\pm$ 1.20
	2	-		
	3	25		
	4	-		
	5	-		
E4	1	25	2/6	25 $\pm$ 0
	2	-		
	3	25		
	4	-		
	5	-		
	6	-		
E5	1	11	2/6	11 $\pm$ 0
	2	-		
	3	11		
	4	-		
	5	-		
	6	-		

E6	1	8	1/4	8 ± 0
	2	-		
	3	-		
	4	-		



UNIVERSITY *of the*  
WESTERN CAPE





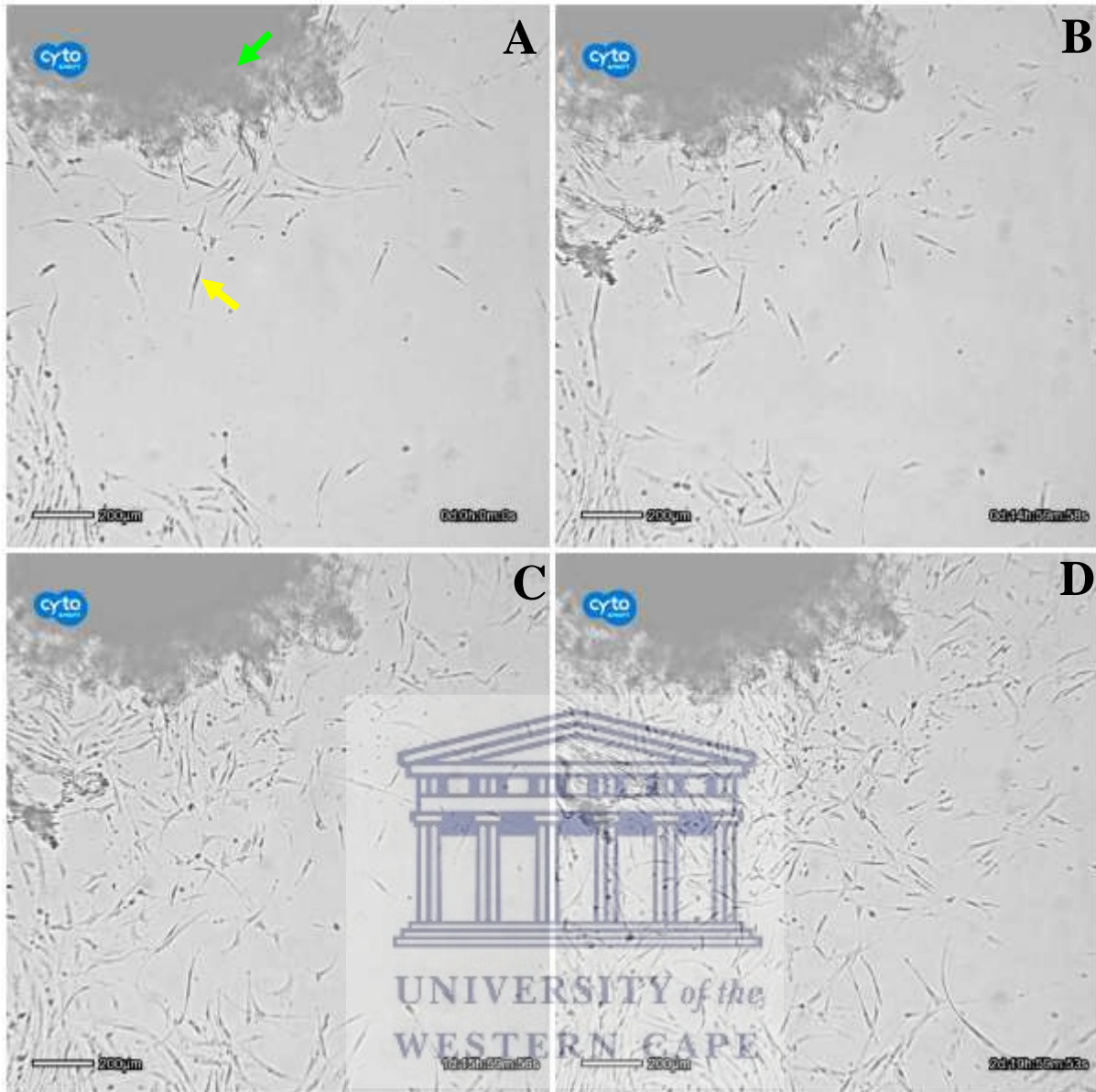


**Figure 38: First radial explant outgrowth of E1 after biopsy fragmentation.** A) The first images were taken of the cells in T25 flasks by the CytoSmart, Lonza® live cell imaging system (scale 200  $\mu\text{m}$ ) after the first visual confirmation of explant outgrowth of fibroblast cells. The green arrow illustrates the elephant biopsy fragment and the yellow arrow illustrates fibroblast cells. B) 15 h, C) 36 h and D) 67 h post initial EDFs confirmation.



### 3.1.2. Primary EDF growth curve

The culture flask confluency of 3 elephant fibroblasts cell lines (E3 – E5) was determined daily with the CytoSmart, Lonza® live cell imaging system over 11 consecutive days. The percentage confluency (y-axis) was plotted in function of the number of days in culture (x-axis). In order to get to a percentage value, the results were standardised before graphically plotted. The fibroblasts of each elephant had their own replication rate and the T25 flasks reached confluency (100%) on day 12, 17 and 11 for E3, E4 and E5, respectively.

The confluency for of all samples increased gradually over time and was on average  $76.45\% \pm 26.56\%$  (average  $\pm$  SD) on day 11 as presented in **Figure 39**.

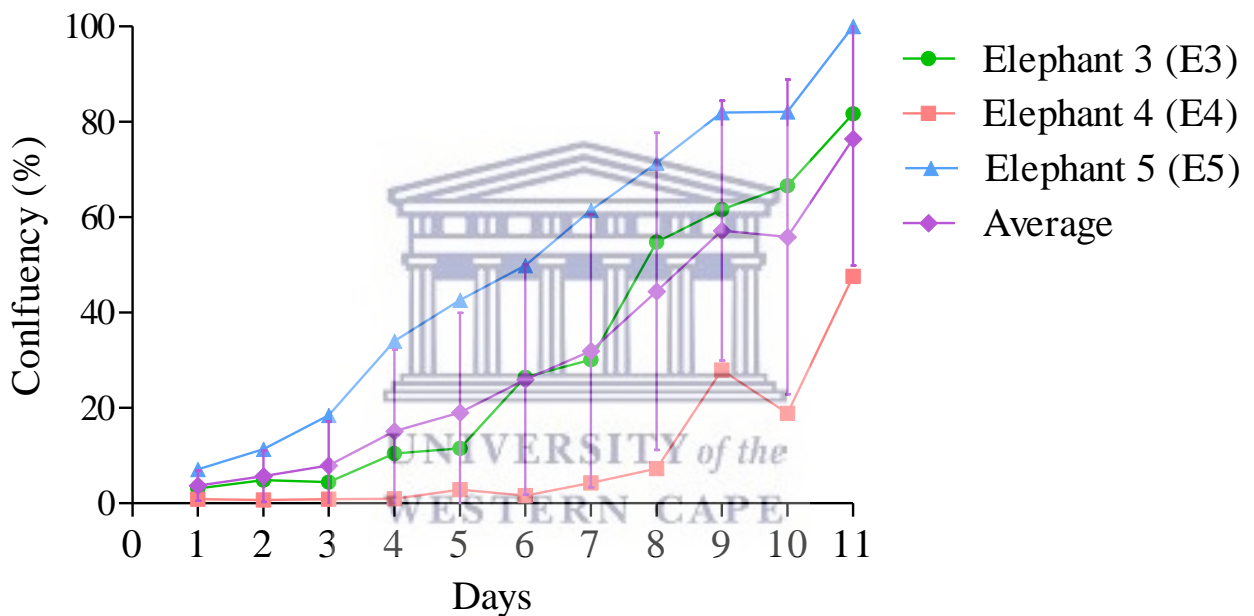


**Figure 39: Growth curve of E3, E4 and E5 determined with CytoSmart, Lonza® live cell imaging system for 11 consecutive days.** The percentage confluency captured over 6 regions of a T25 flask over 11 consecutive days was plotted for E3, E4 and E5. The average confluency for the 3 elephants was  $76.45\% \pm 26.56\%$  (average  $\pm$  SD) on the final day of imaging. The error bars represent the SD (n = 3).

### 3.1.3. Primary EDF doubling time (Td)

Based on the confluency algorithm of the live cell imaging system, CytoSmart, Lonza®, the Td was calculated within the 6 regions of a T25 flask over 6 consecutive days. At passage 1, E3, E4 and E5 had a Td of 53.90, 65.61 and 66.86 h, respectively. This results in an average Td of  $62.13 \pm 7.15$  h (average  $\pm$  SD) for the 3 elephants (**Figure 40**).

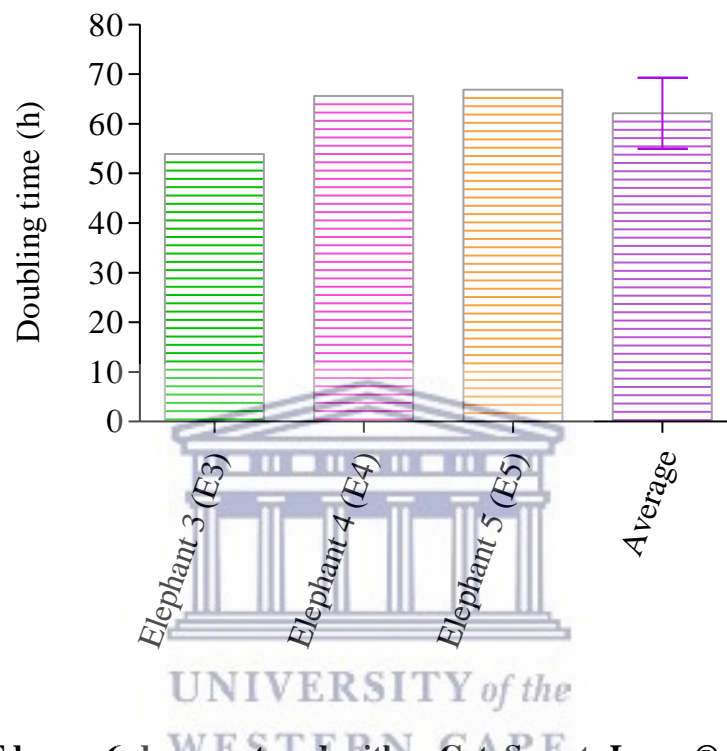


**Figure 40: EDF Td over 6 days captured with a CytoSmart, Lonza® live cell imaging system. E3, E4 and E5 at passage 1 with a Td of 53.90, 65.61 and 66.86, respectively and an average Td of  $62.13 \pm 7$  h (average  $\pm$  SD). The error bars represent the SD (n = 3).**

### 3.2. Metaphase chromosome spread

Once the primary EDF cultures were established, the protocol to obtain a metaphase chromosome spread of the African savanna EDFs was established. A variety of conditions were applied and tested in order to obtain the metaphase chromosome spread of E1.

The EDFs of E1 were in an exponential growth phase throughout all the passages which were used to test the different treatment conditions as presented in **Table 6**. The number of metaphase chromosome spread was manually counted using a Zeiss Primovert under 10× magnification. As the results in **Table 6** indicates, a higher density of EDFs present in the culture flask allowed a higher number of metaphase chromosome spreads. However, it should be noted that the slide evaluation at 10× magnification did not allow to score the number of chromosomes per metaphase, so the number presented in the last column of **Table 6** are only an indication of the working mechanisms of the KaryoMAX™ Colcemid™ and to check if longer exposure times resulted in more metaphases. Further experiments will be needed to evaluate the impact of the time of KaryoMAX™ Colcemid™ exposure and concentration on the quality and completeness of the metaphase chromosome spreads.



**Table 6: The time and cell density conditions applied in obtaining metaphase chromosome spreads.** Cells from E1 were exposed to KaryoMAX™ Colcemid™ at and had a cell density of 70 – 80%, 60 – 70% and 90 – 95%, respectively. A working concentration of 0.05 µg/mL KaryoMAX™ Colcemid™ was added for 3 – 28 h to prevent the EDFs from proceeding to anaphase.

Confluency of EDFs in culture	Time (h)	Number of metaphases
70 – 80%	3	122
	6	192.5
60 – 70%	6	32
	15	274
	24	49.5
	28	29
90 – 95%	3	414
	6	372
	12	543
	24	378

Even though 12 h KaryoMAX™ Colcemid™ yielded the highest number of metaphases, the quality of metaphase chromosome spread decreased with longer KaryoMAX™ Colcemid™ incubation times as what is known in literature. However, as stated previously, further investigations are needed to evaluate the completeness and quality of the metaphase spread for different KaryoMAX™ Colcemid™ exposure scenarios. **Figure 41** represents 2 metaphase chromosome spreads after 3 h KaryoMAX™ Colcemid™ exposure at an EDF density of 90 – 95%.

**Figure 41** metaphase chromosome spreads confirm the diploid number of 56 chromosomes in the *L. Africana* (Frönicke *et al.*, 2003; Hungerford *et al.*, 1966; Yang *et al.*, 2003).

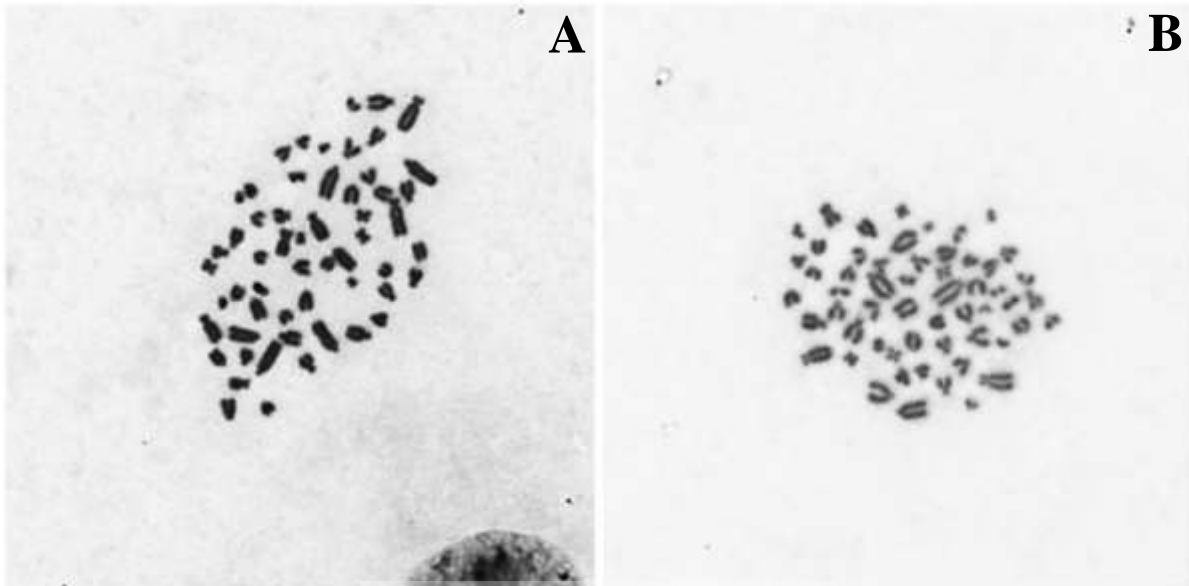
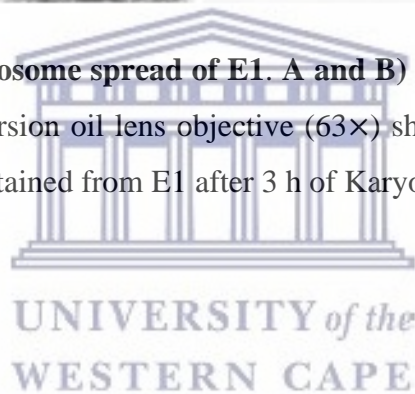


**Figure 41: Metaphase chromosome spread of E1. A and B)** Images were captured using a Metafer 4 platform with immersion oil lens objective (63 $\times$ ) showing a diploid chromosome number of 56 chromosomes obtained from E1 after 3 h of KaryoMAX<sup>TM</sup> Colcemid<sup>TM</sup>.



### 3.3. Cell synchronisation and mitotic index (MI)

Cells from E6 were used to determine the duration of the different cell phases of these fibroblasts. HU was added to the EDF cultures for a period of 36 h to block the cells at G1/S. The block was washed out and the cells were left for 24 h. The coverslips with the cells were removed every 2<sup>nd</sup> h for the 1<sup>st</sup> 6 h and thereafter removed hourly over a period of 24 h.

A MI of <1% is indicative of cells residing in the S phase after removal of a block. In **Figure 42**, the MI 24 h post block removal was at 2.20% which is more than what was expected, based on the doubling time of the cells (Section 3.1.3). A slight but steady increase in the MI was seen from 32 h (7.10%) up to 36 h (7.80%) indicating a G2/M transition period of approximately 5 h. At this stage 59% of the cells were in prophase. A sharp increase in the MI, 38 h after the release of the G1/S block indicated the beginning of mitosis. The MI peaked at 39 h (10.40%), with 64% of the cells still in prophase. As the cells left mitosis, a steady decline in the MI was observed (see **Figure 43** for an example at 39 h after block release for the different mitotic phases).

The length of the S- and M phases of primary EDFs are unknown and seeing that elephants have 10 more chromosomes in comparison to humans, it is not clear if this will conform to what is observed for human fibroblasts. For primary human fibroblasts, the cell cycle lasts between 16 and 28 h with a mean of 20 h (Tamm *et al.*, 1984) while for elephant fibroblasts, according to the MI shown here, that the cell cycle is approximately 39 h. Presuming that the S-, G2- and M phases of the human and elephant cells are similar, which is the case for most mammalian cells, the G1 phase in the elephant fibroblasts is much longer than that of the human fibroblasts known from literature and would also explain their long Td of  $62.13 \pm 7.15$  h at passage 1. However, further studies will have to be done to confirm the length of each cell phase in the elephant fibroblasts, for example by using cell cycle markers, and inter-elephant variations should be included.

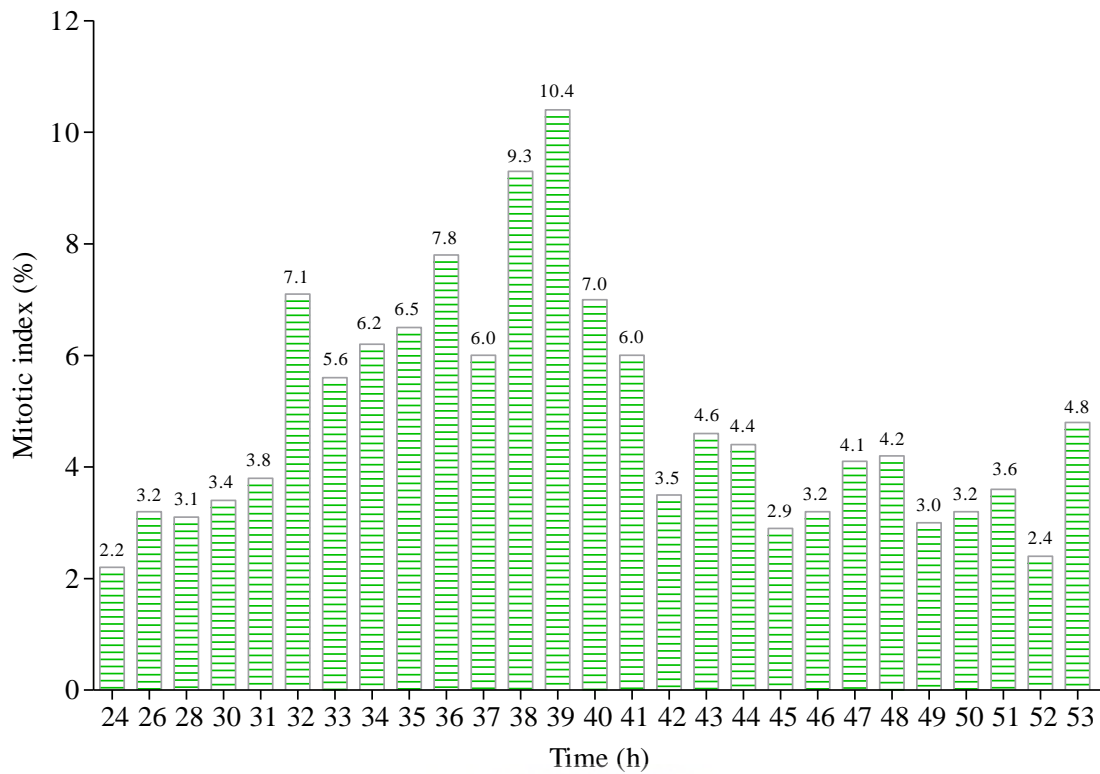


**Figure 42: E6 fluctuation of MI after the release of G1/S block by HU.** Duplicate coverslips were removed every 2<sup>nd</sup> h for the first 6 h and thereafter removed hourly for 24 h. A peak in MI was observed 36 – 39 h after release of the HU.





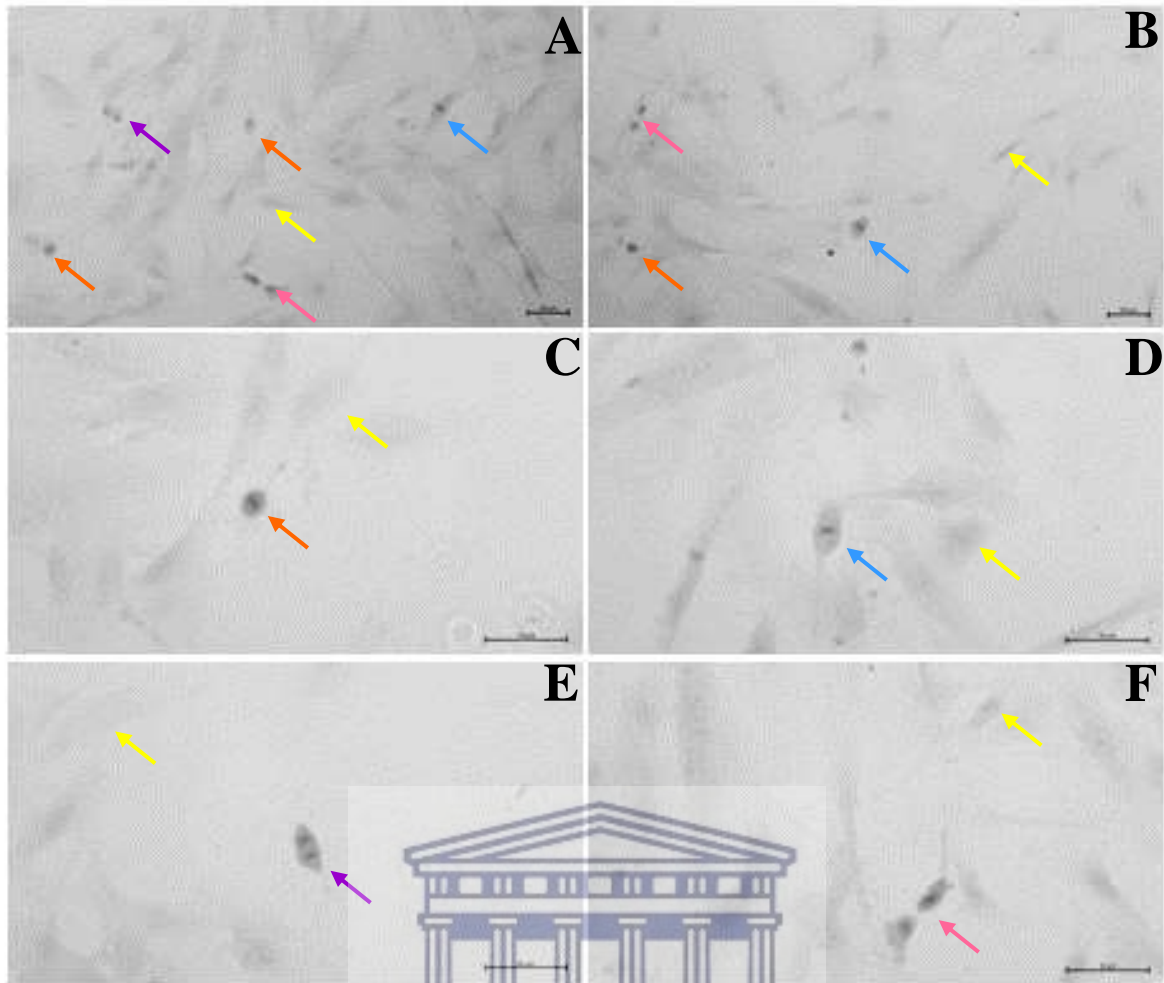


**Figure 43: Mitotic phases of E6 at 39 h after block release.** Viewed with Zeiss Primovert light microscope and images were captured with a Axio 208 colour, scale 50  $\mu\text{m}$ . Fibroblast indicated by a yellow arrow, prophase indicated by an orange arrow, metaphase showed by a blue arrow, purple arrow indicating anaphase and telophase showed by a pink arrow. **A – B)** At 20  $\times$  magnification. **C – D)** At 40  $\times$  magnification.

# CHAPTER 3:

## RESULTS

---

### **Section B: Primary normal human dermal fibroblast (NHDF) vs primary elephant dermal fibroblast (EDF) radiation response post X-ray irradiation**

Primary NHDFs and EDFs (E6) cultures were irradiated with X-rays at GSI and NRF iThemba LABS to investigate the radiation sensitivity of human and elephant fibroblast cells, respectively.



### 3.4. X-ray standardisation

Since 2 different X-ray irradiators were used for the irradiation experiments with EDFs at NRF iThemba LABS and NHDFs at GSI, a CSA was performed with a CHO-K1 cell line. The same cell line of CHO-K1 was present at both facilities and therefore selected for the comparison between the 2 different X-ray irradiators. The CHO-K1 cell line was selected as it is often used in radiobiology studies and its radiosensitivity was well characterised in previous studies at both institutes (Cunningham *et al.*, 2021). As expected, the CHO-K1 cell line showed a decrease in SF with increasing doses at both GSI and NRF iThemba LABS. The SF were fitted using the linear quadratic model (as described in Section 2.9.) and presented in **Figure 44**. The 2 fitted cell survival curves are almost overlapping and no statistically significant difference (paired t test,  $p = 0.32$ ) was observed in SF at all the radiation doses. This indicates that the doses and radiation quality delivered with the X-ray machine at both research facilities results in a similar biological effect.

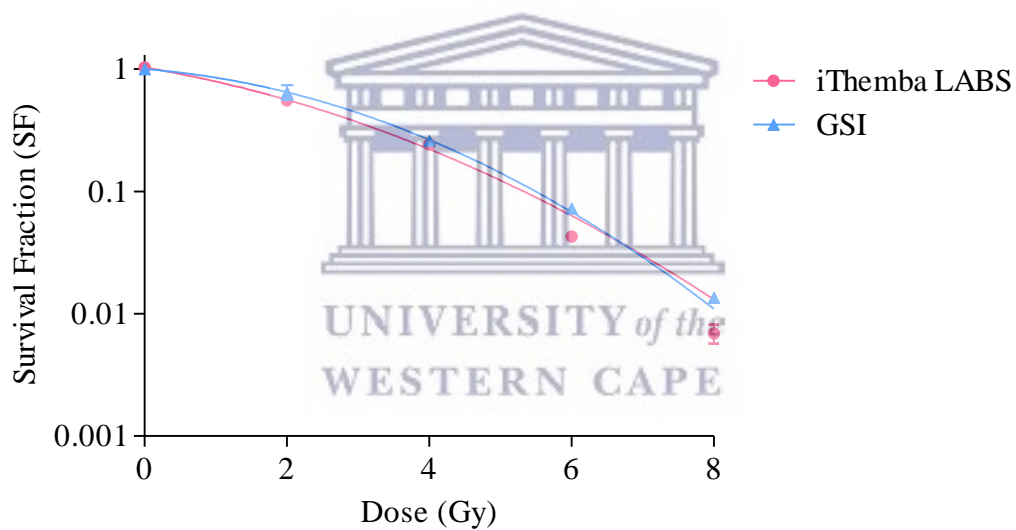


**Figure 44: Standardisation of the X-ray machine at both research facilities by using CHO-K1 cells.** A decrease in SF with higher doses for the CHO-K1 at both GSI (shown in blue) and NRF iThemba LABS (shown in pink). No statistical significance with a paired t test was observed in SF. Error bars represent the SD of the biological triplicates.

### 3.5. Clonogenic survival assay (CSA)

#### 3.5.1. Plating efficiency determination of NHDFs

The NHDF cells were seeded as described in **Table 7** and left to grow for 2 weeks (results of the colonies can be seen in **Figure 45**). The samples where 200 cells were originally seeded, resulted in an average  $\pm$  SD of  $43 \pm 8.29$  counted colonies with a plating efficiency of 21.50%. This was the highest plating efficiency across all samples, compared to the samples with a higher seeding density that showed a decrease in the plating efficiency with 20.38%, 13.38% and 11.84%, for 400, 600 and 800 NHDF cells, respectively.

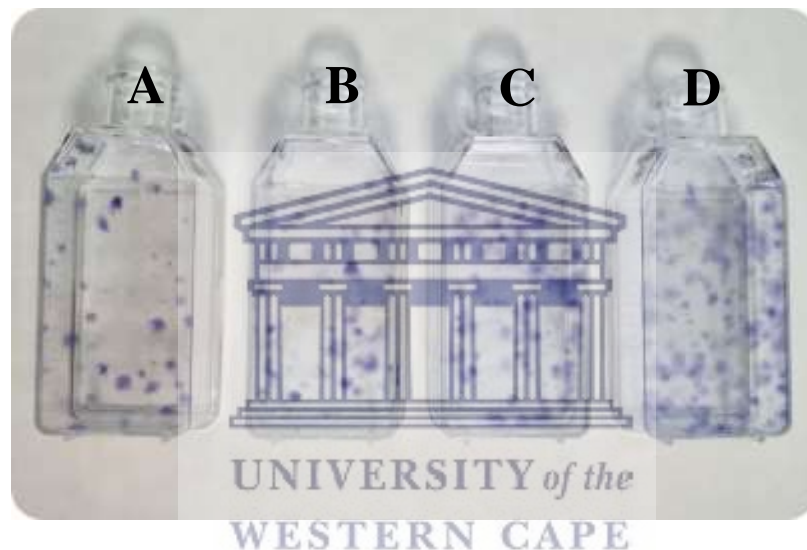


**Figure 45: Plating efficiency determination of the NHDF flask with no IR exposure. A)** 200 cells seeded. **B)** 400 cells seeded. **C)** 600 cells seeded. **D)** 800 cells seeded.

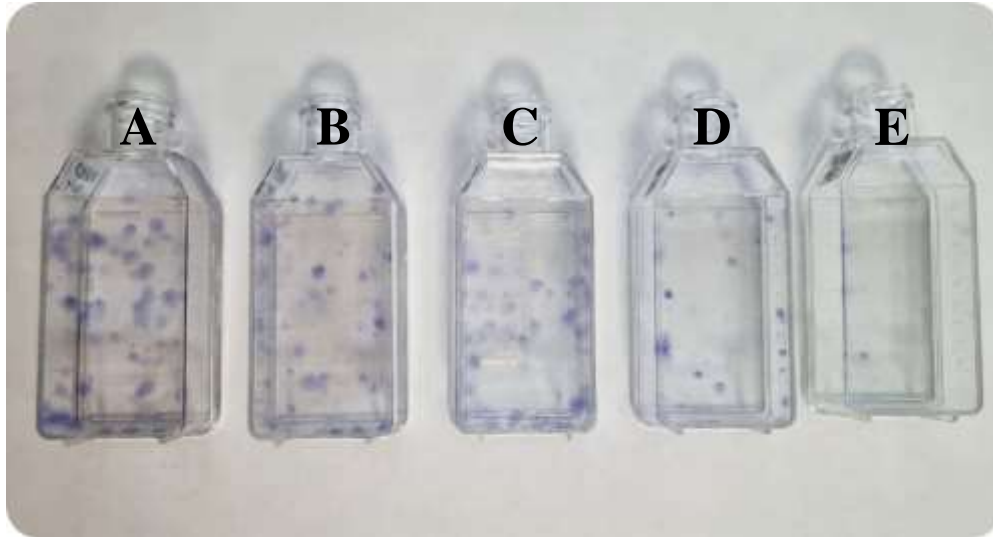
**Table 7: Plating efficiency determination of NHDF cells after 2 weeks of incubation without IR exposure.** The highest plating efficiency was obtained with seeding 200 cells per T25 flask. A decrease in plating efficiency was observed in the samples with a higher seeding density (SD based on the biological triplicates).

Cell seeding density	Average colonies counted	SD	Plating efficiency (%)
200	43.00	8.29	21.50
400	81.50	2.38	20.38
600	80.25	12.97	13.38
800	94.75	20.42	11.84

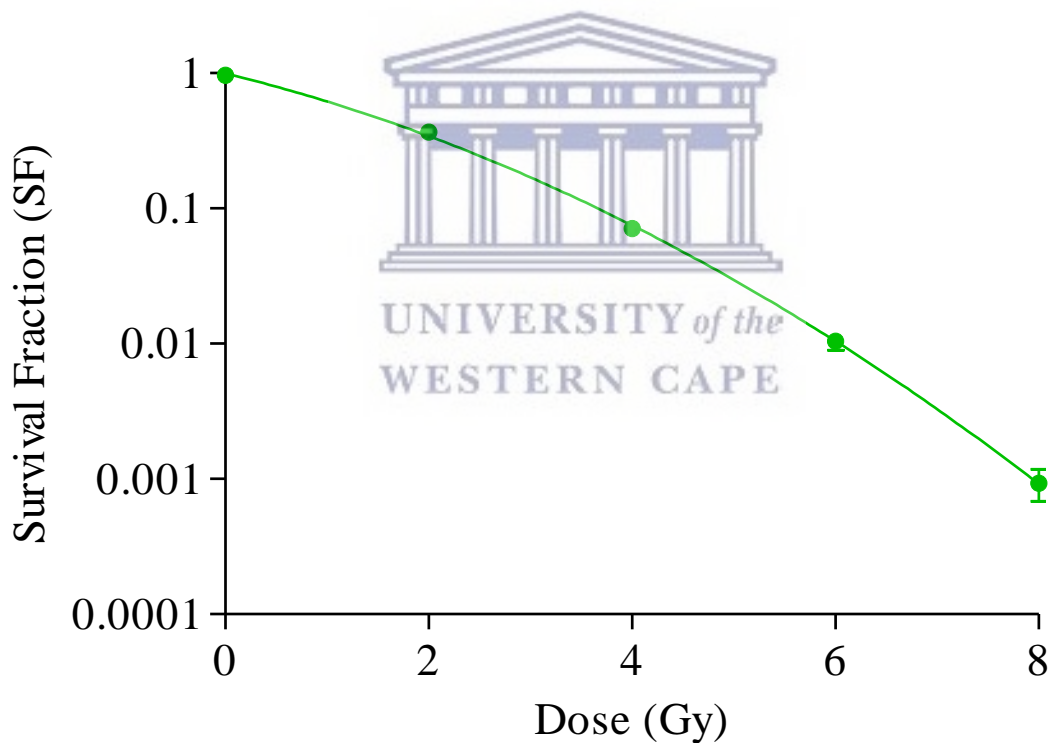
### 3.5.2. Seeding density for IR for the NHDF cells

Based on the plating efficiency results (Table 7), it was concluded that the optimal seeding density for the NHDF cells was 200 cells for the control sample and the dilution route was calculated accordingly. Results of the colonies can be seen in Figure 46.

Figure 47 shows the SF (y-axis) plotted in function of the radiation dose (x-axis). As expected, there was a gradual decrease in the NHDFs SF with radiation dose 2 weeks post-irradiation. The SF for 2 Gy was  $36.83\% \pm 7.02\%$  (SF percentage  $\pm$  SD) and significantly decreased to  $0.09\% \pm 1.53\%$  (SF percentage  $\pm$  SD) for 8 Gy, showing a dose response decrease in colony formation for the NHDF cells.



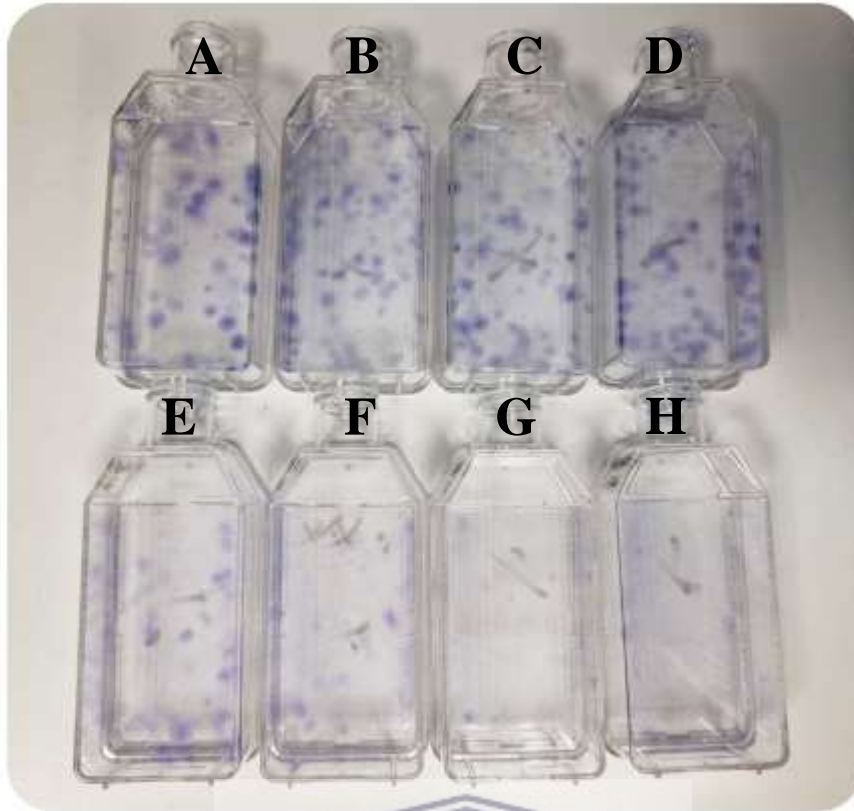
**Figure 46: NHDF flasks post staining to determine seeding densities with IR exposure for CSA dose response curve. A) 200 cells seeded, 0 Gy. B) 400 cells seeded, 2 Gy. C) 2 000 cells seeded, 4 Gy. D) 5 000 cells seeded, 6 Gy. E) 10 000 cells seeded, 8 Gy.**



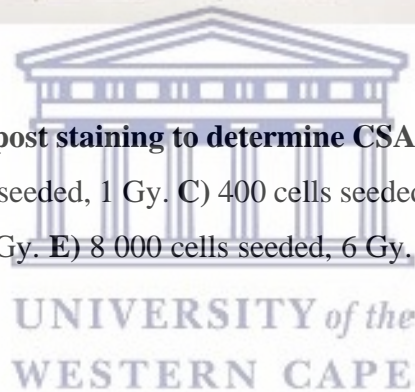
**Figure 47: SF of NHDFs at 2 weeks post irradiation.** Seeding densities of 200, 400, 2 000, 5 000 and 10 000 NHDF cells per T25 flask were used for 0, 2, 4, 6 and 8 Gy, respectively. A decrease in SF was noted with an increase in radiation doses. Error bars represent the SD of the biological triplicates.

### 3.5.3. Clonogenic survival assay (CSA) dose response curve

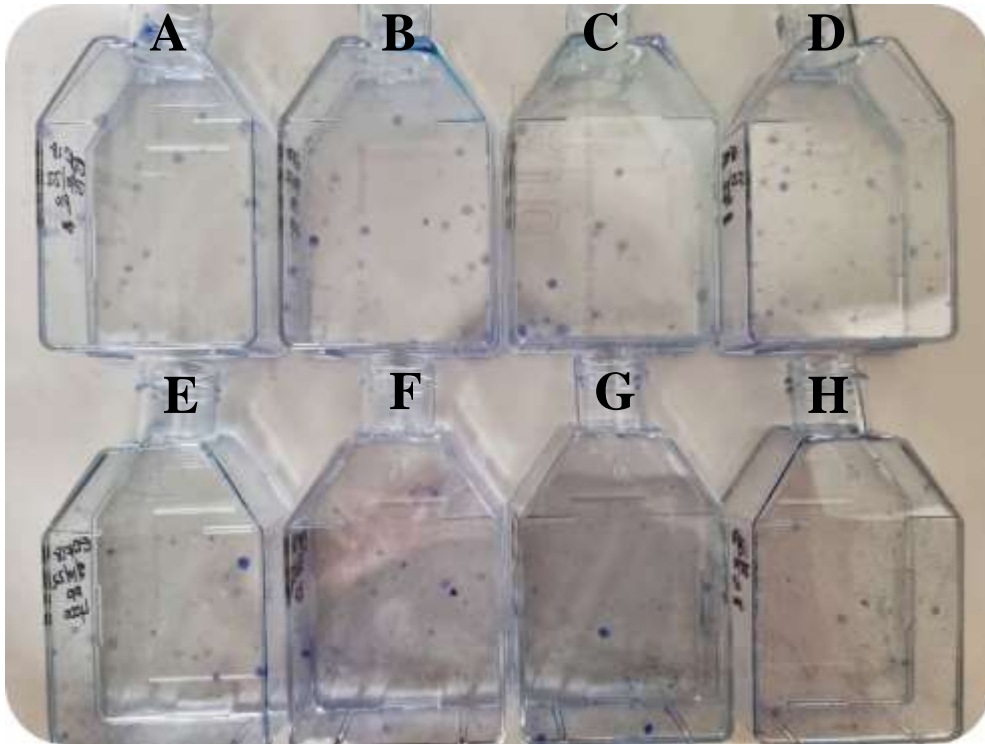
Again, a decrease in SF was noted with an increase in dose. Colony formation can be seen in **Figure 48** and **49** for the NHDFs and EDFs, respectively. NHDFs and EDFs SF had a significant decrease to  $51.18\% \pm 15.31\%$  and  $45.85\% \pm 2.89\%$  (SF percentage  $\pm$  SD) for 1 Gy, respectively. The highest dose (8 Gy) had a notable impact on both the NHDFs and EDFs with a SF of  $0.07\% \pm 2.08\%$  and  $0.26\% \pm 5.29\%$  (SF percentage  $\pm$  SD), respectively. Both NHDF and EDF cells were sensitive to radiation causing a decrease in colony formation with higher doses. In general, no significance was observed in the dose response curve between the 2 cell lines (paired t test,  $p = 0.86$ ). **Figure 50** presents the fitted cell survival curves using the linear quadratic model (described in Section 2.9), resulting in an  $\alpha$ -value of  $0.47 \pm 0.06$  and  $0.62 \pm 0.07$  and  $\beta$ -value of  $0.05 \pm 0.01$  and  $0.02 \pm 0.01$  for NHDFs and EDFs, respectively. Biological triplicates were included, but the experiment was only performed once, which did not allow a statistical comparison between the  $\alpha$ -values. However, the 95% confidence intervals on the  $\alpha$ -values showed significant overlap between the colony survival curve of the NHDF cells (0.35 – 0.60) and the EDF cells (0.48 – 0.780, which indicates that there is no significant difference between the linear component of the linear quadratic model. Lastly, the  $\alpha/\beta$  ratio of the NHDFs was  $9.4 \pm 0.33$  while this was  $31.0 \pm 2.12$  for the EDFs. The lower  $\alpha/\beta$  ratio of the NHDFs could indicate that these cells have a higher repair capacity compared to the EDFs, which appear to be more radiosensitive based on the  $\alpha/\beta$  ratio.



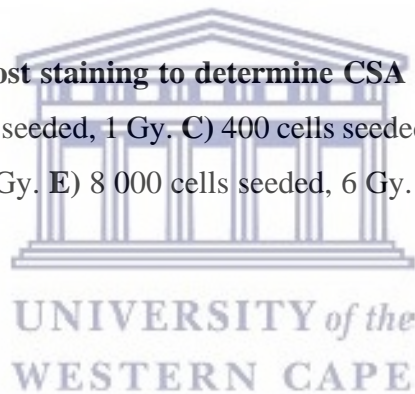
**Figure 48:** NHDF T25 flasks post staining to determine CSA dose response curve. **A)** 200 cells seeded, 0Gy. **B)** 400 cells seeded, 1 Gy. **C)** 400 cells seeded, 2 Gy. **D)** 2 000 cells seeded, 4 Gy. **E)** 5 000 cells seeded, 5 Gy. **F)** 8 000 cells seeded, 6 Gy. **G)** 10 000 cells seeded, 7 Gy. **H)** 20 000 cells seeded, 8 Gy.







**Figure 49: EDF T25 flasks post staining to determine CSA dose response curve. A) 200 cells seeded, 0 Gy. B) 400 cells seeded, 1 Gy. C) 400 cells seeded, 2 Gy. D) 2 000 cells seeded, 4 Gy. E) 5 000 cells seeded, 5 Gy. E) 8 000 cells seeded, 6 Gy. E) 10 000 cells seeded, 7 Gy. E) 20 000 cells seeded, 8 Gy.**



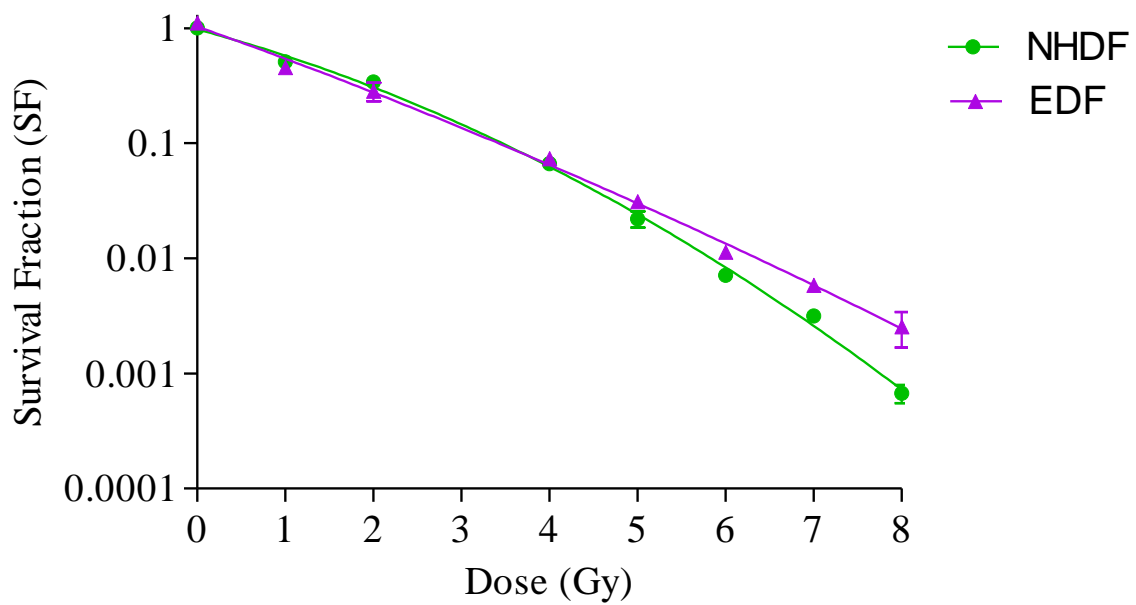
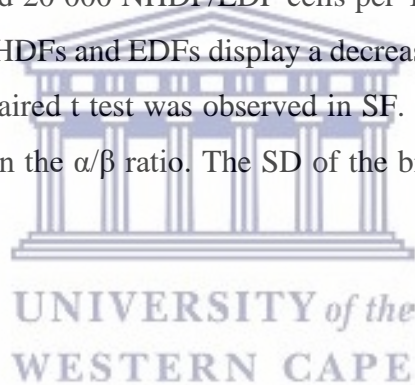


**Figure 50: NHDFs and EDFs CSA dose response curve.** Seeding densities of 200, 400, 400, 2 000, 4 000, 8 000, 10 000 and 20 000 NHDF/EDF cells per T25 flask for 0, 1, 2, 4, 5, 6, 7 and 8 Gy, respectively. Both NHDFs and EDFs display a decrease in SF with higher doses. No statistical significance with a paired t test was observed in SF. However, the EDFs appear to be more radiosensitive based on the  $\alpha/\beta$  ratio. The SD of the biological triplicates represents the error bars.



### 3.6. Proliferation assay

The amount of crystal violet staining in this assay was directly proportional to the cell biomass that was attached to the plate, meaning the live cells. NHDFs proliferation capacity was investigated post-irradiation for 24, 48, 72, 96, 120 and 144 h. The proliferation percentage (y-axis) was plotted in function of the time in culture (x-axis). The control sample (0 Gy) was expressed as 100% and all the doses were standardised to 0 Gy.

After 24 h, there was a decrease in cell proliferation for all the doses for 0, 1, 2, 4, 8 and 16 Gy (**Figure 51**). This could possibly be due to the slow replication capacity of the NHDF cells. Furthermore, the decrease in cell proliferation in the NHDFs is not dose dependent at 24 h.

For 1, 2, 4 and 16 Gy at 48 h post-irradiation, an increase in cell percentage was seen with 143.20%, 226.40%, 123.10% and 102.70%, respectively. A statistically significant increase was observed at 2 Gy (an outlier in these results), while a decrease was observed at 8 Gy but not at 16 Gy. No dose dependent effect was observed warranting further investigation.

A dose dependent decrease in cell proliferation can be observed after 72, 96, 120 and 144 h. The majority of these samples, especially the higher doses, showed a significant decrease in cell proliferation percentage. At 144 h, 1 and 2 Gy showed no significance difference when compared to the non-irradiated control sample with a cell proliferation percentage of 80.90% and 83.18%, respectively. The NHDF cells had the ability to repair the DNA damage that was present, and the cells were able to continue with their cell proliferation without reaching confluency within 144 h when experimentation termination occurred. In summary, the radiation effect on the NHDF cells was not time dependent, however dose dependent from 72 hours onward.

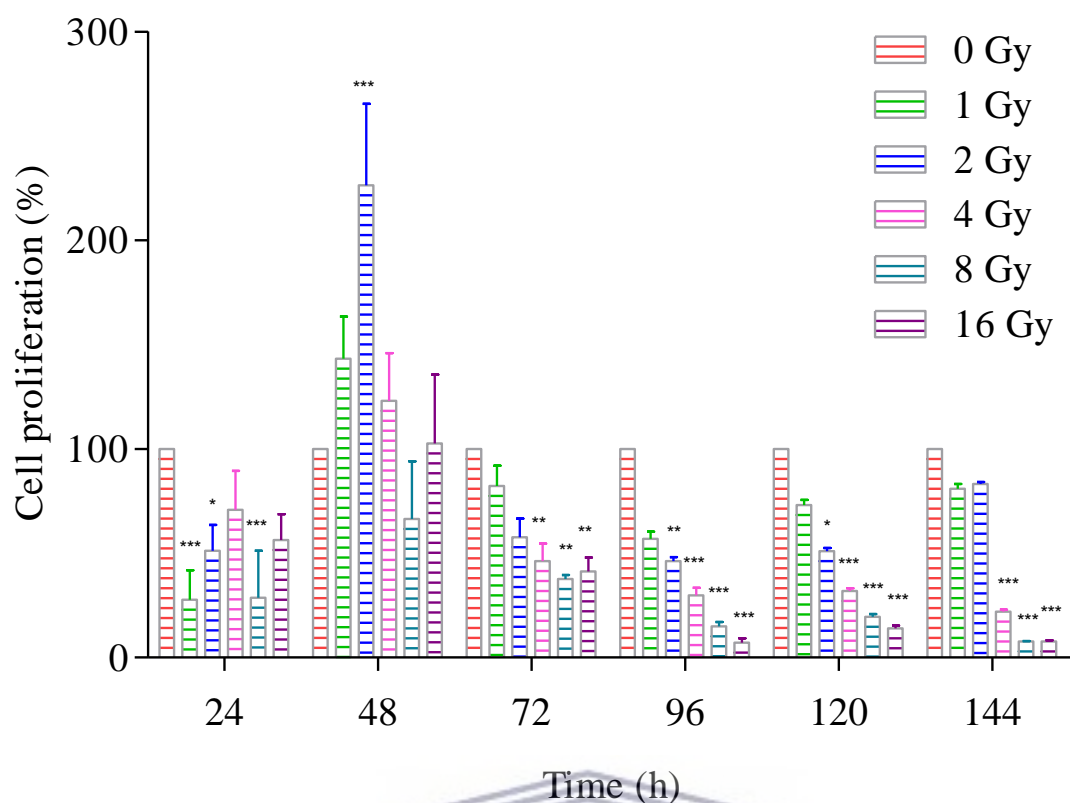


**Figure 51: NHDF cell proliferation after 24, 48, 72, 96, 120 and 144 h of X-ray irradiation.** The NHDF cell proliferation capacity was dose-dependent and not time-dependent. The error bars represent the SD of the biological repeats. The statistically significant comparison between the irradiated and unirradiated was shown as follow: \* represents  $p < 0.05$ , \*\* represents  $p < 0.01$  and \*\*\* represents  $p < 0.0001$ .

Due to the long cell cycle of the EDFs, it was decided to perform the proliferation experiment of EDF cells using only 2 time points, namely 72 and 120 h. The EDF cell proliferation was dose-dependent with a significant decrease at higher doses (**Figure 52**). Similar to the result of the NHDF cells at 72 h, a dose responsive decrease was observed in the EDFs. The cell numbers decreased at 1 Gy and 2 Gy by 13.17% and 23.26%, followed by 30.70%, 42.83% and 54.32% for 4, 8 and 16 Gy, respectively. At 120 h post irradiation, a small increase of 4.34% and 2.34% in the EDF cell numbers was observed at 1 and 2 Gy, and the cells irradiated with 4, 8 and 16 Gy showed an inhibition of 17.54%, 29.95% and 20.63%, respectively. Even though the cell percentages at 120 h were still lower than the control, for 4, 8 and 16 Gy the suppression was not as noticeable as that observed for the EDFs after 72h for the corresponding doses. This

shows a remarkable recovery in the cell numbers when compared to the corresponding decrease at 72 h, see **Table 8** for statistically significant comparison.

Comparing the NHDFs and EDFs in **Figure 52**, at 72 h post-irradiation, a similar dose dependent effect was observed with both cell lines. The NHDFs showed a cell proliferation of 41.26% and the EDFs had a cell proliferation of 45.68% at 16 Gy. However, at 120 h post-irradiation, the EDFs had remarkable recovery after 1 and 2 Gy and slight decrease in cell proliferation at higher doses. In contrast, the NHDFs had a statistically significant decrease in cell proliferation at higher doses confirmed by ANOVA with Bonferroni post-test. The EDFs and NHDFs had a cell proliferation of 79.37% and 15.03% at 16 Gy, respectively. This large difference in cell proliferation at 120 h requires future investigation, in which the time point of 96 h should be included.



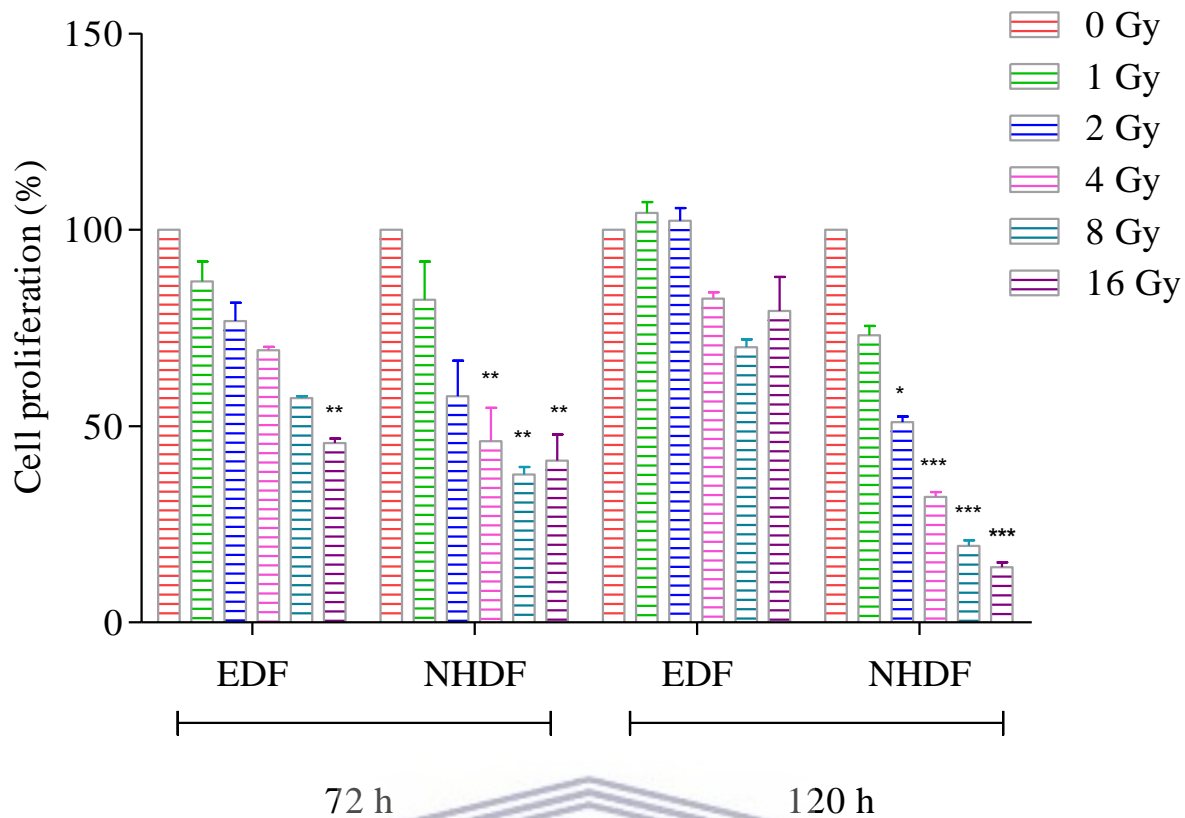


**Figure 52: EDF cell proliferation after 72 and 120 h of X-ray irradiation.** The EDF cell proliferation capacity was dose-dependent and not time-dependent. A cell recovery was observed at 120 h for 1 and 2 Gy. The SD of the biological triplicates represented by the error bars. Significance indication of the irradiated and unirradiated sample was indicated as follow: \* represents  $p < 0.05$ , \*\* represents  $p < 0.01$  and \*\*\* represents  $p < 0.0001$ .

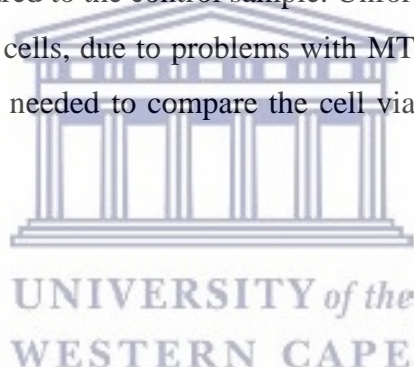
**Table 8: Statistical comparison between 72 and 120 h for the cell proliferation assay.** A significant difference for the NHDFs comparing 72 and 120 h were only observed at 16 Gy. In contrasts, the EDFs showed a significant difference at 1, 2 and 16 Gy. Significance indication: \*  $p < 0.05$ , \*\*  $p < 0.01$ , \*\*\*  $p < 0.0001$  and ns indicates no significance.

Cell line	Dose (Gy)	Statistical significance
NHDF	0	ns
	1	ns
	2	ns
	4	ns
	8	ns
	16	**
EDF	0	ns
	1	*
	2	***
	4	ns
	8	ns
	16	***



### 3.7. MTS assay

The MTS assay is a sensitive quantification of viable cells. Based on the results obtained with the proliferation assays, the same time points of 72 and 120 h were carried out for NHDFs in the MTS assay. The cell viability percentage (y-axis) was plotted in function of the time in culture (x-axis). A significant decrease in NHDFs cell viability was observed when compared to the control sample (expressed as 100%) across both time points. The cell viability decreased from 82.85% for 1 Gy to 45.25% for 16 Gy at 72 h (**Figure 53**). A further decrease in NHDFs cell viability was observed at 120 h at the higher dose points, but not at the lower doses where 1 and 2 Gy exposure resulted in 93.50% and 90.13% cell viability, respectively. This contradicts the findings at 120 h with the cell proliferation assay and is more in line with the observations in the EDFs. Lower doses of 1 and 2 Gy do not have such a damaging effect on the cells when compared to higher doses. Furthermore, 4, 8 and 16 Gy had a significant decrease in cell viability when compared to the non-irradiated control sample at 120 h. This was in contrast to the results obtained at 72 h, where all doses induced a statistically significant decrease in cell viability compared to the control sample. Unfortunately, this assay could only be performed with the NHDFs cells, due to problems with MTS stock and delivery in South Africa. Future experiments are needed to compare the cell viability of the NDHF and EDF cells.





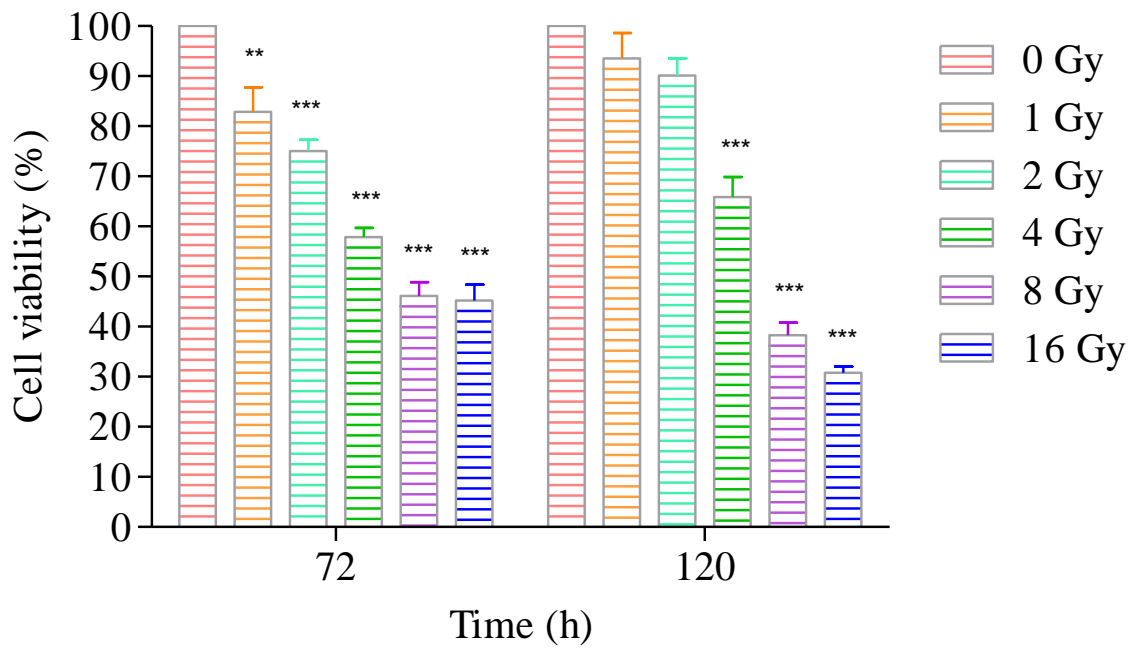
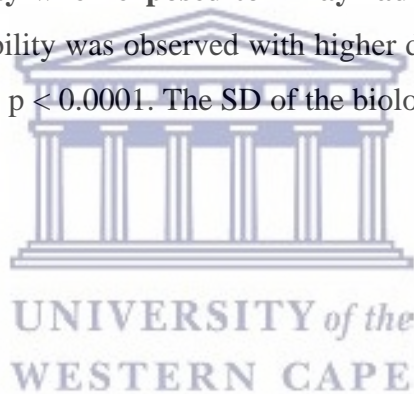


**Figure 53: NHDF cell viability when exposed to X-ray radiation after 72 and 120 h.** A significant decrease in cell viability was observed with higher doses. Significance indication: \*  $p < 0.05$ , \*\*  $p < 0.01$  and \*\*\*  $p < 0.0001$ . The SD of the biological triplicates represents the error bars.



### 3.8. Flow cytometry

#### 3.8.1. Apoptosis assay

NHDFs and EDFs apoptosis analysis was done via flow cytometry to reveal early apoptosis, late apoptosis and necrosis post-irradiation. The cell percentage (y-axis) was plotted in function of the dose for both human and elephant cell lines (x-axis).

After 12 h, a radiation dose of 8 Gy did not affect the number of viable cells compared to the unirradiated control, resulting in 91.93% and 93.73% of living NHDF cells, respectively. In contrast, the EDFs showed a decreased number of viable cells of 79.33% and 73.63% for 0 Gy and 8 Gy, respectively (**Figure 54**). The decrease in viable cells corresponded to a 10% increase in early apoptosis in EDF cells irradiated with 8 Gy, while an increase of only 2.78% and 0.52% was observed in late apoptosis and necrosis, respectively. The EDF apoptosis results were not statistically significant. Future experiments with more technical and biological repeats are warranted to confirm apoptosis induction in a different method.

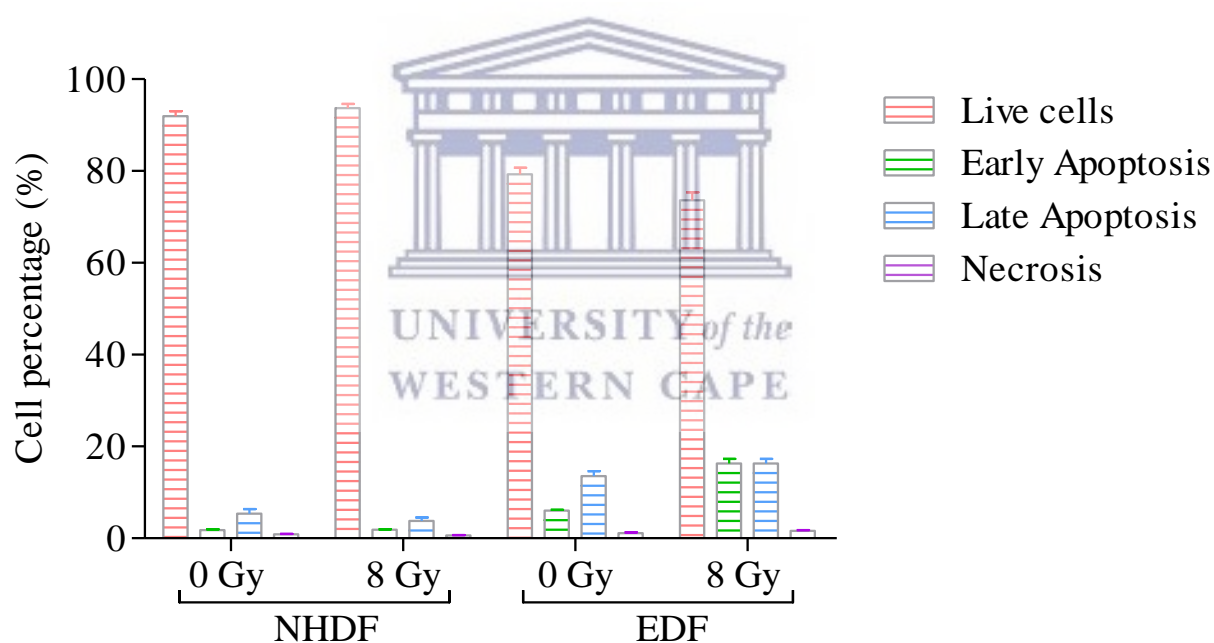


**Figure 54: Apoptosis analysis 12 h post-irradiation for both NHDFs and EDFs.** No significant apoptosis induction was observed for both NHDF and EDF cell lines. A 10% increase from 0 to 8 Gy for the EDFs at early apoptosis was observed. Error bars represent the SD of the biological triplicates.

In the analysis of apoptosis 24 h post-irradiation (**Figure 55**), the majority of the NHDFs cells were still viable. For the EDFs, a decrease in the number of viable cells was observed from

78.80% for 0 Gy to 61.45% for 8 Gy. Interestingly, the 0 Gy value at 24 h remains stable compared to the 0 Gy value at 12 h (79.33%), while the percentage viable cells at 8 Gy decreased further from 73.63% at 12 h to 61.45% at 24 h. This reflects a low level of spontaneous apoptosis in the EDFs. In comparison to the NHDF cell line, apoptotic changes were observed across early apoptosis, late apoptosis and necrosis for the EDFs. Early apoptosis was 6.61% and 13.23% for 0 and 8 Gy, while late apoptosis was 12.90% and 23.65% for 0 and 8 Gy, respectively. These changes were again not statistically significant and different apoptosis methods are warranted to confirm the results obtain.

The EDFs resulted in a higher level of early and late apoptosis. The EDFs late apoptosis was 23.65%, while for the NHDFs was only 5.19% in **Figure 55**. Necrosis remained below 1.72% for both cell lines. Again, the higher early and late apoptosis induction for the EDF cell line was not statistically significant but will be further investigated in future experiments to understand the full working mechanism of cell death in the cell line.

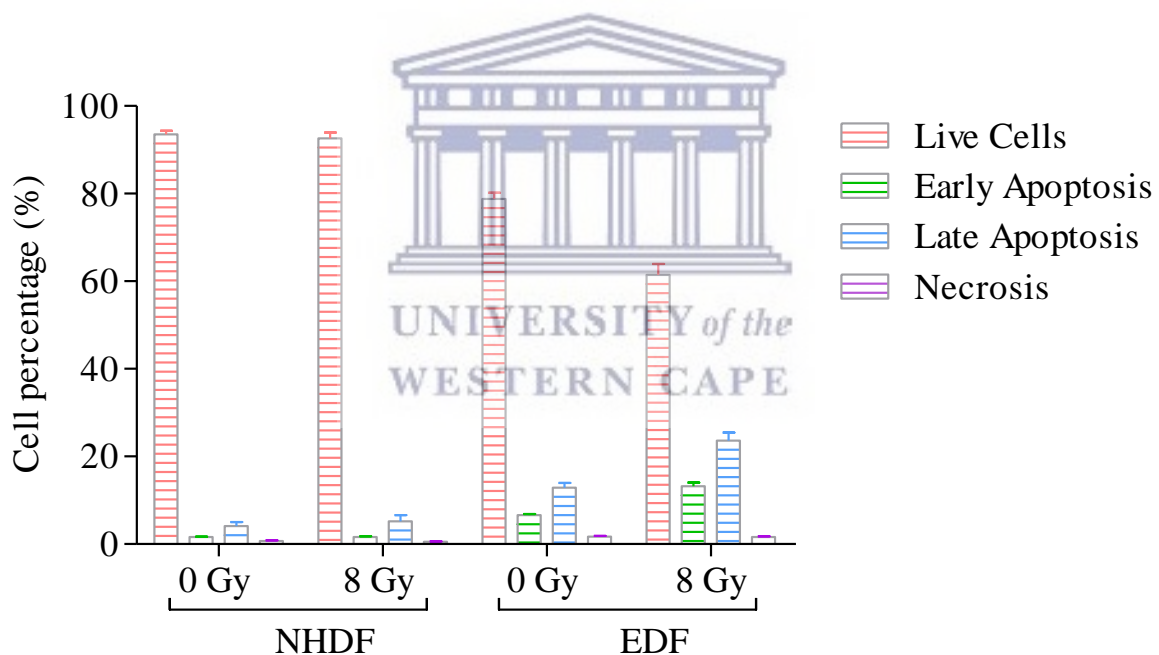


**Figure 55: Apoptosis analysis 24 h post-irradiation of both NHDFs and EDFs.** NHDFs showed a minimal change in apoptosis induction, whilst the EDFs showed a notable increase with 8 Gy in both early and late apoptotic response. However, both NHDF and EDF had no significant apoptosis induction after X-rays irradiations. The error bars indicate the SD.

No significant presence of NHDF apoptotic cells was observed 48 h post-irradiation. Viable cells remained above 94.40%, while early apoptosis ranged from 1.32% to 1.14% and late apoptosis ranged from 3.62% to 4.03% for 0 and 8 Gy, respectively.

In contrast to the NHDFs, the EDFs showed a decrease in the number of viable cells at 48 h post-irradiation with 57.80% for 0 Gy and 48.78% for 8 Gy (**Figure 56**). A decrease of viable cells of more than 10% was observed for 8 Gy from 24 – 48 h. Furthermore, early apoptosis was 14% and 16.70%, whilst late apoptosis was 24.80% and 30.70% for 0 and 8 Gy, respectively. Necrosis remained below 3.90%. A 7.37% and a 7.05% increase in late apoptosis in EDFs was observed from 12 – 24 h and 24 – 48 h, respectively. No significant difference was observed across all the condition when comparing 0 and 8 Gy and 24 – 48 h and warrants further investigation in future experiments with a different apoptosis method.

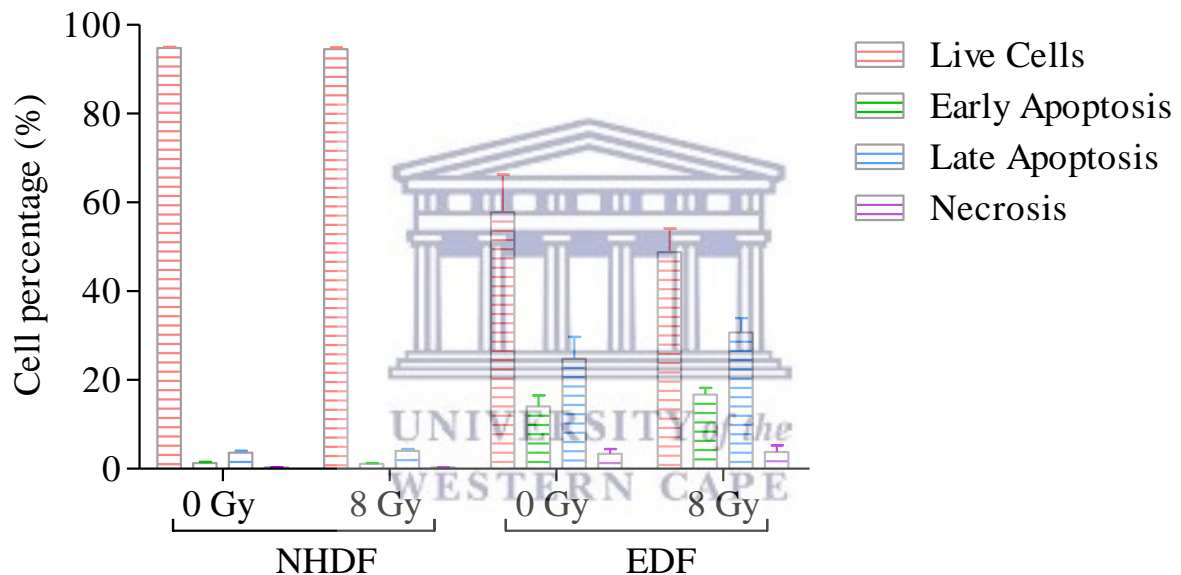


**Figure 56: Apoptosis analysis 48 h post-irradiation for both NHDFs and EDFs.** No significant change was observed with the NHDFs and EDFs. The EDFs had an increase in apoptotic response with late apoptosis having the highest indicator. The error bars show the SD of the biological triplicates.

Overall, the EDFs were more sensitive to X-ray irradiation compared to the NHDFs. A 2-fold increase with both early and late apoptosis were observed for 12, 24 and 48 h for the EDF cell line (**Figure 54 – 56**). Even at 8 Gy, no significant change in apoptosis was observed in NHDFs

and it was previously reported that human dermal fibroblasts are apoptosis resistant (Akasaka *et al.*, 2010; Audo *et al.*, 2007; Hanson *et al.*, 2019).

### 3.8.2. Cell cycle assay

The cell cycle assay quantifies the DNA content to reveal the distribution of NHDF and EDF cells in the different cell cycle phases.

At the start of the experiment (0 h), 84.50% of the NHDF cells were in G0/G1 phase. For the EDFs, 61.80% were in G0/G1 phase and 24.08% were in G2/M phase (**Table 9**). A significant difference was observed between the NHDF and EDF cell line with  $p < 0.0001$  in G0/G1- and G2/M phase at the start of the experiment.

**Table 9: Cell cycle assay of NHDF and EDF cells before X-rays.** The NHDFs were in the G0/G1 phase with 84.50%, whilst 61.80% of the EDFs were in G0/G1 phase and 24.08% was in G2/M phase. NHDF results were displayed in green and EDF results shown in purple. Significant indication of comparison between the NHDF and EDF cell line was shown in orange with \*  $p < 0.05$  and \*\*\*  $p < 0.0001$ .

Time (h)	Dose (Gy)	G0/G1 phase	S phase	G2/M phase
		(Average $\pm$ SD) NHDF/EDF	(Average $\pm$ SD) NHDF/EDF	(Average $\pm$ SD) NHDF/EDF
0	0	84.50 $\pm$ 3.16 ***	5.24 $\pm$ 2.99 *	9.91 $\pm$ 1.79 ***
		61.80 $\pm$ 2.43	9.99 $\pm$ 1.94	24.08 $\pm$ 1.16

It was found that more than 88.35% of the NHDF cells remained in G0/G1 throughout all the radiation doses 24 h post-irradiation (**Table 10**). No statistical significance was observed in the cell cycle distribution between the non-irradiated and irradiated NHDF cells.

In contrast, the EDFs at 24 h showed a shift of cells to G2/M phase. For 0 Gy, 56,83% was in G0/G1 phase and 30,68% was in G2/M phase. For 8 Gy, 12 Gy and 16 Gy, a significant difference was observed with 42,23%, 46,0% and 47,73% of the cells in the G2/M phase, respectively. In the S phase, a small decrease was observed with higher doses with 0 Gy being 8.26% and 16 Gy being 4.69%.

Furthermore, a significant difference was observed in G0/G1-, S- and G2/M phase across all the conditions between the NHDF and EDF cell line with a  $p < 0.0001$  (indicated in orange in **Table 10**). Apart from  $p < 0.01$  at 16 Gy 24 h post-irradiation in the S phase.

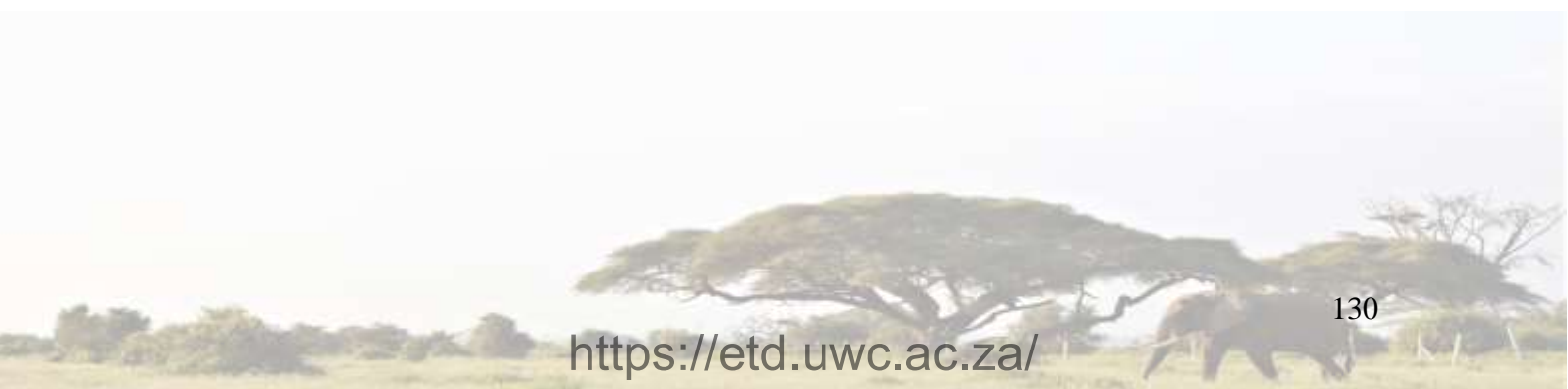


**Table 10: NHDF and EDF cell cycle assay to reveal the cell cycle progression post 24 h X-ray irradiation.** More than 80% of the NHDFs were in the G0/G1 phase for all the doses. For the EDFs a decrease was observed in G0/G1 phase with an increase in the doses and a notable increase in the G2/M phase, shown in bold. Green indicates NHDF results while purple indicates EDF results. The statistically significant comparison between the irradiated and unirradiated sample shown in the colour of the cell line and \*\*\* indicate  $p < 0.0001$ . The significant comparison between the NHDF and EDF cell lines are presented in orange and \*\* represents  $p < 0.01$  and \*\*\* represents  $p < 0.0001$ .

Time (h)	Dose (Gy)	G0/G1 phase	S phase	G2/M phase
		(Average $\pm$ SD) NHDF/EDF	(Average $\pm$ SD) NHDF/EDF	(Average $\pm$ SD) NHDF/EDF
24	0	88.83 $\pm$ 0.80 *** 56.83 $\pm$ 2.70	2.15 $\pm$ 0.80 *** 8.26 $\pm$ 1.94	8.62 $\pm$ 0.93 *** 30.68 $\pm$ 3.02
	4	88.50 $\pm$ 0.76 *** 54.15 $\pm$ 1.04	1.84 $\pm$ 0.52 *** 6.35 $\pm$ 1.49	9.07 $\pm$ 0.36 *** 34.48 $\pm$ 2.00
	8	89.13 $\pm$ 0.68 *** 47.40 $\pm$ 5.45 ***	1.73 $\pm$ 0.52 *** 6.46 $\pm$ 1.35	8.34 $\pm$ 0.30 *** <b>42.23 <math>\pm</math> 5.60 ***</b>
	12	89.05 $\pm$ 1.07 *** 42.63 $\pm$ 1.07 ***	2.12 $\pm$ 0.65 *** 6.31 $\pm$ 1.35	8.23 $\pm$ 0.38 *** <b>46.00 <math>\pm</math> 1.99 ***</b>
	16	89.13 $\pm$ 0.52 *** 40.83 $\pm$ 0.39 ***	1.74 $\pm$ 0.49 ** 4.69 $\pm$ 1.83	8.70 $\pm$ 0.62 *** <b>47.73 <math>\pm</math> 1.84 ***</b>

For the NHDFs, 48 h post-irradiation, 88.73% – 90.65% of the cell population remained in G<sub>0</sub>/G<sub>1</sub> phase throughout all the doses. For the S phase, the NHDFs remained below 3.18% for G<sub>2</sub>/M phase, the highest percentage was 8.33% after 4 Gy.

The EDFs showed a decrease in G<sub>0</sub>/G<sub>1</sub> phase when exposed to higher doses. The EDFs decreased from 55.03% at 0 Gy to 42.70% for 16 Gy, with 12 Gy being the lowest fraction of cells in G<sub>0</sub>/G<sub>1</sub> with 39.48%. The S phase decreased from 9.11% for 0 Gy to 3.74% for 16 Gy. The biggest change was the shift to the G<sub>2</sub>/M phase, indicated in bold in **Table 11**. The cells exposed to 8, 12 and 16 Gy, showed 39.83%, 41.00% and 36.98% of cells in G<sub>2</sub>/M which was a significant increase when compared to the 26.1% cells in G<sub>2</sub>/M in the unirradiated sample. Furthermore, across all the irradiated conditions, the NHDFs and EDFs showed a significant difference for G<sub>0</sub>/G<sub>1</sub>- and G<sub>2</sub>/M phases.





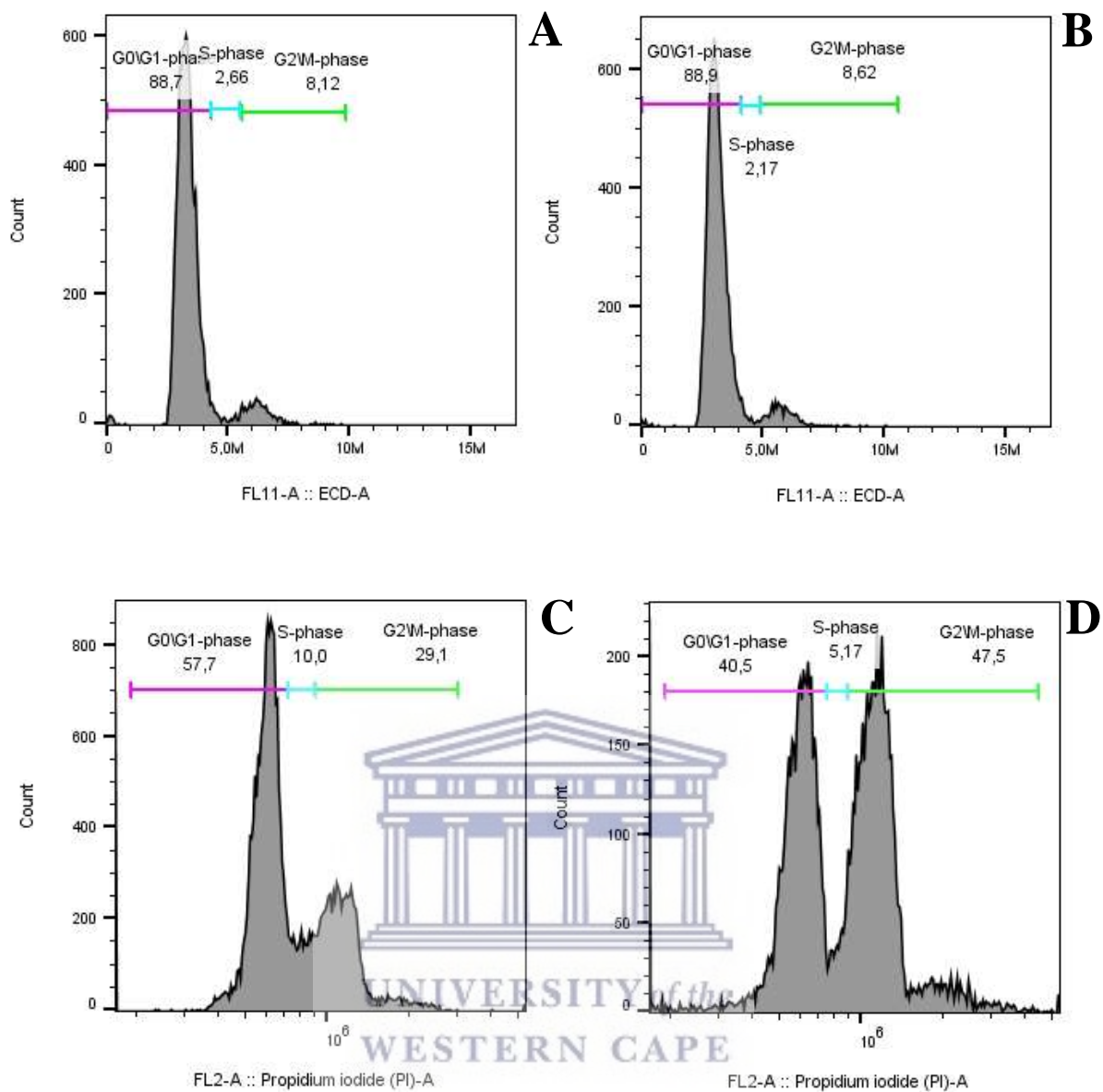
**Table 11: Cell cycle progression of NHDF and EDF cells post 48 h X-ray irradiation.** The NHDFs showed no clear shift in cell cycle progression in response to the IR. The EDFs showed a decreased number of cells in the G0/G1 phase with an increase of cells in the G2/M phase after irradiation with 4, 8, 12 and 16 Gy (bold). NHDF results showed in green and EDF results in purple and both cell line significance of the control and IR was shown in the respective colours. The NHDF and EDF significance comparison is presented in orange. Significance indication: \*  $p < 0.05$ , \*\*  $p < 0.01$  and \*\*\*  $p < 0.0001$ .

Time (h)	Dose (Gy)	G0/G1 phase (Average $\pm$ SD) NHDF/EDF	S phase (Average $\pm$ SD) NHDF/EDF	G2/M phase (Average $\pm$ SD) NHDF/EDF
48	0	90.65 $\pm$ 1.50 *** 55.03 $\pm$ 0.34	3.18 $\pm$ 1.48 *** 9.11 $\pm$ 0.89	5.48 $\pm$ 2.07 *** 26.10 $\pm$ 1.71
	4	88.73 $\pm$ 0.72 * *** 48.70 $\pm$ 1.44 ***	2.38 $\pm$ 0.84 5.06 $\pm$ 0.67 ***	8.33 $\pm$ 0.32 *** *** 31.53 $\pm$ 3.63 ***
	8	90.60 $\pm$ 0.48 *** 44.03 $\pm$ 0.81 ***	2.56 $\pm$ 0.32 2.66 $\pm$ 0.67 ***	6.27 $\pm$ 0.74 *** 39.83 $\pm$ 1.38 ***
	12	89.08 $\pm$ 1.08 *** 39.48 $\pm$ 1.57 ***	2.55 $\pm$ 0.79 4.78 $\pm$ 1.30 ***	7.91 $\pm$ 0.36 ** *** 41.00 $\pm$ 1.69 ***
	16	89.23 $\pm$ 0.79 *** 42.70 $\pm$ 0.69 ***	3.17 $\pm$ 0.59 3.74 $\pm$ 0.56 ***	6.91 $\pm$ 0.55 *** 36.98 $\pm$ 1.58 ***

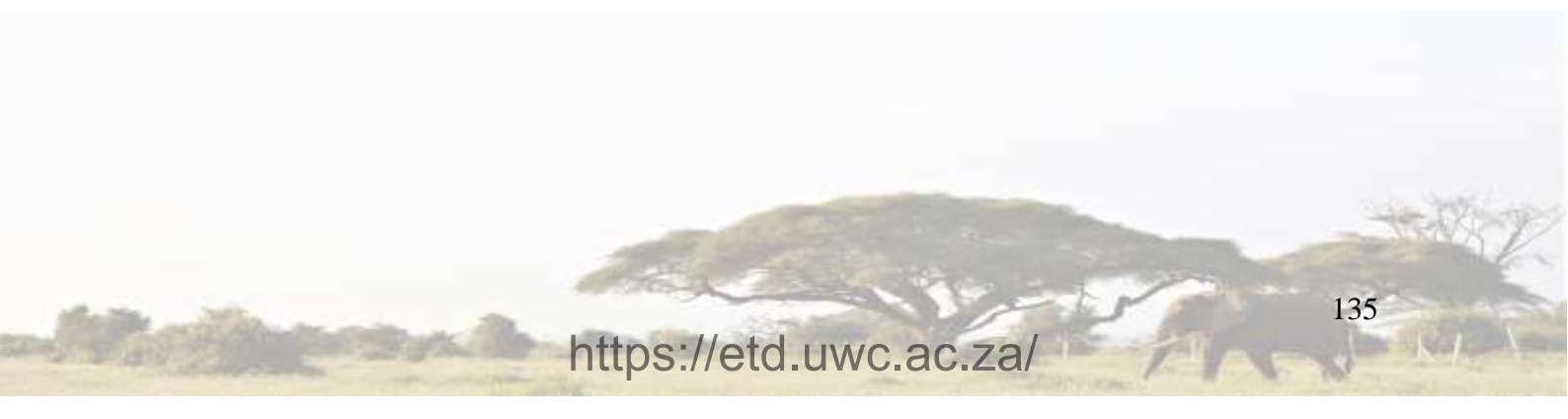
Looking at the results obtained at 24 h and 48 h, the EDF showed a shift from the G1 phase to the G2/M phase which could be indicative of a G2/M block (**Figure 57** and **58 C and D**). The NHDF cells showed no cell cycle shifts or changes after irradiation (**Figure 57** and **58 A and B**). More than 80% of the NHDF cells remained in G0/G1 phase.

The cell cycle progression for the EDFs was dose dependent since at 24 h and 48 h G2/M phase was 47.73% and 36.98%, respectively for 16 Gy, indicating G2/M block after radiation exposure. This was not observed for the NHDF cells which harbour only 1 copy of TP53.





**Figure 57: NHDF and EDF flow cytometry cell cycle progression 24 h post-irradiation.** Example images obtained from 1 sample representing **A)** NDHF: 0 Gy, **B)** NHDF: 16 Gy, **C)** EDF: 0 Gy and **D)** EDF: 16 Gy. A significant increase was observed in EDF at 16 Gy, indicating a possible G2/M cell block.



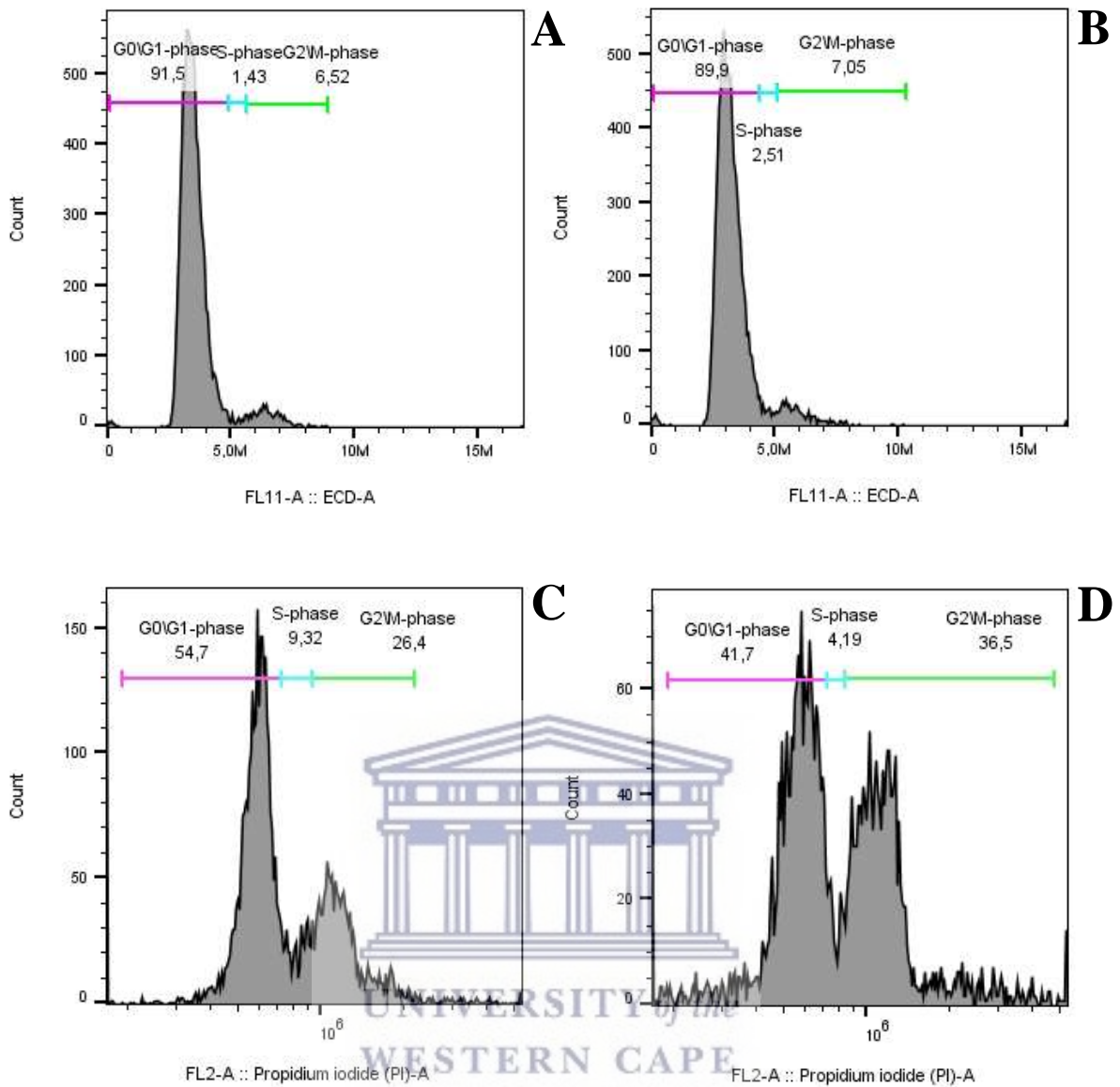
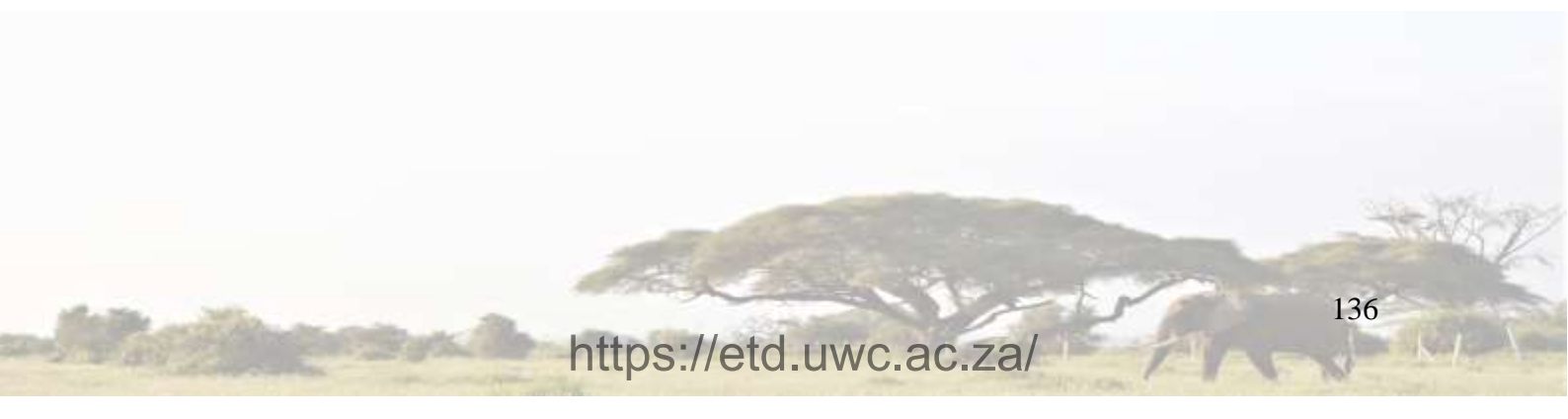


**Figure 58: Flow cytometry cell cycle progression for NHDF and EDF 48 h post-irradiation.** Example images obtained from 1 sample representing **A)** NDHF: 0 Gy, **B)** NDHF: 16 Gy, **C)** EDF: 0 Gy and **D)** EDF: 16 Gy with a significant cell cycle shift indicating a possible G2/M block.



# CHAPTER 4:

## DISCUSSION

---

### Section A: Primary elephant dermal fibroblast (EDF) cell line characterisation

Fibroblasts from a variety of mammals, including Asian elephants (*Elephas maximus*) and hippopotami (*Hippopotamus amphibious*) have successfully been established by researchers over the years (Siengdee *et al.*, 2018; Wang *et al.*, 2021b). EDF cell lines were established for the TUSSC project, from semi-free ranging African savanna elephants (*Loxodonta africana*) undergoing a routine veterinarian intervention. All species of elephants are currently listed as critically endangered on the International Union for Conservation of Nature (IUCN) red list of threatened species (Gobush, *et al.*, 2020; Gobush *et al.*, 2021; Williams *et al.*, 2020). Cryopreserved biomaterial and biobanks might safeguard the genetic material of species for future research and the conservation of species, especially those identified as vulnerable to extinction (Bartels & Kotze, 2006; Leon-Quinto *et al.*, 2009; Ryder & Onuma, 2018). The African elephant cryopreservation of a primary EDF cell line is the first of its kind. These fibroblasts provide the opportunity to unravel cancer suppression mechanisms in elephants and could act as a future source of African elephant genetic information.

In the current study, 5 mm skin punch biopsies were obtained behind the ear of African elephants. In a study conducted by Siengdee *et al.*, 3 × 3 cm<sup>2</sup> biopsies from domesticated adult Asian elephants were collected post-mortem (Siengdee *et al.*, 2018). In both studies, establishment of the respective African and Asian elephant cell lines had a success rate of 83.33%. In this study, the first explant fibroblasts were observed 8 – 25 days for the African elephant. Siengdee *et al.* observed the first fibroblasts 4 – 12 days after culturing (Siengdee *et al.*, 2018). A study on primary human fibroblasts showed that tissue pieces with ragged edges contributed to poor attachment/cell outgrowth (Vangipuram *et al.*, 2013), while in a different study on fibroblast cultures from mouse ear and tail tissues, it was observed that insufficient cutting or digestion resulted in low recovery of fibroblasts (Khan & Gasser, 2016). The poor

outgrowth seen in biopsies from E3, E4 and E5 could possibly be due to insufficient cutting of ragged edged biopsies. The variation in the first EDF outgrowth between the 6 elephants could probably be explained by environmental factors such as the weather conditions, the time of day when samples were obtained and the duration of the transportation to the laboratory. Some researchers proposed specific time windows between sample collection and laboratory procedures and temperatures of  $<4^{\circ}\text{C}$  with no direct contact to ice (Fernandes *et al.*, 2016; Kisiel & Klar, 2019; Siengdee *et al.*, 2018). Silvestre and team did not observe any harmful effects on the viable cell yield after shipping skin samples on ice for several days (Silvestre, Sánchez & Gómez, 2004). In contrast, Siengdee *et al.* reported unsuccessful cultures of elephant biopsies left at high environmental temperatures for long periods before transported to the laboratory (Siengdee *et al.*, 2018).

Despite longer waiting periods to establish primary EDF cultures, direct explant cultures offer the advantage of conserving cell integrity and providing essential growth factors (Wang *et al.*, 2021b). Research teams promote different techniques for successful establishment of fibroblast cultures. For this study, the epidermis-dermis was separated with a scalpel and only the dermis was cut into smaller fragments and incubated as described by Fernandes *et al.* (Fernandes *et al.*, 2016). In a different study, Dos Santos and team established primary skin fibroblast lines of rabbits and hares (*Leporidae*) using dispase II, a protease that allows dermal-epidermal separation, followed by a simple enzymatic digestion with trypsin resulting in viable cells with a purity level higher than 85% (Dos Santos *et al.*, 2021). Siengdee *et al.* established fibroblasts from Asian elephants by cutting the biopsies into smaller fragments and incubating the samples with media containing collagenase type II, for 21 h (Siengdee *et al.*, 2018). In another study with mouse fibroblasts, Khan and Gasser added a collagenase D-pronase solution to the biopsies and had mouse fibroblasts adhering to tissue culture plastic surfaces between day 1 and 3 of culture (Khan & Gasser, 2016). Whereas, for human fibroblasts, Vangipuram *et al.* achieved success by coating the surface of the wells with 0.1% gelatin prior to skin biopsy fragment (Vangipuram *et al.*, 2013).

Villegas and McPhaul did not coat the culture surfaces, but allowed the human explants sufficient time to adhere to the primary culture flask (approximately 15 – 20 min) before adding primary culture medium to the flask in order to prevent floating of the explants. It allowed the residual medium to dry and form a “halo” around the explants (Villegas and McPhaul, 2005). In this study, this floating was avoided by placing the culture flask upside down for 24 hours. Despite all the variations suggested by the researchers, this study followed the less elaborate

method described by Fernandes *et al.* (Fernandes *et al.*, 2016) that resulted in the successful establishment of African elephant fibroblasts. To the best of our knowledge, this is the first successful establishment of African savanna elephant (*Loxodonta africana*) fibroblasts and a paper to this effect has been submitted for publication: Establishment of primary adult skin fibroblast cell lines from African savanna elephants (*Loxodonta africana*) to Heliyon (<https://www.cell.com/heliyon/home>) (see **Annexure VII**).

Fibroblasts are the most abundant cell type of connective tissue, the main function being to synthesise and maintain the extracellular matrix. Fibroblasts are elongated spindle-or star-like cells, with cytoplasmic projections that can be short and wide or long, thin and branched. They have 1 elongated nucleus, limited cytoplasm and the fibroblasts grow aligned and in bundles when confluent (Vangipuram *et al.*, 2013; Villegas & McPhaul, 2005). **Figure 38** in Section 3.1.1. clearly confirms the presence of fibroblasts in the EDF culture based on the typical morphology displayed and the known growth properties of fibroblasts. Fibroblasts are characterised by the expression of mesenchymal cellular markers like vimentin, and type I collagen and labelling for vimentin as done by Khan and Gasser (Khan and Gasser, 2016) and will be done for these newly established fibroblasts in a forthcoming study. Culture media used for fibroblasts differ and while EMEM was used for this study, other research groups used Dulbecco's modified Eagle's medium (DMEM) (Siengdee *et al.*, 2018; Vangipuram *et al.*, 2013; Villegas & McPhaul, 2005). Reports show that both types of media support the growth of fibroblasts unlike e.g. keratinocytes that need additional supplements and growth factors (Siengdee *et al.*, 2018; Vangipuram *et al.*, 2013; Villegas & McPhaul, 2005).

In this study, the skin punch biopsies were obtained in the elephant's natural habitat, which is challenging to control and might increase the risk for microbial contamination. Therefore, a high concentration of 10% P/S/A antibiotics was added to the transport media, 1% P/S/A in the initial culture media and washing PBS which contained 10% P/S/A and 2% Gentamicin (see Section 2.1.1 and 2.1.2.). The high anti-bacterial and anti-fungal agents are in accordance with other research groups (Fernandes *et al.*, 2016; Kisiel & Klar, 2019; Siengdee *et al.*, 2018; Wang *et al.*, 2021b). Siengdee *et al.* reported that as soon as microbial contamination was detected, everything was discarded and the same rule was applied in this study (Siengdee *et al.*, 2018). Additionally, a 16S ribosomal RNA PCR confirmed that the EDF cell lines were clean of bacterial infections. Anti-bacterial and anti-fungal agents can affect cell cycle regulation, differentiation and growth (Ryu *et al.*, 2017), Gentamicin treatment can result in mitochondrial dysfunction and oxidative damage in mammalian cells and Amphotericin B can decrease cell

viability (Elliott & Jiang, 2019; Grela *et al.*, 2018). Therefore, anti-bacterial and anti-fungal agents that could potentially affect the replication rate, was limited to passage 1 of the EDF cell lines.

An Asian elephant skin fibroblast growth curve ( $n = 5$ ) at passage 6 had a Td of about 25 h (Siengdee *et al.*, 2018) and Wang *et al.* showed a Td of 34 h at passage 3 for a hippopotamus fibroblast cell culture (Wang *et al.*, 2021b). The EDF growth curve in this study, was established from 3 elephants (E3, E4 and E5) at passage 1. It was found that the EDF cell line had a significantly longer Td of  $62.13 \pm 7.00$  h (average  $\pm$  SD) compared to the previously mentioned cell lines. Individual variations in Td and outgrowth are expected for skin punch biopsies originating from different elephants. Seluanov *et al.* described a Td of approximately 7 days for naked mole rats, possessing cancer suppression mechanisms similar to that of the elephants, whereas human fibroblasts divide approximately every 2 days (Seluanov & Ribeiro, 2009). The relatively slow Td of the primary EDF cultures could potentially be linked to their underlying cancer suppression mechanism, including a lower somatic mutation rate and BMR (Caulin & Maley, 2011; Totter, 1980). The dissimilarities in fibroblast growth curves obtained in the different animals could be linked to differences at the molecular level such as differences in the number of TP53 genes. The TP53 status of the African elephant was not tested in this study. The presence of the 20 copies of TP53 was based on previous literature (Abegglen *et al.*, 2015, 2022; Callier, 2019; Caulin and Maley, 2011; Ferris *et al.*, 2018; Nunney *et al.*, 2015; Seluanov and Ribeiro, 2009; Sulak *et al.*, 2016; Tollis *et al.*, 2019) however, needs to be confirmed in future studies and is a limitation for this MSc thesis.

Determination of mitotic indices (MI) after the removal of HU was used to determine the durations of the S phase, G2/M transition period and mitosis (Loitering *et al.*, 1996). The MI reached a peak between 36 – 39 h indicating the transition from G2 to mitosis for E6 cells at passage 9. This sharp increase in the MI, 36 h after the release from the G1/S block indicated the beginning of mitosis with some cells mostly in prophase. A mitotic peak was reached at 39 h. At this stage metaphase cells predominated. Evidently the passage number could influence the replication rate and cell cycle duration, since the EDFs at passage 9 had a faster replication rate than the rate mentioned for passage 1 above (see Section 3.1.3). It has been shown that human embryonic stem cells often undergo culture adaptation showing altered growth characteristics, such as increased population Td and plating efficiency (Gokhale *et al.*, 2015). The shorter cell cycle (39 – 40 h), observed in passage 9 EDF cells, was probably due to tissue culture environment adaptation by the cells. The cell cycle duration was only studied in 1 of



the elephant fibroblasts lines and it could be speculated that the average of all the EDF cell lines could probably alter the picture slightly since inter-elephant variability was found with the growth curve at passage 1 (**Figure 39** in Section 3.1.2.). Furthermore, Kasinathan *et al.* observed that the mean cell cycle length in isolated bovine fetal and adult fibroblasts ranged from 9.60 – 15.50 h. This was considerably shorter than they expected and shorter than that observed for cells cultured as a population, even at low confluence (22 h at 25% confluence), indicating that fibroblasts have an inherent cell cycle length similar to that of embryonic cells. Furthermore, this result indicates that cell cycle length is influenced by the degree of contact inhibition in culture (Kasinathan *et al.*, 2001). Cell exposure to inhibitors used for cell synchronisation such HU, thymidine and aphidicolin could lead to activation of ATR and ATM protein kinases other DNA damage signaling (Darzynkiewicz *et al.*, 2011; Halicka *et al.*, 2016; Kurose *et al.*, 2006). In this study, treatment with HU did not have any toxic effect on the EDFs. HU inactivates ribonucleotide reductase. Ribonucleotide reductase is composed of 2 non-identical subunits: M1, which contains the allosteric binding sites for effector molecules, and M2, which contains the tyrosyl radical necessary for the reduction reaction, and to which HU binds (Thelander & Reichard, 1979). HU, by destroying the tyrosyl radical on the M2 subunit of ribonucleotide reductase, is a specific inhibitor of DNA synthesis (Albert & Nodzenski, 1989). Gasparri *et al.* synchronised fibroblasts by starvation. This method, which is also known to induce apoptosis in some cell lines, proved to be ineffective as the starved human skin fibroblasts, at baseline levels, had high mitotic indices ranging from 4.5% to 6.5% (Gasparri *et al.*, 2004). It is now known that serum deprivation leads to apoptosis and changes in oncogene expression (Pucci, Kasten & Giordano, 2000). A maximum MI of 10.4% was reached for this study, indicating the HU had no significant effect on the EDFs and the cells were in a healthy state. Among all cell types, fibroblasts are plastic and resilient cells (Dos Santos *et al.*, 2021). Furthermore, cells synchronised by thymidine and/or HU show higher expression levels of cyclins A and B1 in S- and G2 phases than in mitotically selected cells progressing normally through the cell cycle (Beyrouthy *et al.*, 2008).

Cell cycle arrest at different phases can also be achieved by either Nocodazole, Colchicine or Colcemid that act by inhibiting mitotic spindle formation (Ligasová & Koberna, 2021). Colcemid was used in this study to obtain a chromosome metaphase spread. The quality of the metaphase chromosome spread can decrease with longer Colcemid incubation times such as >6 h due to chromosome condensation and the shorter Colcemid incubation period (3 h) applied in this study is in accordance with previous research (Howe, Umrigar & Tsien, 2014;

Mirzaghaderi, 2010; Nasonova *et al.*, 2009). Insufficient time in Colcemid treatment yields fewer metaphase chromosome spreads and longer incubation times with Colcemid results in shorter and thicker chromosomes which makes analysis difficult (Howe, Umrigar & Tsien, 2014). Howe *et al.* stated that a successful assay yields chromosomes which are well spread and of suitable quality for chromosome morphology analysis (Howe, Umrigar & Tsien, 2014). **Figure 1** (in Section 3.2.) displays a chromosome metaphase spread after a 3 h Colcemid incubation showing the diploid number of 56 chromosomes in the EDF cell line which is in agreement with the Elephantidae family (Frönicke *et al.*, 2003; Hungerford *et al.*, 1966; Yang *et al.*, 2003). This confirms that the EDF cell line originates from an African elephant. The common hippopotamus is diploid with 36 chromosomes, while Great Apes (*Hominidae*) have 48 chromosomes and humans have 46 chromosomes (Stankiewicz, 2016). Frönicke *et al.* reported a predominantly acrocentric karyotype consisting of  $2n = 56$  chromosomes for the African savanna elephant containing only 1 sub-telocentric and 2 metacentric autosomes (Frönicke *et al.*, 2003). Palkopoulou *et al.* formally reported the high-quality reference genome of the African savanna elephant which first became available in 2005 (LoxAfr1) and has been updated in 2014 (LoxAfr4) (Wang *et al.*, 2019). Investigations on the ancestral karyotype of humans and elephants concluded that human painting probes produced identical hybridisation patterns in both the African and Asian elephants, confirming that both species possess karyotypes that differ only in the amount and distribution of C-band positive heterochromatin (Yang *et al.*, 2003). Chromosome rearrangements are a hallmark of genome evolution and essential for understanding the mechanisms of speciation and adaptation (Kim *et al.*, 2017). Potential answers can be obtained in the EDF chromosomes which could provide insight into neoplasia in humans.

A small sample size was used for this study and is a limitation in this MSc thesis however, it is a step closer to cryopreserving the African savanna elephant genome. Due to the variability in biopsy outgrowth, Td and MI, one can conclude that a larger sample size is needed to precisely determine individual variations among the different elephants. Due to the low accessibility, ethical and administrative constraints, it is challenging to obtain larger sample sizes. In addition, the biopsy samples are collected from semi-free ranging elephants in the wild and are influenced by environmental factors and high risk of contamination.

# CHAPTER 4:

## DISCUSSION

---

### Section B: Primary normal human dermal fibroblast (NHDF) vs primary elephant dermal fibroblast (EDF) radiation response post X-ray irradiation

The induction of DNA damage by exposure to X-ray radiation *in vitro* is a method to investigate how the presence of 20 copies of TP53 in elephant fibroblasts cells affect the DNA damage response in comparison to human fibroblast cells containing only 1 copy of TP53.

In the current study, the NHDF and EDF cells showed reduced levels of survival with increasing doses of IR with the CSA. This dose-dependent decrease in colony formation is widely accepted in the radiobiology field and these results confirm previous findings with fibroblasts (Buch *et al.*, 2012; Liu *et al.*, 2019). In preparation of the CSA, the optimal seeding density was determined. Brix *et al.* showed that plating efficiency is cell line dependent (Brix *et al.*, 2020). In this study, the lowest number of cells seeded yielded the highest plating efficiency of 21.50% in the NHDFs. Contact inhibition is a well-known mechanism that enables non-cancerous cells to cease proliferation and growth when they contact each other, which results in a stop of proliferation upon reaching confluency (Eagle & Levine, 1967). While this phenomenon is mainly observed in epithelial cells, fibroblasts exhibit 2 closely related phenomena as described by Ribatti (Ribatti, 2017), contact inhibition of locomotion and contact inhibition of proliferation. Normal fibroblasts migrate across the surface of a culture dish until they contact a neighbouring cell, leading to the inhibition of cell migration and adherence to each other. The latter might explain why the best plating efficiency was obtained with the lowest seeding density of NHDFs in this study. Furthermore, Kuznetsov *et al.* observed that the degree of colony-forming efficiency reduction was species- and donor-related (Kuznetsov *et al.*, 2009). In addition, Panteleeva *et al.* found that there was a decrease in survival rate in murine fibroblasts, but not in human epithelial cell line when exposed to X-

rays (Panteleeva *et al.*, 2003). When looking at how the radiation exposure affected both the NHDF and EDF cell lines in this study, no significant difference ( $p = 0.86$ ) was found between the 2 different mammalian cell lines. Despite the fact that the EDFs had a 3.72-fold higher cell survival at 8 Gy when compared to the NHDF, no conclusive results were obtained with the CSA. However, the NHDFs lower  $\alpha/\beta$  ratio possibly indicated that these cells have a higher repair capacity in comparison with the EDFs. The EDFs appear to be more radiosensitive based on the  $\alpha/\beta$  ratio, but further investigation is needed. The results found does not confirm the hypothesis that the multiple copies of TP53 RTGs found in the African elephant genome result in a higher level of proliferative cell death upon the induction of DNA damage.

The cell proliferation assay revealed that the NHDFs and EDFs responded to IR was dose dependent and not time dependent. At 24 and 48 h the NHDFs cell proliferation capacity showed no dose dependent effect as observed at 72 – 144 h and one can conclude that is it related to the long doubling time of the cells (Tamm *et al.*, 1984). Truong and team concluded that low doses of X-ray radiation might cause an initial pause, followed by a significant increase in proliferation. The initial pause in the cell proliferation could be a protective mechanism of the cells to minimise the DNA damaged caused by the radiation exposure and be the result of the induction of cell cycle arrests (Truong *et al.*, 2018). From 72 h onward, a decrease in cell proliferation was observed with increasing radiation doses in the human fibroblasts.

Based on the initial cell proliferation results obtained with the NHDFs cells covering a time range of 24 h up to 144 h, the 72 and 120 h time points were selected for the comparison in cell proliferation between NHDF and EDF cells in this study. These 2 time points also seemed optimal based on the Td of the EDFs determined in Section 3.1.3 of 62.13 h. As expected, a dose dependent effect was also observed with increasing radiation doses in the EDFs. One could conclude that the cells were initially arrested to repair the DNA damaged inflicted by the IR or induce a cell death pathway or replicative senescence if DNA damaged was irreparable. This could explain why the cell proliferation levels at 72 h in EDFs were lower compared to the 120 h results. At this later time point, the EDFs showed remarkable recovery post 1 and 2 Gy irradiation with a cell proliferation at 104.34% and 102.34%, respectively (**Figure 52** in Section 3.6). This raises the hypothesis that the DNA damage response of the EDFs acts faster compared to NHDFs due to the presence of the TP53 RTGs, which requests for an expansion of the current study where additional time points should be tested for EDFs as well. John and Little observed that radiation in sufficient doses inhibit mitosis which stops the cells ability to divide and proliferate indefinitely (John & Little, 2003). Wang *et al.* reported that that RT

affects fibroblasts negatively through growth arrest and cell senescence or RT promotes activation of normal fibroblasts through inducing a senescence-like phenotype (Wang *et al.*, 2019). Fibroblasts derived from human skin biopsies were treated with either with a single dose of 3.5 Gy or 10.5 Gy in 3 consecutive daily fractions. The pathways that responded to the corresponding radiation were associated with a few biological processes (Wang *et al.*, 2019):

- i. Cell cycle arrest was mainly induced by ATM/ATR signaling pathway and the upregulation of TP53.
- ii. DNA repair process which includes BER, NER, MMR, HR and NHEJ (Chatterjee & Walker, 2017; Hall & Giaccia, 2012; Martín-López & Fishel, 2013; Simonelli *et al.*, 2005). Repairing the DNA damage is a critical process after IR which repeated itself inside the cell (see Section 1.6.1 for more information on the repair processes).
- iii. ROS scavenging, which participates in radiation induced biological processes.

Addis *et al.* stated that fibroblast migration and proliferation bear crucial roles in the healing process by initiating the proliferative phase of repair (Addis *et al.*, 2020). Truong *et al.* observed that low-dose of soft X-ray radiation had stimulating effects on the proliferation of cell types such as fibroblasts and osteoblasts, as well as in animal models (Truong *et al.*, 2018). Liang *et al.* found that low-dose  $\gamma$ - and X- ray irradiation in cell lines have demonstrated a dose-response phenomenon characterised by low-dose stimulation (<0.05 Gy) and high-dose inhibition (>0.075 Gy). They found that low doses induce cell proliferation in the normal human embryonic lung fibroblast cell line, mouse hematopoietic progenitor cells and rat mesenchymal stem cells (Liang *et al.*, 2016). While Wang and team found fibroblasts are able to tolerate harsh extracellular environments for example IR (single dose of 3.5 Gy or 10.5 Gy in 3 consecutive daily fractions), which are usually fatal to all other cells (Wang *et al.*, 2019). Based on the evidence of previous research mentioned above, fibroblasts are able to continue to proliferate after low doses (1 – 2 Gy), however this was only observed for the elephant fibroblasts and not in human fibroblasts in the current study.

The MTS assay revealed a significant decrease in cell viability of the NHDFs 72 and 120 h post-irradiation which is in accordance with the cell proliferation assay. Masson-Meyers *et al.* stated that in their study the cell viability decreased significantly when fibroblast was irradiated and is due to impaired mitochondrial metabolic activity (Masson-Meyers, Bumah & Enwemeka, 2016). Unfortunately, this assay could not be conducted on EDF cells in this study but will be included in future experiments as part of the TUSCC project. It will be most

interesting to see if the cell viability results with MTS will confirm the cell proliferation results described in the previous paragraph. Based on these cell proliferation findings for EDFs at 72 and 120 h, additional earlier time points will be included in the analysis. More copies of TP53 could possibly play a role in the cells ability to function and could ultimately lead to a faster induction to cell cycle arrest to repair the damage DNA inflicted by radiation. However, the induction of cell death if the damage is too severe is also an option to prevent cancerous cell to continue to divide. Abegglen and team stated that elephants cells are hypersensitive to stress factors which enables them to have an enhance apoptosis reaction to prevent cancer formation (Abegglen *et al.*, 2015). Furthermore, Sulak and team determined the consequences of an enhanced TP53 response when treating primary African and Asian elephants and other family members such as South African Rock hyrax (*Procavia capensis capensis*), East African aardvark (*Orycteropus afer lademanni*) and Southern Three-banded armadillo (*Tolypeutes matacus*) dermal fibroblasts with stressors (mitomycin C, doxorubicin or UV-C) and measured cell viability, cytotoxicity and the induction of apoptosis. They found that lower doses of stressors decreased cell viability and induced apoptosis in elephants cells than the other species and that the magnitude of the response was greater in elephant than other species (Sulak *et al.*, 2016). In the current study for cell viability, the elephant fibroblasts showed a low-dose (1 and 2 Gy) stimulation and high-dose (4, 8 and 16 Gy) inhibition at 120 h post X-ray irradiation (**Figure 52** in Section 3.6.), while the human fibroblasts showed a dose dependent effect for all doses at the same time point.

Abegglen *et al.* investigated lymphocytes of the African elephant and humans. African elephant lymphocytes demonstrated apoptosis at significantly higher levels in comparison to human lymphocytes post 18 h 2 Gy IR: late apoptosis was 33.20% (elephant) vs 14.07% (human),  $p < 0.001$  and early apoptosis was 21.07% (elephant) vs 11.73% (human),  $p < 0.001$  (Abegglen *et al.*, 2015). Due to the elephant's distinctive body size and burden to reduce somatic mutations and cancer risk, elephant genes that respond to DNA damage are important candidates for shaping mammalian mutation and cancer resistance phenotypes (Tollis, Boddy & Maley, 2017). Since Abegglen *et al.* observed higher levels of apoptosis in the elephant lymphocytes, it was postulated that for this study on EDFs vs NHDFs, the same trend would transpire. In the current study, apoptosis-mediated cell death was investigated to differentiate between the response of fibroblasts containing TP53 RTGs (elephant cells) and the lack of TP53 RTGs (human cells), respectively. Furthermore, in view of the decrease in cell numbers observed in the CSA SF and cell proliferation assay, it was deemed that the decrease was due to apoptosis.

However, the current study did not show a significant early or late apoptosis induction at 12, 24 and 48 h after exposure to 8 Gy (**Figure 54 – 56** in Section 3.8.1). The EDFs had a higher percentage of cells committed to early and late apoptosis in comparison to the NHDFs, but this result was not statistically significant. The slight increase in apoptosis in the EDFs could be probably due to the extra copies of TP53 in the elephant fibroblasts, but the lack of statistical significance does not allow us to draw decisive conclusions. In addition, the IR dose delivered to the fibroblasts in this study was 4-fold higher than the study of Abegglen *et al.* and no significant presence of apoptosis was seen (Abegglen *et al.*, 2015). However, lymphocytes are known to be one of the most radiosensitive tissues and are prone to radiation-induced apoptosis (Lambin *et al.*, 2020). Therefore, the findings of Abegglen and team in lymphocytes may not necessarily apply to fibroblasts since radiation-induced apoptosis is cell type dependent. Especially since fibroblasts are not prone to apoptosis (Hanson *et al.*, 2019; Mellone *et al.*, 2017), even primary rat fibroblasts do not undergo apoptosis following serum withdrawal or irradiation (McKenna *et al.*, 1996). It is probably due to this reason that the decrease in cell numbers following irradiation in the current study can't be explained via an apoptosis-mediated cell death pathway. Therefore, further investigation is warranted to understand what major cell death pathway the NHDF and EDF cells undertake. The activation of TP53 after genotoxic insults may result in 2 different responses: apoptosis or growth arrest (Attardi, De Vries & Jacks, 2004; Heinrichs and Deppert, 2003). While the former is considered untrue for dermal fibroblasts even when containing extra copies of TP53, the latter is more convincingly observed in the elephant fibroblast cell lines.

Radiation-induced DNA damage triggers the activation of G1/S, G2/M and intra-S cell cycle checkpoints, consequently slowing the progress of radiation-exposed cells in the cell cycle (Khan & Wang, 2022). Cell cycle checkpoints can enhance cell survival and limit mutagenic events following DNA damage which leads to cell cycle arrest, DNA repair and cell death (Clay & Fox, 2021; Kastan *et al.*, 1992). Exposure of eukaryotic cells to IR is known to affect the normal progression through G1-, S- and G2 phases of the cell cycle (Antoccia *et al.*, 2009). For this study, more than 84.50% of the NHDF cells were in G0/G1 phase throughout all the conditions and no clear shift in the cell cycle phases were noted with the different conditions. Similarly, Antoccia *et al.* found that unsynchronised normal human primary fibroblasts cells remained arrested in the G1 phase for several days at doses of 1 – 4 Gy for both X-ray and protons and (Antoccia *et al.*, 2009). Furthermore, primary murine fibroblasts were restricted in a G1 checkpoint activated by IR when both wild-type TP53 alleles were disrupted (Kastan *et*

*al.*, 1992). The signal transduction pathway that controls cell cycle arrest following DNA damage rely on the ataxia-telangiectasia gene, TP53 and GADD45 and abnormalities in this pathway contribute to tumour development (Kastan *et al.*, 1992). Irradiated-human fibroblasts, by persistent expression proteins of p53, p16 and p21, show hallmarks of G0 growth arrest, senescence or differentiation (Antocchia *et al.*, 2009). The NHDFs in this thesis remained in G0/G1 phase 48 h post-irradiation and could possibly have reached a permanent cell cycle arrest remaining in a quiescent state as mentioned by Urban and Cheung showed in **Figure 59**.

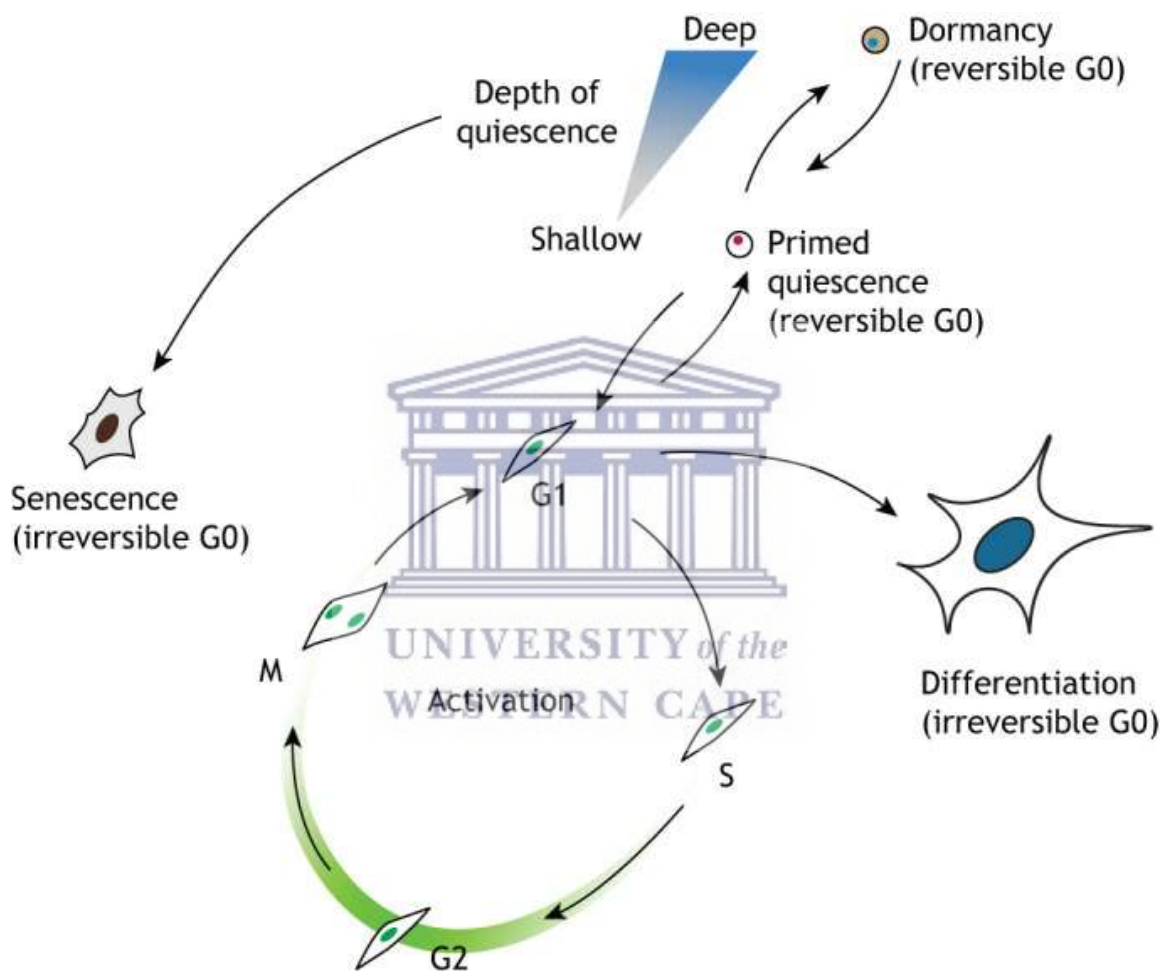


**Figure 59: Cellular states and transitions into quiescence.** Quiescent cells can reversibly transition into an active state in which they enter the cell cycle and generate new differentiated cells to maintain tissue homeostasis. In contrast to differentiation, cells can enter an irreversible senescent (G0) state, therefore hampering the regenerative potential (Urban and Cheung, 2021).



Cell cycle progression of the EDFs displayed a significant G2/M arrest after IR for 24 and 48 h. TP53 has been implicated in the control of G2/M arrest via 3 possible mechanisms (**Figure 14** in Section 1.4.4.2) (Kastan, 2016; Taylor & Stark, 2001). Firstly, TP53 induces the transcription of the GADD45 gene and p21 that disrupts the cyclin B1-CDK1 complex (G2 arrest) (Nosrati, Kapoor & Kumar, 2015; Wang *et al.*, 1999). Secondly, TP3 can induce the transcription of 14-3-3 binds and sequesters the phosphorylated CDC25 in the cytoplasm, preventing its activation (Wang *et al.*, 1999). Thirdly, a direct process of transcriptional down-regulation of cyclin B1 by TP53 could happen (**Figure 59**) (Baus *et al.*, 2003; Liu *et al.*, 2019). The dysfunction of checkpoints leads to uncontrolled proliferation, accumulation of mutations and ultimately, progressive survival advantage (Nosrati, Kapoor & Kumar, 2015). In the 14-3-3 family, 14-3-3 $\sigma$  is overexpressed in some cancers, including colon carcinoma and pancreatic ductal carcinoma, where it has been shown to promote cell survival and invasiveness (Pennington *et al.*, 2018). The p21 protein exerts a key role in driving the G2 phase exit both by inhibiting cyclin B-CDK1 and cyclin A-CDK1/2 complexes, which control G2/M progression and by blocking the phosphorylation of pRB family proteins (Baus *et al.*, 2003; Liu *et al.*, 2019). Agarwal *et al.* reported that regulated expression of wild-type TP53 in TP53-null human fibroblasts causes growth arrest in both G1 and G2/M and the arrest is associated with high levels of p21 and is reversible (Agarwal *et al.*, 1995). Therefore, the results of the current study support Agarwal results since a dose dependent stimulation occurred at 120 h for 1 and 2 Gy in the cell proliferation assay (**Figure 52** in Section 3.6). At low doses, one can conclude that the G2/M block might have allowed the cells to repair the DNA damage, followed by a lift of the cell cycle arrest and a continuation of cell proliferation after 120 h as seen in the cell proliferation assay. Unfortunately, at this stage of the project, it remains speculation if the presence of TP53 RTGs in EDFs provide a better control of cell cycle checkpoints and switch on the cell cycle arrest faster compared to the NHDF cells where no changes in cell cycle distribution were observed during irradiation. In addition, the outcome of the DNA damage repair (or misrepair) was not investigated in this study, which does not allow us to draw conclusion on chromosomal instability and potential radiation-induced cancer risks.

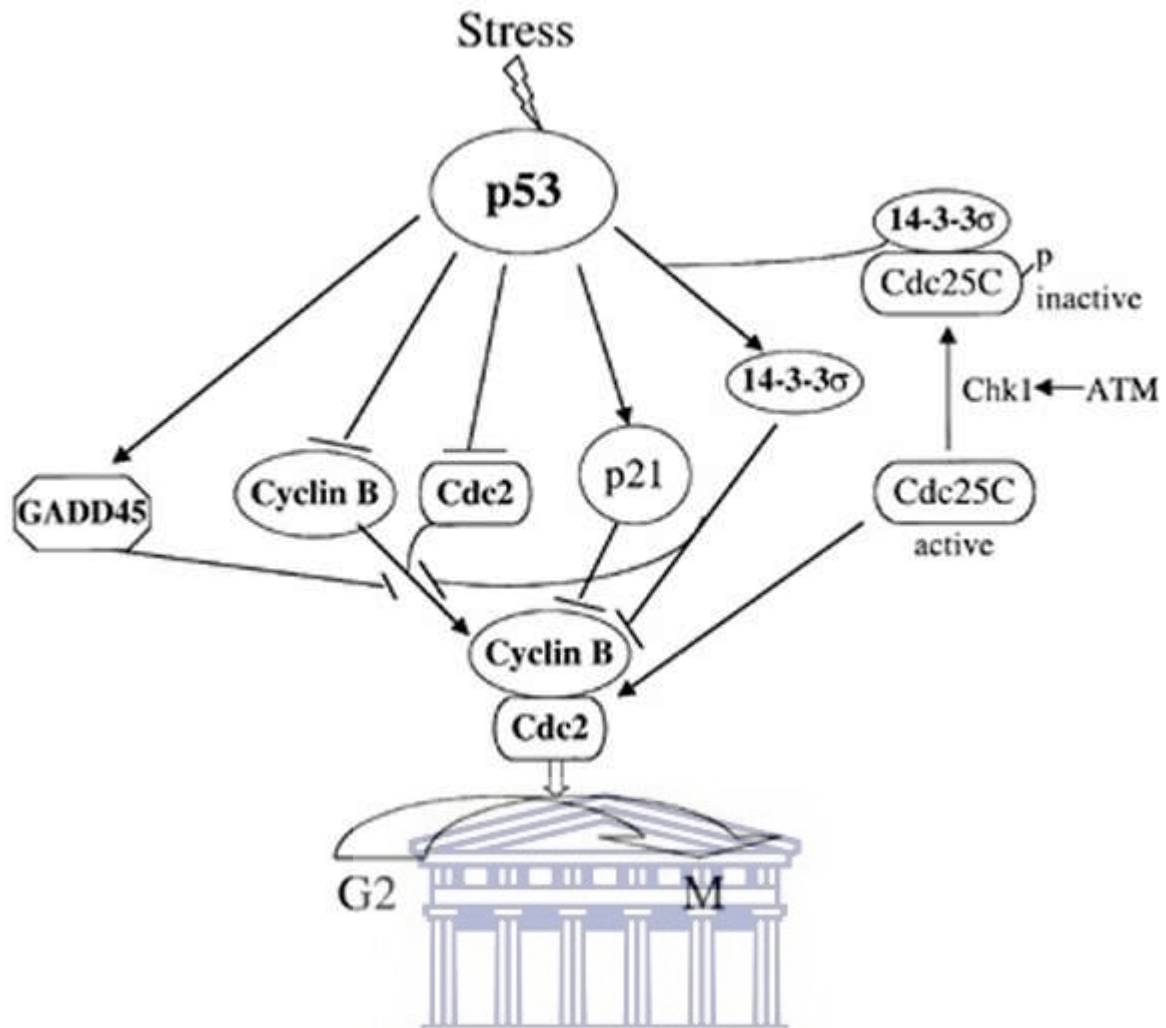


**Figure 60: Contribution of the p53 protein to induce G2/M cell cycle arrest.** When DNA damage is present within the cell, the p53 protein triggers several parallel pathways that block the formation of the mitotic cyclin B-CDC2 complex and inhibit its activity to allow cell cycle continuation. The p53 protein targets the upregulation of p21 and causes an inhibition of the cyclin B-CDK complex acting as a cell cycle block. The upregulation of p53 acts on GADD45 and results in the binding to CDC2 and prevent the cyclin B complex activation. The p53 protein sequesters 14-3-3 $\sigma$  and inhibits the phosphorylated form of CDC25 isoform C which in turn dephosphorylate cyclin B-CDK complex. In addition, 14-3-3 $\sigma$  recruits CDC2 in the cytoplasm, preventing it from translocating into the nucleus in the late G2 phase. The p21 protein, GADD45, 14-3-3 $\sigma$  all are upregulated in the presence of TP53 in response to DNA damage inducing a G2/M cell cycle block (Sionov, Hayon & Haupt, 2013).

G2/M arrest occurs in the presence of DSBs, which prevents cells from entering the M phase and repair the DNA damage (Wang, 2014). Post-irradiation the recovery process can be delayed and sometimes if the DNA damage is irreparable it can lead to mitotic catastrophes that result in cell death (Khan & Wang, 2022). Since a high-dose inhibition effect was observed at 120 h for the cell proliferation assay one can conclude that EDFs entered the G2/M block indicated by the cell cycle assay, however, were unable to repair the DNA damage. However, comparing 72 and 120 h, a higher cell proliferation was observed indicating that some cell death occurred at high doses but also the remaining cells were able to repair the DNA damage and started to proliferate again (considering the Td of > 60 h, see Section 3.1.3.) Liu *et al.* observed with increasing irradiation doses, a gradual decrease in G0/G1 phase and a gradual increase in G2/M phase which support the results found in this study (Liu *et al.*, 2019). The hypersensitivity to DNA damage in elephant cells gives them the ability to eliminate cancerous cells at a very early stage (Abegglen *et al.*, 2015). Lui *et al.*, also reported that the more severe the IR induces DNA damages, the longer the cells were blocked in a specific cell phase (Liu *et al.*, 2019).

Furthermore, Sulak and team data suggested that at least 2 non-exclusive models of TP53 RTG action in elephants (Sulak *et al.*, 2016):

- i. TP53 RTGs may act as ‘decoys’ for the MDM2 complex allowing the canonical p53 protein to escape negative regulation; and
- ii. TP53 RTGs may protect canonical TP53 from MDM2 mediated ubiquitination, which requires tetramerisation by dimerising with canonical TP53 and thereby preventing the formation of tetramers.

The upregulation of TP53 RTGs results in a rapid respond to lower levels of DNA damage and stress compared to African elephant family members such as South African Rock hyrax, East African armadillo and Southern Three-banded armadillo fibroblasts (Sulak *et al.*, 2016). Their RNA sequencing data suggests that at least TP53 RTG 12, TP53 RTG 18/19 and TP53 RTG 13 are transcribed in African elephant dermal fibroblasts (Sulak *et al.*, 2016). Abegglen *et al.* reported on TP53 RTG 14 or TP53 RTG 5 expression in adipose, placenta or fibroblasts suggesting that the expression of some TP53 RTG is tissue specific (Abegglen *et al.*, 2015). In our study, it looks like the TP53 RTGs present in elephants induce growth arrest in G2/M phase, while this was not observed in the NHDFs, however needs to be confirmed in future studies.

Over the course of evolution, the African elephant underwent a series of adaptations which enabled them to have an enhanced monitoring of genomic integrity and to have the ability to eliminate pre-cancer cells, which decreases the cancer incidence rate in these mammals. The observations of Sulak *et al.* confirm that elephant cells may have an altered TP53 signalling system compared to species without expanded TP53/TP53 RTG (Sulak *et al.*, 2016). To determine which subpopulation of the p53 protein or other molecules for controlling the cell cycle are upregulated in response to DNA damage, needs to be understood in future studies. This MSc study encountered several limitations, of which the Covid-19 pandemic was the most severe one. However, it lays the foundation for future studies, particularly by the establishment of primary EDF cell lines which simplifies future experiments drastically, since experiments can now be scheduled and do not necessarily depend on the availability of an elephant sample. These future experiments are essential to understand whether TP53 RTG genes are casually related to the resolution of Peto's paradox in Proboscidean lineage or if they are irrelevant relicts of ancient transposition events, like so many other pseudogenes that riddle mammalian genomes (Sulak *et al.*, 2016).



# CHAPTER 5:

## CONCLUSION

---

Developing novel cancer treatments or prevention strategies based on naturally occurring cancer resistance shaped by species evolution, lifestyle and body characteristics is an important trademark of biomimetics. The findings of this research project could rapidly advance the development of new strategies for the prevention of radiation-induced cancers or the sensitisation of cancer cells to RT. Cancer resistance has evolved over the course of evolution in the animal kingdom. Species such as the African savanna elephant display cancer resistance and one of the possible mechanisms is the duplication of TP53 RTGs in their genome. The TP53 RTGs mechanism is beginning to be understood by conducting novel research with the African savanna elephant. However, other possible mechanisms can also play a role in their cancer resistance and will be part of future experiments as a continuation of this project.

Primary dermal fibroblast cell lines, using small skin punch biopsies from living, semi- and free-roaming African savanna elephants, were established and characterised. On average, the first explant of fibroblasts outgrowth was observed after 8 – 25 days (n = 6). An overall biopsy success rate of 83.33% was obtained. The EDF Td was  $62.13 \pm 7.00$  h (average  $\pm$  SD) at passage 1 (n = 3). A metaphase chromosome spread was obtained which confirm the diploid number of 56 chromosomes in the *Loxodonta africana*. This opens the scope for future cytogenetic studies on the EDF cells of African savannah elephants. Investigating the cell cycle kinetics of the EDFs at passage 9, revealed a peak in the MI at 39 h after the release of G1/S block. Preliminary results indicate a length of the G0/G1 phase of 20 – 22 h, the S phase 10 h, the G2/M phase 5 h and M phase 1 h. Furthermore, the establishment of a primary cell line from African savanna elephants allows the preservation of their genetic material for conservation efforts.

The radiation sensitivity of elephant and human dermal fibroblasts cells were investigated using 250 kVp X-ray irradiation in order to evaluate the impact of the 20 copies and 1 copy of TP53 in EDFs and NHDFs, respectively. The NHDFs and EDFs were sensitive to radiation and showed a decrease in SF and cell proliferation when exposed to higher doses of X-ray

irradiation. No significant differences were found in the CSA between the NHDFs and EDFs. However, the EDFs showed to be more radiosensitive based on the  $\alpha/\beta$  ratio in comparison to the NHDFs. While the cell proliferation assay showed a significant decrease in NHDFs after the higher doses, the EDFs showed a remarkable recovery 120 h after irradiation with the lower doses (1 – 2 Gy) and a slight recovery after the higher doses (4 – 16 Gy). The extend of TP53-mediated apoptosis is cell line dependent and fibroblasts are known to preferentially go into senescence rather than apoptosis. No significant difference in radiation-induced apoptosis was observed between NHDFs and EDFs in this study after a radiation dose of 8 Gy. Additional experiments will be required in the future to confirm this finding with different apoptosis visualisation methods. TP53-mediated cell death will require further investigation to understand what type of cell death pathway fibroblasts induce after high doses of radiation exposure.

Furthermore, more than 84.50% of the NHDF cells were in G0/G1 phase throughout all the control and irradiation conditions at different time points. The NHDFs remained in G0/G1 phase with higher doses and no change in the S- or M phase of the cell cycle was observed with different radiation doses. The radiation-induced cell cycle effects were more pronounced in the EDFs, showing a significant increase in the G2/M phase and a decrease in G0/G1 phase with higher doses at 24 and 48 h, indicating a possible G2/M cell cycle block. Moreover, an increase in cell proliferation capacity was observed at 120 h for 1 and 2 Gy with the cell proliferation assay, indicating that the G2/M was lifted. It is possible that the TP53 RTGs provided the EDFs a stricter cell cycle arrest to allow damaged DNA to be repaired before entering the M phase.

The RTGs present in the EDFs may provide an enhanced sensitivity for cell cycle arrests, but the apoptosis results do not confirm the previous observations from other research groups where an elevated sensitivity to apoptosis induction was observed in elephant lymphocytes compared to human lymphocytes. The mechanism might be cell type dependent and future studies, such as on radiation-induced senescence and different cell death pathways are warranted to explain the results reported in this thesis. In addition, further investigation is needed to understand the molecular underpinnings of TP53/TP53 RTG and other mechanisms which could play a role in elephant cancer resistance and the resolution of Peto's paradox in Proboscidean lineage. In the end, the knowledge gained during this project could be harnessed for cancer prevention and treatment in humans.

# FUTURE PERSPECTIVES

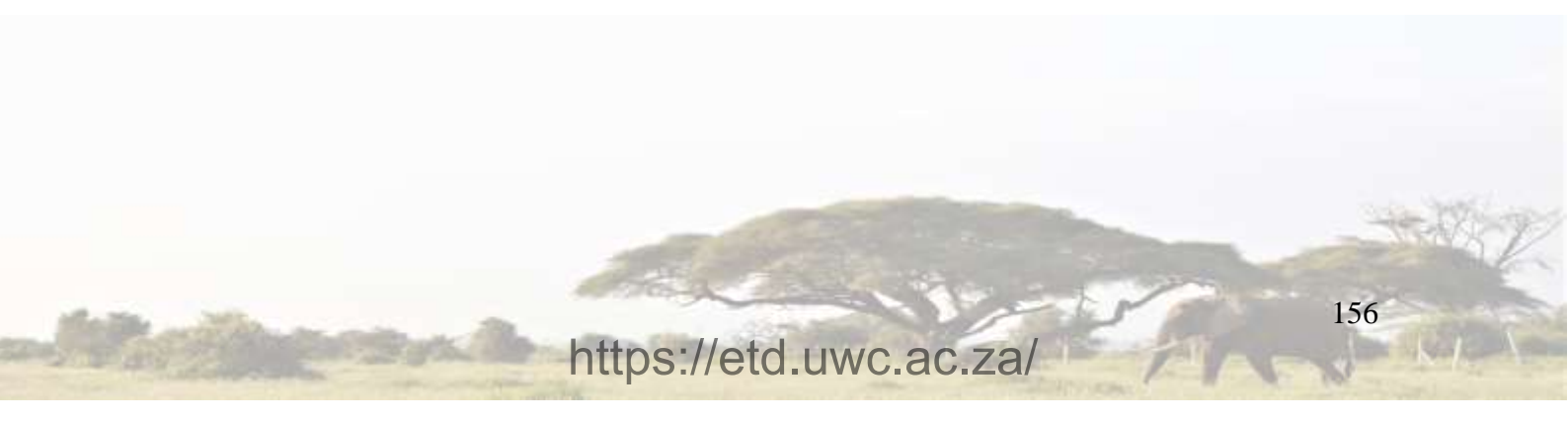
---

It is well known that primary human dermal fibroblasts cells placed in an artificial culture environment exhibit a limited replicative potential. However, the extent to which the culture environment influences proliferation life span is not completely understood but “cellular senescence” does exist (Balin *et al.*, 2002; Kuilman *et al.*, 2010; Mammone, Gan & Foyouzi-Youssefi, 2006). Senescence is a process by which cells stop replication and is characterised as distinct metabolic activity and dramatic changes in cell morphology (Mammone, Gan & Foyouzi-Youssefi, 2006; Gire & Dulic, 2015). The cellular proliferation and the transition into senescence can vary depending on the tissue of origin and the age of the source tissue (Schäuble *et al.*, 2012). Senescence is recognised as a critical feature of mammalian cells to suppress tumourigenesis, acting alongside cell death and DNA repair pathways (Nunney, 2018).

In 2013, Chen *et al.* stated that cellular senescence occurs when cultures are unable to complete 1 population doubling during a 4-week period that includes 3 consecutive weeks of refeeding with fresh medium (Chen, Li & Tollefsbol, 2013). For this methodology, the EFDs were kept in culture for up to passage 14 without seeing any clear signs of cellular senescence based on morphology and as defined by Chen and team (Chen, Li & Tollefsbol, 2013). Similarly, Wang *et al.* who established a hippopotamus primary fibroblast cell line, did not identify dramatic changes in cell size, shape and proliferation rate upon reaching passage 12 (Wang *et al.*, 2021b). Mammone and team observed an increase in cell death with increased DNA fragmentation in NHDFs *in vitro* as a function of increasing cell passage (passage 71). Serial passage of human fibroblasts also resulted in mitochondrial dysfunction, represented by a loss of mitochondrial membrane potential (Mammone, Gan & Foyouzi-Youssefi, 2006). Additionally, Kuilman *et al.* highlight the power and limitations of the biomarkers such as the increase in senescence-associated  $\beta$ -galactosidase (SA- $\beta$ -GAL) activity currently used to identify senescent cells *in vitro* and *in vivo* (Nunney, 2018).

Moreover, the upregulation of TP53 had been found in senescence cultures (Capuozzo *et al.*, 2022; Di Leonardo *et al.*, 1994; Gire & Dulic, 2015). It is not known how the 20 copies of TP53 in elephants play a role in senescence and it is possible that elephants may have an extended protection of reaching cellular senescence which aids their longevity. Qian reported that mouse studies have shown that the activation of TP53 induce premature senescence and promotes tumour regression *in vivo*. However, TP53-mediated cellular senescence also leads to aging-related phenotypes, such as tissue atrophy, stem cell depletion and impaired wound healing (Qian & Chen, 2013). As already reported in Section 1.2.3., Tyner and team studied the increase of TP53 copy number in mice and found resistance to spontaneous tumorigenesis compared to wild type TP53, but also observed premature aging (Tyner *et al.*, 2002).

Telomeres have a direct link with replicative senescence and telomere length is a molecular marker of cell aging and genomic instability due to the link between telomere shortening and aging-related diseases, especially cancer (Han *et al.*, 2009). Allsopp *et al.* said that aging in cells occur at many levels and is polygenic, however, several observation implicate a role of telomere shortening in replicative senescence of cells and telomeres shorten during aging of cultured human fibroblasts (Allsopp *et al.*, 1992). Yin and Jiang observed a rapid telomere shortening after radiation to human dermal fibroblasts (Yin & Jiang, 2013). Therefore, an active role of telomere length in ageing-related human diseases could occur since short telomeres increase the risk of diseases related to restricted cell proliferation and tissue degeneration, while long telomeres increase the risk of diseases related to increased proliferative growth, including major cancers (Aviv & Shay, 2018). As mentioned in Section 1.2.1. a possible reason why elephants can better suppress cancer can also be related to the telomere length. Research suggest that larger animals could have a shorter telomere length and therefore constrict cell replication (Tollis, Boddy & Maley, 2017; Vaiserman & Krasnienkov, 2021). Mammalian species have different telomere lengths and the rate of telomere shortening rates determine species longevity.





To understand the properties of the primary fibroblasts cell culture more comprehensively and to be able to take full advantage of it in future studies, it might be necessary to serially passage the cells for a longer period of time to determine when both the elephant and human fibroblasts enter an irreversible cell cycle arrest and induce replicative senescence with the upregulation of SA- $\beta$ -GAL activity for example (Domogauer *et al.*, 2021; Wang *et al.*, 2021b). The p53 protein isoforms: p63 and p73, have been shown to play a role in cellular senescence and/or aging. Importantly, p53, p63 and p73 proteins are necessary for the maintenance of adult stem cells and therefore, understanding the dual role the p53 protein family in cancer and aging is critical to solve cancer and longevity in the future (Qian & Chen, 2013). Furthermore, cell immortalisation is one way to eliminate the need for establishing cell cultures from the tissue samples frequently. Therefore, it might be worth to immortalise the fibroblast culture using methods as reported in previous literature to better facilitate future applications (Gouko *et al.*, 2018; Petkov *et al.*, 2018). However, the cancer suppression mechanism of elephants might require the induction of more mutations compared to rodent and human cell lines, in order to obtain immortalisation. An example is the fact that for the malignant transformation of mouse fibroblasts, 2 hits are needed (the inactivation of transformation-related protein 53 (TRP53) or pRB and an activating mutation of Harvey Rat sarcoma virus (HRAS)) (Rangarajan *et al.*, 2004). In contrast, 5 hits are needed to transform human fibroblasts, which already demonstrates that humans have evolved much more robust anticancer defence mechanisms than mice (Seluanov *et al.*, 2018). Therefore, Seluanov *et al.* suggest to establish primary cells from long-lived and/or cancer resistant species and try to induce a known set of mutational hits into these cells, such as the inactivation of tumour suppressors and activation of oncogenes (Seluanov *et al.*, 2018). This will allow us to see if a number of hits beyond those that are known from human and mouse studies are needed for tumour formation. Since primary EDF cell lines have already been established in this MSc study, these experiments can now be executed in the continuation of the TUSCC project.

Furthermore, the biopsy technique described in Section 2.1. allows for remote biopsy darting, a technique which eliminates the need for sedation and causes minimal harm to the animal (Mijele *et al.*, 2016). It provides the opportunity to collect skin tissue samples from a variety of free-ranging terrestrial animals, including the elusive African forest elephant. In the case of remote biopsy darting, it might be more challenging to obtain samples originated from the skin behind the ear of the elephant where the epidermis is thin and Global Positioning System tracking might be required to retrieve the biopsy darts. In addition, there is a risk that the dart

penetrates the skin at an oblique angle which would make the biopsy to superficial to reach fibroblasts. Remote darting might be crucial to allow future studies on telomere length and telomere shortening rate in elephants of different ages. It will reduce the stress for the elephants and the risk induced by repetitive sedation.

Comprehending replicative senescence, studies on telomere shortening rate and the possible to enable immortalisation of the primary EDF cell lines will be important steps in the future studies of the TUSCC project.



# LIST OF REFERENCES

---

Abegglen, L.M., Caulin, A.F., Chan, A., Lee, K., Robinson, R., Campbell, M.S., Kiso, W.K., Schmitt, D.L., Waddell, P.J., Bhaskara, S., Jensen, S.T., Maley, C.C. and Schiffman, J.D. (2015) 'Potential mechanisms for cancer resistance in elephants and comparative cellular response to DNA Damage in Humans', *JAMA - Journal of the American Medical Association*, 314(17), pp. 1850–1860. Available at: <https://doi.org/10.1001/jama.2015.13134>.

Abegglen, L.M., Harrison, T.M., Moresco, A., Fowles, J.S., Troan, B. V, Kiso, W.K., Schmitt, D., Boddy, A.M. and Schiffman, J.D. (2022) 'Of Elephants and Other Mammals: A Comparative Review of Reproductive Tumors and Potential Impact on Conservation', *Animals*. Available at: <https://doi.org/10.3390/ani12152005>.

Abraham, J. and Staffurth, J. (2016) 'Hormonal therapy for cancer', *Medicine (United Kingdom)*. Crit Rev Biotechnol, pp. 30–33. Available at: <https://doi.org/10.1016/j.mpmmed.2015.10.014>.

Addis, R., Cruciani, S., Santaniello, S., Bellu, E., Sarais, G., Ventura, C., Maioli, M. and Pintore, G. (2020) 'Fibroblast Proliferation and Migration in Wound Healing by Phytochemicals: Evidence for a Novel Synergic Outcome', *International Journal of Medical Sciences*, 17(8), p. 1030. Available at: <https://doi.org/10.7150/IJMS.43986>.

Agarwal, M.L., Agarwal, A., Taylor, W.R. and Stark, G.R. (1995) 'p53 controls both the G2/M and the G1 cell cycle checkpoints and mediates reversible growth arrest in human fibroblasts', *Proceedings of the National Academy of Sciences of the United States of America*, 92(18), pp. 8493–8497. Available at: <https://doi.org/10.1073/pnas.92.18.8493>.

Akasaka, Y., Ono, I., Kamiya, T., Ishikawa, Y., Kinoshita, T., Ishiguro, S., Yokoo, T., Imaizumi, R., Inomata, N., Fujita, K., Akishima-Fukasawa, Y., Uzuki, M., Ito, K. and Ishii, T. (2010) 'The mechanisms underlying fibroblast apoptosis regulated by growth factors during wound healing', *Journal of Pathology*, 221(3), pp. 285–299. Available at: <https://doi.org/10.1002/path.2710>.

Albert, D.A. and Nodzenski, E. (1989) 'M2 subunit of ribonucleotide reductase is a target of cyclic AMP-dependent protein kinase', *Journal of Cellular Physiology*, 138(1), pp. 129–136. Available at: <https://doi.org/10.1002/JCP.1041380118>.

Albuquerque, T.A.F., Drummond do Val, L., Doherty, A. and de Magalhães, J.P. (2018) 'From humans to hydra: patterns of cancer across the tree of life', *Biological Reviews*, 93(3), pp. 1715–1734. Available at: <https://doi.org/10.1111/brv.12415>.

Allsopp, R.C., Vaziri, H., Patterson, C., Goldstein, S., Younglai, E. V., Futcher, A.B., Greider, C.W. and Harley, C.B. (1992) 'Telomere length predicts replicative capacity of human fibroblasts', *Proceedings of the National Academy of Sciences of the United States of America*, 89(21), pp. 10114–10118. Available at: <https://doi.org/10.1073/pnas.89.21.10114>.

Antocchia, A., Sgura, A., Berardinelli, F., Cavinato, M., Cherubini, R., Gerardi, S. and Tanzarella, C. (2009) 'Cell cycle perturbations and genotoxic effects in human primary fibroblasts induced by low-energy protons and X/gamma-rays', *Journal of radiation research*, 50(5), pp. 457–468. Available at: <https://doi.org/10.1269/JRR.09008>.

Appella, E. and Anderson, C.W. (2001) 'Post-translational modifications and activation of p53 by genotoxic stresses', *European journal of biochemistry*, 268(10), pp. 2764–2772. Available at: <https://doi.org/10.1046/J.1432-1327.2001.02225.X>.

Aslantürk, Ö.S. (2017) 'In Vitro Cytotoxicity and Cell Viability Assays: Principles, Advantages, and Disadvantages', *Genotoxicity - A Predictable Risk to Our Actual World* [Preprint]. Available at: <https://doi.org/10.5772/INTECHOPEN.71923>.

Atanassova, N. and Grainge, I. (2008) 'Biochemical characterization of the minichromosome maintenance (MCM) protein of the crenarchaeote *Aeropyrum pernix* and its interactions with the origin recognition complex (ORC) proteins', *Biochemistry*, 47(50), pp. 13362–13370. Available at: <https://doi.org/10.1021/bi801479s>.

Athena Aktipis, C., Boddy, A.M., Jansen, G., Hibner, U., Hochberg, M.E., Maley, C.C. and Wilkinson, G.S. (2015) 'Cancer across the tree of life: Cooperation and cheating in multicellularity', *Philosophical Transactions of the Royal Society B: Biological Sciences*, 370(1673). Available at: <https://doi.org/10.1098/rstb.2014.0219>.

Attardi, L.D., De Vries, A. and Jacks, T. (2004) 'Activation of the p53-dependent G1 checkpoint response in mouse embryo fibroblasts depends on the specific DNA damage inducer', *Oncogene*, 23(4), pp. 973–980. Available at: <https://doi.org/10.1038/sj.onc.1207026>.

Aubrey, B.J., Kelly, G.L., Janic, A., Herold, M.J. and Strasser, A. (2018) 'How does p53 induce apoptosis and how does this relate to p53-mediated tumour suppression?', *Cell Death and Differentiation*, pp. 104–113. Available at: <https://doi.org/10.1038/cdd.2017.169>.

Aviv, A. and Shay, J.W. (2018) 'Reflections on telomere dynamics and ageing-related diseases in humans', *Philosophical Transactions of the Royal Society B: Biological Sciences*, 373(1741). Available at: <https://doi.org/10.1098/rstb.2016.0436>.

Avivi, A., Ashur-Fabian, O., Amariglio, N., Nevo, E. and Rechavi, G. (2005) 'p53 - A key player in tumoral and evolutionary adaptation: A lesson from the Israeli blind subterranean mole rat', *Cell Cycle*, 4(3), pp. 368–372. Available at: <https://doi.org/10.4161/cc.4.3.1534>.

Babaei, M. and Ganjalikhani, M. (2014) 'The potential effectiveness of nanoparticles as radio sensitizers for radiotherapy', *BioImpacts: BI*, 4(1), p. 15. Available at: <https://doi.org/10.5681/BI.2014.003>.

Balin, A.K., Fisher, A.J., Anzelone, M., Leong, I. and Allen, R.G. (2002) 'Effects of establishing cell cultures and cell culture conditions on the proliferative life span of human fibroblasts isolated from different tissues and donors of different ages', *Experimental Cell Research*, 274(2), pp. 275–287. Available at: <https://doi.org/10.1006/excr.2002.5485>.

Bálint, É. and Vousden, K.H. (2001) 'Activation and activities of the p53 tumour suppressor protein', *British Journal of Cancer*, 85(12), pp. 1813–1823. Available at: <https://doi.org/10.1054/bjoc.2001.2128>.

Barberis, M., Klipp, E., Vanoni, M. and Alberghina, L. (2007) 'Cell Size at S Phase Initiation: An Emergent Property of the G1/S Network', *PLoS Computational Biology*, 3(4), pp. 649–666. Available at: <https://doi.org/10.1371/JOURNAL.PCBI.0030064>.

Barnett, G.C., West, C.M.L., Dunning, A.M., Elliott, R.M., Coles, C.E., Pharoah, P.D.P. and Burnet, N.G. (2009) 'Normal tissue reactions to radiotherapy: Towards tailoring treatment dose by genotype', *Nature Reviews Cancer*. *Nat Rev Cancer*, pp. 134–142. Available at: <https://doi.org/10.1038/nrc2587>.

Barnum, K.J. and O'Connell, M.J. (2014) 'Cell cycle regulation by checkpoints', *Methods in Molecular Biology*, 1170, pp. 29–40. Available at: [https://doi.org/10.1007/978-1-4939-0888-2\\_2](https://doi.org/10.1007/978-1-4939-0888-2_2).

Bartas, M., Brázda, V., Volná, A., Červeň, J., Pečinka, P. and Zawacka-Pankau, J.E. (2021) 'The changes in the p53 protein across the animal kingdom point to its involvement in longevity', *International Journal of Molecular Sciences*, 22(16). Available at: <https://doi.org/10.3390/ijms22168512>.

Bartek, J. and Lukas, J. (2003) 'Chk1 and Chk2 kinases in checkpoint control and cancer', *Cancer Cell*. Cell Press, pp. 421–429. Available at: [https://doi.org/10.1016/S1535-6108\(03\)00110-7](https://doi.org/10.1016/S1535-6108(03)00110-7).

Bartels, P. and Kotze, A. (2006) 'Wildlife biomaterial banking in Africa for now and the future', *Journal of Environmental Monitoring*, 8(8), pp. 779–781. Available at: <https://doi.org/10.1039/B602809H>.

Barton, M.B., Frommer, M. and Shafiq, J. (2006) 'Role of radiotherapy in cancer control in low-income and middle-income countries', *The Lancet. Oncology*, 7(7), pp. 584–595. Available at: [https://doi.org/10.1016/S1470-2045\(06\)70759-8](https://doi.org/10.1016/S1470-2045(06)70759-8).

Baskar, R., Lee, K.A., Yeo, R. and Yeoh, K.W. (2012) 'Cancer and radiation therapy: Current advances and future directions', *International Journal of Medical Sciences*. Ivyspring International Publisher, pp. 193–199. Available at: <https://doi.org/10.7150/ijms.3635>.

Baskar, R., Yap, S.P., Chua, K.L.M. and Itahana, K. (2012) 'The diverse and complex roles of radiation on cancer treatment: therapeutic target and genome maintenance.', *American journal of cancer research*, 2(4), pp. 372–82. Available at: [/pmc/articles/PMC3410581/](https://pubmed.ncbi.nlm.nih.gov/2410581/) (Accessed: 24 October 2022).

Baus Charrier-Savournin, F., Marie-Thérèse Château, †, Gire, V., Sedivy, J., Piette, J. and Dulic\*, V.D. (2004) 'p21-Mediated Nuclear Retention of Cyclin B1-Cdk1 in Response to Genotoxic Stress □ D', *Molecular Biology of the Cell*, 15, pp. 3965–3976. Available at: <https://doi.org/10.1091/mbc.E03-12-0871>.

Beresford, P.J., Zhang, D., Oh, D.Y., Fan, Z., Greer, E.L., Russo, M.L., Jaju, M. and Lieberman, J. (2001) 'Granzyme A Activates an Endoplasmic Reticulum-associated Caspase-independent Nuclease to Induce Single-stranded DNA Nicks', *Journal of Biological Chemistry*, 276(46), pp. 43285–43293. Available at: <https://doi.org/10.1074/jbc.M108137200>.

Berridge, M.J. (2014) 'Module 9: Cell Cycle and Proliferation', *Cell Signalling Biology*, 6, p. csb0001009. Available at: <https://doi.org/10.1042/csb0001009>.

Beyrouthy, M.J., Alexander, K.E., Baldwin, A., Whitfield, M.L., Bass, H.W., McGee, D. and Hurt, M.M. (2008) 'Identification of G1-regulated genes in normally cycling human cells', *PLoS ONE*, 3(12). Available at: <https://doi.org/10.1371/journal.pone.0003943>.

Bieging, K.T., Mello, S.S. and Attardi, L.D. (2014) 'Unravelling mechanisms of p53-mediated tumour suppression', *Nature reviews. Cancer*, 14(5), p. 359. Available at: <https://doi.org/10.1038/NRC3711>.

Blow, J.J. and Tanaka, T.U. (2005) 'The chromosome cycle: Coordinating replication and segregation', *EMBO Reports*. European Molecular Biology Organization, pp. 1028–1034. Available at: <https://doi.org/10.1038/sj.embor.7400557>.

Borlado, L.R. and Méndez, J. (2008) 'CDC6: from DNA replication to cell cycle checkpoints and oncogenesis', *Carcinogenesis*, 29(2), pp. 237–243. Available at: <https://doi.org/10.1093/carcin/bgm268>.

Borner, C. and Monney, L. (1999) 'Apoptosis without caspases: An inefficient molecular guillotine?', *Cell Death and Differentiation*, 6(6), pp. 497–507. Available at: <https://doi.org/10.1038/sj.cdd.4400525>.

Brix, N., Samaga, D., Hennel, R., Gehr, K., Zitzelsberger, H. and Lauber, K. (2020) 'The clonogenic assay: robustness of plating efficiency-based analysis is strongly compromised by cellular cooperation', *Radiation Oncology*, 15(1), pp. 1–12. Available at: <https://doi.org/10.1186/s13014-020-01697-y>.

Brooks, C.L. and Gu, W. (2006) 'p53 ubiquitination: Mdm2 and beyond', *Molecular Cell*. NIH Public Access, pp. 307–315. Available at: <https://doi.org/10.1016/j.molcel.2006.01.020>.

Brooks, C.L. and Gu, W. (2010) 'New insights into p53 activation', *Cell Research 2010 20:6*, 20(6), pp. 614–621. Available at: <https://doi.org/10.1038/cr.2010.53>.

Brown, N.R., Noble, M.E.M., Lawrie, A.M., Morris, M.C., Tunnah, P., Divita, G., Johnson, L.N. and Endicott, J.A. (1999) 'Effects of phosphorylation of threonine 160 on cyclin-dependent kinase 2 structure and activity', *Journal of Biological Chemistry*, 274(13), pp. 8746–8756. Available at: <https://doi.org/10.1074/JBC.274.13.8746>.

Bruce, W.R., Pearson, M.L. and Freedhoff, H.S. (1963) 'The Linear Energy Transfer Distributions Resulting From Primary And Scattered X-rays And Gamma Rays With Primary HVL'S From 1.25 mm Cu To 11 mm PB.', *Radiation research*, 19, pp. 606–620. Available at: <https://doi.org/10.2307/3571481>.

Buck, S.H., Chiu, D. and Saito, R.M. (2009) 'The cyclin-dependent kinase inhibitors, cki-1 and cki-2, act in overlapping but distinct pathways to control cell-cycle quiescence during *C. elegans* development', *Cell cycle (Georgetown, Tex.)*, 8(16), p. 2613. Available at: <https://doi.org/10.4161/CC.8.16.9354>.

Cairncross, L., Parkes, J., Craig, H. and Are, C. (2021) *Cancer on the Global Stage: Incidence and Cancer-Related Mortality in Kenya - The ASCO Post*, *ASCO Post*. Available at: <https://ascopost.com/issues/september-10-2021/cancer-on-the-global-stage-incidence-and-cancer-related-mortality-in-south-africa/> (Accessed: 20 April 2022).

Caldecott, K.W. (2008) 'Single-strand break repair and genetic disease', *Nature Reviews Genetics* 2008 9:8, 9(8), pp. 619–631. Available at: <https://doi.org/10.1038/nrg2380>.

Callier, V. (2019) 'Solving Peto's Paradox to better understand cancer', *Proceedings of the National Academy of Sciences of the United States of America*, 116(6), pp. 1825–1828. Available at: <https://doi.org/10.1073/pnas.1821517116>.

Candé, C., Cecconi, F., Dessen, P. and Kroemer, G. (2002) 'Apoptosis-inducing factor (AIF): Key to the conserved caspase-independent pathways of cell death?', *Journal of Cell Science*, 115(24), pp. 4727–4734. Available at: <https://doi.org/10.1242/jcs.00210>.

Capuozzo, M., Santorsola, M., Bocchetti, M., Perri, F., Cascella, M., Granata, V., Celotto, V., Gualillo, O., Cossu, A.M., Nasti, G., Caraglia, M. and Ottaiano, A. (2022) 'p53: From Fundamental Biology to Clinical Applications in Cancer'.

Caulin, A.F. and Maley, C.C. (2011) 'Peto's Paradox: Evolution's prescription for cancer prevention', *Trends in Ecology and Evolution*, 26(4), pp. 175–182. Available at: <https://doi.org/10.1016/j.tree.2011.01.002>.



Chatterjee, N. and Walker, G.C. (2017) 'Mechanisms of DNA damage, repair and mutagenesis', *Environmental and molecular mutagenesis*, 58(5), p. 235. Available at: <https://doi.org/10.1002/EM.22087>.

Chen, H., Li, Y. and Tollefsbol, T.O. (2013) 'Cell Senescence Culturing Methods', *Methods in molecular biology (Clifton, N.J.)*, 1048, pp. 1–10. Available at: [https://doi.org/10.1007/978-1-62703-556-9\\_1](https://doi.org/10.1007/978-1-62703-556-9_1).

Chen, S. (2015) *Radiation types and the degree of penetration... | Download Scientific Diagram*. Available at: [https://www.researchgate.net/figure/11-Radiation-types-and-the-degree-of-penetration\\_fig9\\_286590827](https://www.researchgate.net/figure/11-Radiation-types-and-the-degree-of-penetration_fig9_286590827) (Accessed: 14 September 2022).

Chu, D.T., Nguyen, T.T., Tien, N.L.B., Tran, D.K., Jeong, J.H., Anh, P.G., Thanh, V. Van, Truong, D.T. and Dinh, T.C. (2020) 'Recent Progress of Stem Cell Therapy in Cancer Treatment: Molecular Mechanisms and Potential Applications', *Cells*. Multidisciplinary Digital Publishing Institute (MDPI). Available at: <https://doi.org/10.3390/cells9030563>.

Clay, D.E. and Fox, D.T. (2021) 'DNA Damage Responses during the Cell Cycle: Insights from Model Organisms and Beyond', *Genes* 2021, Vol. 12, Page 1882, 12(12), p. 1882. Available at: <https://doi.org/10.3390/GENES12121882>.

Cobrinik, D. (2005) 'Pocket proteins and cell cycle control', *Oncogene*, pp. 2796–2809. Available at: <https://doi.org/10.1038/sj.onc.1208619>.

Cocker, J.H., Piatti, S., Santocanale, C., Nasmyth, K. and Diffley, J.F.X. (1996) 'An essential role for the Cdc6 protein in forming the pre-replicative complexes of budding yeast', *Nature* 1996 379:6561, 379(6561), pp. 180–182. Available at: <https://doi.org/10.1038/379180a0>.

Coverley, D., Laman, H. and Laskey, R.A. (2002) 'Distinct roles for cyclins E and A during DNA replication complex assembly and activation', *Nature cell biology*, 4(7), pp. 523–528. Available at: <https://doi.org/10.1038/NCB813>.

Cunningham, C., de Kock, M., Engelbrecht, M., Miles, X., Slabbert, J. and Vandevoorde, C. (2021) 'Radiosensitization Effect of Gold Nanoparticles in Proton Therapy', *Frontiers in Public Health*, 9, p. 1065. Available at: <https://doi.org/10.3389/FPUBH.2021.699822/BIBTEX>.

Cuttler, J.M. and Pollycove, M. (2009) 'Nuclear energy and health and the benefits of low-dose radiation hormesis', *Dose-Response*, 7(1), pp. 52–89. Available at: <https://doi.org/10.2203/dose-response.08-024.Cuttler>.

Danial, N.N. and Korsmeyer, S.J. (2004) 'Cell Death: Critical Control Points', *Cell*. Cell Press, pp. 205–219. Available at: [https://doi.org/10.1016/S0092-8674\(04\)00046-7](https://doi.org/10.1016/S0092-8674(04)00046-7).

Darzynkiewicz, Z., Halicka, H.D., Zhao, H. and Podhorecka, M. (2011) 'Cell synchronization by inhibitors of DNA replication induces replication stress and DNA damage response: Analysis by flow cytometry', *Methods in Molecular Biology*, 761, pp. 85–96. Available at: [https://doi.org/10.1007/978-1-61779-182-6\\_6](https://doi.org/10.1007/978-1-61779-182-6_6).

Davis, B.W. and Ostrander, E.A. (2014) 'Domestic dogs and cancer research: A breed-based genomics approach', *ILAR Journal*, 55(1), pp. 59–68. Available at: <https://doi.org/10.1093/ilar/ilu017>.

Debela, D.T., Muzazu, S.G., Heraro, K.D., Ndalama, M.T., Mesele, B.W., Haile, D.C., Kitui, S.K. and Manyazewal, T. (2021) 'New approaches and procedures for cancer treatment: Current perspectives', *SAGE Open Medicine*, 9, p. 205031212110343. Available at: <https://doi.org/10.1177/20503121211034366>.

Demchenko, A.P. (2013) 'Beyond annexin V: Fluorescence response of cellular membranes to apoptosis', *Cytotechnology*. Springer, pp. 157–172. Available at: <https://doi.org/10.1007/s10616-012-9481-y>.

Deng, W., Tsao, S.W., Lucas, J.N., Leung, C.S. and Cheung, A.L.M. (2003) 'A New Method for Improving Metaphase Chromosome Spreading', *Cytometry Part A*, 51(1), pp. 46–51. Available at: <https://doi.org/10.1002/cyto.a.10004>.

Desouky, O., Ding, N. and Zhou, G. (2015) 'Targeted and non-targeted effects of ionizing radiation', *Journal of Radiation Research and Applied Sciences*, 8(2), pp. 247–254. Available at: <https://doi.org/10.1016/j.jrras.2015.03.003>.

Ding, L., Cao, J., Lin, W., Chen, H., Xiong, X., Ao, H., Yu, M., Lin, J. and Cui, Q. (2020) 'The Roles of Cyclin-Dependent Kinases in Cell-Cycle Progression and Therapeutic Strategies in Human Breast Cancer', *International Journal of Molecular Sciences*, 21(6). Available at: <https://doi.org/10.3390/IJMS21061960>.

Domogauer, J.D., de Toledo, S.M., Howell, R.W. and Azzam, E.I. (2021) ‘Acquired radioresistance in cancer associated fibroblasts is concomitant with enhanced antioxidant potential and DNA repair capacity’, *Cell Communication and Signaling*, 19(1), pp. 1–17. Available at: <https://doi.org/10.1186/S12964-021-00711-4/FIGURES/9>.

Duncker, B.P., Chesnokov, I.N. and McConkey, B.J. (2009) ‘The origin recognition complex protein family.’, *Genome biology*, 10(3), p. 214. Available at: <https://doi.org/10.1186/GB-2009-10-3-214/FIGURES/4>.

Durante, M. and Loeffler, J.S. (2010) ‘Charged particles in radiation oncology’, *Nature Reviews Clinical Oncology*, 7(1), pp. 37–43. Available at: <https://doi.org/10.1038/nrclinonc.2009.183>.

Eagle, H. and Levine, E.M. (1967) ‘Growth regulatory effects of cellular interaction’, *Nature*, 213(5081), pp. 1102–1106. Available at: <https://doi.org/10.1038/2131102a0>.

Eccles, L.J., O’Neill, P. and Lomax, M.E. (2011) ‘Delayed repair of radiation induced clustered DNA damage: Friend or foe?’, *Mutation Research*, 711(1–2), p. 134. Available at: <https://doi.org/10.1016/J.MRFMMM.2010.11.003>.

Elliott, R.L. and Jiang, X.P. (2019) ‘The adverse effect of gentamicin on cell metabolism in three cultured mammary cell lines: “Are cell culture data skewed?”’, *PLoS ONE*, 14(4), p. e0214586. Available at: <https://doi.org/10.1371/journal.pone.0214586>.

Elmore, S. (2007) ‘Apoptosis: A Review of Programmed Cell Death’, *Toxicologic Pathology*, pp. 495–516. Available at: <https://doi.org/10.1080/01926230701320337>.

Enk, J.M., Devault, A.M., Kuch, M., Murgha, Y.E., Rouillard, J.M. and Poinar, H.N. (2014) ‘Ancient Whole Genome Enrichment Using Baits Built from Modern DNA’, *Molecular Biology and Evolution*, 31(5), pp. 1292–1294. Available at: <https://doi.org/10.1093/MOLBEV/MSU074>.

Fan, T.J., Han, L.H., Cong, R.S. and Liang, J. (2005) ‘Caspase family proteases and apoptosis’, *Acta Biochimica et Biophysica Sinica*, 37(11), pp. 719–727. Available at: <https://doi.org/10.1111/j.1745-7270.2005.00108.x>.

Fang Khoo, L. and Foley, P. (2001) ‘Harry Potter and the omen of value added’, *European Business Review*, 13(4). Available at: <https://doi.org/10.1108/EBR.2001.05413DAB.001/FULL/HTML>.

Fang, S., Jensen, J.P., Ludwig, R.L., Vousden, K.H. and Weissman, A.M. (2000) 'Mdm2 is a RING finger-dependent ubiquitin protein ligase for itself and p53', *Journal of Biological Chemistry*, 275(12), pp. 8945–8951. Available at: <https://doi.org/10.1074/jbc.275.12.8945>.

Fernandes, I.R., Russo, F.B., Pignatari, G.C., Evangelinellis, M.M., Tavolari, S., Muotri, A.R. and Beltrão-Braga, P.C.B. (2016) 'Fibroblast sources: Where can we get them?', *Cytotechnology*, 68(2), pp. 223–228. Available at: <https://doi.org/10.1007/s10616-014-9771-7>.

Ferris, E., Abegglen, L.M., Schiffman, J.D. and Gregg, C. (2018) 'Accelerated Evolution in Distinctive Species Reveals Candidate Elements for Clinically Relevant Traits, Including Mutation and Cancer Resistance', *Cell reports*, 22(10), pp. 2742–2755. Available at: <https://doi.org/10.1016/J.CELREP.2018.02.008>.

Fischer, A.H., Jacobson, K.A., Rose, J. and Zeller, R. (2008) 'Hematoxylin and eosin staining of tissue and cell sections', *CSH protocols*, 2008(5). Available at: <https://doi.org/10.1101/PDB.PROT4986>.

Frangioni, J. V (2008) 'New technologies for human cancer imaging', *Journal of Clinical Oncology*, pp. 4012–4021. Available at: <https://doi.org/10.1200/JCO.2007.14.3065>.

Frankel, R. 1 (1995) 'Articles Centennial of Rontgen's Discovery of X-rays'.

Franken, N.A.P., Rodermond, H.M., Stap, J., Haveman, J. and van Bree, C. (2006) 'Clonogenic assay of cells in vitro', *Nature protocols*, 1(5), pp. 2315–2319. Available at: <https://doi.org/10.1038/NPROT.2006.339>.

Frönicke, L., Wienberg, J., Stone, G., Adams, L. and Stanyon, R. (2003) 'Towards the delineation of the ancestral eutherian genome organization: Comparative genome maps of human and the African elephant (*Loxodonta africana*) generated by chromosome painting', *Proceedings of the Royal Society B: Biological Sciences*, 270(1522), pp. 1331–1340. Available at: <https://doi.org/10.1098/rspb.2003.2383>.

Frouin, I., Montecucco, A., Biamonti, G., Hübscher, U., Spadari, S. and Maga, G. (2002) 'Cell cycle-dependent dynamic association of cyclin/Cdk complexes with human DNA replication proteins', *The EMBO Journal*, 21(10), p. 2485. Available at: <https://doi.org/10.1093/EMBOJ/21.10.2485>.

Galluzzi, L., Vitale, I., Aaronson, S.A., Abrams, J.M., Adam, D., ... Kroemer, G. (2018) 'Molecular mechanisms of cell death: Recommendations of the Nomenclature Committee on Cell Death 2018', *Cell Death and Differentiation*. Nature Publishing Group, pp. 486–541. Available at: <https://doi.org/10.1038/s41418-017-0012-4>.

Galluzzi, L., Vitale, I., Abrams, J.M., Alnemri, E.S., Baehrecke, E.H., Blagosklonny, M. V., Dawson, T.M., Dawson, V.L., El-Deiry, W.S., Fulda, S., Gottlieb, E., Green, D.R., Hengartner, M.O., Kepp, O., Knight, R.A., Kumar, S., Lipton, S.A., Lu, X., Madeo, F., Malorni, W., Mehlen, P., Nñez, G., Peter, M.E., Piacentini, M., Rubinsztein, D.C., Shi, Y., Simon, H.U., Vandenabeele, P., White, E., Yuan, J., Zhivotovsky, B., Melino, G. and Kroemer, G. (2011) 'Molecular definitions of cell death subroutines: recommendations of the Nomenclature Committee on Cell Death 2012', *Cell Death & Differentiation* 2012 19:1, 19(1), pp. 107–120. Available at: <https://doi.org/10.1038/cdd.2011.96>.

García-Cao, I., García-Cao, M., Martín-Caballero, J., Criado, L.M., Klatt, P., Flores, J.M., Weill, J.C., Blasco, M.A. and Serrano, M. (2002) "Super p53" mice exhibit enhanced DNA damage response, are tumor resistant and age normally', *EMBO Journal*, 21(22), pp. 6225–6235. Available at: <https://doi.org/10.1093/emboj/cdf595>.

García-Reyes, B., Kretz, A.L., Ruff, J.P., Karstedt, S. von, Hillenbrand, A., Knippschild, U., Henne-Bruns, D. and Lemke, J. (2018) 'The emerging role of cyclin-dependent kinases (CDKs) in pancreatic ductal adenocarcinoma', *International Journal of Molecular Sciences*. Multidisciplinary Digital Publishing Institute, p. 3219. Available at: <https://doi.org/10.3390/ijms19103219>.

Garrett, S., Barton, W.A., Knights, R., Jin, P., Morgan, D.O. and Fisher, R.P. (2001) 'Reciprocal Activation by Cyclin-Dependent Kinases 2 and 7 Is Directed by Substrate Specificity Determinants outside the T Loop', *Molecular and Cellular Biology*, 21(1), pp. 88–99. Available at: <https://doi.org/10.1128/mcb.21.1.88-99.2001>.

Gasco, M., Shami, S. and Crook, T. (2002) 'The p53 pathway in breast cancer', *Breast Cancer Research*, 4(2), pp. 70–76. Available at: <https://doi.org/10.1186/bcr426>.

Gasparri, F., Mariani, M., Sola, F. and Galvani, A. (2004) 'Quantification of the proliferation index of human dermal fibroblast cultures with the ArrayScan™ high-content screening reader', *Journal of Biomolecular Screening*, 9(3), pp. 232–243. Available at: <https://doi.org/10.1177/1087057103262836>.

Gerschenson, L.E. and Rotello, R.J. (1992) 'Apoptosis: a different type of cell death', *The FASEB Journal*, 6(7), pp. 2450–2455. Available at: <https://doi.org/10.1096/fasebj.6.7.1563596>.

Gewin, V. (2013) 'Massive animals may hold secrets of cancer suppression', *Nature* [Preprint]. Available at: <https://doi.org/10.1038/NATURE.2013.12258>.

Gherardini, L., Ciuti, G., Tognarelli, S. and Cinti, C. (2014) 'Searching for the Perfect Wave: The Effect of Radiofrequency Electromagnetic Fields on Cells', *Int. J. Mol. Sci*, 15, pp. 5366–5387. Available at: <https://doi.org/10.3390/ijms15045366>.

Ghobrial, I.M., Witzig, T.E. and Adjei, A.A. (2005) 'Targeting Apoptosis Pathways in Cancer Therapy', *CA: A Cancer Journal for Clinicians*, 55(3), pp. 178–194. Available at: <https://doi.org/10.3322/canjclin.55.3.178>.

Giaccia, A.J. and Kastan, M.B. (1998) *The complexity of p53 modulation: emerging patterns from divergent signals*. Available at: [www.genesdev.org](http://www.genesdev.org).

Gire, V. and Dulic, V. (2015) 'Senescence from G2 arrest, revisited', *Cell Cycle*. Taylor & Francis, pp. 297–304. Available at: <https://doi.org/10.1080/15384101.2014.1000134>.

Gobush, K.S., Edwards, C.T.T, Balfour, D., Wittemyer, G., M., F. & Taylor, R.D. and View (2020) 'The IUCN Red List of Threatened Species', *The IUCN Red List of Threatened Species*, 8235. Available at: [https://www.iucn.org/sites/dev/files/import/downloads/iucn\\_brochure\\_low\\_res.pdf](https://www.iucn.org/sites/dev/files/import/downloads/iucn_brochure_low_res.pdf).

Gobush, K.S., Edwards, C.T., Balfour, D., Wittemyer, G., Maisels, F.& and Taylor, R.D. (2021) 'Loxodonta cyclotis (African Forest Elephant)', *The IUCN Red List of Threatened Species*, 8235(March), p. e.T181007989A181019888. Available at: <https://doi.org/10.2305/IUCN.UK.2021-1.RLTS.T181007989A181019888.en>.

Goel, S., DeCristo, M.J., McAllister, S.S. and Zhao, J.J. (2018) 'CDK4/6 Inhibition in Cancer: Beyond Cell Cycle Arrest', *Trends in Cell Biology*. NIH Public Access, pp. 911–925. Available at: <https://doi.org/10.1016/j.tcb.2018.07.002>.

Gokhale, P.J., Au-Young, J.K., Dadi, S.V., Keys, D.N., Harrison, N.J., Jones, M., Soneji, S., Enver, T., Sherlock, J.K. and Andrews, P.W. (2015) 'Culture Adaptation Alters Transcriptional Hierarchies among Single Human Embryonic Stem Cells Reflecting Altered Patterns of Differentiation', *PLOS ONE*, 10(4), p. e0123467. Available at: <https://doi.org/10.1371/JOURNAL.PONE.0123467>.

Gorbunova, V., Hine, C., Tian, X., Ablueva, J., Gudkov, A. V., Nevo, E. and Seluanov, A. (2012) 'Cancer resistance in the blind mole rat is mediated by concerted necrotic cell death mechanism', *Proceedings of the National Academy of Sciences of the United States of America*, 109(47), pp. 19392–19396. Available at: <https://doi.org/10.1073/pnas.1217211109>.

Gouko, R., Onuma, M., Eitsuka, T., Katayama, M., Takahashi, K., Nakagawa, K., Inoue-Murayama, M., Kiyono, T. and Fukuda, T. (2018) 'Efficient immortalization of cells derived from critically endangered Tsushima leopard cat (*Prionailurus bengalensis euptilurus*) with expression of mutant CDK4, Cyclin D1, and telomerase reverse transcriptase', *Cytotechnology*, 70(6), pp. 1619–1630. Available at: <https://doi.org/10.1007/S10616-018-0254-0/FIGURES/5>.

Gould, K.L., Owen, D.J., Sazer, S., Nurse, P. and Moreno, S. (1991) 'Phosphorylation at Thr167 is required for *Schizosaccharomyces pombe* p34(cdc2) function', *EMBO Journal*, 10(11), pp. 3297–3309. Available at: <https://doi.org/10.1002/j.1460-2075.1991.tb04894.x>.

Green, J., Cairns, B.J., Casabonne, D., Wright, F.L., Reeves, G. and Beral, V. (2011) 'Height and cancer incidence in the Million Women Study: prospective cohort, and meta-analysis of prospective studies of height and total cancer risk', *The Lancet Oncology*, 12(8), pp. 785–794. Available at: [https://doi.org/10.1016/S1470-2045\(11\)70154-1](https://doi.org/10.1016/S1470-2045(11)70154-1).

Grela, E., Piet, M., Luchowski, R., Grudzinski, W., Paduch, R. and Gruszecki, W.I. (2018) 'Imaging of human cells exposed to an antifungal antibiotic amphotericin B reveals the mechanisms associated with the drug toxicity and cell defence', *Scientific Reports*, 8(1), pp. 1–7. Available at: <https://doi.org/10.1038/s41598-018-32301-9>.

Grodzinski, P., Silver, M. and Molnar, L.K. (2006) 'Expert Review of Molecular Diagnostics Nanotechnology for cancer diagnostics: promises and challenges Nanotechnology for cancer diagnostics: promises and challenges', *Expert Rev. Mol. Diagn*, 6(3), pp. 307–318. Available at: <https://doi.org/10.1586/14737159.6.3.307>.

Gurina, T.S. and Simms, L. (2022) 'Histology, Staining', pp. 1–15. Available at: <https://www.ncbi.nlm.nih.gov/books/NBK557663/> (Accessed: 13 October 2022).

Haines, B.P., Voyle, R.B. and Rathjen, P.D. (2000) 'Intracellular and Extracellular Leukemia Inhibitory Factor Proteins Have Different Cellular Activities That Are Mediated by Distinct Protein Motifs', *Molecular Biology of the Cell*, 11(4), p. 1369. Available at: <https://doi.org/10.1091/MBC.11.4.1369>.

Halicka, D., Zhao, H., Li, J., Garcia, J., Podhorecka, M. and Darzynkiewicz, Z. (2016) 'DNA damage response resulting from replication stress induced by synchronization of cells by inhibitors of DNA replication: Analysis by flow cytometry', in *Methods in Molecular Biology*. Humana Press Inc., pp. 107–119. Available at: [https://doi.org/10.1007/978-1-4939-6603-5\\_7](https://doi.org/10.1007/978-1-4939-6603-5_7).

Hall, E.J. and Giaccia, A.J. (2012) 'Radiobiology for the Radiologist 7th Edition', *Radiation Research*, 141(3), p. 347. Available at: <https://doi.org/10.2307/3579017>.

Hamdi, Y., Abdeljaoued-Tej, I., Zatchi, A.A., Abdelhak, S., Boubaker, S., Brown, J.S. and Benkahla, A. (2021) 'Cancer in Africa: The Untold Story', *Frontiers in Oncology*, 11, p. 1011. Available at: <https://doi.org/10.3389/FONC.2021.650117/BIBTEX>.

Han, J., Qureshi, A.A., Prescott, J., Guo, Q., Ye, L., Hunter, D.J. and De Vivo, I. (2009) 'A Prospective Study of Telomere Length and the Risk of Skin Cancer', *The Journal of investigative dermatology*, 129(2), p. 415. Available at: <https://doi.org/10.1038/JID.2008.238>.

Hanahan, D. and Weinberg, R.A. (2000) 'The hallmarks of cancer', *Cell*, pp. 57–70. Available at: [https://doi.org/10.1016/S0092-8674\(00\)81683-9](https://doi.org/10.1016/S0092-8674(00)81683-9).

Hanson, K.M., Hernady, E.B., Reed, C.K., Johnston, C.J., Groves, A.M. and Finkelstein, J.N. (2019a) 'Apoptosis Resistance in Fibroblasts Precedes Progressive Scarring in Pulmonary Fibrosis and Is Partially Mediated by Toll-Like Receptor 4 Activation', *Toxicological Sciences*, 170(2), pp. 489–498. Available at: <https://doi.org/10.1093/toxsci/kfz103>.

Hanson, K.M., Hernady, E.B., Reed, C.K., Johnston, C.J., Groves, A.M. and Finkelstein, J.N. (2019b) 'Apoptosis Resistance in Fibroblasts Precedes Progressive Scarring in Pulmonary Fibrosis and Is Partially Mediated by Toll-Like Receptor 4 Activation', *Toxicological Sciences*, 170(2), p. 489. Available at: <https://doi.org/10.1093/TOXSCI/KFZ103>.

Harbour, J.W. and Dean, D.C. (2000) 'The Rb/E2F pathway: expanding roles and emerging paradigms'. Available at: <https://doi.org/10.1101/gad.813200>.



Haupt, S., Berger, M., Goldberg, Z. and Haupt, Y. (2003) 'Apoptosis - the p53 network', *Journal of cell science*, 116(Pt 20), pp. 4077–4085. Available at: <https://doi.org/10.1242/JCS.00739>.

Haupt, S. and Haupt, Y. (2017) 'P53 at the start of the 21st century: Lessons from elephants', *F1000Research*. Available at: <https://doi.org/10.12688/f1000research.12682.1>.

Higgins, L.J. and Pomper, M.G. (2011) 'The evolution of imaging in cancer: Current state and future challenges', *Seminars in Oncology*, 38(1), pp. 3–15. Available at: <https://doi.org/10.1053/j.seminoncol.2010.11.010>.

Hill, R., Kuncic, Z. and Baldock, C. (2010) 'The water equivalence of solid phantoms for low energy photon beams', *Medical Physics*, 37(8), pp. 4355–4363. Available at: <https://doi.org/10.1118/1.3462558>.

Holler, N., Tardivel, A., Kovacsovics-Bankowski, M., Hertig, S., Gaide, O., Martinon, F., Tinel, A., Deperthes, D., Calderara, S., Schulthess, T., Engel, J., Schneider, P. and Tschopp, J. (2003) 'Two Adjacent Trimeric Fas Ligands Are Required for Fas Signaling and Formation of a Death-Inducing Signaling Complex', *Molecular and Cellular Biology*, 23(4), pp. 1428–1440. Available at: <https://doi.org/10.1128/MCB.23.4.1428-1440.2003>.

Holley, A.K., Miao, L., St. Clair, D.K. and St. Clair, W.H. (2014) 'Redox-modulated phenomena and radiation therapy: The central role of superoxide dismutases', *Antioxidants and Redox Signaling*. Mary Ann Liebert, Inc., pp. 1567–1589. Available at: <https://doi.org/10.1089/ars.2012.5000>.

Hossain, M.A., Lin, Y. and Yan, S. (2018) 'Single-Strand Break End Resection in Genome Integrity: Mechanism and Regulation by APE2', *International Journal of Molecular Sciences*, 19(8). Available at: <https://doi.org/10.3390/IJMS19082389>.

Howe, B., Umrigar, A. and Tsien, F. (2014) 'Chromosome preparation from cultured cells', *Journal of Visualized Experiments*, (83), p. e50203. Available at: <https://doi.org/10.3791/50203>.

Hristu, R., Stanciu, S.G., Dumitru, A., Paun, B., Floroiu, I., Costache, M. and Stanciu, G.A. (2021) 'Influence of hematoxylin and eosin staining on the quantitative analysis of second harmonic generation imaging of fixed tissue sections', *Biomedical Optics Express*, 12(9), p. 5829. Available at: <https://doi.org/10.1364/boe.428701>.

Huang, C.Y., Ju, D.T., Chang, C.F., Muralidhar Reddy, P. and Velmurugan, B.K. (2017) 'A review on the effects of current chemotherapy drugs and natural agents in treating non-small cell lung cancer', *BioMedicine (France)*, pp. 12–23. Available at: <https://doi.org/10.1051/bmdcn/2017070423>.

Huijbregts, R.P.H., Svitin, A., Stinnett, M.W., Renfrow, M.B. and Chesnokov, I. (2009) 'Drosophila Orc6 facilitates GTPase activity and filament formation of the septin complex', *Molecular Biology of the Cell*, 20(1), pp. 270–281. Available at: <https://doi.org/10.1091/mbc.E08-07-0754>.

Hungerford, D.A., Chandra, H.S., Snyder, R.L. and Ulmer, F.A. (1966) 'Chromosomes of Three Elephants, Two Asian (*Elephas maximus*) and One African (*Loxodonta africana*)', *Cytogenetic and Genome Research*, 5(3–4), pp. 243–246. Available at: <https://doi.org/10.1159/000129900>.

Imoto, Y., Yoshida, Y., Yagisawa, F., Kuroiwa, H. and Kuroiwa, T. (2011) 'The cell cycle, including the mitotic cycle and organelle division cycles, as revealed by cytological observations', *Journal of Electron Microscopy*, 60(SUPPL. 1). Available at: <https://doi.org/10.1093/jmicro/dfr034>.

International Agency for Research on Cancer (2022) *Cancer Topics – IARC, Cancer Topics*. Available at: <https://www.iarc.who.int/cancer-topics/> (Accessed: 21 October 2022).

International Atomic Energy Agency (2010) *Radiation biology: A Handbook for Teachers and Students*, International Atomic Energy Agency Vienna International Centre. Available at: <https://doi.org/10.1259/bjr/20995428>.

Ishikawa, H., Tsuji, H., Murayama, S., Sugimoto, M., Shinohara, N., Maruyama, S., Murakami, M., Shirato, H. and Sakurai, H. (2019) 'Particle therapy for prostate cancer: The past, present and future', *International Journal of Urology*, 26(10), pp. 971–979. Available at: <https://doi.org/10.1111/IJU.14041>.

Jan, R. and Chaudhry, G.-S. (2019) 'Understanding Apoptosis and Apoptotic Pathways Targeted Cancer Therapeutics', *Tabriz University of Medical Sciences*, 7(2), pp. 113–117. Available at: <https://doi.org/10.15171/apb.2019.024>.

Jang, T.H., Park, S.C., Yang, J.H., Kim, J.Y., Seok, J.H., Park, U.S., Choi, C.W., Lee, S.R. and Han, J. (2017) ‘Cryopreservation and its clinical applications’, *Integrative Medicine Research*, 6(1), p. 12. Available at: <https://doi.org/10.1016/J.IMR.2016.12.001>.

Joerger, A.C. and Fersht, A.R. (2010) ‘The Tumor Suppressor p53: From Structures to Drug Discovery’, *Cold Spring Harbor Perspectives in Biology*, 2(6), p. a000919. Available at: <https://doi.org/10.1101/CSHPERSPECT.A000919>.

John, B. and Little, M. (2003) ‘Principal Cellular and Tissue Effects of Radiation’, *Cancer Medicine*, pp. 1–7. Available at: <https://www.ncbi.nlm.nih.gov/books/NBK12344/> (Accessed: 22 August 2022).

Jung, M., Lee, J., Seo, H.Y., Lim, J.S. and Kim, E.K. (2015) ‘Cathepsin Inhibition-Induced Lysosomal Dysfunction Enhances Pancreatic Beta-Cell Apoptosis in High Glucose’, *PLOS ONE*, 10(1), p. e0116972. Available at: <https://doi.org/10.1371/JOURNAL.PONE.0116972>.

Kaldis, P., Tsakraklides, V., Ross, K. and Winter, E. (2013) ‘Activating Phosphorylation of Cyclin-Dependent Kinases in Budding Yeast’, *Madame Curie Bioscience Database [Internet]*, pp. 1–40. Available at: <https://www.ncbi.nlm.nih.gov/books/NBK6329/> (Accessed: 16 September 2022).

Kasinathan, P., Knott, J.G., Moreira, P.N., Jerry, A.S., Burnside, D.J. and Robl, J.M. (2001) ‘Effect of fibroblast donor cell age and cell cycle on development of bovine nuclear transfer embryos in vitro’, *Biology of Reproduction*, 64(5), pp. 1487–1493. Available at: <https://doi.org/10.1095/biolreprod.64.5.1487>.

Kastan, M.B. (2016) ‘Commentary on “participation of p53 protein in the cellular response to DNA damage”’, *Cancer Research*, 76(13), pp. 3663–3665. Available at: <https://doi.org/10.1158/0008-5472.CAN-16-1560>.

Kastan, M.B. and Bartek, J. (2004) ‘Cell-cycle checkpoints and cancer’, *Nature*. Nature Publishing Group, pp. 316–323. Available at: <https://doi.org/10.1038/nature03097>.

Kastan, M.B., Zhan, Q., El-Deiry, W.S., Carrier, F., Jacks, T., Walsh, W. V., Plunkett, B.S., Vogelstein, B. and Fornace, A.J. (1992) ‘A mammalian cell cycle checkpoint pathway utilizing p53 and GADD45 is defective in ataxia-telangiectasia’, *Cell*, 71(4), pp. 587–597. Available at: [https://doi.org/10.1016/0092-8674\(92\)90593-2](https://doi.org/10.1016/0092-8674(92)90593-2).

Kernan, J., Bonacci, T. and Emanuele, M.J. (2018) ‘Who guards the guardian? Mechanisms that restrain APC/C during the cell cycle.’, *Biochimica et biophysica acta. Molecular cell research*, 1865(12), p. 1924. Available at: <https://doi.org/10.1016/J.BBAMCR.2018.09.011>.

Khan, M. and Gasser, S. (2016) ‘Generating Primary Fibroblast Cultures from Mouse Ear and Tail Tissues’, *Journal of Visualized Experiments : JoVE*, 2016(107), p. 53565. Available at: <https://doi.org/10.3791/53565>.

Khan, M.G.M. and Wang, Y. (2022) ‘Advances in the Current Understanding of How Low-Dose Radiation Affects the Cell Cycle’, *Cells*. Multidisciplinary Digital Publishing Institute, p. 356. Available at: <https://doi.org/10.3390/cells11030356>.

Kim, B.M., Hong, Yunkyung, Lee, S., Liu, P., Lim, J.H., Lee, Y.H., Lee, T.H., Chang, K.T. and Hong, Yonggeun (2015) ‘Therapeutic implications for overcoming radiation resistance in cancer therapy’, *International Journal of Molecular Sciences*, pp. 26880–26913. Available at: <https://doi.org/10.3390/ijms161125991>.

Kim, H., Kim, K., Choi, J., Heo, K., Baek, H.J., Roeder, R.G. and An, W. (2012) ‘P53 requires an intact C-terminal domain for DNA binding and transactivation’, *Journal of Molecular Biology*, 415(5), pp. 843–854. Available at: <https://doi.org/10.1016/j.jmb.2011.12.001>.

Kim, H.J., Lee, H.J., Kim, E. and Yun, J. (2018) ‘Abrupt hemodynamic changes accompanying intrapleural hyperthermic chemotherapy’, *Medicine (United States)*, 97(25). Available at: <https://doi.org/10.1097/MD.00000000000010982>.

Kim, J., Farré, M., Auvil, L., Capitanu, B., Larkin, D.M., Ma, J. and Lewin, H.A. (2017) ‘Reconstruction and evolutionary history of eutherian chromosomes’, *Proceedings of the National Academy of Sciences of the United States of America*, 114(27), pp. E5379–E5388. Available at: <https://doi.org/10.1073/pnas.1702012114>.

Kirkby, K.J., Kirkby, N.F., Burnet, N.G., Owen, H., Mackay, R.I., Crellin, A. and Green, S. (2020) ‘Heavy charged particle beam therapy and related new radiotherapy technologies: The clinical potential, physics and technical developments required to deliver benefit for patients with cancer’, *British Journal of Radiology*, 93(1116). Available at: <https://doi.org/10.1259/bjr.20200247>.

Kisiel, M.A. and Klar, A.S. (2019) ‘Chapter 6 Isolation and Culture of Human Dermal Fibroblasts’, 1993, pp. 71–78.

Kögel, D. and Prehn., J.H.M. (2018) ‘Caspase-Independent Cell Death Mechanisms’, *NCBI Bookshelf*, 1, pp. 1–12. Available at: <https://www.ncbi.nlm.nih.gov/books/NBK6197/> (Accessed: 24 October 2022).

Kottou, S. (2014) ‘How Safe is the Environmental Electromagnetic Radiation?’, *Journal of Physical Chemistry & Biophysics*, 4(3), pp. 1–10. Available at: <https://doi.org/10.4172/2161-0398.1000146>.

Kousholt, A.N., Menzel, T. and Sørensen, C.S. (2012) ‘Pathways for genome integrity in G2 phase of the cell cycle’, *Biomolecules*, 2(4), pp. 579–607. Available at: <https://doi.org/10.3390/BIOM2040579>.

Kroemer, G., Galluzzi, L. and Brenner, C. (2007) ‘Mitochondrial membrane permeabilization in cell death’, *Physiological reviews*, 87(1), pp. 99–163. Available at: <https://doi.org/10.1152/PHYSREV.00013.2006>.

Kroemer, G., Galluzzi, L., Vandenabeele, P., Abrams, J., Alnemri, E.S., Baehrecke, E.H., Blagosklonny, M. V., El-Deiry, W.S., Golstein, P., Green, D.R., Hengartner, M., Knight, R.A., Kumar, S., Lipton, S.A., Malorni, W., Nuñez, G., Peter, M.E., Tschopp, J., Yuan, J., Piacentini, M., Zhivotovsky, B. and Melino, G. (2009) ‘Classification of cell death: Recommendations of the Nomenclature Committee on Cell Death 2009’, *Cell Death and Differentiation*. NIH Public Access, pp. 3–11. Available at: <https://doi.org/10.1038/cdd.2008.150>.

Kruse, J.P. and Gu, W. (2009) ‘Modes of p53 Regulation’, *Cell*. NIH Public Access, pp. 609–622. Available at: <https://doi.org/10.1016/j.cell.2009.04.050>.

Kurose, A., Tanaka, T., Huang, X., Traganos, F. and Darzynkiewicz, Z. (2006) ‘Synchronization in the cell cycle by inhibitors of DNA replication induces histone H2AX phosphorylation: An indication of DNA damage’, *Cell Proliferation*, 39(3), pp. 231–240. Available at: <https://doi.org/10.1111/j.1365-2184.2006.00380.x>.

Kuru, K. (2014) ‘Optimization and enhancement of H&E stained microscopical images by applying bilinear interpolation method on lab color mode’, *Theoretical Biology and Medical Modelling*, 11(1), pp. 1–22. Available at: <https://doi.org/10.1186/1742-4682-11-9/FIGURES/21>.

Kuznetsov, S.A., Mankani, M.H., Bianco, P. and Robey, P.G. (2009) 'Enumeration of the colony-forming units-fibroblast from mouse and human bone marrow in normal and pathological conditions', *Stem Cell Research*, 2(1), pp. 83–94. Available at: <https://doi.org/10.1016/j.scr.2008.07.007>.

Labib, K., Tercero, J.A. and Diffley, J.F.X. (2000) 'Uninterrupted MCH2-7 function required for DNA replication fork progression', *Science*, 288(5471), pp. 1643–1647. Available at: <https://doi.org/10.1126/science.288.5471.1643>.

Laconi, E., Marongiu, F. and DeGregori, J. (2020) 'Cancer as a disease of old age: changing mutational and microenvironmental landscapes', *British Journal of Cancer*. Nature Publishing Group, pp. 943–952. Available at: <https://doi.org/10.1038/s41416-019-0721-1>.

Lai, Z.C., Wei, X., Shimizu, T., Ramos, E., Rohrbaugh, M., Nikolaidis, N., Ho, L.L. and Li, Y. (2005) 'Control of cell proliferation and apoptosis by mob as tumor suppressor, mats', *Cell*, 120(5), pp. 675–685. Available at: <https://doi.org/10.1016/J.CELL.2004.12.036>.

Lakshmanan, I. and Batra, S. (2013) 'Protocol for Apoptosis Assay by Flow Cytometry Using Annexin V Staining Method', *BIO-PROTOCOL*, 3(6). Available at: <https://doi.org/10.21769/bioprotoc.374>.

Lambin, P., Lieverse, R.I.Y., Eckert, F., Marcus, D., Oberije, C., van der Wiel, A.M.A., Guha, C., Dubois, L.J. and Deasy, J.O. (2020) 'Lymphocyte-Sparing Radiotherapy: the rationale for protecting lymphocyte-rich organs when combining radiotherapy with immunotherapy', *Seminars in radiation oncology*, 30(2), p. 187. Available at: <https://doi.org/10.1016/J.SEMRADONC.2019.12.003>.

Landolfi, J.A., Gaffney, P.M., McManamon, R., Gottdenker, N.L., Ellis, A.E., Rech, R.R., Han, S., Lowenstine, L.J., Agnew, D., Garner, M.M., McAloose, D., Hollinger, C., St. Leger, J., Terrell, S.P., Duncan, M. and Pessier, A.P. (2021) 'Reproductive tract neoplasia in adult female Asian elephants (*Elephas maximus*)', *Veterinary Pathology*, 58(6), pp. 1131–1141. Available at: <https://doi.org/10.1177/030098582111031843>.

Laricchiuta, P., Russo, V., Costagliola, A., Piegari, G., Capasso, M., Silvestre, P., Martano, M. and Paciello, O. (2018) 'Histological and immunohistochemical characterisation of uterine adenocarcinoma in an Asian elephant (*Elephas Maximus*)', *Folia Morphol*, 77(4), pp. 771–774. Available at: <https://doi.org/10.5603/FM.a2018.0025>.

Lee, Y., Jin, Y.W., Wilkins, R.C. and Jang, S. (2019) 'Validation of the dicentric chromosome assay for radiation biological dosimetry in South Korea', *Journal of Radiation Research*, 60(5), pp. 555–563. Available at: <https://doi.org/10.1093/jrr/rrz039>.

LeMaire-Adkins, R., Radke, K. and Hunt, P.A. (1997) 'Lack of checkpoint control at the metaphase/anaphase transition: A mechanism of meiotic nondisjunction in mammalian females', *Journal of Cell Biology*, 139(7), pp. 1611–1619. Available at: <https://doi.org/10.1083/jcb.139.7.1611>.

Leon-Quinto, T., Simon, M.A., Cadenas, R., Jones, J., Martinez-Hernandez, F.J., Moreno, J.M., Vargas, A., Martinez, F. and Soria, B. (2009) 'Developing biological resource banks as a supporting tool for wildlife reproduction and conservation: The Iberian lynx bank as a model for other endangered species', *Animal Reproduction Science*, 112(3–4), pp. 347–361. Available at: <https://doi.org/10.1016/J.ANIREPROSCI.2008.05.070>.

Di Leonardo, A., Linke, S.P., Clarkin, K. and Wahl, G.M. (1994) 'DNA damage triggers a prolonged p53-dependent G1 arrest and long-term induction of Cip1 in normal human fibroblasts', *Genes and Development*, 8(21), pp. 2540–2551. Available at: <https://doi.org/10.1101/gad.8.21.2540>.

Leroi, A.M., Koufopanou, V. and Burt, A. (2003) 'Cancer selection', *Nature Reviews Cancer*. Nature Publishing Group, pp. 226–231. Available at: <https://doi.org/10.1038/nrc1016>.

Leslie, M. (2015) 'How elephants crush cancer', *Science* [Preprint]. Available at: <https://doi.org/10.1126/science.aad4687>.

Li, X. and Heyer, W.D. (2008) 'Homologous recombination in DNA repair and DNA damage tolerance', *Cell research*, 18(1), p. 99. Available at: <https://doi.org/10.1038/CR.2008.1>.

Li, X., Wilson, A.F., Du, W. and Pang, Q. (2018) 'Cell-Cycle-Specific Function of p53 in Fanconi Anemia Hematopoietic Stem and Progenitor Cell Proliferation', *Stem Cell Reports*, 10(2), pp. 339–346. Available at: <https://doi.org/10.1016/j.stemcr.2017.12.006>.

Liang, X., Gu, J., Yu, D., Wang, G., Zhou, L., Zhang, X., Zhao, Y., Chen, X., Zheng, S., Liu, Q., Cai, L., Cui, J. and Li, W. (2016) ‘Low-dose radiation induces cell proliferation in human embryonic lung fibroblasts but not in lung cancer cells: Importance of ERK1/2 and AKT signaling pathways’, *Dose-Response*, 14(1), pp. 1–10. Available at: [https://doi.org/10.1177/1559325815622174/ASSET/IMAGES/LARGE/10.1177\\_1559325815622174-FIG2.JPEG](https://doi.org/10.1177/1559325815622174/ASSET/IMAGES/LARGE/10.1177_1559325815622174-FIG2.JPEG).

LibreTexts (2020) 7.2: *Carcinogenesis - Medicine LibreTexts*. Available at: [https://med.libretexts.org/Courses/American\\_Public\\_University/APUS%3A\\_An\\_Introduction\\_to\\_Nutrition\\_\(Byerley\)/APUS%3A\\_An\\_Introduction\\_to\\_Nutrition\\_1st\\_Edition/07%3A\\_Nutrition\\_and\\_Cancer/7.02%3A\\_Carcinogenesis](https://med.libretexts.org/Courses/American_Public_University/APUS%3A_An_Introduction_to_Nutrition_(Byerley)/APUS%3A_An_Introduction_to_Nutrition_1st_Edition/07%3A_Nutrition_and_Cancer/7.02%3A_Carcinogenesis) (Accessed: 4 August 2022).

Ligasová, A. and Koberna, K. (2021) ‘Strengths and Weaknesses of Cell Synchronization Protocols Based on Inhibition of DNA Synthesis’, *International Journal of Molecular Sciences*, 22(19). Available at: <https://doi.org/10.3390/IJMS221910759>.

Lim, S. and Kaldis, P. (2013) ‘Cdks, cyclins and CKIs: Roles beyond cell cycle regulation’, *Development (Cambridge)*. Development, pp. 3079–3093. Available at: <https://doi.org/10.1242/dev.091744>.

Lindqvist, A., Källström, H., Lundgren, A., Barsoum, E. and Rosenthal, C.K. (2005) ‘Cdc25B cooperates with Cdc25A to induce mitosis but has a unique role in activating cyclin B1-Cdk1 at the centrosome’, *Journal of Cell Biology*, 171(1), pp. 35–45. Available at: <https://doi.org/10.1083/jcb.200503066>.

Lindqvist, A., Rodríguez-Bravo, V. and Medema, R.H. (2009) ‘The decision to enter mitosis: feedback and redundancy in the mitotic entry network’, *Journal of Cell Biology*, 185(2), pp. 193–202. Available at: <https://doi.org/10.1083/JCB.200812045>.

Liu, C., Nie, J., Wang, R. and Mao, W. (2019) ‘The Cell Cycle G2/M Block Is an Indicator of Cellular Radiosensitivity’, *Dose-Response*, 17(4), pp. 1–7. Available at: <https://doi.org/10.1177/1559325819891008>.

Liu, G., Zou, H., Luo, T., Long, M., Bian, J., Liu, X., Gu, J., Yuan, Y., Song, R., Wang, Y., Zhu, J. and Liu, Z. (2016) ‘Caspase-dependent and caspase-independent pathways are involved in cadmium-induced apoptosis in primary rat proximal tubular cell culture’, *PLoS ONE*, 11(11), p. e0166823. Available at: <https://doi.org/10.1371/journal.pone.0166823>.



Liu, Y., Li, Y., Li, N., Teng, W., Wang, M., Zhang, Y. and Xiao, Z. (2016) 'TGF- $\beta$ 1 promotes scar fibroblasts proliferation and transdifferentiation via up-regulating MicroRNA-21', *Scientific Reports* 2016 6:1, 6(1), pp. 1–9. Available at: <https://doi.org/10.1038/srep32231>.

Löbrich, M., Cooper, P.K. and Rydberg, B. (1996) 'Non-random distribution of DNA double-strand breaks induced by particle irradiation', *International Journal of Radiation Biology*, 70(5), pp. 493–503. Available at: <https://doi.org/10.1080/095530096144680>.

Locksley, R.M., Killeen, N. and Lenardo, M.J. (2001) 'The TNF and TNF receptor superfamilies: integrating mammalian biology', *Cell*, 104(4), pp. 487–501. Available at: [https://doi.org/10.1016/S0092-8674\(01\)00237-9](https://doi.org/10.1016/S0092-8674(01)00237-9).

Loitering, M.L., De Kock, M., Viljoen, T.C., Grobler, C.J.S. and Seegers, J.C. (1996) '17 $\beta$ -Estradiol metabolites affect some regulators of the MCF-7 cell cycle', *Cancer Letters*, 110(1–2), pp. 181–186. Available at: [https://doi.org/10.1016/S0304-3835\(96\)04489-8](https://doi.org/10.1016/S0304-3835(96)04489-8).

Loreto, C., La Rocca, G., Anzalone, R., Caltabiano, R., Vespasiani, G., Castorina, S., Ralph, D.J., Celtek, S., Musumeci, G., Giunta, S., Djinic, R., Basic, D. and Sansalone, S. (2014) 'The role of intrinsic pathway in apoptosis activation and progression in Peyronie's disease', *BioMed Research International*, 2014. Available at: <https://doi.org/10.1155/2014/616149>.

Ma, C.M., Coffey, C.W., DeWerd, L.A., Liu, C., Nath, R., Seltzer, S.M. and Seuntjens, J.P. (2001) 'AAPM protocol for 40-300 kV x-ray beam dosimetry in radiotherapy and radiobiology', *Medical physics*, 28(6), pp. 868–893. Available at: <https://doi.org/10.1118/1.1374247>.

Malumbres, M., Harlow, E., Hunt, T., Hunter, T., Lahti, J.M., Manning, G., Morgan, D.O., Tsai, L.H. and Wolgemuth, D.J. (2009) 'Cyclin-dependent kinases: A family portrait', *Nature Cell Biology*. NIH Public Access, pp. 1275–1276. Available at: <https://doi.org/10.1038/ncb1109-1275>.

Mammone, T., Gan, D. and Foyouzi-Youssefi, R. (2006) 'Apoptotic cell death increases with senescence in normal human dermal fibroblast cultures', *Cell Biology International*, 30(11), pp. 903–909. Available at: <https://doi.org/10.1016/j.cellbi.2006.06.010>.

Martín-López, J. V. and Fishel, R. (2013) 'The mechanism of mismatch repair and the functional analysis of mismatch repair defects in Lynch syndrome', *Familial Cancer*, 12(2), pp. 159–168. Available at: <https://doi.org/10.1007/s10689-013-9635-x>.

Massagué, J. (2004) 'G1 cell-cycle control and cancer', *Nature* 2004 432:7015, 432(7015), pp. 298–306. Available at: <https://doi.org/10.1038/nature03094>.

Masson-Meyers, D.S., Bumah, V. V. and Enwemeka, C.S. (2016) 'A comparison of four methods for determining viability in human dermal fibroblasts irradiated with blue light', *Journal of Pharmacological and Toxicological Methods*, 79, pp. 15–22. Available at: <https://doi.org/10.1016/j.vascn.2016.01.001>.

Mathers, C.D. and Loncar, D. (2006) 'Projections of global mortality and burden of disease from 2002 to 2030', *PLoS Medicine*, 3(11), pp. 2011–2030. Available at: <https://doi.org/10.1371/journal.pmed.0030442>.

McColl, N., Auvinen, A., Kesminiene, A., Espina, C., Erdmann, F., de Vries, E., Greinert, R., Harrison, J. and Schüz, J. (2015) 'European Code against Cancer 4th Edition: Ionising and non-ionising radiation and cancer', *Cancer Epidemiology*, 39, pp. S93–S100. Available at: <https://doi.org/10.1016/j.canep.2015.03.016>.

Mcintosh, J.R. (2016) 'Mitosis', *Cold Spring Harbor Perspectives in Biology*, 8(9), p. a023218. Available at: <https://doi.org/10.1101/CSHPERSPECT.A023218>.

McKenna, W.G., Bernhard, E.J., Markiewicz, D.A., Rudoltz, M.S., Maity, A. and Muschel, R.J. (1996) 'Regulation of radiation-induced apoptosis in oncogene-transfected fibroblasts: Influence of H-ras on the G2 delay', *Oncogene*, 12(2), pp. 237–245. Available at: <https://europepmc.org/article/med/8570201> (Accessed: 22 August 2022).

McKinnon, K.M. (2018) 'Flow cytometry: An overview', *Current Protocols in Immunology*, 2018, pp. 5.1.1-5.1.11. Available at: <https://doi.org/10.1002/cpim.40>.

McLean, J.R., Chaix, D., Ohi, M.D. and Gould, K.L. (2011) 'State of the APC/C: Organization, function, and structure', *Critical Reviews in Biochemistry and Molecular Biology*, pp. 118–136. Available at: <https://doi.org/10.3109/10409238.2010.541420>.

Medema, R.H. and MacÜrek, L. (2012) 'Checkpoint control and cancer', *Oncogene*, pp. 2601–2613. Available at: <https://doi.org/10.1038/onc.2011.451>.

Melino, G. (2001) 'The Sirens' song', *Nature*. Nature Publishing Group, p. 23. Available at: <https://doi.org/10.1038/35083653>.

Mellone, M., Hanley, C.J., Thirdborough, S., Mellows, T., Garcia, E., Woo, J., Tod, J., Frampton, S., Jenei, V., Moutasim, K.A., Kabir, T.D., Brennan, P.A., Venturi, G., Ford, K.,

Herranz, N., Lim, K.P., Clarke, J., Lambert, D.W., Prime, S.S., Underwood, T.J., Vijayanand, P., Eliceiri, K.W., Woelk, C., King, E. V., Gil, J., Ottensmeier, C.H. and Thomas, G.J. (2017) 'Induction of fibroblast senescence generates a non-fibrogenic myofibroblast phenotype that differentially impacts on cancer prognosis', *Aging*, 9(1), pp. 114–132. Available at: <https://doi.org/10.18632/aging.101127>.

Merlo, D.F., Rossi, L., Pellegrino, C., Ceppi, M., Cardellino, U., Capurro, C., Ratto, A., Sambucco, P.L., Sestito, V., Tanara, G. and Bocchini, V. (2008) 'Cancer incidence in pet dogs: Findings of the animal tumor registry of Genoa, Italy', *Journal of Veterinary Internal Medicine*, 22(4), pp. 976–984. Available at: <https://doi.org/10.1111/j.1939-1676.2008.0133.x>.

Meulmeester, E. and Jochemsen, A. (2008) 'p53: a guide to apoptosis', *Current cancer drug targets*, 8(2), pp. 87–97. Available at: <https://doi.org/10.2174/156800908783769337>.

Mijele, D., Iwaki, T., Chiyo, P.I., Otiende, M., Obanda, V., Rossi, L., Soriguer, R. and Angelone-Alasaad, S. (2016) 'Influence of Massive and Long Distance Migration on Parasite Epidemiology: Lessons from the Great Wildebeest Migration', *EcoHealth*, 13(4), pp. 708–719. Available at: <https://doi.org/10.1007/s10393-016-1156-2>.

Milanese, Jean-S ´, Wang, & E., Milanese, Jean-Sébastien and Wang, E. (2019) 'Germline mutations and their clinical applications in cancer', <https://doi.org/10.2217/bmt-2019-0005>, 8(1), p. BMT23. Available at: <https://doi.org/10.2217/BMT-2019-0005>.

Miles, B. and Tadi, P. (2020) *Genetics, Somatic Mutation, StatPearls*. Available at: <http://europepmc.org/books/NBK557896> (Accessed: 25 March 2022).

Mirzaghaderi, G. (2010) 'A simple metaphase chromosome preparation from meristematic root tip cells of wheat for karyotyping or in situ hybridization', *African Journal of Biotechnology*, 9(3), pp. 314–318.

Mohammed, B. (2018) (PDF) *The Relationship between Cigarette Smoking and Some Genetic and Immune Aspects in a Sample of Iraqi Smokers Supervised by*. Available at: [https://www.researchgate.net/publication/327824733\\_The\\_Relationship\\_between\\_Cigarette\\_Smoking\\_and\\_Some\\_Genetic\\_and\\_Immune\\_Aspects\\_in\\_a\\_Sample\\_of\\_Iraqi\\_Smokers\\_Supervised\\_by](https://www.researchgate.net/publication/327824733_The_Relationship_between_Cigarette_Smoking_and_Some_Genetic_and_Immune_Aspects_in_a_Sample_of_Iraqi_Smokers_Supervised_by) (Accessed: 16 May 2022).

Momand, J., Zambetti, G.P., Olson, D.C., George, D. and Levine, A.J. (1992) 'The mdm-2 oncogene product forms a complex with the p53 protein and inhibits p53-mediated transactivation', *Cell*, 69(7), pp. 1237–1245. Available at: [https://doi.org/10.1016/0092-8674\(92\)90644-R](https://doi.org/10.1016/0092-8674(92)90644-R).

Mombach, J.C.M., Bugs, C.A. and Chaouiya, C. (2014) 'Modelling the onset of senescence at the G1/S cell cycle checkpoint', *BMC Genomics*, 15(7). Available at: <https://doi.org/10.1186/1471-2164-15-S7-S7>.

Monti, P., Menichini, P., Speciale, A., Cutrona, G., Fais, F., Taiana, E., Neri, A., Bomben, R., Gentile, M., Gattei, V., Ferrarini, M., Morabito, F. and Fronza, G. (2020) 'Heterogeneity of TP53 Mutations and P53 Protein Residual Function in Cancer: Does It Matter?', *Frontiers in Oncology*. Frontiers Media S.A., p. 2313. Available at: <https://doi.org/10.3389/fonc.2020.593383>.

Nasonova, E., Füßel, K., Berger, S., Gudowska-Nowak, E. and Ritter, S. (2004) 'Cell cycle arrest and aberration yield in normal human fibroblasts. I. Effects of X-rays and 195 MeV  $u^{-1}$  C ions', *International Journal of Radiation Biology*, 80(9), pp. 621–634. Available at: <https://doi.org/10.1080/095533000400001006>.

National Cancer Institute (2021) *Risk Factors: Age - NCI*. Available at: <https://www.cancer.gov/about-cancer/causes-prevention/risk/age> (Accessed: 11 May 2022).

Neshasteh-Riz, A., Pashazadeh, A.M. and Mahdavi, S.R. (2013) 'Relative biological effectiveness (RBE) of 131I radiation relative to 60Co gamma rays', *Cell Journal*, 15(3), pp. 224–229. Available at: <https://pmc/articles/PMC3769604/> (Accessed: 13 November 2022).

Ngwa, W., Kumar, R., Sridhar, S., Korideck, H., Zygmanski, P., Cormack, R.A., Berbeco, R. and Makrigiorgos, G.M. (2014) 'Targeted radiotherapy with gold nanoparticles: Current status and future perspectives', *Nanomedicine*. NIH Public Access, pp. 1063–1082. Available at: <https://doi.org/10.2217/nnm.14.55>.

Nikitaki, Z., Nikolov, V., Mavragani, I. V., Mladenov, E., Mangelis, A., Laskaratou, D.A., Fragkoulis, G.I., Hellweg, C.E., Martin, O.A., Emfietzoglou, D., Hatzi, V.I., Terzoudi, G.I., Iliakis, G. and Georgakilas, A.G. (2016) 'Measurement of complex DNA damage induction and repair in human cellular systems after exposure to ionizing radiations of varying linear energy transfer (LET)', *Free Radical Research*, 50(sup1), pp. S64–S78. Available at: <https://doi.org/10.1080/10715762.2016.1232484>.

Nosrati, N., Kapoor, N.R. and Kumar, V. (2015) 'DNA damage stress induces the expression of ribosomal protein S27a gene in a p53-dependent manner', *Gene*, 559(1), pp. 44–51. Available at: <https://doi.org/10.1016/j.gene.2015.01.014>.

Nouraini, S., Six, E., Matsuyama, S., Krajewski, S. and Reed, J.C. (2000) 'The Putative Pore-Forming Domain of Bax Regulates Mitochondrial Localization and Interaction with Bcl-X L', *Molecular and Cellular Biology*, 20(5), pp. 1604–1615. Available at: <https://doi.org/10.1128/mcb.20.5.1604-1615.2000>.

Nunney, L. (2018) 'Size matters: Height, cell number and a person's risk of cancer', *Proceedings of the Royal Society B: Biological Sciences*, 285(1889), p. 2463. Available at: <https://doi.org/10.1098/rspb.2018.1743>.

Nunney, L., Maley, C.C., Breen, M., Hochberg, M.E. and Schiffman, J.D. (2015) 'Peto's paradox and the promise of comparative oncology', *Philosophical Transactions of the Royal Society B: Biological Sciences*, 370(1673). Available at: <https://doi.org/10.1098/rstb.2014.0177>.

Olivier, M., Hollstein, M. and Hainaut, P. (2010) 'TP53 mutations in human cancers: origins, consequences, and clinical use.', *Cold Spring Harbor perspectives in biology*. Available at: <https://doi.org/10.1101/cshperspect.a001008>.

Padma, V.V. (2015) 'An overview of targeted cancer therapy', *BioMedicine*, 5(4), pp. 1–6. Available at: <https://doi.org/10.7603/S40681-015-0019-4>.

Panteleeva, A., Słonina, D., Brankovic, K., Spekl, K., Pawelke, J., Hoinkis, C. and Dörr, W. (2003) 'Clonogenic survival of human keratinocytes and rodent fibroblasts after irradiation with 25 kV x-rays', *Radiation and Environmental Biophysics*, 42(2), pp. 95–100. Available at: <https://doi.org/10.1007/S00411-003-0199-2/TABLES/3>.

Parkin, D.M., Bray, F., Ferlay, J. and Jemal, A. (2014) 'Cancer in Africa 2012', *Cancer Epidemiology Biomarkers and Prevention*, 23(6), pp. 953–966. Available at: <https://doi.org/10.1158/1055-9965.EPI-14-0281>.

Parry, D.H. and O'Farrell, P.H. (2001) 'The schedule of destruction of three mitotic cyclins can dictate the timing of events during exit from mitosis', *Current biology: CB*, 11(9), pp. 671–683. Available at: [https://doi.org/10.1016/S0960-9822\(01\)00204-4](https://doi.org/10.1016/S0960-9822(01)00204-4).

Pennington, K., Chan, T., Torres, M. and Andersen, J. (2018) ‘The dynamic and stress-adaptive signaling hub of 14-3-3: emerging mechanisms of regulation and context-dependent protein–protein interactions’, *Oncogene*. Nature Publishing Group, pp. 5587–5604. Available at: <https://doi.org/10.1038/s41388-018-0348-3>.

Percuoco, R. (2013) ‘Plain Radiographic Imaging’, in *Clinical Imaging: With Skeletal, Chest, & Abdominal Pattern Differentials: Third Edition*. Elsevier Inc., pp. 1–43. Available at: <https://doi.org/10.1016/B978-0-323-08495-6.00001-4>.

Petkov, S., Kahland, T., Shomroni, O., Lingner, T., Salinas, G., Fuchs, S., Debowski, K. and Behr, R. (2018) ‘Immortalization of common marmoset monkey fibroblasts by piggyBac transposition of hTERT’, *PLOS ONE*, 13(9), p. e0204580. Available at: <https://doi.org/10.1371/JOURNAL.PONE.0204580>.

Peto, H., Roe, F.J.C., Lee, P.N., Levy, L. and Clack, J. (1975) ‘Cancer and ageing in mice and men’, *British Journal of Cancer*, 32(4), pp. 411–426. Available at: <https://doi.org/10.1038/bjc.1975.242>.

Pfister, N.T. and Prives, C. (2017) ‘Transcriptional regulation by wild-type and cancer-related mutant forms of p53’, *Cold Spring Harbor Perspectives in Medicine*, 7(2). Available at: <https://doi.org/10.1101/cshperspect.a026054>.

Porcel, E., Liehn, S., Remita, H., Usami, N., Kobayashi, K., Furusawa, Y., Sech, C. Le and Lacombe, S. (2010) ‘Platinum nanoparticles: A promising material for future cancer therapy?’, *Nanotechnology*, 21(8). Available at: <https://doi.org/10.1088/0957-4484/21/8/085103>.

Positive Bioscience (2019) *Somatic Mutations vs Germline Mutations*, *Positive Bioscience*. Available at: <https://ib.bioninja.com.au/standard-level/topic-3-genetics/33-meiosis/somatic-vs-germline-mutatio.html> (Accessed: 27 April 2022).

Prasanth, S.G., Méndez, J., Prasanth, K. V and Stillman, B. (2003) ‘Dynamics of pre-replication complex proteins during the cell division cycle’. Available at: <https://doi.org/10.1098/rstb.2003.1360>.

Pucci, B., Kasten, M. and Giordano, A. (2000) ‘Cell Cycle and Apoptosis’, *Neoplasia (New York, N.Y.)*, 2(4), p. 291. Available at: <https://doi.org/10.1038/SJ.NEO.7900101>.

Pucci, C., Martinelli, C. and Ciofani, G. (2019) 'Innovative approaches for cancer treatment: Current perspectives and new challenges', *ecancermedicalscience*. ecancer Global Foundation. Available at: <https://doi.org/10.3332/ecancer.2019.961>.

Qian, Y. and Chen, X. (2013) 'Senescence regulation by the p53 protein family', *Methods in Molecular Biology*, 965, pp. 37–61. Available at: [https://doi.org/10.1007/978-1-62703-239-1\\_3](https://doi.org/10.1007/978-1-62703-239-1_3).

Rafehi, H., Orlowski, C., Georgiadis, G.T., Ververis, K., El-Osta, A. and Karagiannis, T.C. (2011) 'Clonogenic assay: Adherent cells', *Journal of Visualized Experiments*, (49), p. 49. Available at: <https://doi.org/10.3791/2573>.

Rangarajan, A., Hong, S.J., Gifford, A. and Weinberg, R.A. (2004) 'Species- and cell type-specific requirements for cellular transformation', *Cancer Cell*, 6(2), pp. 171–183. Available at: <https://doi.org/10.1016/j.ccr.2004.07.009>.

Rao, R. V., Hermel, E., Castro-Obregon, S., Del Rio, G., Ellerby, L.M., Ellerby, H.M. and Bredesen, D.E. (2001) 'Coupling endoplasmic reticulum stress to the cell death program. Mechanism of caspase activation', *The Journal of biological chemistry*, 276(36), pp. 33869–33874. Available at: <https://doi.org/10.1074/JBC.M102225200>.

Ravichandran, R. (2009) 'Has the time come for doing away with Cobalt-60 teletherapy for cancer treatments', *Journal of Medical Physics*. Wolters Kluwer -- Medknow Publications, pp. 63–65. Available at: <https://doi.org/10.4103/0971-6203.51931>.

Reed, J.C. (2000) 'Warner-Lambert/Parke Davis award lecture: Mechanisms of apoptosis', *American Journal of Pathology*. American Society for Investigative Pathology, pp. 1415–1430. Available at: [https://doi.org/10.1016/s0002-9440\(10\)64779-7](https://doi.org/10.1016/s0002-9440(10)64779-7).

Ribatti, D. (2017) 'A revisited concept: Contact inhibition of growth. From cell biology to malignancy', *Experimental Cell Research*. Academic Press, pp. 17–19. Available at: <https://doi.org/10.1016/j.yexcr.2017.06.012>.

Rieger, A.M., Nelson, K.L., Konowalchuk, J.D. and Barreda, D.R. (2011) 'Modified Annexin V/Propidium Iodide Apoptosis Assay For Accurate Assessment of Cell Death', *Journal of Visualized Experiments : JoVE*, (50), p. 2597. Available at: <https://doi.org/10.3791/2597>.

Rodman, T.C., Flehinger, B.J. and Rohlf, F.J. (1980) 'Metaphase chromosome associations: Colcemid distorts the pattern', *Cytogenetic and Genome Research*, 27(2–3), pp. 98–110. Available at: <https://doi.org/10.1159/000131471>.

Rohland, N., Reich, D., Mallick, S., Meyer, M., Green, R.E., Georgiadis, N.J., Roca, A.L. and Hofreiter, M. (2010) 'Genomic DNA sequences from mastodon and woolly mammoth reveal deep speciation of forest and savanna elephants', *PLoS Biology*, 8(12), p. e1000564. Available at: <https://doi.org/10.1371/journal.pbio.1000564>.

Roobol, S.J., van den Bent, I., van Cappellen, W.A., Abraham, T.E., Paul, M.W., Kanaar, R., Houtsmuller, A.B., van Gent, D.C. and Essers, J. (2020) 'Comparison of high-and low-let radiation-induced dna double-strand break processing in living cells', *International Journal of Molecular Sciences*, 21(18), pp. 1–19. Available at: <https://doi.org/10.3390/ijms21186602>.

Ryder, O.A. and Onuma, M. (2018) 'Viable Cell Culture Banking for Biodiversity Characterization and Conservation', *Annual Review of Animal Biosciences*, 6, pp. 83–98. Available at: <https://doi.org/10.1146/annurev-animal-030117-014556>.

Ryu, A.H., Eckalbar, W.L., Kreimer, A., Yosef, N. and Ahituv, N. (2017) 'Use antibiotics in cell culture with caution: genome-wide identification of antibiotic-induced changes in gene expression and regulation', *Scientific reports*, 7(1). Available at: <https://doi.org/10.1038/S41598-017-07757-W>.

Sabatinos, S.A. and Forsburg, S.L. (2010) 'Molecular genetics of schizosaccharomyces pombe', *Methods in Enzymology*, 470(C), pp. 759–795. Available at: [https://doi.org/10.1016/S0076-6879\(10\)70032-X](https://doi.org/10.1016/S0076-6879(10)70032-X).

Sacristan, C. and Kops, G.J.P.L. (2015) 'Joined at the hip: kinetochores, microtubules, and spindle assembly checkpoint signaling', *Trends in cell biology*, 25(1), pp. 21–28. Available at: <https://doi.org/10.1016/J.TCB.2014.08.006>.

Sancar, A., Lindsey-Boltz, L.A., Ünsal-Kaçmaz, K. and Linn, S. (2004) 'Molecular mechanisms of mammalian DNA repair and the DNA damage checkpoints', *Annual Review of Biochemistry*. Annu Rev Biochem, pp. 39–85. Available at: <https://doi.org/10.1146/annurev.biochem.73.011303.073723>.



Dos Santos, F.A.A., Carvalho, C.L., Almeida, I., Fagulha, T., Rammos, F., Barros, S.C., Henriques, M., Luís, T. and Duarte, M.D. (2021) ‘Simple method for establishing primary leporidae skin fibroblast cultures’, *Cells*, 10(8), p. 2100. Available at: <https://doi.org/10.3390/cells10082100>.

Sarkar, S., Horn, G., Moulton, K., Oza, A., Byler, S., Kokolus, S. and Longacre, M. (2013) ‘Cancer development, progression, and therapy: An epigenetic overview’, *International Journal of Molecular Sciences*. Multidisciplinary Digital Publishing Institute (MDPI), pp. 21087–21113. Available at: <https://doi.org/10.3390/ijms141021087>.

Scalliet, P. and Gueulette, J. (2017) ‘Radiobiological characterization of clinical proton and carbon-ion beams’, *CERN Yellow Reports: School Proceedings*, 1(May), pp. 1–11. Available at: <https://doi.org/10.23730/CYRSP-2017-001.1>.

Schäuble, S., Klement, K., Marthandan, S., Münch, S., Heiland, I., Schuster, S., Hemmerich, P. and Diekmann, S. (2012) ‘Quantitative model of cell cycle arrest and cellular senescence in primary human fibroblasts’, *PLoS ONE*, 7(8). Available at: <https://doi.org/10.1371/journal.pone.0042150>.

Seaman, J.E., Julien, O., Lee, P.S., Rettenmaier, T.J., Thomsen, N.D. and Wells, J.A. (2016) ‘Cacidas: Caspases can cleave after aspartate, glutamate and phosphoserine residues’, *Cell Death and Differentiation*, 23(10), pp. 1717–1726. Available at: <https://doi.org/10.1038/cdd.2016.62>.

Seluanov, A., Gladyshev, V.N., Vijg, J. and Gorbunova, V. (2018) ‘Mechanisms of cancer resistance in long-lived mammals’, *Nature Reviews Cancer*, 18(7), pp. 433–441. Available at: <https://doi.org/10.1038/s41568-018-0004-9>.

Seluanov, A., Hine, C., Azpurua, J., Feigenson, M., Bozzella, M., Mao, Z., Catania, K.C. and Gorbunova, V. (2009) ‘Hypersensitivity to contact inhibition provides a clue to cancer resistance of naked mole-rat’, *Proceedings of the National Academy of Sciences of the United States of America*, 106(46), pp. 19352–19357. Available at: <https://doi.org/10.1073/pnas.0905252106>.

Seluanov, A. and Ribeiro, A.A.C.M. (2009) ‘That Differ in Size and Lifespan’, *Aging*, 7(6), pp. 813–823. Available at: <https://doi.org/10.1111/j.1474-9726.2008.00431.x>.Distinct.

Sharpless, N.E. and DePinho, R.A. (2004) 'Telomeres, stem cells, senescence, and cancer', *The Journal of Clinical Investigation*, 113(2), pp. 160–168. Available at: <https://doi.org/10.1172/JCI20761>.

Shen, T. and Huang, S. (2012) 'The Role of Cdc25A in the Regulation of Cell Proliferation and Apoptosis', *Anti-Cancer Agents in Medicinal Chemistry*, 12(6), pp. 631–639. Available at: <https://doi.org/10.2174/187152012800617678>.

Siegel, R.L., Miller, K.D., Fuchs, H.E. and Jemal, A. (2021) 'Cancer Statistics, 2021', *CA: A Cancer Journal for Clinicians*, 71(1), pp. 7–33. Available at: <https://doi.org/10.3322/caac.21654>.

Siengdee, P., Klinhom, S., Thitaram, C. and Nganvongpanit, K. (2018) 'Isolation and culture of primary adult skin fibroblasts from the Asian elephant (*Elephas maximus*)', *PeerJ*, 2018(1), pp. 1–16. Available at: <https://doi.org/10.7717/peerj.4302>.

Silvestre, M.A., Sánchez, J.P. and Gómez, E.A. (2004) 'Vitrification of goat, sheep, and cattle skin samples from whole ear extirpated after death and maintained at different storage times and temperatures', *Cryobiology*, 49(3), pp. 221–229. Available at: <https://doi.org/10.1016/j.cryobiol.2004.08.001>.

Simonelli, V., Narciso, L., Dogliotti, E. and Fortini, P. (2005) 'Base excision repair intermediates are mutagenic in mammalian cells', *Nucleic Acids Research*, 33(14), pp. 4404–4411. Available at: <https://doi.org/10.1093/nar/gki749>.

Sionov, R.V., Hayon, I.L. and Haupt, Y. (2002) 'The Regulation of p53 Growth Suppression', in *Cell cycle checkpoints and cancer*. Landes Bioscience, pp. 106–125. Available at: <https://www.ncbi.nlm.nih.gov/books/NBK6412/> (Accessed: 15 November 2022).

Slee, E.A., Adrain, C. and Martin, S.J. (2001) 'Executioner Caspase-3, -6, and -7 Perform Distinct, Non-redundant Roles during the Demolition Phase of Apoptosis \*', *Journal of Biological Chemistry*, 276(10), pp. 7320–7326. Available at: <https://doi.org/10.1074/JBC.M008363200>.

Smith, F. (1890) 'Histology of the Skin of the Elephant', *Journal of anatomy and physiology*, 24(Pt 4), pp. 493–503.

Smith, S.D., Kawash, J.K., Karaiskos, S., Biluck, I. and Grigoriev, A. (2017) 'Evolutionary adaptation revealed by comparative genome analysis of woolly mammoths and elephants', *DNA Research*, 24(4), pp. 359–369. Available at: <https://doi.org/10.1093/dnares/dsx007>.

Smith, T.A., Kirkpatrick, D.R., Smith, S., Smith, T.K., Pearson, T., Kailasam, A., Herrmann, K.Z., Schubert, J. and Agrawal, D.K. (2017) 'Radioprotective agents to prevent cellular damage due to ionizing radiation', *Journal of Translational Medicine*. BioMed Central Ltd., pp. 1–18. Available at: <https://doi.org/10.1186/s12967-017-1338-x>.

Soussi, T. (2010) 'The history of p53. A perfect example of the drawbacks of scientific paradigms', *EMBO Reports*, pp. 822–826. Available at: <https://doi.org/10.1038/embor.2010.159>.

Sowa, P., Rutkowska-Talipska, J., Sulkowska, U., Rutkowski, K. and Rutkowski, R. (2012) 'Ionizing and non-ionizing electromagnetic radiation in modern medicine', *Polish Annals of Medicine*, 19(2), pp. 134–138. Available at: <https://doi.org/10.1016/j.poamed.2012.07.001>.

Stankiewicz, P. (2016) 'One pedigree we all may have come from - Did Adam and Eve have the chromosome 2 fusion?', *Molecular Cytogenetics*, 9(1), pp. 1–5. Available at: <https://doi.org/10.1186/S13039-016-0283-3/FIGURES/2>.

Staszak, K. and Makałowska, I. (2021) 'Cancer, retrogenes, and evolution', *Life*. Multidisciplinary Digital Publishing Institute (MDPI), pp. 1–16. Available at: <https://doi.org/10.3390/life11010072>.

Statement, P. and Cancer, C. (2013) 'The Cancer Association of South Africa ( CANSA )', (June), pp. 1–9. Available at: <https://cansa.org.za/mens-health/> (Accessed: 17 October 2021).

Stenvinkel, P., Painer, J., Johnson, R.J. and Natterson-Horowitz, B. (2020) 'Biomimetics – Nature's roadmap to insights and solutions for burden of lifestyle diseases', *Journal of Internal Medicine*, pp. 238–251. Available at: <https://doi.org/10.1111/joim.12982>.

Stockert, J.C., Blázquez-Castro, A., Cañete, M., Horobin, R.W. and Villanueva, Á. (2012) 'MTT assay for cell viability: Intracellular localization of the formazan product is in lipid droplets', *Acta Histochemica*, 114(8), pp. 785–796. Available at: <https://doi.org/10.1016/j.acthis.2012.01.006>.

Stoka, V., Turk, B., Schendel, S.L., Kim, T.H., Cirman, T., Snipas, S.J., Ellerby, L.M., Bredesen, D., Freeze, H., Abrahamson, M., Brömme, D., Krajewski, S., Reed, J.C., Yin, X.M., Turk, V. and Salvesen, G.S. (2001) 'Lysosomal protease pathways to apoptosis: Cleavage of Bid, not pro-caspases, is the most likely route', *Journal of Biological Chemistry*, 276(5), pp. 3149–3157. Available at: <https://doi.org/10.1074/jbc.M008944200>.

Strober, W. (2001) 'Trypan blue exclusion test of cell viability.', *Current protocols in immunology / edited by John E. Coligan ... [et al.]*, Appendix 3(1), p. A.3B.1-A.3B.2. Available at: <https://doi.org/10.1002/0471142735.ima03bs21>.

Sulak, M., Fong, L., Mika, K., Chigurupati, S., Yon, L., Mongan, N.P., Emes, R.D. and Lynch, V.J. (2016) 'TP53 copy number expansion is associated with the evolution of increased body size and an enhanced DNA damage response in elephants', *eLife*, 5(September2016). Available at: <https://doi.org/10.7554/eLife.11994>.

Suryadinata, R., Sadowski, M. and Sarcevic, B. (2010) 'Control of cell cycle progression by phosphorylation of cyclin-dependent kinase (CDK) substrates', *Bioscience reports*, 30(4), pp. 243–255. Available at: <https://doi.org/10.1042/BSR20090171>.

Sutherland, B.M., Bennett, P. V., Sidorkina, O. and Laval, J. (2000) 'Clustered DNA damages induced in isolated DNA and in human cells by low doses of ionizing radiation', *Proceedings of the National Academy of Sciences of the United States of America*, 97(1), pp. 103–108. Available at: <https://doi.org/10.1073/pnas.97.1.103>.

Suzuki, Y., Imai, Y., Nakayama, H., Takahashi, K., Takio, K. and Takahashi, R. (2001) 'A serine protease, HtrA2, is released from the mitochondria and interacts with XIAP, inducing cell death', *Molecular Cell*, 8(3), pp. 613–621. Available at: [https://doi.org/10.1016/S1097-2765\(01\)00341-0](https://doi.org/10.1016/S1097-2765(01)00341-0).

Sy, E., Samboju, V. and Mukhdomi, T. (2021) 'X-ray Image Production Procedures', *StatPearls* [Preprint]. Available at: <https://www.ncbi.nlm.nih.gov/books/NBK564352/> (Accessed: 14 September 2022).

Szegezdi, E., Fitzgerald, U. and Samali, A. (2003) 'Caspase-12 and ER-Stress-Mediated Apoptosis: The Story so Far', in *Annals of the New York Academy of Sciences*. John Wiley & Sons, Ltd, pp. 186–194. Available at: <https://doi.org/10.1196/annals.1299.032>.

Tamm, I., Kikuchi, T., Wang, E. and Pfeffer, L.M. (1984) 'Growth Rate of Control and  $\beta$ -Interferon-treated Human Fibroblast Populations over the Course of Their in Vitro Life Span', *Cancer Research*, 44(6), pp. 2291–2296.

Taylor, W.R. and Stark, G.R. (2001) 'Regulation of the G2/M transition by p53', *Oncogene*. *Oncogene*, pp. 1803–1815. Available at: <https://doi.org/10.1038/sj.onc.1204252>.

*Templates* (no date). Available at: <http://www.cellsignet.com/media/templ.html> (Accessed: 27 January 2023).

Thelander, L. and Reichard, P. (1979) 'Reduction of +12005 ribonucleotides', *Biochem*, (48), pp. 133–158. Available at: [https://doi.org/0066-4154/79/0701-0133\\$01.00](https://doi.org/0066-4154/79/0701-0133$01.00).

Tian, X., Azpurua, J., Hine, C., Vaidya, A., Myakishev-Rempel, M., Ablaeva, J., Mao, Z., Nevo, E., Gorbunova, V. and Seluanov, A. (2013) 'High-molecular-mass hyaluronan mediates the cancer resistance of the naked mole rat', *Nature*, 499(7458), pp. 346–349. Available at: <https://doi.org/10.1038/nature12234>.

Tidière, M., Gaillard, J.M., Berger, V., Müller, D.W.H., Lackey, L.B., Gimenez, O., Clauss, M. and Lemaître, J.F. (2016) 'Comparative analyses of longevity and senescence reveal variable survival benefits of living in zoos across mammals', *Scientific Reports 2016 6:1*, 6(1), pp. 1–7. Available at: <https://doi.org/10.1038/srep36361>.

Tollis, M., Boddy, A.M. and Maley, C.C. (2017) 'Peto's Paradox: How has evolution solved the problem of cancer prevention?', *BMC Biology*, 15(1), pp. 1–5. Available at: <https://doi.org/10.1186/s12915-017-0401-7>.

Tollis, M., Robbins, J., Webb, A.E., Kuderna, L.F.K., Caulin, A.F., Garcia, J.D., Bèrubè, M., Pourmand, N., Marques-Bonet, T., O'Connell, M.J., Palsbøll, P.J., Maley, C.C. and Shapiro, B. (2019) 'Return to the Sea, Get Huge, Beat Cancer: An Analysis of Cetacean Genomes Including an Assembly for the Humpback Whale (*Megaptera novaeangliae*)', *Molecular Biology and Evolution*, 36(8), pp. 1746–1763. Available at: <https://doi.org/10.1093/molbev/msz099>.

Totter, J.R. (1980) 'Spontaneous cancer and its possible relationship to oxygen metabolism', *Proceedings of the National Academy of Sciences of the United States of America*, 77(4 D), pp. 1763–1767. Available at: <https://doi.org/10.1073/pnas.77.4.1763>.

Trimarchi, J.M. and Lees, J.A. (2002) 'Sibling rivalry in the E2F family', *Nature Reviews Molecular Cell Biology*. *Nat Rev Mol Cell Biol*, pp. 11–20. Available at: <https://doi.org/10.1038/nrm714>.

Truong, K., Bradley, S., Baginski, B., Wilson, J.R., Medlin, D., Zheng, L., Wilson, R.K., Rusin, M., Takacs, E. and Dean, D. (2018) 'The effect of well-characterized, very low-dose x-ray radiation on fibroblasts', *PLoS ONE*, 13(1), p. e0190330. Available at: <https://doi.org/10.1371/journal.pone.0190330>.

Tuieng, R.J., Cartmell, S.H., Kirwan, C.C. and Sherratt, M.J. (2021) 'The effects of ionising and non-ionising electromagnetic radiation on extracellular matrix proteins', *Cells*. Available at: <https://doi.org/10.3390/cells10113041>.

Tyner, S.D., Venkatachalam, S., Choi, J., Jones, S., Ghebranious, N., Igelmann, H., Lu, X., Soron, G., Cooper, B., Brayton, C., Sang, H.P., Thompson, T., Karsenty, G., Bradley, A. and Donehower, L.A. (2002) 'P53 mutant mice that display early ageing-associated phenotypes', *Nature*, 415(6867), pp. 45–53. Available at: <https://doi.org/10.1038/415045a>.

Urbain, N. and Cheung, T.H. (2021) 'Stem cell quiescence: the challenging path to activation', *Development (Cambridge, England)*, 148(3). Available at: <https://doi.org/10.1242/DEV.165084>.

Uttamatin, R., Yuvapoositanon, P., Intarapanich, A., Kaewkamnerd, S., Phuksaritanon, R., Assawamakin, A. and Tongshima, S. (2013) 'MetaSel: A metaphase selection tool using a Gaussian-based classification technique', *BMC Bioinformatics*, 14(SUPPL16), pp. 1–13. Available at: <https://doi.org/10.1186/1471-2105-14-S16-S13/TABLES/1>.

Vaiserman, A. and Krasnienkov, D. (2021) 'Telomere Length as a Marker of Biological Age: State-of-the-Art, Open Issues, and Future Perspectives', *Frontiers in Genetics*, 11, p. 1816. Available at: <https://doi.org/10.3389/FGENE.2020.630186/BIBTEX>.

Vangipuram, M., Ting, D., Kim, S., Diaz, R. and Schüle, B. (2013) 'Skin Punch Biopsy Explant Culture for Derivation of Primary Human Fibroblasts', *Journal of Visualized Experiments : JoVE*, (77), p. 3779. Available at: <https://doi.org/10.3791/3779>.

Vazquez, J.M., Sulak, M., Chigurupati, S. and Lynch, V.J. (2018) 'A Zombie LIF Gene in Elephants Is Upregulated by TP53 to Induce Apoptosis in Response to DNA Damage', *Cell Reports*, 24(7), pp. 1765–1776. Available at: <https://doi.org/10.1016/j.celrep.2018.07.042>.

Vermeulen, K., Van Bockstaele, D.R. and Berneman, Z.N. (2003) 'The cell cycle: A review of regulation, deregulation and therapeutic targets in cancer', *Cell Proliferation*, pp. 131–149. Available at: <https://doi.org/10.1046/j.1365-2184.2003.00266.x>.

Villegas, J. and McPhaul, M. (2005) 'Establishment and culture of human skin fibroblasts.', *Current protocols in molecular biology / edited by Frederick M. Ausubel ... [et al.]*, Chapter 28, pp. 1–9. Available at: <https://doi.org/10.1002/0471142727.mb2803s71>.

Vincze, O., Colchero, F., Lemaître, J.F., Conde, D.A., Pavard, S., Bieuvre, M., Urrutia, A.O., Ujvari, B., Boddy, A.M., Maley, C.C., Thomas, F. and Giraudeau, M. (2022) 'Cancer risk across mammals', *Nature*, 601(7892), pp. 263–267. Available at: <https://doi.org/10.1038/s41586-021-04224-5>.

Visconti, R., Della Monica, R. and Grieco, D. (2016) 'Cell cycle checkpoint in cancer: a therapeutically targetable double-edged sword', *Journal of experimental & clinical cancer research : CR*, 35(1). Available at: <https://doi.org/10.1186/S13046-016-0433-9>.

Waldman, A.D., Fritz, J.M. and Lenardo, M.J. (2020) 'A guide to cancer immunotherapy: from T cell basic science to clinical practice', *Nature Reviews Immunology*. Nature Publishing Group, pp. 651–668. Available at: <https://doi.org/10.1038/s41577-020-0306-5>.

Wang, B. (2014) 'Analyzing cell cycle checkpoints in response to ionizing radiation in mammalian cells', *Methods in Molecular Biology*, 1170, pp. 313–320. Available at: [https://doi.org/10.1007/978-1-4939-0888-2\\_15](https://doi.org/10.1007/978-1-4939-0888-2_15).

Wang, G.Q., Wieckowski, E., Goldstein, L.A., Gastman, B.R., Rabinovitz, A., Gambotto, A., Li, S., Fang, B., Yin, X.M. and Rabinowich, H. (2001) 'Resistance to granzyme B-mediated cytochrome c release in Bak-deficient cells', *Journal of Experimental Medicine*, 194(9), pp. 1325–1337. Available at: <https://doi.org/10.1084/jem.194.9.1325>.

Wang, T., Li, Z., Wei, J., Zheng, D., Wang, C., Xu, C., Chen, W. and Wang, B. (2021) 'Establishment and characterization of fibroblast cultures derived from a female common hippopotamus (*Hippopotamus amphibius*) skin biopsy', *Cell Biology International*, 45(7), pp. 1571–1578. Available at: <https://doi.org/10.1002/CBIN.11596>.

Wang, X.W., Zhan, Q., Coursen, J.D., Khan, M.A., Kontny, H.U., Yu, L., Hollander, M.C., O'Connor, P.M., Fornace, A.J. and Harris, C.C. (1999) 'GADD45 induction of a G2/M cell cycle checkpoint', *Proceedings of the National Academy of Sciences of the United States of America*, 96(7), pp. 3706–3711. Available at: <https://doi.org/10.1073/pnas.96.7.3706>.

Wang, Y., Nguyen, D.T., Yang, G., Anesi, J., Kelly, J., Chai, Z., Ahmady, F., Charchar, F. and Golledge, J. (2021) 'A Modified MTS Proliferation Assay for Suspended Cells to Avoid the Interference by Hydralazine and  $\beta$ -Mercaptoethanol', *Assay and Drug Development Technologies*, 19(3), pp. 184–190. Available at: [https://doi.org/10.1089/ADT.2020.1027/ASSET/IMAGES/LARGE/ADT.2020.1027\\_FIGURE6.JPG](https://doi.org/10.1089/ADT.2020.1027/ASSET/IMAGES/LARGE/ADT.2020.1027_FIGURE6.JPG).

Wang, Y., Plewa, M.J., Mukherjee, U.K. and Verma, V. (2018) 'Assessing the cytotoxicity of ambient particulate matter (PM) using Chinese hamster ovary (CHO) cells and its relationship with the PM chemical composition and oxidative potential', *Atmospheric Environment*, 179, pp. 132–141. Available at: <https://doi.org/10.1016/j.atmosenv.2018.02.025>.

Wang, Z., Tang, Y., Tan, Y., Wei, Q. and Yu, W. (2019) 'Cancer-associated fibroblasts in radiotherapy: Challenges and new opportunities', *Cell Communication and Signaling*. National Academy of Sciences, pp. E2566–E2574. Available at: <https://doi.org/10.1186/s12964-019-0362-2>.

Ward, J.F., Blakely, W.F. and Joner, E.I. (1985) 'Mammalian cells are not killed by DNA single-strand breaks caused by hydroxyl radicals from hydrogen peroxide', *Radiation Research*, 103(3), pp. 383–392. Available at: <https://doi.org/10.2307/3576760>.

Whaley, D., Damyar, K., Witek, R.P., Mendoza, A., Alexander, M. and Lakey, J.R. (2021) 'Cryopreservation: An Overview of Principles and Cell-Specific Considerations', *Cell Transplantation*. Available at: <https://doi.org/10.1177/0963689721999617>.

Widmer, H.R., Hoppeler, H., Nevo, E., Taylor, C.R. and Weibel, E.R. (1997) 'Working underground: Respiratory adaptations in the blind mole rat', *Proceedings of the National Academy of Sciences of the United States of America*, 94(5), pp. 2062–2067. Available at: <https://doi.org/10.1073/PNAS.94.5.2062/ASSET/EDADBDBE-7BC2-44B0-8D58-0EB74CAFCA64/ASSETS/GRAPHIC/PQ0473671004.JPG>.



Williams, C., Tiwari, S.K., Goswami, V.R., De Silva, S., Kumar, A., Baskaran, N., Yoganand, K. and Menon, V.& (2020) ‘Elephas maximus. The IUCN Red List of Threatened Species’, *Elephas maximus*, 2020(The IUCN Red List of Threatened Species 2020), pp. 1–29. Available at: <https://www.iucnredlist.org/species/7140/45818198>.

Wlodkovic, D., Telford, W., Skommer, J. and Darzynkiewicz, Z. (2011) ‘Apoptosis and Beyond: Cytometry in Studies of Programmed Cell Death’, *Methods in Cell Biology*, 103, p. 55. Available at: <https://doi.org/10.1016/B978-0-12-385493-3.00004-8>.

Wong, R.S.Y. (2011) ‘Apoptosis in cancer: From pathogenesis to treatment’, *Journal of Experimental and Clinical Cancer Research*. BioMed Central, pp. 1–14. Available at: <https://doi.org/10.1186/1756-9966-30-87>.

World Cancer Research Fund (2020) *Worldwide cancer data | World Cancer Research Fund International*. Available at: <https://www.wcrf.org/cancer-trends/worldwide-cancer-data/> (Accessed: 14 June 2022).

World Health Organisation (2022) *Cancer*. Available at: <https://www.who.int/news-room/fact-sheets/detail/cancer> (Accessed: 25 April 2022).

Xie, D., Pei, Q., Li, J., Wan, X. and Ye, T. (2021) ‘Emerging Role of E2F Family in Cancer Stem Cells’, *Frontiers in Oncology*. Available at: <https://doi.org/10.3389/fonc.2021.723137>.

Yam, C.H., Fung, T.K. and Poon, R.Y.C. (2002) ‘Cyclin A in cell cycle control and cancer’, *Cellular and molecular life sciences: CMLS*, 59(8), pp. 1317–1326. Available at: <https://doi.org/10.1007/S00018-002-8510-Y>.

Yang, F., Alkalaeva, E.Z., Perelman, P.L., Pardini, A.T., Harrison, W.R., O’Brien, P.C.M., Fu, B., Graphodatsky, A.S., Ferguson-Smith, M.A. and Robinson, T.J. (2003) ‘Reciprocal chromosome painting among human, aardvark, and elephant (superorder Afrotheria) reveals the likely eutherian ancestral karyotype’, *Proceedings of the National Academy of Sciences of the United States of America*, 100(3), pp. 1062–1066. Available at: <https://doi.org/10.1073/pnas.0335540100>.

Yanumula, A. and Cusick, J.K. (2020) *Biochemistry, Extrinsic Pathway of Apoptosis, StatPearls*. Available at: <https://www.ncbi.nlm.nih.gov/books/NBK560811/> (Accessed: 30 March 2022).

Yin, B. and Jiang, X. (2013) 'Telomere shortening in cultured human dermal fibroblasts is associated with acute photodamage induced by UVA irradiation', *Postepy Dermatologii i Alergologii*, 30(1), pp. 13–18. Available at: <https://doi.org/10.5114/pdia.2013.33374>.

Yousef, H., Alhajj, M. and Sharma, S. (2020) 'Anatomy, Skin (Integument), Epidermis - StatPearls - NCBI Bookshelf', *StatPearls Publishing, Treasure Island (FL)*, pp. 1–12. Available at: <https://www.ncbi.nlm.nih.gov/books/NBK470464/> (Accessed: 10 June 2022).

Zhang, W., Moore, L. and Ji, P. (2011) 'Mouse models for cancer research', *Chinese Journal of Cancer*, 30(3), pp. 149–152. Available at: <https://doi.org/10.5732/cjc.011.10047>.

Zhou, R., Si, J., Zhang, H., Wang, Z., Li, J., Zhou, X., Gan, L. and Liu, Y. (2014) 'The effects of x-ray radiation on the eye development of zebrafish', <http://dx.doi.org/10.1177/0960327114522278>, 33(10), pp. 1040–1050. Available at: <https://doi.org/10.1177/0960327114522278>.

Ziegler, U. and Groscurth, P. (2004) 'Morphological features of cell death', *News in Physiological Sciences*. American Physiological Society, pp. 124–128. Available at: <https://doi.org/10.1152/nips.01519.2004>.

Zilfou, J.T. and Lowe, S.W. (2009) 'Tumor suppressive functions of p53.', *Cold Spring Harbor perspectives in biology*. Available at: <https://doi.org/10.1101/cshperspect.a001883>.

Zorin, V., Zorina, A., Smetanina, N., Kopnin, P., Ozerov, I. V., Leonov, S., Isaev, A., Klovov, D. and Osipov, A.N. (2017) 'Diffuse colonies of human skin fibroblasts in relation to cellular senescence and proliferation', *Aging*, 9(5), pp. 1404–1413. Available at: <https://doi.org/10.18632/aging.101240>.

# APPENDIX

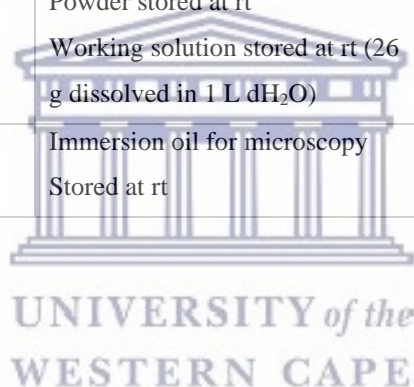
## Appendix I: Reagents and consumables for primary EDF cell culture.

Reagent/Consumable	Additional Information	Vendor
Thianil®	Dosage/body mass: 3 mg/1 000 kg Stored at room temperature (rt)	Wildlife Pharmaceuticals Pty LTD., Nelspruit, Mpumalanga, South Africa
Punch biopsy needles	Standard Store at rt	Supplied by the veterinarian
Eagle's Minimum Essential Medium (EMEM)	Contains Earle's Balanced Salt Solution and L-Glutamine Stored at 2 – 8°C	Lonza, Walkersville, Maryland, Delaware, United States of America (USA)
Fetal Bovine Serum (FBS) Gamma Irradiated	Heat-inactivated, sterile-filtered Stored at -20°C	Gibco™, Dun Laohaire, Dublin, Leinster, United Kingdom (UK)
Phosphate Buffered Saline (PBS)	Buffered saline solution Modified without calcium chloride (CaCl <sub>2</sub> ) and magnesium chloride (MgCl <sub>2</sub> ), liquid, sterile-filtered, suitable for cell culture Stored at 2 – 8°C	Gibco™, Dun Laohaire, Dublin, Leinster, UK
Trypsin Ethylenediaminetetraacetic acid (EDTA) solution 1×	0.12% trypsin, 0.02% EDTA Sterile filtered Working solution stored at 2 – 8°C Stock solution stored at -20°C	Lonza, Walkersville, Maryland, Delaware, USA
Penicillin/Streptomycin/Amphotericin B (P/S/A)	10 000 units penicillin/mL, 10 000 µg streptomycin/mL and 25 µg amphotericin B/mL in 0.85% saline Working solution stored at 2 – 8°C Stock solution stored at -20°C	Lonza, Walkersville, Maryland, Delaware, USA

Penicillin/Streptomycin (P/S)	10 000 units penicillin/mL and 10 000 µg streptomycin/mL in 0.85% saline Working solution stored at 2 – 8°C Stock solution stored at -20°C	Lonza, Walkersville, Maryland, Delaware, USA
Gentamicin reagent solution	50 mg/mL in distilled water Stored at rt	Gibco™, Grand Island, New York, USA
Ethanol (EtOH)	95% denatured	Labchem, Johannesburg, Gauteng, South Africa
T25/T75 Tissue cultured treated flasks	Sterilised by E-Beam Vent caps (with breathable 0.22 µm membrane) Non-Pyrogenic, deoxyribonuclease (DNase-)/ Ribonucleases (RNase-) free Stored at rt	Nest®, Biotechnology Co, Ltd, Wuxi, Jiangsu, China
15/50 mL Conical centrifuge tubes	Sterilised by E-Beam Non-Pyrogenic, DNase-/RNase- free Stored at rt	Nest®, Biotechnology Co, Ltd, Wuxi, Jiangsu, China
Scalpels and surgical blades	Size 11 scalpels, individually wrapped Sterilised by Gamma radiation (25 kGy) Stored at rt	Hi-Care International, Cape Town, Western Cape, South Africa
150 mm Glass Pasteur pipets	Autoclaved Stored at rt	Lasec®, Am Wollerspfad, Lauda-Koningshofen, Germany
100 mm Glass petri dishes	Autoclaved and reused Stored at rt	Pyrex®, Birmingham, England, UK
2-, 5-, 10- and 25 mL Serological pipets	Sterilised by E-beam Non-pyrogenic, non-cytotoxic and non-haemolytic DNase-/RNase- free Stored at rt	Nest®, Biotechnology Co, Ltd, Wuxi, Jiangsu, China
35 × 12 mm Petri dish	Tissue Culture Treated Polystyrene, DNase-/RNase- free, non-pyrogenic Stored at rt	Nest®, Biotechnology Co, Ltd, Wuxi, Jiangsu, China

Hydroxyurea (HU)	Molecular formula: NH <sub>2</sub> CONHOH Molecular Weight: 76.05 g/mol 98%, powder Powder stored at rt Stock solution stored at 2 – 8°C (200 mM: 0.15 g in 10 mL cEMEM (EMEM, 20% FBS and 1% P/S) Working solution of 2 mM: 20 uL/petri dish in 2 mL cEMEM	Sigma-Aldrich® Co, LLC, St.Louis, Missouri, USA
20 × 20 mm and 24 × 50 mm Glass coverslips	Autoclaved Stored at rt	Lasec®, Am Wollerspfad, Lauda-Koningshofen, Germany
Bouin's Solution	Contains formaldehyde Stored at rt	Sigma-Aldrich® Co, LLC, St.Louis, Missouri, USA
Mayer's Haematoxylin solution	Stored at rt	Sigma-Aldrich® Co, LLC, St.Louis, Missouri, USA
Eosin Y solution alcoholic	General purpose counterstains Stored at rt	Sigma-Aldrich® Co, LLC, St.Louis, Missouri, USA
Xylene	Molecular formula: C <sub>6</sub> H <sub>4</sub> (CH <sub>3</sub> ) <sub>2</sub> Molecular weight: 106.17 g/mol Histological grade Stored at rt	Sigma-Aldrich® Co, LLC, St.Louis, Missouri, USA
Glass slides	Microscopic use Stored at rt	Lasec®, Am Wollerspfad, Lauda-Koningshofen, Germany
DPX mountant for histology	Mixture of distyrene, a plasticizer and xylene Stored at rt	Kreatech Biotechnology, Villerweg, Amsterdam, Netherlands
KaryoMAX™ Colcemid™	Stock solution: 10 µg/mL in PBS. Working solution: 0.05 µg/mL Stored at 2 – 8 °C	Gibco™, Grand Island, New York, USA
Potassium Chloride (KCl)	Molecular formula: KCl Molecular Weight: 74,55 g/mol Powder stored at rt Working solution stored at 2 – 8°C (0.075 M: 5.6 g KCl powder was dissolved in 1 L dH <sub>2</sub> O)	Sigma-Aldrich® Co, LLC, St.Louis, Missouri, USA

Methanol	Molecular formula: CH <sub>3</sub> OH Molecular weight: 32.04 g/mol Stored at rt	Sigma-Aldrich® Co, LLC, St.Louis, Missouri, USA
Acetic acid solution	Molecular formula: CH <sub>3</sub> COOH Molecular weight: 60.05 g/mol Stored at rt	Sigma-Aldrich® Co, LLC, St.Louis, Missouri, USA
Giemsa's Azur Eosin Methylene Blue Solution	Protected from light Stored at rt	Gurr®, BDH chemicals LTD., Poole, UK
2-[4-(2-hydroxyethyl) piperazin-1-yl] ethanesulfonic acid (HEPES) Solution A	Molecular formula: C <sub>8</sub> H <sub>18</sub> N <sub>2</sub> O <sub>4</sub> S Molecular Weight: 238.30 g/mol Powder stored at rt Working solution stored at rt (23.83 g dissolved in 1 L dH <sub>2</sub> O)	Santa Cruz Biotechnology Inc., Dallas, Texas, USA
HEPES solution B	HEPES sodium salt Molecular formula: C <sub>8</sub> H <sub>17</sub> N <sub>2</sub> NaO <sub>4</sub> S Molecular Weight: 260.28 g/mol Powder stored at rt Working solution stored at rt (26 g dissolved in 1 L dH <sub>2</sub> O)	Santa Cruz Biotechnology Inc., Dallas, Texas, USA
Immersol™ 518 F	Immersion oil for microscopy Stored at rt	Carl Zeiss SMT GmbH, Roßdorf, Hessen, Germany



## Appendix II: Reagents and consumables for primary NHDF cell culture.

Reagent/Consumable	Additional Information	Vendor
Primary NHDF cell line (adult donor)	1 × cryovial with >500 000/1 mL Stored in liquid nitrogen	PromoCell®, Heidelberg, Baden-Württemberg, Germany
Fibroblast Growth Medium (FGM)	Basal medium Stored at 2 – 8°C	PromoCell®, Heidelberg, Baden-Württemberg, Germany
Supplement mix	0.02 mL/mL FBS, 1 ng/mL Basic fibroblast growth factor (recombinant human) and 5 µg/mL insulin (recombinant human) Stored at -20°C	PromoCell®, Heidelberg, Baden-Württemberg, Germany
Hanks Buffered Saline Solution (HBSS)	Balanced salt solution Contains no CaCl <sub>2</sub> , MgCl <sub>2</sub> with phenol red indicator, liquid, sterile-filtered, suitable for cell culture Stored at 2 – 8°C	Gibco™, Dun Laohaire, Dublin, UK
EtOH	≥99.8% Molecular formula: C <sub>2</sub> H <sub>6</sub> O Molecular weight: 46.07 g/mol Stored at rt	Carl Roth® GmbH & Co, Karlsruhe, Baden-Württemberg, Germany
DMSO	Molecular formula: C <sub>2</sub> H <sub>6</sub> OS Molecular weight: 78.13 g/mol Stored at rt	AppliChem GmbH, Darmstadt, Hessen, Germany
Trypsin EDTA solution 1×	0.05% trypsin, 0.02% EDTA in PBS Sterile filtered Working solution stored at 2 – 8°C Stock solution -20°C	PAN-Biotech GmbH, Aidenback, Bavaria, Germany
T12.5/T25/T75 Tissue culture treated flasks	Non-pyrogenic RNase-/ DNase- free Vented caps incorporate a 0.2 µm hydrophobic membrane for optimal gas exchange	Falcon®, Corning Incorporated, Corning, New York, USA
15/50 mL Conical centrifuge tubes	Sterile DNA-, DNase-/RNase-free Non-pyrogenic, non-cytotoxic	Sarstedt AG & Co. KG, Nümbrecht, North Rhine-Westphalia, Germany
2-, 5-, 10- and 25 mL Serological pipets	Sterile DNase-/RNase-free Non-pyrogenic	Costar®, Corning Incorporated, Corning, New York, USA

**Appendix III:** Reagents and consumables for biological assays at GSI for the NHDF cell line.

Reagent/Consumable	Additional Information	Vendor
Counting slides	Dual chamber for cell counter Stored at rt	Bio-Rad Laboratories, Inc, Hercules, California, USA
Trypan blue dye, 0.4% solution	Molecular formula: $C_{34}H_{24}N_6Na_4O_{14}S_4$ Molecular weight: 960.81 g/mol Stored at rt	Bio-Rad Laboratories, Inc, Hercules, California, USA
Roswell Park Memorial Institute (RPMI) 1640	RPMI Medium 1640 and GlutaMAX™ Stored at 2 – 8°C	Gibco™, Dun Laohaire, Dublin, Leinster, UK
P/S	10 000 units penicillin/mL and 10 mg/mL streptomycin/mL Working solution stored at 2 – 8°C and stock solution -20°C	Pan-Biotech GmbH, Aidenbach, Bavaria, Germany
Loeffler's methylene blue solution	For microscopy and cell payment Stored at rt	Carl Roth® GmbH & Co, Karlsruhe, Baden-Württemberg, Germany
Potassium Hydroxide (KOH)	Molecular formula: KOH Molecular weight: 56.11 g/mol Working solution: 0.1% (1 g KOH dissolved in 1 L dH <sub>2</sub> O) Stored at rt	Carl Roth® GmbH & Co, Karlsruhe, Baden-Württemberg, Germany
Methanol	Molecular formula: CH <sub>3</sub> OH Molecular weight: 32.04 g/mol Stored at rt	AppliChem GmbH, Darmstadt, Hessen, Germany
96-well Tissue culture plates	Growth-enhanced treated Sterilised by radiation Free from pyrogens DNA-/RNA-, DNase-/RNase-free	TPP® Techno Plastic Products AG, Trasadingen, Switzerland
Crystal violet	Molecular formula: C <sub>25</sub> H <sub>30</sub> ClN <sub>3</sub> Molecular weight: 407.99 g/mol Stored at rt Working solution: 0.1% crystal violet dye (1 g crystal violet powder + 50 mL EtOH, adjusted to final volume of 1 L in dH <sub>2</sub> O)	Merck KGaA, Darmstadt, Hessen, Germany



Glutaraldehyde solution 25% for synthesis	Molecular formula: C <sub>5</sub> H <sub>8</sub> O <sub>2</sub> Molecular weight: 100.12 g/mol Working solution: 1% (40 mL adjusted to final volume of 1 L in PBS) Stored at rt	AppliChem GmbH, Darmstadt, Hessen, Germany
Triton-X 100	Molecular formula: C <sub>33</sub> H <sub>60</sub> O <sub>10</sub> Molecular weight: 624.00 g/mol Working solution: 0.1% (1 mL adjusted to final volume of 1 L in PBS) Stored at rt	Carl Roth® GmbH & Co, Karlsruhe, Baden-Württemberg, Germany
3-[4,5-dimethylthiazol-2-yl]-5-[3-carboxymethoxyphenyl]-2-[4-sulfophenyl]-2H-tetrazolium (MTS) Assay Kit	MTS reagent in electron coupling solution Stored at -20°C	Abcam plc, Trumpington, Cambridge, UK
phycoerythrin (PE) Annexin V	Protect from light Stored at 2 – 8°C	BD Biosciences Pharmingen™, Basel, Allschwil, Switzerland
7-Amino-Actinomycin (7-AAD)	Protect from light Stored at 2 – 8°C	BD Biosciences Pharmingen™, Basel, Allschwil, Switzerland
HEPES for buffer solutions	Molecular formula: C <sub>8</sub> H <sub>18</sub> N <sub>2</sub> O <sub>4</sub> S Molecular weight: 238.31 g/mol Working solution: 0.1 M (pH7.4) Stored at rt	AppliChem GmbH, Darmstadt, Hessen, Germany
CaCl <sub>2</sub>	Molecular formula: CaCl <sub>2</sub> Molecular weight: 147.01 g/mol Working solution: 25 mM Stored at rt	Sigma-Aldrich® Co, LLC, St.Louis, Missouri, USA
Sodium Chloride (NaCl)	Molecular formula: NaCl Molecular weight: 58.44 g/mol Working solution: 1.4 M Stored at rt	Carl Roth® GmbH & Co, Karlsruhe, Baden-Württemberg, Germany
1.5 mL Eppendorf tubes	DNA-, DNase-/RNase-free Store at rt	Eppendorf®, Eppendorf, Hamburg, Germany
Ribonuclease A (RNase A)	100 000 U Stored at -20°C	Thermo Fisher Scientific, Graičiūno, Vilnius, Lithuania
Propidium iodide (PI)	10 mg/mL solution in water Protect from light Stored at 2 – 8°C	Invitrogen™, Thermo Fisher Scientific, Eugene, Oregon, USA

**Appendix IV:** Reagents and consumables for biological assays at NRF iThemba LABS for the EDF cell line.

Reagent/Consumable	Additional Information	Vendor
RPMI 1640	Contains L-Glutamine, with a phenol red indicator Stored at 2 – 8°C	Lonza, Walkersville, Maryland, Delaware, USA
Trypan blue dye, 0.4% solution	Molecular formula: $C_{34}H_{24}N_6Na_4O_{14}S_4$ Molecular weight: 960.81 g/mol Stored at rt	Gibco™, Dun Laohaire, Dublin, Leinster, UK
Loeffler's methylene blue solution	For microscopy and cell payment Stored at rt	Sigma-Aldrich® Co, LLC, St.Louis, Missouri, USA
KOH	Molecular formula: KOH Molecular weight: 56.1056 g/mol Working solution: 0.1% (1 g KOH dissolved in 1 L dH <sub>2</sub> O) Stored at rt	Sigma-Aldrich® Co, LLC, St.Louis, Missouri, USA
Methanol	Molecular formula: CH <sub>3</sub> OH Molecular weight: 32.04 g/mol Stored at rt	Sigma-Aldrich® Co, LLC, St.Louis, Missouri, USA
96-well Tissue culture plates	Growth-enhanced treated Sterilised by radiation Pyrogens-, DNA-/RNA- and DNase-/RNase-free Store at rt	Nest®, Biotechnology Co, Ltd, Wuxi, Jiangsu, China
MTS Assay Kit	MTS reagent in electron coupling solution Stored at -20°C	Biocom Africa (Pty) Ltd, Centurion, Gauteng, South Africa
Annexin V-FITC (fluorescein isothiocyanate)	Protect from light Stored at 2 – 8°C	BD Biosciences Pharmigen™, Basel, Allschwil, Switzerland
Fluorescence-activated single cell sorting (FACS) tubes	Polypropylene, non-pyrogenic Store at rt	SPL Life Sciences, Pocheon, Gyeonggi-do, South Korea
10× Annexin V Binding Buffer	Stock solution: 0.1 M HEPES (pH 7.4), 1.4 M NaCl and 25 mM CaCl <sub>2</sub> solution Working solution: 1× in dH <sub>2</sub> O Store at 2 – 8°C	BD Biosciences Pharmigen™, Basel, Allschwil, Switzerland

PI Solution	50 µg/mL Protect from light Stored at 2 – 8°C	BD Biosciences Pharmigen™, Basel, Allschwil, Switzerland
FxCycle™ PI/RNase Staining Solution	Protect from light Stored at rt	Invitrogen™, Thermo Fisher Scientific, Eugene, Oregon, USA



UNIVERSITY *of the*  
WESTERN CAPE



# ANNEXURE

---

**Annexure I:**

AREC of UWC ethical approval form, reference number AR21/6/4.

**Annexure II:**

DFFE standing permit, registration number: 02307 and permit number: S-65761.

**Annexure III:**

Section 20 granted by DALRRD formerly DAFF.

**Annexure IV:**

Botlierskop Private Game Reserves landowner permission letter.

**Annexure V:**

Sanbona Wildlife Reserve landowner permission letter.

**Annexure VI:**

Pathcare 16S ribosomal RNA gene PCR test.

**Annexure VII:**

Publication submission to Heliyon: Establishment of primary adult skin fibroblast cell lines from African savanna elephants (*L. africana*).



## Annexure I



UNIVERSITY of the  
WESTERN CAPE



03 September 2021

Dr F Rahiman  
Medical Biosciences  
Faculty of Natural Science

Ethics Reference Number: AR21/6/4

Protocol Title: *Tumour Suppression and Subdual of Cancer (TUSSC) in elephants: An in vitro study to shed light on Peto's Paradox*

Principal Investigator: F Rahiman

Approval Period: 31 August 2021 – 30 August 2024

Date of Approval by UWC Animal Research Ethics Committee: 31 August 2021

I hereby certify that the Animal Research Ethics Committee (AREC) of the University of the Western Cape (UWC) approved the ethics application of the above-mentioned protocol.

This approval is subject to the UWC Principal Investigator submitting a satisfactory annual progress report to the UWC AREC by 30 November each year for the duration of the protocol and subsequent approval of the annual progress report by the AREC. Following the completion of the protocol or termination of the study, a final report must be submitted to the UWC AREC no later than two months after completion. Annual progress and final reports must be submitted using form AREC (APR).

Any amendments, extensions or other modifications to the protocol must be submitted to the UWC AREC for review and approval, prior to initiating any amendments. Amendment requests must be submitted using form AREC (A).

The UWC AREC must be informed of any deviations from the approved protocol, unanticipated problems, serious incidents or adverse events, using form AREC (E).

The UWC Principal Investigator is responsible to ensure adherence to all applicable UWC Policies, UWC AREC requirements, as well as the regulatory framework of the protocol.

Any further requirements will be stipulated as an Addendum accompanying this letter.

All forms, policies, and guidelines are available from <https://uwcacza.sharepoint.com/sites/UWCIntranet> under Support Units, Office of Research & Development.

Prof TK Monsees, PhD  
Chairperson: Animal Research Ethics Committee (AREC)  
University of the Western Cape

NHREC Registration Number: AREC-130416-019

Director: Research Development  
University of the Western Cape  
Private Bag X 17  
Bellville 7535  
Republic of South Africa  
Tel: +27 21 959 4111  
Email: [research-ethics@uwc.ac.za](mailto:research-ethics@uwc.ac.za)

FROM HOPE TO ACTION THROUGH KNOWLEDGE.

**ADDENDUM: AR21/6/4**

The approval of this project is subject to special conditions set out hereunder:

- **NOTES:**
  - AREC only approve the animal tissue portion of the project
  - The application has to provide AREC with signed permission letters from the landowners prior to collection of samples.
  - Monthly reports be submitted to AREC. The permission letters from the landowners can be submitted via the monthly reports to the committee



UNIVERSITY *of the*  
WESTERN CAPE

*NHREC Registration Number: AREC-130416-019*

# Annexure II



## REGISTRATION CERTIFICATE

(Issued in terms of the provisions of the National Environmental Management: Biodiversity Act 2004, Act 10 of 2004)

CERTIFICATE NUMBER: **02307**

NAME OF ISSUING AUTHORITY	
NAME	DEPT OF ENVIROMENTAL AFFAIRS
ADDRESS	PRIVATE BAG X 447
ADDRESS	PRETORIA 0001
PROVINCE	NATIONAL DEPARTMENT

PROVINCIAL DEPARTMENT	NATIONAL DEPARTMENT
CAPTIVE BREEDING OPERATIONS	COMMERCIAL EXHIBITION EXHIBITION
GAME FARMS	NURSERIES
<input checked="" type="checkbox"/> SCIENTIFIC INSTITUTIONS	SANCTUARIES
REHABILITATION FACILITIES	WILDLIFE TRADERS
UNIQUE REGISTRATION NUMBER	<b>V369/EN019926</b>

DETAILS OF CERTIFICATE HOLDER	
NAME	National Research Foundation
SURNAME	C/o Charlot Vandevorcke
POSTAL ADDRESS	RESIDENTIAL ADDRESS
ADDRESS	No 8 Union Street
ADDRESS	Lochnerhof
ADDRESS	Strand
TOWN	
POSTAL CODE	7139
PROVINCE	Western Cape
PROPERTY WHERE OPERATION WILL BE CONDUCTED	
NAME AND SURNAME OF APPLICANT	National Research Foundation
NAME AND SURNAME OF AGENT	
PHYSICAL ADDRESS OF FACILITY	See attached annexure A
PHYSICAL ADDRESS OF FACILITY	
DISTRICT NAME	
PROVINCE	
REGISTERED NAME AND NUMBER (in the case of game farm)	

PARTICULARS OF SPECIES			
SPECIES		SEX	QUANTITY
COMMON NAME	SCIENTIFIC NAME	(if known)	
Specimens of all plant and animal species that are listed as threatened or protected in terms of the National Environmental Management Biodiversity Act no 10 of 2004.			

CERTIFICATE VALIDATION	
PERIOD OF VALIDITY	FROM: 22/04/2022 TO: 21-04-2025
RECEIPT NUMBER	
SIGNATURE ISSUING OFFICER	SIGNATURE CERTIFICATE HOLDER

DEPT. VAN OMGEWINGSAKE
DATE STAMP
PRETORIA / PRIVATE BAG X 447
2022-04-22
PRETORIA 0001
DEPT. OF ENVIROMENTAL AFFAIRS

## ANNEXURE A



## REGISTRATION CERTIFICATE

(Issued in terms of the provisions of the National Environmental Management: Biodiversity Act 2004, Act 10 of 2004)

Registration certificate no: 02307

NAME OF ISSUING AUTHORITY	
NAME	DEPARTMENT OF FORESTRY, FISHERIES AND THE ENVIRONMENT
ADDRESS	PRIVATE BAG X 447
	PRETORIA 0001
PROVINCE	NATIONAL DEPARTMENT

DETAILS OF SPECIES INVOLVED	
SCIENTIFIC NAME	COMMON NAME
Specimens of all plant and animal species that are listed as threatened or protected in terms of section 56 of the National Environmental Management: Biodiversity Act, 2004 (Act No 10 of 2004)	
DETAILS OF THE FACILITY FOR REGISTRATION CERTIFICATE	
1. National Research Foundation IThemba Laboratory Old Faure Road Eerste River Somerset West Western Cape Registration applies to: Scientific Institution	
SPECIAL CONDITIONS TO THE REGISTRATION CERTIFICATE:	
1. This registration certificate does not authorise the carrying out of any restricted activities. 2. This registration certificate applies only to the facility as indicated in this annexure A. 3. In the event that the certificate holder intends to operate a facility that is not authorised in terms of this registration the registration holder must therefore apply for registration of such facility. 4. This registration certificate applies only to the specimens referred to in this annexure A.	

PERMIT VALIDATION			
PERIOD OF VALIDITY	FROM	22-04-2022	TO: 21-04-2025
SIGNATURE OF ISSUING OFFICER		SIGNATURE PERMIT HOLDER	
DATE STAMP DEPT. VAN OMGEWINGSAKE PRIVAATSAK / PRIVATE BAG X 447 2022 -04- 22 PRETORIA 0001 DEPT. OF ENVIROMENTAL AFFAIRS			





**STANDING PERMIT**

(Issued in terms of the provisions of the National Environmental Management Biodiversity Act 2004, Act 10 of 2004)

**PERMIT NUMBER: S 65761**

NAME OF ISSUING AUTHORITY	
NAME	DEPT OF ENVIROMENTAL AFFAIRS
ADDRESS	PRIVATE BAG X 447
	PRETORIA 0001
PROVINCE	NATIONAL DEPARTMENT

PROVINCIAL DEPARTMENT	NATIONAL DEPARTMENT	
PROTECTED AREA MANAGEMENT AUTHORITY	VETERINARIAN	
REGISTERED CAPTIVE BREEDING OPERATION	REGISTERED SCIENTIFIC INSTITUTION	X
REGISTERED SANCTUARY	REGISTERED REHABILITATION FACILITY	
REGISTERED COMMERCIAL EXHIBITION FACILITY	REGISTERED GAME FARM	
REGISTERED WILDLIFE TRADER	REGISTERED NURSERY	
UNIQUE REGISTRATION NUMBER <b>N369/EN 019926</b>		

DETAILS OF HUNTER			
NAME	National Research Foundation		ID NO.
SURNAME	C/o Charlot Vanderhorde		PASSPORT NO. EN019926
	POSTAL ADDRESS	RESIDENTIAL ADDRESS	
ADDRESS	National Research Foundation	Nog Union Street	
ADDRESS	Ilumbo laboratories	Lochnerhof	
ADDRESS	Old Fourie Road	Strand	
TOWN	Essexia River, Somerset West		
POSTAL CODE	7100	7139	
PROVINCE	Western Cape	Western Cape	

PROPERTY WHERE RESTRICTED ACTIVITIES WILL BE CARRIED OUT	
NAME AND SURNAME OF APPLICANT	National Research Foundation
NAME AND SURNAME: RESPONSIBLE PERSON	Charlot Vanderhorde
NAME AND SURNAME OF AGENT	
PHYSICAL ADDRESS OF FACILITY	See attached annexure A
PHYSICAL ADDRESS OF FACILITY	
DISTRICT	
PROVINCE	
REGISTERED NAME AND NUMBER (in the case of game farm)	

DETAILS OF SPECIES INVOLVED					
COMMON NAME	SPECIES	SCIENTIFIC NAME	SEX (if known)	QUANTITY	MARKING (if applicable)
African elephant		Loxodonta africana	Males Females	22	

DETAILS OF RESTRICTED ACTIVITIES INVOLVED	
Collect, receive, transport and temporary possess	

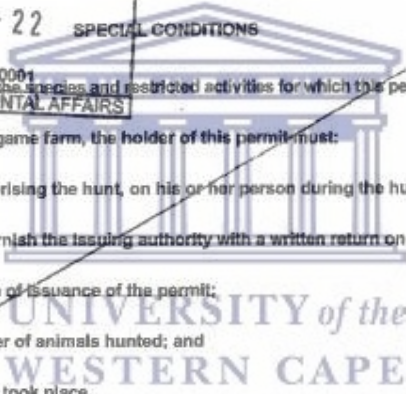
PERMIT VALIDATION		
PERIOD OF VALIDITY	FROM: 22-04-2022	TO: 21-04-2025
RECEIPT NUMBER		
SIGNATURE ISSUING OFFICER:	SIGNATURE PERMIT HOLDER:	
DATE STAMP:	2022-04-22	
	PRETORIA 0001	
	DEPT. OF ENVIROMENTAL AFFAIRS	



STANDING PERMIT CONDITIONS

1. This permit is not transferable.
2. Any unauthorised alteration to this permit shall render it invalid.
3. This permit is subject to the provisions of any applicable law in force during the period of validity of the permit.
- ~~4. This permit is valid only within the province where it was issued;~~
5. The holder of this permit shall, at the request of a person authorised in terms of applicable legislation so to demand, forthwith produce such permit to such person.
6. This permit shall be invalid until such time that it is signed by the permit holder.
7. This permit shall be deemed invalid when it is lost or destroyed and no copy thereof shall be issued.
8. This permit may be withdrawn by an authorised person if the execution of any activity may be detrimental to the welfare of any wild animal or the safety of any person, provided that the permit holder is given notice of such intention and be granted the opportunity to appeal to such withdrawal.
- ~~9. The prescribed fees paid for the issuing of this permit shall not be refunded.~~
10. If the holder of this permit contravenes or fails to comply with any permit condition or requirement to which this permit is subject, he or she shall be guilty of an offence.
11. This permit shall be subject to any applicable norms and standards in existence at the time of issuance of this permit.

DEPT. VAN OMGEWINGSAKE  
PRIVAATSAK / PRIVATE BAG X 447  
2022-04-22  
PRETORIA 0001  
DEPT. OF ENVIRONMENTAL AFFAIRS



1. The issuing authority shall determine the species and restricted activities for which this permit will apply.
2. If this permit applies to a registered game farm, the holder of this permit must:
  - a. Have a copy of this permit authorising the hunt, on his or her person during the hunt;
  - b. Within 21 days after the hunt, furnish the issuing authority with a written return on the hunt stating:
    - (i) the permit number and date of issuance of the permit;
    - (ii) the species, sex and number of animals hunted; and
    - (iii) the location where the hunt took place.
  - c. Return all used copies of the game farm hunting permits within 3 weeks after the end of the calendar year following the issuance of the game farm hunting permit, to the Issuing Authority.

05-03-2022  
05-03-2022



## ANNEXURE A



## STANDING PERMIT

(Issued in terms of the provisions of the National Environmental Management: Biodiversity Act 2004, Act 10 of 2004)

Permit number: S - 65761


Registration number: 02307

NAME OF ISSUING AUTHORITY	
NAME	DEPARTMENT OF FORESTRY FISHERIES AND THE ENVIRONMENT
ADDRESS	PRIVATE BAG X 447 PRETORIA 0001
PROVINCE	NATIONAL DEPARTMENT

DETAILS OF SPECIES INVOLVED				
COMMON NAME	SCIENTIFIC NAME	QUANTITY	SEX	DESCRIPTION
African Elephant	<i>Loxodonta africana</i>	32	Males and females	blood and skin biopsy samples
DETAILS OF RESTRICTED ACTIVITIES INVOLVED AND SPECIAL CONDITIONS				
<ol style="list-style-type: none"> <li>This permit authorizes the permit holder to collect, receive, transport and temporary possess specimens of species referred to in this annexure A for research purposes.</li> <li>This permit authorizes the permit holder to possess specimens of species referred to in this annexure A at the National Research Foundation IThaba Laboratory.</li> <li>This permit authorizes the permit holder to receive samples of specimens of species referred to in this annexure A <b>only</b> from a veterinarian that is in possession of a permit issued in terms of National Environmental Management: Biodiversity Act, 2004 (Act No. 10 of 2004) authorizing the collection and giving of such specimens.</li> <li>The permit holder must keep a register and record all restricted activities carried out involving specimens of species referred to in this annexure A.</li> <li>The register referred to in paragraph 4 must include the following information: <ul style="list-style-type: none"> <li>➤ Name and surname of the veterinarian who the specimens were received from.</li> <li>➤ Permit number of the veterinarian who the specimens were received from.</li> <li>➤ Details of the specimens collected/ received from the veterinarian. i.e. blood, tissue etc</li> <li>➤ Date of collection/ receiving.</li> <li>➤ Purpose for collection.</li> <li>➤ Destination where the sample were transported to.</li> </ul> </li> <li>The permit holder must make the register available to the Department of Forestry, Fisheries and the Environment (DFFE) upon request by the DFFE.</li> <li>The permit holder must submit a copy of the register referred to in paragraph 4 to the DFFE upon the expiry of this permit.</li> <li>The permit holder must obtain a letter of consent from the landowner before carrying out the restricted activities referred to in paragraph 1 in other people's property.</li> <li>The permit holder must submit a report to the DFFE on the findings after the research has been completed or</li> </ol>				

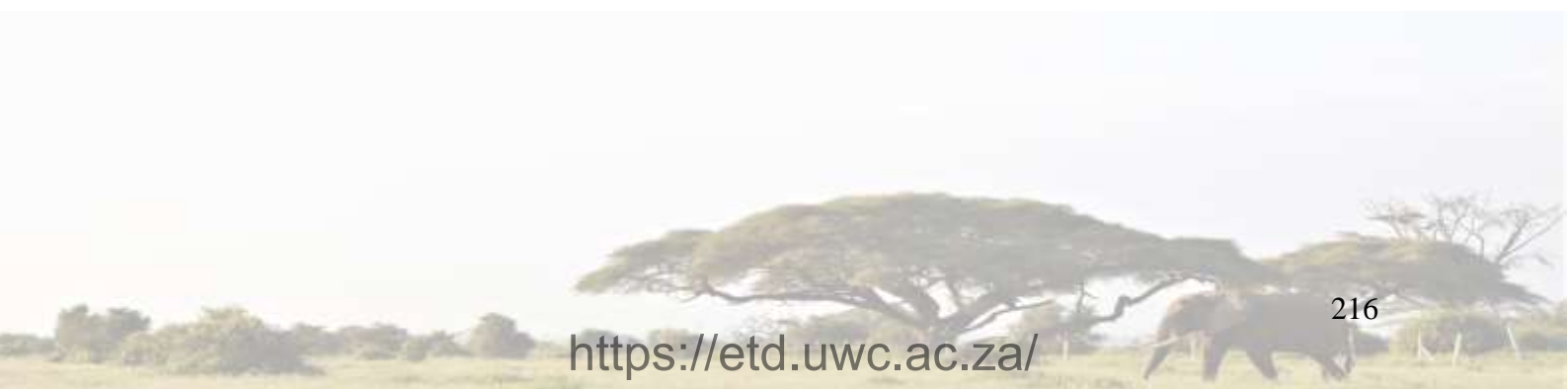
Permit number: S – 65761

- progress report upon expiry of this permit.
10. This permit does not absolve the permit holder to obtain additional import, export or re-export permits required in terms of the National Environmental Management: Biodiversity Act, 2004 (Act No.10 of 2004) or the Convention on International Trade in Endangered Species of Wild Fauna and Flora (CITES) for the specimens of species referred to in this annexure A.
  11. The permit holder must also obtain any permit that may be required in terms of any applicable legislation.

PERMIT VALIDATION								
PERIOD OF VALIDITY	FROM:	22 / 04 / 2022	TO: 21 - 04 - 2025					
								
SIGNATURE OF ISSUING OFFICER		SIGNATURE PERMIT HOLDER						
DATE STAMP:								
<table border="1"><tr><td>DEPT. VAN OMGEWINGSAKE</td></tr><tr><td>PRIVAATSAK / PRIVATE BAG X 447</td></tr><tr><td>2022 -04- 22</td></tr><tr><td>PRETORIA 0001</td></tr><tr><td>DEPT. OF ENVIROMENTAL AFFAIRS</td></tr></table>				DEPT. VAN OMGEWINGSAKE	PRIVAATSAK / PRIVATE BAG X 447	2022 -04- 22	PRETORIA 0001	DEPT. OF ENVIROMENTAL AFFAIRS
DEPT. VAN OMGEWINGSAKE								
PRIVAATSAK / PRIVATE BAG X 447								
2022 -04- 22								
PRETORIA 0001								
DEPT. OF ENVIROMENTAL AFFAIRS								



UNIVERSITY of the  
WESTERN CAPE



## Annexure III



### agriculture, land reform & rural development

Department:  
Agriculture, Land Reform and Rural Development  
REPUBLIC OF SOUTH AFRICA

Directorate Animal Health, Department of Agriculture, Land Reform and Rural Development  
Private Bag X250, Pretoria 0001  
Enquiries: Ms. Marna Laing · Tel: 012 319 7442 · Fax: +27 12 319 7470 E-mail:  
MarnaL@dalrrd.gov.za  
Reference: 12/11/1/7 (2412 SR)

Dr Charlot Vandevoorde  
University of the Western Cape

Robert Sobukwe Road  
Bellville  
Cape Town  
7535

E-mail: mengelbrecht@tlabs.ac.za

#### RE: PERMISSION TO DO RESEARCH IN TERMS OF SECTION 20 OF THE ANIMAL DISEASES ACT, 1984 (ACT NO. 35 OF 1984)

Dear Dr Charlot Vandevoorde

Your email received 22 April 2022, requesting permission under Section 20 of the Animal Disease Act, 1984 (Act No. 35 of 1984) to perform a research project or study, refers. I am pleased to inform you that permission is hereby granted to perform the following research/study, with the following conditions:

#### Conditions:

1. This permission does not relieve the researcher of any responsibility which may be placed on him by any other act of the Republic of South Africa;
2. The research project is approved as per the application form received 22 April 2022 and the correspondence thereafter. Written permission from the Director: Animal Health must be obtained prior to any deviation from the conditions approved for this research project under this Section 20 permit. Please apply in writing to MarnaL@dalrrd.gov.za;
3. All potentially infectious material utilised or collected during the study is to be destroyed at the completion of the study using the specified waste contractor (BCL Medical Waste Management Service).
4. Records must be kept for five years for audit purposes.
5. A dispensation application may be made to the Director Animal Health in the event that any of the above is to be stored or distributed;

6. Permission in terms of the Fertilizers, Farm Feeds, Agricultural Remedies and Stock Remedies Act, 1947 (Act No 36 of 1947) and/or the Medicines and Related Substances Control Act, 1965 (Act No 101 of 1965) may be needed prior to the start of the study;
7. Ethics approval must be obtained prior to the start of the study;
8. Samples may only be collected from African Elephants in the Botlierskop private game reserve and Sanbona wildlife reserve;
9. Only *in vitro* testing may be done during this study;
10. The following field samples may be collected from African Elephant: blood and skin biopsies;
11. Samples to be exported may only be exported if in full compliance with the importing conditions of the importing country;
12. If required, an application for an extension must be made by the responsible researcher at least one month prior to the expiry of this Section 20 permit. Please apply in writing to [MamaL@dalrrd.gov.za](mailto:MamaL@dalrrd.gov.za);
13. This Section 20 approval is valid until 31 August 2025.

**Title of research/study:** "Tumour Suppression and Subdual of Cancer (TUSSC) in elephants: An *in vitro* study to shed light on Peto's Paradox."

**Researcher (s):** Dr Farzana Rahiman and Dr Charlot Vandevoorde

**Institution:** University of the Western Cape

**Your Ref./ Project Number:** AR21/6/4

**Our ref Number:** 12/11/17 (2412 SR)

Kind regards,



**DR. MPHO MAJA**  
**DIRECTOR OF ANIMAL HEALTH**

**Date:** 2022-05-03



- 2 -

**SUBJECT:** RE: Permission to do research in terms of Section 20 of the ANIMAL DISEASES ACT, 1984 (ACT NO. 35 of 1984)

## Annexure IV



**Ref: Landowner permission letter for elephant research project**

Dear Dr Burger and research team,

With this letter we would like to express Botlierskop's support for the project on "Tumor Suppression and Subdual of Cancer (TUSSC) in elephants: An in vitro study to shed let on Peto's Paradox".

Botlierskop Private Game Reserve welcomes this new collaboration and approves the collection of blood and skin tissue samples from our elephants by Dr Willem Burger in the framework of this interesting research project. We are of the opinion that this is a project unique to Southern Africa, that brings together the expertise of different people and has the potential to discover novel mechanisms that could be used to prevent cancer development as well as improve existing cancer treatment strategies in humans. We are pleased to be able to contribute to this project and it fits well in the spirit of our African Wildlife Conservation Foundation.

We would like to express our commitment to this project once ethics approval has been obtained. The male elephants on our premises have to be darted and immobilized two times per year by Dr Willem Burger in order reduce their testosterone levels via vaccination. Without this control, the mature bulls could cause problems and might react aggressive to human approach. This presents an ideal opportunity to collect samples for this project.

Please do not hesitate to contact us if you require any further information.

Sincerely,

A handwritten signature in black ink, appearing to read "Mnr T. A. Neethling".

Mnr T. A. Neethling

**Owner/Director Botlierskop  
Private Game Reserve  
083 3799949**

A handwritten signature in black ink, appearing to read "Dr W. Burger".

Dr W. Burger

**AWCF Founder/Wildlife Vet**

**082 5705710**

## Annexure V



**Ref: Landowner permission letter for elephant research project**

Dear Dr Burger and research team,

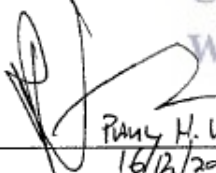
With this letter we would like to express Sanbona's support for the project on "Tumour Suppression and Subdual of Cancer (TUSSC) in elephants: An In vitro Study to shed light on Peto's Paradox".

Sanbona Wildlife Reserve welcomes this new collaboration and approves the collection of blood and skin samples from our elephants by Dr Willem Burger in the framework of his interesting research project. We are of the opinion that this is a project unique to Southern Africa that brings together the expertise of different people and has the potential to discover novel mechanisms that could be used to prevent cancer development as well as improve existing cancer treatment strategies in humans. We are pleased to be able to contribute to this project.

The elephants on our premises have to be darted and immobilized by Dr Willem Burger in order to place a new collar on the elephant to trace the elephant herd. This presents an ideal opportunity to collect samples for this project.

Please do not hesitate to contact us if you require any future information.

Sincerely,

X   
PAUL H. VORSTER  
16/12/2021  
Legal representative Sanbona Wildlife Reserve

UNIVERSITY of the  
WESTERN CAPE

X   
Dr W. Burger  
AWCF Founder/Responsible Wildlife Veterinarian



# Annexure VI

## Final Report

Drs Izak Loftus and Linda Steyn  
 MEDICLINIC VERGELEGEN  
 Somerset West  
 Tel: 021 852 3144



Practice No:5200539

**Report to:**  
 ITHEMBA LABS - RADIOBIOLOGY  
 ATT: DR MONIQUE ENGELBRECHT  
 OLD FAURE RD  
 7130 FAURE SOMERSET WEST

**Referred by:** ITHEMBA LABS - RADIOBIOLOGY

**Requisition No:** 678108213  
**Specimen No:** 0223:PA02976R  
**Collection Date:** 23-02-2022 UNK  
**Received Date:** 2022-02-23 17:54  
**Reported Date:** 2022-02-28 14:18

**Patient:**  
**N/A CP.EDF-P11**  
**Patient ID No:** N/A  
**Age:Sex:DoB:** U  
**Contact No:** N/A

**Guarantor:**  
 ITHEMBA LABS - RADIOBIOLOGY  
**Contact No:** U

**Clinical Data:** Please note that the collection date or time was not provided and could not be verified by PathCare.  
 TWO NEGATIVE CONTROLS : (1) NEGATIVE CONTROL (NC) PBS AND  
 (2) NEGATIVE CONTROL (NC) COMPLETE CULTURE MEDIA

**Tests requested:** PCR 16s rRNA

P.C.R. Department			
Test Name	Result	Flag	Reference Range
16s rRNA PCR			
SPECIMEN SOURCE	Cultured Cells		
DNA AMPLIFICATION	NOT DETECTED		
BACTERIA ID	No bacterial DNA (including Mycoplasma sp.) was detected in this culture specimen.		

Authorised on 2022-02-28 13:52:00

For consultation, contact a Clinical Pathologist - +27 21 596 3400

H=High, L=Low, H=Critically High, L=Critically Low

File [ ] Phone Patient [ ] Appointment [ ] Prescription [ ] Draw File [ ]

UNIVERSITY of the WESTERN CAPE

## Annexure VII

-----Original Message-----

From: em.heliyon.0.7ef018.60d33205@editorialmanager.com <em.heliyon.0.7ef018.60d33205@editorialmanager.com> On Behalf Of Heliyon  
Sent: Wednesday, October 26, 2022 5:30 PM  
To: Vandevorde, Charlot <C.Vandevorde@gsi.de>  
Subject: Confirming submission to Heliyon

CC: "Bolcaen Julie" jbolcaen@tlabs.ac.za, "Engelbrecht Monique" mengelbrecht@tlabs.ac.za, "Jansen van Vuuren Amèlia" ameliavv.1@gmail.com, "Miles Xanthene" xmuller@tlabs.ac.za, "Nair Shankari" snair@tlabs.ac.za, "Fisher Randall" rfisher@tlabs.ac.za, "Tinganelli Walter" w.tinganelli@gsi.de, "Burger Willem" willem@willemburger.co.za, "Farzana Rahiman" frahiman@uwc.ac.za, "Durante Marco" m.durante@gsi.de, "De Kock Maryna" mdekock@uwc.ac.za, "Martinez Lopez Wilner" wilnermartinezlopez@gmail.com

\*This is an automated message.\*

Establishment of primary adult skin fibroblast cell lines from African savanna elephants (*Loxodonta africana*)

Dear Dr Vandevorde,

We have received the above referenced manuscript you submitted to the Life Sciences section of Heliyon. It has been assigned the manuscript number HELIYON-D-22-26335. To track the status of your manuscript, please log in as an author at <https://www.editorialmanager.com/heliyon/>, and navigate to the "Submissions Being Processed" folder.

Thank you in advance for your understanding, and best wishes for the holiday season.

Kind regards,  
Heliyon

More information and support

You will find information relevant for you as an author on Elsevier's Author Hub: <https://www.elsevier.com/authors>

FAQ: How can I reset a forgotten password?

[https://service.elsevier.com/app/answers/detail/a\\_id/28452/supporthub/publishing/](https://service.elsevier.com/app/answers/detail/a_id/28452/supporthub/publishing/)

For further assistance, please visit our customer service site: <https://service.elsevier.com/app/home/supporthub/publishing/>

Here you can search for solutions on a range of topics, find answers to frequently asked questions, and learn more about Editorial Manager via interactive tutorials. You can also talk 24/7 to our customer support team by phone and 24/7 by live chat and email

#AU\_HELIYON#

To ensure this email reaches the intended recipient, please do not delete the above code

In compliance with data protection regulations, you may request that we remove your personal registration details at any time. (Use the following URL: <https://www.editorialmanager.com/heliyon/login.asp?a=r>). Please contact the publication office if you have any questions.



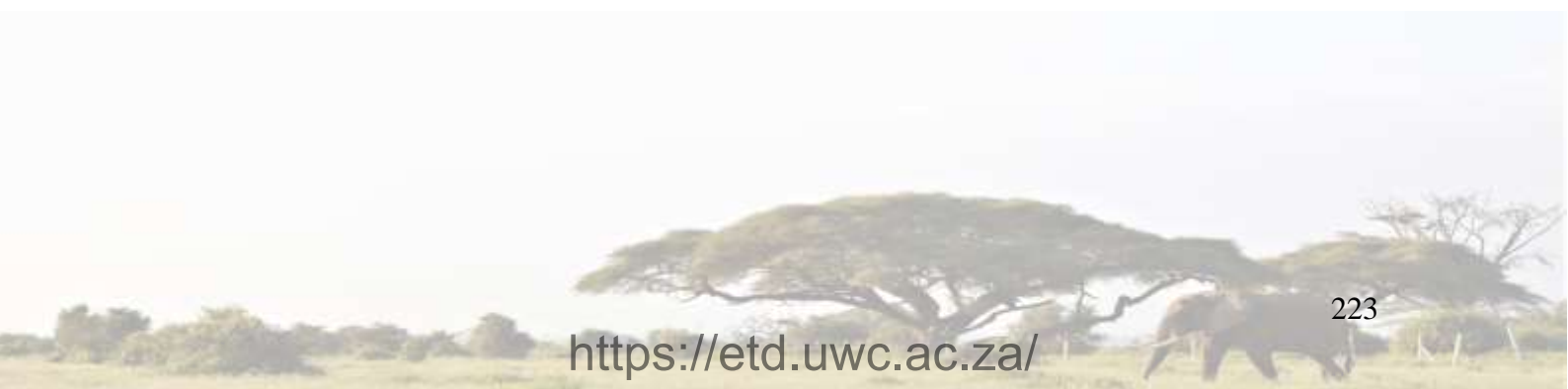
UNIVERSITY of the  
WESTERN CAPE

## Heliyon

### Establishment of primary adult skin fibroblast cell lines from African savanna elephants (*Loxodonta africana*) --Manuscript Draft--

<b>Manuscript Number:</b>	HELIYON-D-22-26335
<b>Article Type:</b>	Protocol
<b>Section/Category:</b>	Life Sciences
<b>Keywords:</b>	African elephant; <i>Loxodonta africana</i> ; dermal fibroblast; primary cell line; metaphase; skin punch biopsy; explant culture; Peto's paradox
<b>Manuscript Classifications:</b>	80.100: Animal Science; 90.120.160: Wildlife Ecology; 90.230.120: Nature Conservation; 110.110.100: Cell Culture; 110.130: Evolutionary Biology; 110.140.140: Biodiversity; 110.290: Cancer Research; 110.350: Zoology; 130.360: Oncology
<b>Corresponding Author:</b>	Charlot Vandevoorde, PhD GSI Helmholtz Centre for Heavy Ion Research GmbH Darmstadt, GERMANY
<b>First Author:</b>	Bolcaen Julie
<b>Order of Authors:</b>	Bolcaen Julie Engelbrecht Monique Jansen van Vuuren Amélia Miles Xanthene Nair Shankari Fisher Randall Tinganelli Walter Burger Willem Farzana Rahiman Durante Marco De Kock Maryna Martinez Lopez Winer Charlot Vandevoorde, PhD
<b>Abstract:</b>	<p>Following population declines of the African savanna elephant (<i>Loxodonta africana</i>) across the African continent, the establishment of primary cell lines of this endangered wildlife species can be paramount for the preservation of their genetic resources and studies on their cancer suppression mechanisms. The low cancer incidence in elephants was previously described as Peto's paradox and more recently linked to a redundancy of tumor suppressor genes TP53. However, the exact working mechanisms of the TP53 retrogenes remain unclear and elephants might have developed additional adaptations to balance enhanced p53-mediated apoptosis against the increasing need for cell replacement, which could result in premature stem cell exhaustion.</p> <p>The methodology presented here, described a technique to establish primary dermal fibroblast cell lines from elephant skin punch biopsy samples. The applied tissue collection technique is minimally invasive and paves the way for future remote biopsy darting of more elusive elephant populations. On average, the first explant outgrowth was observed after <math>15.75 \pm 6.30</math> days and a mean doubling time of <math>62.13 \pm 7.00</math> hours was calculated. Metaphase spreads were obtained, confirming the diploid number of 56 chromosomes, which opens the scope for future cytogenetic studies.</p> <p>The successful establishment of elephant dermal fibroblast cell lines allows future studies on the molecular mechanisms of cancer resistance in this species, which could be harnessed for cancer prevention and treatment in humans.</p>

*Powered by Editorial Manager® and ProduXion Manager® from Arles Systems Corporation*



<b>Suggested Reviewers:</b>	<p>Alexsandra Fernandes alexandra.pereira@ufersa.edu.br Corresponding author of two methodology papers on the establishment of skin-derived fibroblast cells from endangered species.</p> <p>Dino J Martins dmartins@princeton.edu Evolutionary biologist affiliated with Princeton University and also director of Mpala Research Centre which undertakes valuable work on elephant conservation. We believe he will be able to provide a good perspective on the value of the elephant dermal fibroblast cell lines for research and conservation purposes.</p> <p>Andrei Seluanov andrei.seluanov@rochester.edu Published a wide range of papers on cancer suppression mechanisms in long-lived mammals. Expert in the field of Peto's paradox.</p>
<b>Opposed Reviewers:</b>	



UNIVERSITY *of the*  
WESTERN CAPE

*Powered by Editorial Manager® and ProduXion Manager® from Aries Systems Corporation*



26 October 2022

Dear Editor in Chief,

We present our methodology manuscript "*Establishment of primary adult skin fibroblasts from African elephants (*Loxodonta africana*)*" for your consideration and evaluation for publication in the journal Heliyon. This submission is part of a manuscript transfer process that was suggested by Dr Zearfoss from Cell Reports Methods. Based on the author guidelines of Cell Reports Methods, the STAR Methods guidelines were applied in our manuscript. However, based on the recommendation of the Heliyon editorial office, this can be adjusted.

There have been a number of recent methodology papers on the establishment of primary dermal fibroblast cell lines from endangered wildlife species (Silva et al. – 2021; Wang et al. – 2021; Jenuit et al. – 2021), illustrating the value and necessity to obtain this material for species and biodiversity conservation. However, most of these techniques are based on skin biopsy samples obtained from post-mortem or captive animals. For elephants specifically, there is one previously published protocol which makes use of relatively large ear biopsy samples ( $3 \times 3 \text{ cm}^2$  pieces) from Asian elephant carcasses (Siengdee et al. – 2018). While this protocol is very valuable, we were looking for a technique in which we could use minimally invasive punch skin biopsy samples from free-roaming African savanna elephants, resulting in the methodology we are presenting in this manuscript.

The motivation for our study was twofold. Firstly, the isolation and establishment of primary dermal fibroblast cell lines from African savanna elephants allows the acquisition of large amounts of cells that have conserved most of their original characteristics, making them extremely valuable for biobanking and conservation efforts. Secondly, the elephant cell lines are also of high interest to further unravel the cancer suppression mechanisms of elephants (Abegglen et al. – 2015; Tollis et al. – 2017; Sulak et al. – 2018). The observation that cancer incidence in large long-living mammals, such as elephants and whales, does not correlate with species body size is known as Peto's Paradox (Peto et al. – 1975). In elephants, the answer to this paradox lies, at least in part, in the redundancy of Tumor Protein p53 (TP53) and the more recently discovered copies of leukemia inhibitory factor (LIF) (Abegglen et al. – 2015; Sulak et al. – 2018; Gaughan et al. – 2016; Vazquez et al. – 2018). This suggests that the cancer defence of elephants is mediated by an enhanced apoptotic response to DNA damage, in order to kill potentially cancerous cells at an early stage. However, it still remains unclear how elephants balance the enhanced apoptosis response with the increasing need for cell replacement, which could lead to premature aging. The primary elephant dermal fibroblast cell lines that have been established in this study, can assist the research community to further unravel how evolution has fine-tuned the elephant genome.

Next to the methodology, the manuscript aims to illustrate the broad range of research perspectives these cell lines can bring, which we believe are of interest to the all-science multi-disciplinary readership of Heliyon. In order to translate the underlying mechanisms of Peto's Paradox to new strategies to improve cancer prevention and treatment in humans, a close collaboration will be required between multiple disciplines ranging from biomimetics, conservation, evolutionary biology and genetics, to cancer research.



---

Lastly, we would like to confirm that the manuscript has not been published, nor is it currently under consideration for publication elsewhere. There has been a prior submission to the journal Cell Reports Methods, resulting in an article transfer process to this journal.

Thank you for considering our methodology paper for publication in Heliyon.

Yours sincerely,

Charlot Vandevoorde, PhD

Lead author

---

Group Leader Space Radiobiology

Biophysics Department

Phone: +49 6159 71 3478

Email: C.Vandevoorde@gsi.de

GSI Helmholtzzentrum für Schwerionenforschung GmbH

Planckstraße 1

64291 Darmstadt - Germany

[www.gsi.de/biophysik](http://www.gsi.de/biophysik)



UNIVERSITY *of the*  
WESTERN CAPE



## Establishment of primary adult skin fibroblast cell lines from African savanna elephants (*Loxodonta africana*)

Bolcaen Julie<sup>1</sup>, Engelbrecht Monique<sup>1</sup>, Jansen van Vuuren Amélia<sup>2</sup>, Miles Xanthene<sup>1</sup>, Nair Shankari<sup>1</sup>, Fisher Randall<sup>1</sup>, Tinganelli Walter<sup>3</sup>, Burger Willem<sup>4</sup>, Durante Marco<sup>3,5</sup>, Rahiman Farzana<sup>2</sup>, De Kock Maryna<sup>2</sup>, Martinez Lopez Wilner<sup>6</sup>, Vandevoorde Charlot<sup>3\*</sup>

<sup>1</sup> SSC Laboratory, Radiation Biophysics Division, NRF-iThemba LABS, Cape Town, Western Cape, South Africa

<sup>2</sup> Faculty of Natural Sciences, Department of Medical Biosciences, University of the Western Cape, Cape Town, Western Cape, South Africa

<sup>3</sup> Biophysics Department, GSI Helmholtzzentrum für Schwerionenforschung, Darmstadt, Hesse, Germany

<sup>4</sup> Dr Willem Burger Consulting, Mossel Bay, Western Cape, South Africa

<sup>5</sup> Institut für Physik Kondensierter Materie, Technische Universität (TU) Darmstadt, , Darmstadt, Hesse, Germany

<sup>6</sup> Genetics Department and Biodosimetry Service. Instituto de Investigaciones Biológicas Clemente Estable. Montevideo, Uruguay

\* Corresponding author: [c.vandevoorde@gsi.de](mailto:c.vandevoorde@gsi.de)

**Abstract:** Following population declines of the African savanna elephant (*Loxodonta africana*) across the African continent, the establishment of primary cell lines of this endangered wildlife species can be paramount for the preservation of their genetic resources and studies on their cancer suppression mechanisms. The low cancer incidence in elephants was previously described as Peto's paradox and more recently linked to a redundancy of tumor suppressor genes TP53. However, the exact working mechanisms of the TP53 retrogenes remain unclear and elephants might have developed additional adaptations to balance enhanced p53-mediated apoptosis against the increasing need for cell replacement, which could result in premature stem cell exhaustion.

The methodology presented here, described a technique to establish primary dermal fibroblast cell lines from elephant skin punch biopsy samples. The applied tissue collection technique is minimally invasive and paves the way for future remote biopsy darting of more elusive elephant populations. On average, the first explant outgrowth was observed after  $15.75 \pm 6.30$  days and a mean doubling time of  $62.13 \pm 7.00$  hours was calculated. Metaphase spreads were obtained, confirming the diploid number of 56 chromosomes, which opens the scope for future cytogenetic studies.

The successful establishment of elephant dermal fibroblast cell lines allows future studies on the molecular mechanisms of cancer resistance in this species, which could be harnessed for cancer prevention and treatment in humans.

**Keywords:** African elephant, *Loxodonta africana*, dermal fibroblast, primary cell line, metaphase, skin punch biopsy, explant culture, Peto's paradox

### 1. Introduction

The elephant population continues to decline across the African continent due to poaching, disease susceptibility, habitat loss and threats related to climate change<sup>1</sup>. As a result, all species of elephants

1  
2  
3  
4  
5  
6  
7  
8  
9  
10  
11  
12  
13  
14  
15  
16  
17  
18  
19  
20  
21  
22  
23  
24  
25  
26  
27  
28  
29  
30  
31  
32  
33  
34  
35  
36  
37  
38  
39  
40  
41  
42  
43  
44  
45  
46  
47  
48  
49  
50  
51  
52  
53  
54  
55  
56  
57  
58  
59  
60  
61  
62  
63  
64  
65

are currently listed as critically endangered, with the African forest elephant even as critically endangered on the International Union for Conservation of Nature (IUCN) red list of threatened species<sup>2-4</sup>. Cryopreserved biomaterial and biobanks might have a promising value to conserve the genetic material of elephants for future research and conservation efforts<sup>5-8</sup>. Projects like the 'Frozen Zoo' and 'Frozen Ark' have been launched internationally with the goal to safeguard the genetic resources of threatened, rare and elusive animal species for the next generations<sup>9</sup>. Hence, the establishment of primary elephant dermal fibroblast (EDF) cell lines would allow the acquisition of large amounts of cells which conserved most of their original characteristics for functional and genetic analyses<sup>10</sup>. Primary fibroblast cell lines have previously been established from several endangered animal species in captivity such as collared peccaries<sup>11</sup>, jaguars<sup>12</sup>, a wild corsac fox<sup>13</sup>, as well as from fresh carcasses of a common hippopotamus calf<sup>14</sup>, a Chinese muntjac<sup>15</sup>, a Sumatran rhinoceros<sup>16</sup> and Asian elephants<sup>17</sup>, to name a few examples. The establishment of these somatic cell lines is considered to be a valuable resource for modern somatic cell nucleus transfer as part of biodiversity conservation<sup>10,18,19</sup>.

In addition to wildlife conservation, a primary elephant cell line is also of high interest to the cancer research community since elephants appear to have developed cancer suppression mechanisms throughout their evolution<sup>20-23</sup>. The African elephant is the largest land mammal with a body mass up to 7 000 kg and longevity of up to 60 years in the wild. A simplified multi-stage model of carcinogenesis is based on the old observations that the age-specific incidence of cancer was consistent with the stepwise accumulation of 6 to 7 mutational 'hits' within a cell<sup>24,25</sup>. However, if cancers are initiated by a series of somatic mutations, species with a larger body size (more cells) and longer lifespans (more lifetime cell division) should have cancer incidences that are order of magnitude greater than smaller species<sup>26,27</sup>. The observation that cancer incidence in large long-living mammals, such as elephants and whales, does not correlate with species body size and longevity was first described in 1975 by epidemiologist and statistician Richard Peto and is known as Peto's Paradox<sup>28</sup>. This suggests that elephants have evolved enhanced cancer suppression mechanisms in order to offset the trade-off associated with their large bodies and long lifespan.

Several recent studies investigated the genetic mechanisms responsible for cancer suppression in elephants, leading to the discovery of multiple copies of the tumor suppressor genes TP53 (19 extra copies of TP53 retrogenes) and 11 extra copies of leukemia inhibitory factor (LIF)<sup>20,21,29,30</sup>. Particularly TP53 is a well-known tumor suppressor gene, mutated in approximately 50% of human cancers, and often referred to as the "guardian of the genome"<sup>31</sup>. This suggests that the cancer defense of elephants is mediated by an enhanced apoptotic response to DNA damage, in order to kill potentially cancerous cells at an early stage<sup>23,32,33</sup>. However, this enhanced apoptotic response in elephants needs to be balanced by other adaptations to prevent stem cell exhaustion due to the increasing need for cell replacement, which could lead to premature aging, as confirmed in a study on mutant mice with





1  
2  
3  
4  
5  
6  
7  
8  
9  
10  
11  
12  
13  
14  
15  
16  
17  
18  
19  
20  
21  
22  
23  
24  
25  
26  
27  
28  
29  
30  
31  
32  
33  
34  
35  
36  
37  
38  
39  
40  
41  
42  
43  
44  
45  
46  
47  
48  
49  
50  
51  
52  
53  
54  
55  
56  
57  
58  
59  
60  
61  
62  
63  
64

increased p53 activity<sup>34</sup>. To the best of our knowledge, no primary nor immortalized commercial elephant cell line is currently available and the successful establishment of *in vitro* primary EDF cell lines would allow a broad range of scientists to further unravel the mechanisms of cancer resistance in elephants.

This methodology describes the first collection, establishment, and cryopreservation of a primary EDF cell line of African savanna elephants (*Loxodonta africana*). In addition, we describe a method to obtain metaphase spreads from the primary EDF cultures to enable future cytogenetic studies. In contrast to previous protocols where primary fibroblast cell lines were established from relatively large pieces of skin of captive animals or postmortem samples, this protocol starts from a small skin punch biopsy sample (3 - 4 mm) from free-roaming elephants. This biopsy technique allows remote biopsy darting, a technique which eliminates the need for sedation and causes minimal harm to the animal<sup>35</sup>. It provides the opportunity to collect skin tissue samples from a variety of free-ranging terrestrial animals, including the elusive African forest elephant. Thus, this method can lay the foundation for future research in a broad range of research fields, including biomimetic, conservation and evolutionary biology, as well as oncology.

## 2. Results

### Establishment of primary elephant dermal fibroblast cell lines

Skin punch biopsy samples were collected with a punch biopsy needle behind the ear, where the corium and epidermis are the thinnest<sup>36</sup>, of five adult elephants (E1 - E5) on different days (Table 1). The samples were transported on ice (0 - 4°C) in transport media (STAR Methods) to prevent dehydration and contamination (Figure 1A-D) and processed within 24 hours upon arrival in the laboratory. Since the samples were not taken under sterile conditions, the skin biopsy sample was washed thrice with washing PBS containing antibiotics (STAR Methods; Key Resource Table) (Figure 1E). Two scalpels were used to remove the epidermis and cut the biopsies in smaller fragments (Figure 1F). A few drops of culturing media (STAR Methods; Key Resource Table) were added to prevent dehydration and the small tissue fragments were transferred to a T25 tissue culture treated flask using a sterile glass Pasteur pipet (Figure 1G). To prevent floating of the tissue fragments, 0.5 mL Fetal Bovine Serum (FBS) was added and the flask were incubated under standard conditions (STAR Methods). After 24 hours, the flasks were placed upside down for the following 24 hours and 1 mL of initial culturing media was added on day three.

**Table 1. Overview of elephant samples.** Information on the African savanna elephants (*Loxodonta Africana*) such gender, age and location of the sample collection at two different wildlife reserves in South Africa. In addition, more results on the individual cultures are listed, such as the days until the first explant outgrowth was visible and the number of successful outgrowths per biopsy sample.

Code name elephants	Gender (Male/Female)	Age	Days until first EDF outgrowth	Success rate (successful outgrowth /n biopsies)	Location of sample collection
E1	M	25	9	4/5	Botlierskop Game Reserve
E2	M	14	/	0/5	Botlierskop Game Reserve
E3	F	35	18	4/5	Sanbona Wildlife Reserve
E4	M	25	25	2/6	Sanbona Wildlife Reserve
E5	M	26	11	2/6	Botlierskop Game Reserve



**Figure 1: Skin punch biopsy procedure and biopsy preparation.** A - B) The skin behind the ear of the elephant was cleaned with 70% ethanol. C) The punch biopsy area was surgically draped and a punch biopsy needle was used to collect the sample. D) Punch biopsies were collected and transferred in tubes containing transport media. E) In the laboratory, the biopsies were washed thrice with washing PBS and transferred to a sterile glass petri-dish. F) Two scalpels were used to remove the epidermis and cut the biopsies into small tissue fragments. G) The tissue fragments were transferred to a T25 tissue culture treated flask using a sterile Pasteur pipet and 0.5 mL FBS was added.

#### Explant culture outgrowth and cell characteristics

The first outgrowth of fibroblast cells around the explant pieces was visible as early as day 9 (Figure 2A), but varied between individuals. Overall, the first outgrowth appeared within the first 9 - 25 days of culture ( $15.75 \pm 6.30$  days, mean  $\pm$  SD) (Table 1). Explant cultures of 4 out of the 5 elephants exhibited outgrowth, resulting in a success rate of 80.00%. However, not all skin punch biopsies of the same individual resulted in successful cultures. While 4 out of the 5 biopsies presented outgrowth for E1 and E3, only 2 out of the 6 biopsies for E4 and E5 were successful. No fibroblast outgrowth was observed in any of the E2 biopsy samples and culture flasks were discarded after 40 days. The outgrowth

1  
2  
3  
4  
5  
6  
7  
8  
9  
10  
11  
12  
13  
14  
15  
16  
17  
18  
19  
20  
21  
22  
23  
24  
25  
26  
27  
28  
29  
30  
31  
32  
33  
34  
35  
36  
37  
38  
39  
40  
41  
42  
43  
44  
45  
46  
47  
48  
49  
50  
51  
52  
53  
54  
55  
56  
57  
58  
59  
60  
61  
62  
63

of cells from the explant source resulted initially in a dense area with high cell numbers, which gradually migrated and spread outward over time.

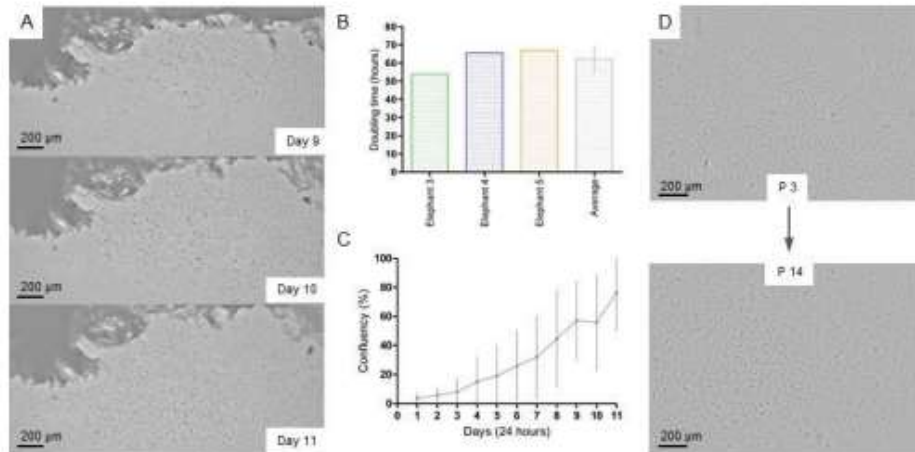


**Figure 2: The characteristic outgrowth of the primary EDF cells from tissue explants. A)** The radial outgrowth of EDFs from a biopsy fragment of E1 on day 9, 10, and 11. **B)** The average doubling time of EDFs obtained from E3, E4, and E5 was  $62.13 \pm 7.00$  hours (mean  $\pm$  SD). **C)** A growth curve was plotted (normalized mean  $\pm$  SD calculated within six regions of a T25 flask) of E3, E4 and E5 based on the % confluency over 11 consecutive days. **D)** The morphology of the EDFs appeared to be normal throughout passage 3 up to 14 with elongated, disc-like structures. All images are captured with a live cell imaging system (Cytosmart, Lonza<sup>®</sup>).

Upon 70% confluency, the cultures were passaged (STAR Methods) into 4 new T25 flasks at a cell density of 3 500 - 7 000 cells per cm<sup>2</sup>. At passage 1, the mean doubling time was determined of three different EDF cultures resulting in an average value of  $62.13 \pm 7.00$  hours (Figure 2B). In addition, a growth curve was established as a parameter of cell viability and proliferation capacity (Figure 2C). Culture flasks of three individuals (E3-E5) were monitored for 11 consecutive days and the percentage confluency (y-axis) was plotted in function of the number of days in culture (x-axis). Throughout the culturing process, the tissue explants and cells were monitored daily for potential microbial or fungal contamination. If contamination was suspected, the flask was washed daily with washing PBS containing antibiotics (Key resource table) and the concentration of antibiotics in the initial culturing media was increased to a maximum of 5%. Additionally, a 16S ribosomal RNA gene polymerase chain reaction (PCR) was performed and no bacterial DNA (including Mycoplasma species) was detected in the cell lines.

1  
2  
3  
4  
5  
6  
7  
8  
9  
10  
11  
12  
13  
14  
15  
16  
17  
18  
19  
20  
21  
22  
23  
24  
25  
26  
27  
28  
29  
30  
31  
32  
33  
34  
35  
36  
37  
38  
39  
40  
41  
42  
43  
44  
45  
46  
47  
48  
49  
50  
51  
52  
53  
54  
55  
56  
57  
58  
59  
60  
61  
62  
63  
64  
65

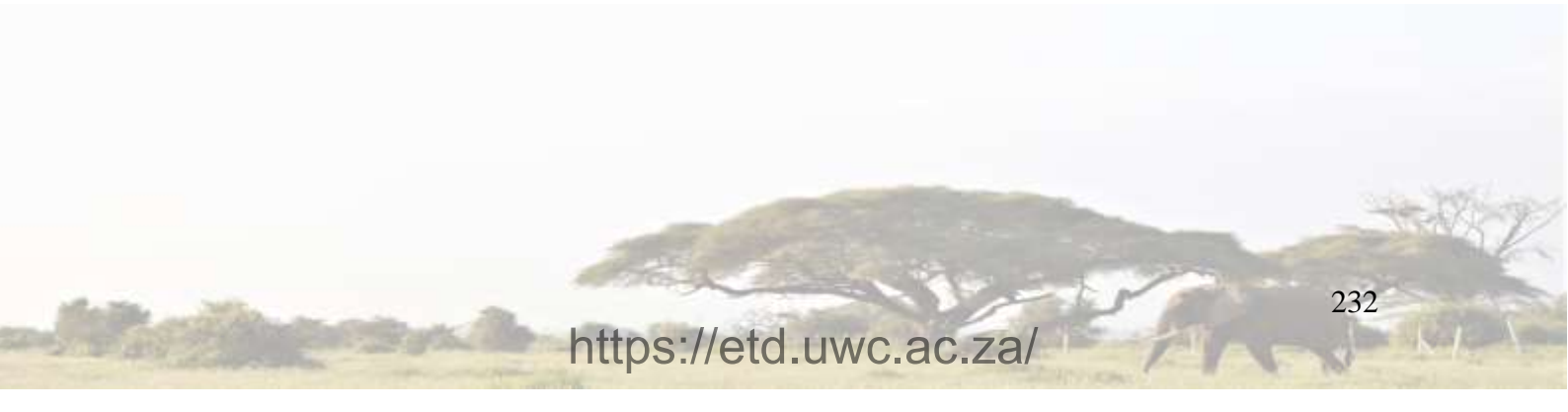
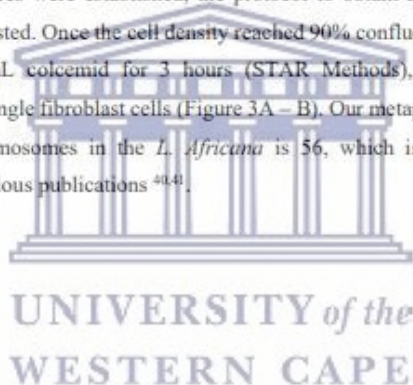
A potential limitation of establishing a primary cell culture is the occurrence of senescence after sequential passaging, which can vary depending on the tissue of origin and the age of the tissue source<sup>37</sup>. After continuous sub-culturing over a period of 2 - 3 months, the morphology of the EDFs was monitored closely from passage 3 up to 14. No significant changes in the cellular size and shape, which could point to senescence, were observed (Figure 2D). In addition, the EDF cultures maintained a steady proliferation rate. The EDFs exhibit a long, thin and multipolar appearance with disc-like structures, similar to descriptions in other reports on primary skin dermal fibroblasts of different species<sup>14,15,38</sup>. Methods to achieve cellular immortalization could facilitate future applications but are out of the scope of the current study<sup>14,39</sup>.

#### **Cryopreservation and recovery**

From the first passage onwards, EDFs cells were frozen away for cryopreservation at a cell density of 500 000 – 700 000 cells/mL by resuspension in freezing media (Key resource table) and transferred to a freezing container containing isopropyl alcohol (STAR Methods) to acclimate to -20°C overnight. Thereafter, the cryovials can be transferred to -80°C or liquid nitrogen for long term storage. After quick thawing (STAR Methods), the EDFs attached after approximately 4 hours. The cell cultures were in a healthy state and the cell doubling time remained similar after recovery.

#### **Chromosome analysis**

Once the primary EDF cultures were established, the protocol to obtain a metaphase spread of the African savanna EDFs was tested. Once the cell density reached 90% confluency, cultures at passage 6 were exposed to 0.05 µg/mL colcemid for 3 hours (STAR Methods), which yielded scattered chromosomes spreads from single fibroblast cells (Figure 3A – B). Our metaphase spreads confirm that the diploid number of chromosomes in the *L. africana* is 56, which is in accordance with the Elephantidae family and previous publications<sup>40,41</sup>.



1  
2  
3  
4  
5  
6  
7  
8  
9  
10  
11  
12  
13  
14  
15  
16  
17  
18  
19  
20  
21  
22  
23  
24  
25  
26  
27  
28  
29  
30  
31  
32  
33  
34  
35  
36  
37  
38  
39  
40  
41  
42  
43  
44  
45  
46  
47  
48  
49  
50  
51  
52  
53  
54  
55  
56  
57  
58  
59  
60  
61  
62  
63  
64  
65

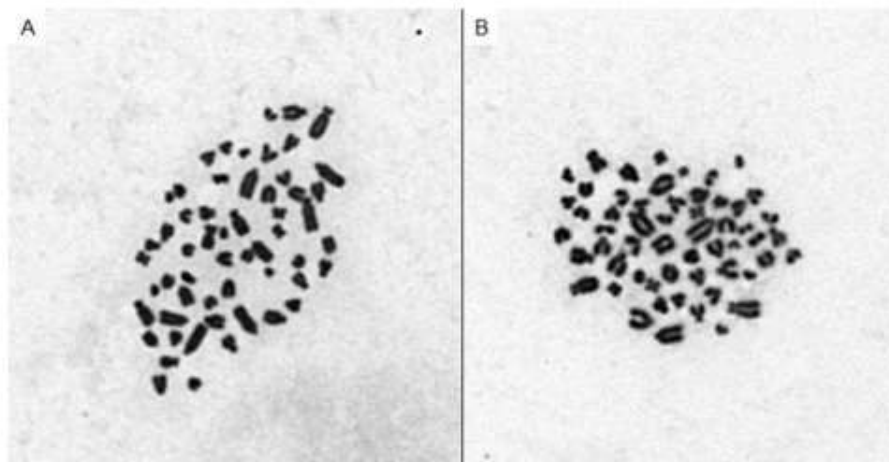
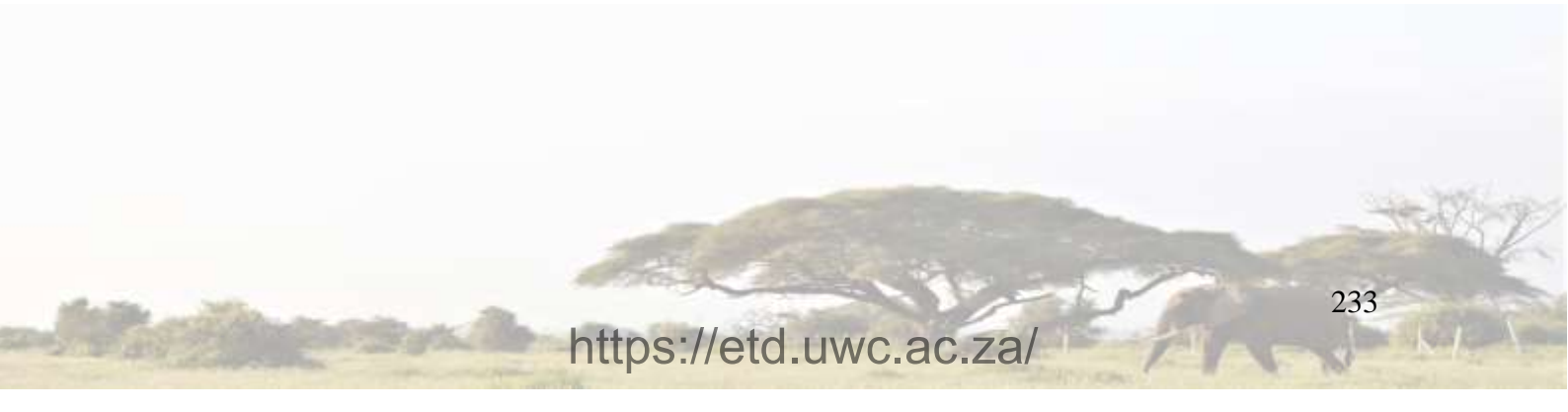


**Figure 3: Metaphase spread of primary EDF cells.** Image A and B were captured using a Metafer 4 platform, showing a diploid chromosome number of 56 chromosomes obtained from elephant E5.

### 3. Discussion

Four primary EDF cell lines were established, characterized and cryopreserved from living, free-roaming African savanna elephants using this protocol. To the best of our knowledge, this methodology described the establishment of the first primary EDF cell lines of *Loxodonta africana*, which can be used for future cytogenetics and conservation studies, as well as to study the mechanism of action of the TP53 retrogenes in elephants. These retrogenes contain various deletions but appear to have some transcriptional activity. Hence, they might play a crucial regulatory role in balancing the two tightly connected biological processes of cancer and aging in elephants<sup>20,33,42</sup>. There is currently only one previously published protocol on the establishment of primary fibroblast cultures from Asian elephants (*Elephas maximus*)<sup>17</sup>. Larger ear samples (3 × 3 cm<sup>2</sup> pieces) from Asian elephant carcasses were used in this protocol, while the current protocol makes use of small skin punch biopsy samples (3 - 4 mm) from African savanna elephants. This biopsy technique will allow remote biopsy darting in the future, a technique that can be used to collect skin tissue samples from a variety of free-ranging terrestrial animals and will allow sample collection from free-ranging elusive African forest and savanna elephants without the need for sedation and causing minimal harm to the animal. A success rate of 83.30% was obtained with the protocol starting from post-mortem ear skin tissue, with a first outgrowth of cells was seen 4 - 12 days after explantation<sup>17</sup>. These values are very similar to what we obtained with the currently protocol, with on average 15.75 ± 6.30 days to see the first outgrowth and a success rate of 80.00%. Vangipuram *et al.* presented a protocol to start up human patient-derived fibroblast cultures from 4 mm human skin biopsies<sup>43</sup>. In contrast to our protocol, this group coated the surface of the wells with 0.1% gelatin prior to skin biopsy fragment transfer. The first outgrowth of fibroblasts was observed

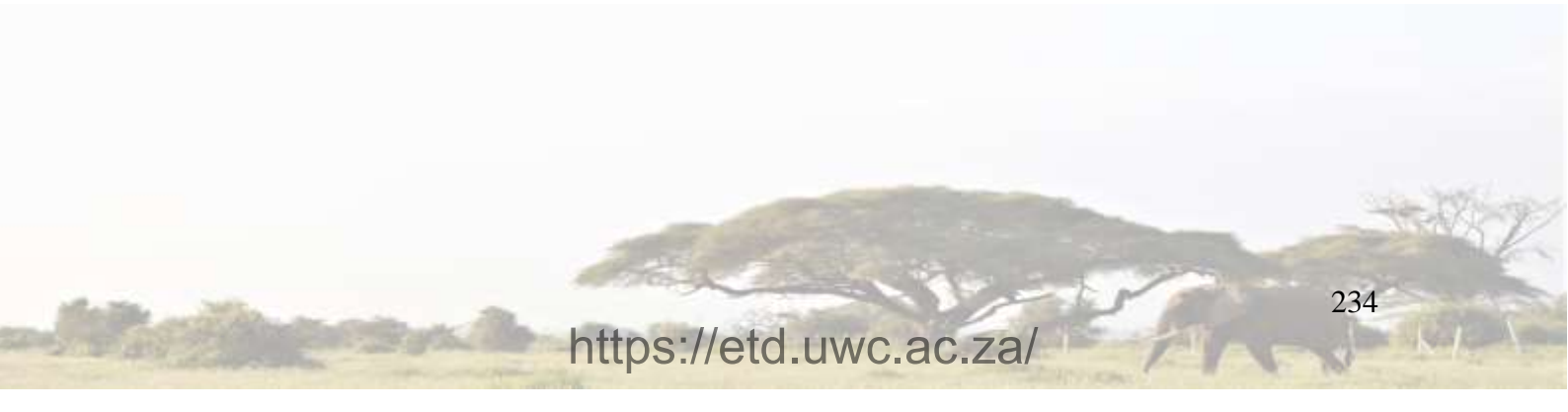


1  
2  
3  
4  
5  
6  
7  
8  
9  
10  
11  
12  
13  
14  
15  
16  
17  
18  
19  
20  
21  
22  
23  
24  
25  
26  
27  
28  
29  
30  
31  
32  
33  
34  
35  
36  
37  
38  
39  
40  
41  
42  
43  
44  
45  
46  
47  
48  
49  
50  
51  
52  
53  
54  
55  
56  
57  
58  
59  
60  
61  
62  
63  
64  
65

at 7 - 14 days, which is slightly earlier than our observations for EDFs. Interestingly, Seluanov *et al.* described a doubling time of approximately 7 days for long-lived small rodents (e.g. naked mole rats) possessing cancer suppression mechanisms, whereas human fibroblast divide approximately every 2 days<sup>44</sup>. The relatively slow doubling time of the primary EDF cultures could potentially be linked to their underlying cancer suppression mechanism, including a lower somatic mutation rate and basal metabolic rate<sup>27</sup>. While we used Eagle's Minimum Essential Medium (EMEM) instead of Dulbecco's modified Eagle's medium (DMEM) as used by Siengdee *et al.* and Vangipuram *et al.*, the principle is the same since both types of media support the growth of fibroblasts whereas other cell populations (e.g. keratinocytes) need additional supplements and growth factors<sup>17,43</sup>. This is a relatively simple way to obtain pure fibroblast cultures. Next to the cultivation of fibroblasts as monolayers in tissue culture dishes, Rittie *et al.* also presented a protocol applying three-dimensional collagen lattices and co-culture with human keratinocytes to form so-called skin reconstructs<sup>45</sup>.

The variation in days upon first EDF outgrowth between the five elephants could be caused by environmental factors, such as the weather conditions when samples were obtained and the duration and conditions of the transportation. We tried to keep transport under 10 hours (depending on the location of the elephant in the game reserve) and a relatively constant temperature of < 4°C with no direct ice contact. However, others documented no effect on the cell viability upon a shipment of skin samples on ice for several days<sup>46-48</sup>, so there could be other factors at play such as the depth and composition of the biopsy sample. The doubling time of our primary EDF cultures of  $62.13 \pm 7.00$  hours (mean  $\pm$  SD) was significantly longer compared to the previously established hippopotamus primary fibroblast culture (34 hours) and the Asian elephant fibroblast culture (25 hours)<sup>14,17</sup>. It is unlikely that age plays a role as the African savanna elephant age range (14 - 36 years) is much younger compared to the Asian elephant age range (2.9 - 68 years)<sup>17</sup>. In this study, the punch skin biopsies were obtained in the elephant's natural habitat, which is challenging to control and might increase the risk for microbial contamination. Therefore, a high concentration of 10% Penicillin-Streptomycin-Amphotericin B (P/S/A) antibiotics was applied in the transport media, in the media upon starting the cultures (1% P/S/A) and PBS washes of the first passage (10% P/S/A and 2% Gentamicin). This could potentially affect the replication rate and hence, the 1% P/S/A treatment was limited to passage 0<sup>17,49</sup>. Anti-bacterial and anti-fungal agents in cell culture, even standardly used Penicillin-Streptomycin (P/S), can affect cell cycle regulation, differential, and growth<sup>50</sup>. Gentamicin treatment can result in mitochondrial dysfunction and oxidative damage in mammalian cells, while Amphotericin B has shown to cause impaired physiological processes causing a decrease in cell viability<sup>51,52</sup>.

Finally, we opted for a direct tissue explant culture instead of enzymatic digestion. Collagenase digestion has been successful for the establishment of primary cell cultures of the Asian elephant, Jaguar (*Panthera onca*) and nonhuman primates from skin biopsies<sup>10,17,48</sup>. A protocol using dispase II, a proteolytic enzyme, followed by a simple incubation with trypsin solution was also optimized for



1  
2  
3  
4  
5  
6  
7  
8  
9  
10  
11  
12  
13  
14  
15  
16  
17  
18  
19  
20  
21  
22  
23  
24  
25  
26  
27  
28  
29  
30  
31  
32  
33  
34  
35  
36  
37  
38  
39  
40  
41  
42  
43  
44  
45  
46  
47  
48  
49  
50  
51  
52  
53  
54  
55  
56  
57  
58  
59  
60  
61  
62  
63  
64  
65

obtaining primary fibroblasts from living, wild leporid species (hares and rabbits)<sup>53</sup>. However, our method brings the advantage of establishing a primary EDF cell line in a relatively short time from a small skin biopsy, with a great efficiency regarding cell density, viability and purity. Despite a longer waiting period to establish a primary EDF culture, direct explant culture offers the advantage of conserving cell integrity and providing essential growth factors<sup>14,54</sup>.

Our result confirm the diploid number of 56 chromosomes in the *Loxodonta africana*, which is in accordance with the Elephantidae family and previous publications<sup>40,41,55,56</sup>. Frönicke *et al.* reported a predominantly acrocentric karyotype consisting of  $2n = 56$  chromosomes for the African savanna elephant containing only one subtelocentric and two metacentric autosomes<sup>40</sup>. Palkopoulou *et al.* formally reported the high quality reference genome of the African savanna elephant which first became available in 2005 (LoxAfr1) and has been updated in 2014 (LoxAfr4)<sup>57</sup>. Investigations on the ancestral karyotype of humans and elephants concluded that human painting probes produced identical hybridization patterns in both the African and Asian elephants, confirming that both species possess karyotypes that differ only in the amount and distribution of C - band positive heterochromatin<sup>41</sup>. This type of information provides a departure point to address fundamental questions in mammalian genome architecture, including possible correlation with chromosomal polymorphisms or translocations causing neoplasia in humans. The cell lines of different elephants that were generated as part of this study, might further contribute these type of investigations<sup>58,59</sup>.

This is the first experiment of its kind in South Africa with a relatively small sample size of five African savanna elephants. Due to the variability in biopsy outgrowth and doubling times, a larger sample size is needed to accurately determine intra- and inter-individual variations in these parameters. However, the low accessibility, ethical and administrative constraints make it challenging to obtain a large amount of elephant samples. In addition, repetitive sampling of the same elephant should be avoided according to ethics guidelines. In addition, biopsy samples of free-roaming elephants have to be collected at game reserves, resulting in often unpredictable environmental challenges and higher risks for sample contamination compared to samples obtained from captive Zoo elephants. As part of this proof-of-concept study, we performed opportunistic sampling and collected samples from elephants who were sedated for vaccination and collar replacements. In the case of remote biopsy darting, it might be more challenging to obtain samples originated from the skin behind the ear of the elephant where the epidermis is thin and GPS tracking might be required to retrieve the biopsy darts throughout the game reserves. In addition, there is a risk that the dart penetrates the skin at an oblique angle which would make the biopsy too superficial to reach fibroblasts. These variables will require further investigation and experimentation in order to make the remote darting technique for sample collection more successful.

1  
2  
3  
4  
5  
6  
7  
8  
9  
10  
11  
12  
13  
14  
15  
16  
17  
18  
19  
20  
21  
22  
23  
24  
25  
26  
27  
28  
29  
30  
31  
32  
33  
34  
35  
36  
37  
38  
39  
40  
41  
42  
43  
44  
45  
46  
47  
48  
49  
50  
51  
52  
53  
54  
55  
56  
57  
58  
59  
60  
61  
62  
63  
64  
65

In this methodology paper, we present a simple method to isolate and establish a primary EDF cell line from small skin punch biopsies of wild, living African savanna elephants residing in South Africa. The EDF cell line brings us a step closer to cryopreserve the genome of African savanna elephants. Furthermore, the cell line provides opportunities to further investigate the Peto's paradox and unravel the biological and genetic mechanisms that lead to cancer suppression in elephants.

#### 4. Acknowledgements

We thank the owners, field guides and staff members of Botlierskop Game Reserve and Sanbona Wildlife Reserve in the Western Cape (South-Africa) for their welcoming attitude, support and help during the sample collections in the field. In particular, we would like to thank the African Wildlife Conservation Foundation to create awareness about our project on cancer suppression mechanisms in elephants and for their fundraising endeavors. We also have to thank the Animal Research Ethics Committee of the University of the Western Cape for their advice and to guide us through the administrative requirements to collect and transport elephant samples in South Africa. Lastly, we would also like to thank David Chancellor and Diana Maclean, for covering the project from the very beginning and for their guidance in the field of elephant conservation. following The experimental work was funded by the internal running budget of the National Research Foundation (NRF) iThemba Laboratory for Accelerator Based Sciences (LABS) (Cape Town, South Africa). Furthermore, MSc and research funding for A.JvV. was provided by NRF iThemba LABS, the IAEA Marie Sklodowska Curie MSc funding scheme, as well as GetInvolved at GSI Helmholtzzentrum für Schwerionenforschung (Darmstadt, Germany).

#### 5. Author contributions

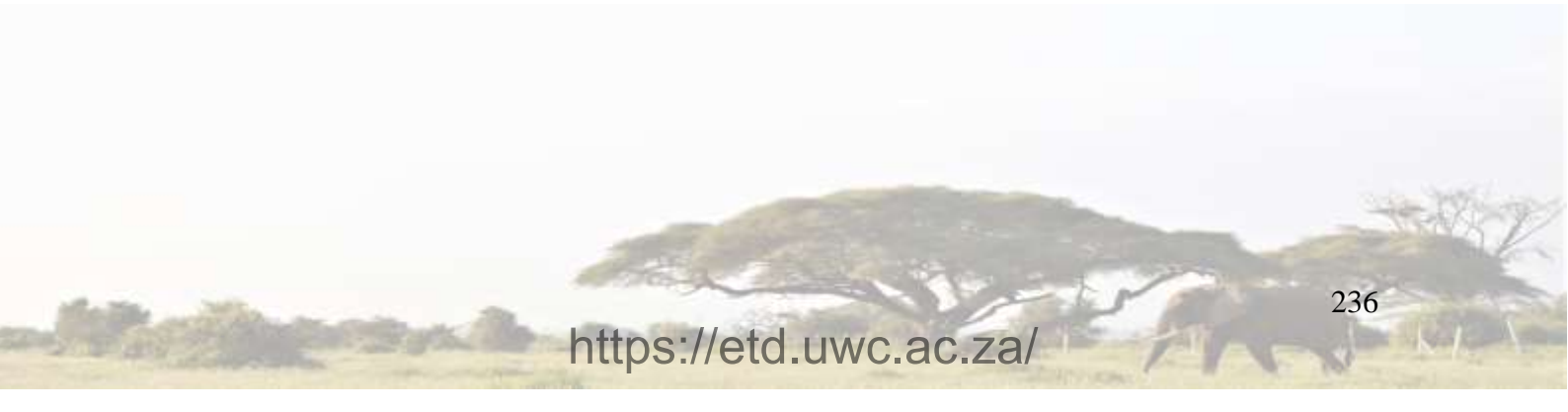
Conceptualization of the project, C.V., M.D. and W.B. Methodology development and design, J.B., M.E., W.T., W.B., M.D., F.R., M.d.K., W.M.L., C.V.; Sample collection, W.B. Experimental laboratory procedure, J.B., C.V., M.E., A.JvV., S.N., X.M. and R.F; Data capturing and analysis, J.B., C.V., M.E. and A.JvV. Ethics approval and project administration, F.R., R.F., M.E. and C.V. Resources, C.V., W.T. and M.D. Writing - original draft, J.B., M.E., A.JvV., W.M.L., C.V.; Writing - review and editing, all authors; Study supervision, W.T., C.V., M.D., M.E. and M.d.K. All authors have read and approved the final version of the manuscript.

#### 6. Declaration of interests

The authors declare no competing interests.

#### 7. Figure titles and legends

**Figure 1: Skin punch biopsy procedure and biopsy preparation. A - B)** The skin behind the ear of the elephant was cleaned with 70% ethanol. **C)** The punch biopsy area was surgically draped and a





1 punch biopsy needle was used to collect the sample. **D)** Punch biopsies were collected and transferred  
2 in tubes containing transport media. **E)** In the laboratory, the biopsies were washed thrice with washing  
3 PBS and transferred to a sterile glass petri-dish. **F)** Two scalpels were used to remove the epidermis  
4 and cut the biopsies into small tissue fragments. **G)** The tissue fragments were transferred to a T25  
5 tissue culture treated flask using a sterile Pasteur pipet and 0.5 mL FBS was added.  
6  
7

8  
9 **Figure 2: The characteristic outgrowth of the primary EDF cells from tissue explants.** **A)** The  
10 radial outgrowth of EDFs from a biopsy fragment of E1 on day 9, 10, and 11. **B)** The average doubling  
11 time of EDFs obtained from E3, E4, and E5 was  $62.13 \pm 7.00$  hours (mean  $\pm$  SD). **C)** A growth curve  
12 was plotted (normalized mean  $\pm$  SD calculated within six regions of a T25 flask) of E3, E4 and E5  
13 based on the % confluence over 11 consecutive days. **D)** The morphology of the EDFs appeared to be  
14 normal throughout passage 3 up to 14 with elongated, disc - like structures. All images are captured  
15 with a live cell imaging system (Cytosmart, Lonza®).  
16  
17  
18  
19  
20

21 **Figure 3: Metaphase spread of primary EDF cells.** Image A and B were captured using a Metafer 4  
22 platform, showing a diploid chromosome number of 56 chromosomes obtained from elephant E5.  
23  
24

## 25 8. Tables titles and legends

26  
27  
28 **Table 1. Overview of elephant samples.** Information on the African savanna elephants (*Loxodonta*  
29 *Africana*) such gender, age and location of the sample collection at two different wildlife reserves in  
30 South Africa. In addition, more results on the individual cultures are listed, such as the days until the  
31 first explant outgrowth was visible and the number of successful outgrowths per biopsy sample.  
32  
33

## 34 9. STAR Methods

### 35 10.1 Resource availability

#### 36 *Lead contact*

37  
38 Further information and requests for resources and reagents should be directed to and will be fulfilled  
39 by the lead contact, Dr Charlot Vandevoorde (c.vandevoorde@gsi.de)  
40  
41

#### 42 *Materials availability*

43  
44 The availability of the primary EDF cell line is limited due to the requirement to obtain the necessary  
45 ethics approval letters as well as transport and wildlife permits. For any research conducted on wildlife  
46 species, threatened species and/or endangered species, relevant conservation permits may be required  
47 and the responsible local authorities in the country of relevance should be contacted prior to distribution  
48 of the cell line.  
49  
50  
51  
52  
53  
54  
55  
56

#### 57 *Data and code availability:*

58  
59  
60  
61  
62  
63  
64  
65

1  
2  
3  
4  
5  
6  
7  
8  
9  
10  
11  
12  
13  
14  
15  
16  
17  
18  
19  
20  
21  
22  
23  
24  
25  
26  
27  
28  
29  
30  
31  
32  
33  
34  
35  
36  
37  
38  
39  
40  
41  
42  
43  
44  
45  
46  
47  
48  
49  
50  
51  
52  
53  
54  
55  
56  
57  
58  
59  
60  
61  
62  
63  
64

Any additional information required to analyze the data reported in this paper is available from the lead author upon request.

## 10.2 Experimental model and subject details

Ethical approval was obtained from the Animal Research Ethics Committee of the University of the Western Cape, South Africa (AR21/6/4). In addition, landowner permission letters and permits for transport of the wildlife samples were obtained prior to sample collection. The Section 20 approval was granted by the South African Department of Agriculture, Land Reform and Rural Development (DALRRD) formerly the Department of Agriculture, Forestry, and Fisheries (DAFF Section 20: 12/11/1/7). The Threatened Or Protected Species (TOPS) permit (permit number: s65761) and registration application (certificate number: 02307) process for the carrying out of restricted activities in terms of the National Environmental Management: Biodiversity Act 2004 (No. 10 of 2004) was also obtained. Biological samples of five free-ranging African savanna elephants (*Loxodonta africana*) aged between 14 - 35 years old (four male and one female elephant) residing in their natural habitat at Botlierskop Game Reserve and Sanbona Wildlife Reserve, South-Africa were collected (Table 1). The elephants had to undergo a scheduled veterinary intervention (vaccination or replacement of tracking collar) requiring sedation via a single intramuscular injection of Thianil (Wildlife Pharmaceuticals Pty Ltd, Mpumalanga, South Africa, 3 mg/1000kg). No analysis of the influence of sex was performed in this study because of the small sample size. During the period of sedation, oxygen levels and general body conditions of the elephant were closely monitored by the wildlife veterinarian and experienced field rangers made sure that the elephant was cooled down with water to assist body temperature regulation. When the elephants were immobilized, 5-6 skin punch biopsy samples of approximately 3-4 mm in diameter were collected behind the ear of the elephant (where the epidermis is the thinnest) by using a punch biopsy needle

## 10.3 Method details

### *Tissue sample collection*

The skin was cleaned with 70% ethanol and surgically draped (Figure 1A - C). Five skin punch biopsies of 5 mm in diameter were collected with a punch biopsy needle behind the ear comparative thinness of the corium and epidermis<sup>36</sup>. The biopsies were transferred to a sterile 15 mL conical tube containing 10 mL transport media, consisting of 90% Eagle's Minimum Essential Medium (EMEM), and 10% Penicillin/Streptomycin/Amphotericin B (P/S/A). Samples were transported at 0 - 4°C and processed within 24 hours. All reagents and consumables are listed in the Key Resource Table.

### *Establishment of the primary EDF culture*

All cell culture consumables and reagents (Key Resource Table) were sterile and all the reagents were pre-warmed in a water bath (37°C) before usage. The skin biopsy was transferred to a glass petri-dish

12

1 with a pair of tweezers (Figure 1E) and washed thrice with washing phosphate buffered saline (PBS),  
2 containing 10% P/S/A, and 2% gentamicin. Two scalpels (size 11) were used to remove the epidermis  
3 and cut the biopsies in smaller fragments (Figure 1F). A few drops of initial culturing media (EMEM  
4 supplemented with 20% Fetal Bovine Serum (FBS) and 1% P/S/A) were added to prevent dehydration.  
5 The small tissue fragments were transferred to a T25 tissue culture treated flask using a sterile glass  
6 Pasteur pipet (Figure 1G). To prevent floating of the tissue fragments, 0.5 mL FBS was added. The T25  
7 flasks were incubated under standard conditions at 37°C in a humidified 5% CO<sub>2</sub> incubator. After 24  
8 hours, the flasks were placed upside down for the next 24 hours. On day three, 1 mL initial culturing  
9 media was added. The tissue fragments were monitored daily under an inverted microscope (Zeiss  
10 Primovert, Carl Zeiss Pty LTD, Munich, Germany) at 10X magnification to observe explant dislodging  
11 and the overall radial migration of the primary EDFs. Microbial or fungal contamination was closely  
12 monitored at 40X magnification. If contamination was suspected, the flask was washed daily with 2 mL  
13 washing PBS. In case of persistent contamination, the amount of P/S/A in the initial culturing media  
14 was increased to a maximum of 5%. Additionally, a commercial 16S ribosomal RNA gene polymerase  
15 chain reaction (PCR) assay was performed and no bacterial DNA (including Mycoplasma species) was  
16 detected (Key Resource Table).  
17  
18  
19  
20  
21  
22  
23  
24  
25  
26

27 Once a T25 flask reached 70% confluency or when over confluent localized cell densities were observed  
28 along tissue fragments, the EDFs were washed twice with PBS and 1 mL of 1X trypsin EDTA solution  
29 (0.12% trypsin, 0.02% EDTA) was added and incubated for maximum 3 min. Upon detachment, 4 mL  
30 cEMEM (EMEM containing 20% FBS, 1% P/S) was added and the cell suspension was transferred to  
31 a 15 ml conical tube. To ensure recovery of > 95% of the cells, this step was repeated. After 8 min  
32 centrifugation at 201 relative centrifugal force (RCF) the pellet was gently resuspended in 2 mL  
33 cEMEM and transferred to a new T25 flask. A confluent T25 flask (approximately 5x10<sup>5</sup> cells) was  
34 subcultured/frozen in a 1 to 4 ratio in T25 flasks/cryovials, respectively. A seeding density of 3 500 - 7  
35 000 cells per cm<sup>2</sup> is recommended.  
36  
37  
38  
39  
40  
41  
42

43 The mean double time (Td) was determined for three primary EDF cultures after the first passage (Td  
44 = (normalised mean ± SD,  $t_2 = t_1 \times 2^{\frac{\log(\text{end cell coverage}/\text{start cell coverage})}{\log(2)}}$ ). Post  
45 seeding, the cells were incubated for two days. From day three onwards, six images were taken daily in  
46 six different regions of the T25 flask until a confluent monolayer was reached (field of view 2.40 x 1.40  
47 mm) using the live cell imaging system (Cytosmart, Eindhoven, The Netherlands). The confluency was  
48 defined using the Cytosmart confluency algorithm<sup>60</sup> (Key Resource Table).  
49  
50  
51  
52

#### 53 *Primary EDF cryopreservation*

54 After trypsinization and centrifugation, the cell pellet was resuspended in freezing media (90% FBS,  
55 10% Dimethyl sulfoxide (DMSO)) and transferred to a Mr. Frosty™ Freezing Container containing  
56 isopropyl alcohol acclimated to -20°C overnight. Thereafter, the cryovials were transferred to -80°C or  
57  
58  
59  
60  
61  
62  
63  
64  
65

1 liquid nitrogen for long term storage. A cooling rate of  $-10^{\circ}\text{C}/\text{min}$  is satisfactory<sup>61</sup>. To resuscitate the  
2 EDFs, the cryovials were thawed quickly by placing them in a warm water bath ( $37^{\circ}\text{C}$ ) until a small  
3 frozen clump remained and the cell suspension was added to 6 mL prewarmed cEMEM. After  
4 centrifugation, the supernatant was discarded and the pellet was resuspended in 2 mL cEMEM and  
5 transferred to a T25 flask. Attachment was observed after approximately 4 hours. A media change was  
6 performed every third day.  
7  
8  
9

#### 10 *Metaphase spread of the African savanna EDFs*

11  
12  
13 Once a confluent monolayer was obtained, 50 000 cells were seeded into a petri dish (35 mm). After  
14 90% confluency was reached, 0.05  $\mu\text{g}/\text{mL}$  of KaryoMAX™ Colcemid™ Solution in PBS (stock  
15 solution 10  $\mu\text{g}/\text{mL}$ ) was added for 3 hours to inactivate spindle fiber formation and amass cells in  
16 metaphase<sup>62</sup>. Cells were harvested by trypsination, transferred to a conical 15 mL tube and 5 mL  
17 prewarmed hypotonic solution (0.075 M Potassium Chloride) was added in a dropwise manner while  
18 stirring vigorously and left for 10 minutes at  $37^{\circ}\text{C}$ . The cells were fixed in methanol - acetic acid (3:1  
19 ratio, freshly prepared at room temperature) using a Pasteur pipette, by slowly adding 1.5 mL fixative  
20 from the bottom to the top of the 15 mL conical tube before centrifugation for 10 minutes at 201 RCF.  
21 The supernatant was discarded, and this fixation step was repeated two more times (5 mL fixative) until  
22 the fixative was clear. The cell pellet was resuspended in 200  $\mu\text{L}$  of the left over supernatant and 50  $\mu\text{L}$   
23 of the cell suspension was dropped from 30 cm height on wet slides (stored in  $\text{dH}_2\text{O}$  with 10%  
24 methanol, at  $4^{\circ}\text{C}$ ). Slides were left to air dry. Slides with fixed metaphase spreads were stained for 3  
25 min with Giemsa's Azur Eosin Methylene Blue Solution in HEPES buffer working solution (1:25 ratio,  
26 freshly prepared and protected from light). The slides were rinsed in  $\text{dH}_2\text{O}$  trice and left to dry and  
27 mounted with DPX. The slides with metaphase chromosome spreads were initially detected by 10X  
28 objective lens using the metaphase finder algorithm of Metafer (MetaSystems, Heidelberg, Germany)  
29 and subsequently captured with an immersion oil lens objective (63X).  
30  
31  
32  
33  
34  
35  
36  
37  
38  
39  
40  
41

#### 42 **10.4 Quantification and statistical analysis**

43  
44 The average and corresponding standard deviations (SD) were calculated for the results from the  
45 individual experiments, Td determined and results visualized using Microsoft Office Excel 2019  
46 (Microsoft Corporation, Washington DC, USA) and GraphPad Prism Software Version 5.01 for  
47 Windows (GraphPad Software, San Diego, CA, USA). As a result of limited availability and  
48 opportunistic sample collection, not all the experiments were performed on the same day.  
49  
50  
51  
52

#### 53 **10.5 Key resource table**

54 REAGENT or RESOURCE	SOURCE	IDENTIFIER
55 Penicillin-Streptomycin-Amphotericin B Mixture (Peni/Strep/Amph)	Lonza	Cat#: 17-745E
56 Gentamycin (50 mg/ml)	Lonza	Cat#: 17-518L

1	Penicillin-Streptomycin (P/S)	Capricorn Scientific	Cat#: PS-B
2	Eagle's Minimum Essential Medium (EMEM)	Capricorn Scientific	Cat#: MEM-A
3	Fetal Bovine Serum (FBS)	Capricorn Scientific	Cat#: FBS-GI-HI-12A
4	Phosphate Buffered Saline (PBS)	Gibco	Cat#: 15374875
5	Trypsin EDTA solution (1X)	Capricorn Scientific	Cat#: TRY-1B
6	Chemicals, peptides, and recombinant proteins		
7	Dimethyl Sulfoxide (DMSO)	Sigma-Aldrich	Cat#: 34869
8	KaryoMAX™ Colcemid™	Gibco	Cat#: 15212012
9	Potassium Chloride (KCl)	Sigma-Aldrich	Cat#: 7447-40-7
10	Methanol acid	Merck	Cat#:67-56-1
11	Acetic acid	Merck	Cat#:64-19-7
12	Giemsa's Azur Eosin Methylene Blue Solution	Merck	Cat#: 109204
13	HEPES sodium salt, C <sub>8</sub> H <sub>17</sub> N <sub>2</sub> NaO <sub>4</sub> S (Molecular Weight: 260.28)	ChemCruz	Cat#: sc-216092
14	HEPES, C <sub>8</sub> H <sub>18</sub> N <sub>2</sub> O <sub>4</sub> S (Molecular Weight: 238.30)	ChemCruz	Cat#: 7635-45-9
15	DPX Mountant for histology	Merck	Cat#: 44581
16	Isopropanol	Kimix Chemicals & Lab Supplies	Cat#: IPR001
17	Critical commercial assays		
18	Add PCR done commercially	PathCare	Practice #: 5200539
19	Experimental models: Cell lines		
20	Primary African elephant ( <i>Loxodonta africana</i> ) dermal fibroblast (EDF) cell lines	This paper.	N/A
21	Software and algorithms		
22	Cytosmart confluency algorithm	Lonza	<a href="https://cytosmart.com/applications/cell-confluence">https://cytosmart.com/applications/cell-confluence</a>
23	Metafer 4 platform	MetaSystems	<a href="https://metasystems-international.com/en/products/metafer">https://metasystems-international.com/en/products/metafer</a>
24	GraphPad Prism	Graphpad	<a href="http://www.graphpad.com">www.graphpad.com</a>
25	Other		
26	Tissue cultured treated flasks (T25)	Nest	Cat#: 707003
27	Conical centrifuge tubes (15 mL)	Nest	Cat#: 601002
28	Scalpels (size11)	Hi-care	Cat#: SCALPEL11
29	Glass petri dish (100 mm)	Pyrex	Cat#: SLW1480/08D
30	Serological pipets (2 and 10 mL)	Nest	Cat#:325001/327001
31	Tissue cultured treated petri dish (35 mm x 12 mm)	Nest	Cat#:706001
32	Mr. Frosty™ Freezing Container	ThermoFisher Scientific	Cat#:5100-0001
33	Glass slides	Lasec	Cat#: GLAS4S22M3000F
34	Glass coverslips	Lasec	Cat#: GLAS2C29M2450REC

## 10. References

1. Chase, M.J., Schlossberg, S., Griffin, C.R., Bouché, P.J.C., Djene, S.W., Elkan, P.W., Ferreira, S., Grossman, F., Kohi, E.M., Landen, K., et al. (2016). Continent-wide survey reveals massive decline in African savannah elephants. *PeerJ* 2016, 1–24. 10.7717/peerj.2354.
2. Gobush, K., Edwards, C.T.T., Balfour, D., Wittemyer, G., Maisels, F., and Taylor, R.D. (2021). *Loxodonta africana*. The IUCN Red List of Threatened Species 2021.

1  
2  
3  
4  
5  
6  
7  
8  
9  
10  
11  
12  
13  
14  
15  
16  
17  
18  
19  
20  
21  
22  
23  
24  
25  
26  
27  
28  
29  
30  
31  
32  
33  
34  
35  
36  
37  
38  
39  
40  
41  
42  
43  
44  
45  
46  
47  
48  
49  
50  
51  
52  
53  
54  
55  
56  
57  
58  
59  
60  
61  
62  
63  
64  
65

primary adult skin fibroblasts from the Asian elephant (*Elephas maximus*). *PeerJ* 2018, 1–16. 10.7717/peerj.4302.

18. Iqbal, A., Ping, J., Ali, S., Zhen, G., Kang, J.Z., Yi, P.Z., Huixian, L., and Zhihui, Z. (2021). Conservation of endangered species through somatic cell nuclear transfer (SCNT). *Conserv. Genet. Resour.* 13, 349–357. 10.1007/s12686-021-01204-9.

19. Ogura, A., Inoue, K., and Wakayama, T. (2013). Recent advancements in cloning by somatic cell nuclear transfer. *Philos. Trans. R. Soc. B Biol. Sci.* 368, 13–16. 10.1098/rstb.2011.0329.

20. Abegglen, L.M., Caulin, A.F., Chan, A., Lee, K., Robinson, R., Campbell, M.S., Kiso, W.K., Schmitt, D., Waddell, P.J., Bhaskara, S., et al. (2015). Potential Mechanisms for Cancer Resistance in Elephants and Comparative Cellular Response to DNA Damage in Humans. *JAMA* 314, 1850–1860. 10.1001/jama.2015.13134.

21. Sulak, M., Fong, L., Mika, K., Chigurupati, S., Yon, L., Mongan, N.P., Emes, R.D., and Lynch, V.J. (2016). TP53 copy number expansion is associated with the evolution of increased body size and an enhanced DNA damage response in elephants. *Elife* 5, 3–5. 10.7554/eLife.11994.

22. Tollis, M., Boddy, A.M., and Maley, C.C. (2017). Peto’s Paradox: How has evolution solved the problem of cancer prevention? *BMC Biol.* 15, 1–5. 10.1186/s12915-017-0401-7.

23. Nunney, L. (2022). Cancer suppression and the evolution of multiple retrogene copies of TP53 in elephants: A re-evaluation. *Evol. Appl.* 15, 891–901. 10.1111/eva.13383.

24. Armitage, P., and Doll, R. (1954). The age distribution of cancer and a multi-stage theory of carcinogenesis. *Br. J. Cancer* 8, 1–12. 10.1038/bjc.1954.1.

25. Nordling, C.O. (1953). A new theory on the cancer-inducing mechanism. *Br. J. Cancer* 7, 68–72. 10.1038/bjc.1953.8.

26. Nunney, L., and Muir, B. (2015). Peto’s paradox and the hallmarks of cancer: Constructing an evolutionary framework for understanding the incidence of cancer. *Philos. Trans. R. Soc. B Biol. Sci.* 370, 1–7. 10.1098/rstb.2015.0161.

27. Caulin, A.F., and Maley, C.C. (2011). Peto’s Paradox: Evolution’s prescription for cancer prevention. *Trends Ecol. Evol.* 26, 175–182. 10.1016/j.tree.2011.01.002.

28. Peto, H., Roe, F.J.C., Lee, P.N., Levy, L., and Clack, J. (1975). Cancer and ageing in mice and men. *Br. J. Cancer* 32, 411–426. 10.1038/bjc.1975.242.

29. Gaughran, S.J., Pless, E., and Stearns, S.C. (2016). How elephants beat cancer. *Elife* 5, e21864. 10.7554/eLife.21864.

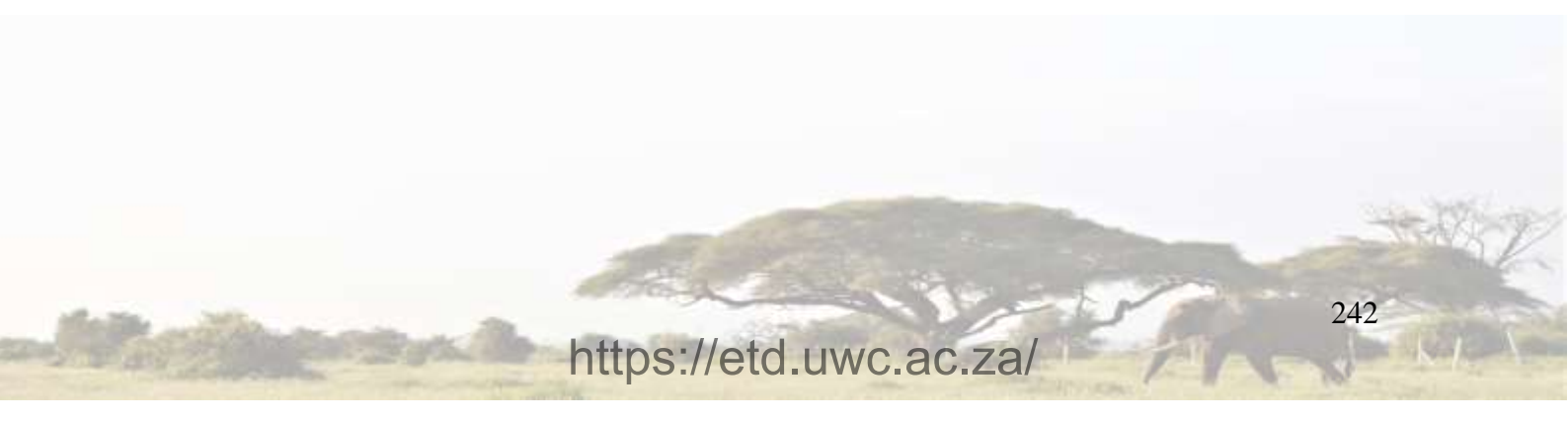
30. Vazquez, J.M., Sulak, M., Chigurupati, S., and Lynch, V.J. (2018). A Zombie LIF Gene in Elephants Is Upregulated by TP53 to Induce Apoptosis in Response to DNA Damage. *Cell Rep.* 24, 1765–1776. 10.1016/j.celrep.2018.07.042.

31. Kumari, R., Kohli, S., and Das, S. (2014). P53 Regulation Upon Genotoxic Stress: Intricacies and Complexities. *Mol. Cell. Oncol.* 1, 1–8. 10.4161/23723548.2014.969653.

32. Aubrey, B.J., Kelly, G.L., Janic, A., Herold, M.J., and Strasser, A. (2018). How does p53 induce apoptosis and how does this relate to p53-mediated tumour suppression? *Cell Death Differ.* 25, 104–113. 10.1038/cdd.2017.169.

33. Haupt, S., and Haupt, Y. (2017). P53 at the start of the 21st century: Lessons from elephants. *F1000Research* 6, 1–8. 10.12688/f1000research.12682.1.

34. Tyner, S.D., Venkatachalam, S., Choi, J., Jones, S., Ghebranious, N., Igelmann, H., Lu, X., Soron, G., Cooper, B., Brayton, C., et al. (2002). P53 mutant mice that display early ageing-associated phenotypes. *Nature* 415, 45–53. 10.1038/415045a.



- 1 35. Mijele, D., Omondi, P., Gakuya, F., Rossi, L., Chiyo, P.I., Soriguer, R.C., and Angelone-  
2 Alasaad, S. (2016). A practical guideline to remote biopsy darting of wildebeests for genetic  
3 sampling. *Int. J. Vet. Sci. Med.* *4*, 27–32. 10.1016/j.ijvsm.2016.10.004.
- 4 36. Smith, F. (1890). Histology of the skin of the elephant. *J. Anat. Physiol.* *24*, 493-503.
- 5 37. Schäuble, S., Klement, K., Marthandan, S., Münch, S., Heiland, I., Schuster, S., Hemmerich, P.,  
6 and Diekmann, S. (2012). Quantitative model of cell cycle arrest and cellular senescence in  
7 primary human fibroblasts. *PLoS One* *7*, 22–24. 10.1371/journal.pone.0042150.
- 8 38. Dick, M.K., Miao, J.H., and Limaiei, F. (2022). Histology, Fibroblast (StatPearls Publishing).
- 9 39. Gouko, R., Onuma, M., Eitsuka, T., Katayama, M., Takahashi, K., Nakagawa, K., Inoue-  
10 Murayama, M., Kiyono, T., and Fukuda, T. (2018). Efficient immortalization of cells derived  
11 from critically endangered Tsushima leopard cat (*Prionailurus bengalensis euptilurus*) with  
12 expression of mutant CDK4, Cyclin D1, and telomerase reverse transcriptase. *Cytotechnology*  
13 *70*, 1619–1630. 10.1007/s10616-018-0254-0.
- 14 40. Frönicke, L., Wienberg, J., Stone, G., Adams, L., and Stanyon, R. (2003). Towards the  
15 delineation of the ancestral eutherian genome organization: Comparative genome maps of  
16 human and the African elephant (*Loxodonta africana*) generated by chromosome painting. *Proc.*  
17 *R. Soc. B Biol. Sci.* *270*, 1331–1340. 10.1098/rspb.2003.2383.
- 18 41. Yang, F., Alkalaeva, E.Z., Perelman, P.L., Pardini, A.T., Harrison, W.R., O'Brien, P.C.M., Fu,  
19 B., Graphodatsky, A.S., Ferguson-Smith, M.A., and Robinson, T.J. (2003). Reciprocal  
20 chromosome painting among human, aardvark, and elephant (superorder Afrotheria) reveals the  
21 likely eutherian ancestral karyotype. *Proc. Natl. Acad. Sci. U. S. A.* *100*, 1062–1066.  
22 10.1073/pnas.0335540100.
- 23 42. Tollis, M., Ferris, E., Campbell, M.S., Harris, V.K., Rupp, S.M., Harrison, T.M., Kiso, W.K.,  
24 Schmitt, D.L., Garner, M.M., Aktipis, C.A., et al. (2021). Elephant Genomes Reveal Accelerated  
25 Evolution in Mechanisms Underlying Disease Defenses. *Mol. Biol. Evol.* *38*, 3606–3620.  
26 10.1093/molbev/msab127.
- 27 43. Vangipuram, M., Ting, D., Kim, S., Diaz, R., and Schüle, B. (2013). Skin punch biopsy explant  
28 culture for derivation of primary human fibroblasts. *J. Vis. Exp.*, 9–11. 10.3791/3779.
- 29 44. Seluanov, A., and Ribeiro, A.A.C.M. (2009). That Differ in Size and Lifespan. *Aging (Albany*  
30 *NY)*. *7*, 813–823. 10.1111/j.1474-9726.2008.00431.
- 31 45. Rittie, L., and Fisher, G.J. (2005). Isolation and culture of skin fibroblasts. In *Fibrosis Research.*  
32 *Methods in Molecular Medicine*, J. Varga, D. A. Brenner, and S. H. Phan, eds. (Humana Press),  
33 pp. 83–98. 10.1385/1-59259-940-0:083.
- 34 46. Okonkwo, C., and Singh, M. (2015). Recovery of fibroblast-like cells from refrigerated goat  
35 skin up to 41 d of animal death. *Vitr. Cell. Dev. Biol.- Anim.* *51*: 463–469. 10.1007/s11626-  
36 014-9856-9.
- 37 47. Silvestre, M.A., Sánchez, J.P., and Gómez, E.A. (2004). Vitrification of goat, sheep, and cattle  
38 skin samples from whole ear extirpated after death and maintained at different storage times and  
39 temperatures. *Cryobiology* *49*, 221–229.
- 40 48. Mishra, A., Qiu, Z., Farnsworth, S., Hemmi, J., Li, M., Pickering, A., and Hornsby, P. (2016).  
41 Induced Pluripotent Stem Cells from Nonhuman Primates. *Methods Mol. Biol.* *1357*, 183–193.  
42 10.1007/7651\_2014\_159.
- 43 49. Yap, N.Y., Ong, T.A., Morais, C., Pailoor, J., Gobe, G.C., and Rajandram, R. (2019).  
44 Establishment of epithelial and fibroblast cell cultures and cell lines from primary renal cancer  
45 nephrectomies. *Cell Biol. Int.* *43*, 715–725. 10.1002/cbin.11150.

- 1 50. Ryu, A.H., Eckalbar, W.L., Kreimer, A., Yosef, N., and Ahituv, N. (2017). Use antibiotics in  
2 cell culture with caution: Genome-wide identification of antibiotic-induced changes in gene  
3 expression and regulation. *Sci. Rep.* 7, 1–9. 10.1038/s41598-017-07757-w.
- 4 51. Elliott, R.L., and Jiang, X.P. (2019). The adverse effect of gentamicin on cell metabolism in  
5 three cultured mammary cell lines: “Are cell culture data skewed?” *PLoS One* 14.  
6 10.1371/journal.pone.0214586.
- 7 52. Grella, E., Piet, M., Luchowski, R., Grudzinski, W., Paduch, R., and Gruszecki, W.I. (2018).  
8 Imaging of human cells exposed to an antifungal antibiotic amphotericin B reveals the  
9 mechanisms associated with the drug toxicity and cell defence. *Sci. Rep.* 8, 1–7.  
10 10.1038/s41598-018-32301-9.
- 11 53. Dos Santos, F.A.A., Carvalho, C.L., Almeida, I., Fagulha, T., Rammos, F., Barros, S.C.,  
12 Henriques, M., Luis, T., and Duarte, M.D. (2021). Simple method for establishing primary  
13 leporidae skin fibroblast cultures. *Cells* 10, 1–9. 10.3390/cells10082100.
- 14 54. Hendijani, F. (2017). Explant culture: An advantageous method for isolation of mesenchymal  
15 stem cells from human tissues. *Cell Prolif.* 50, 1–14. 10.1111/cpr.12334.
- 16 55. Houck, M.L., Kumamoto, A.T., Gallagher, D.S., and Benirschke, K. (2001). Comparative  
17 cytogenetics of the african elephant (*Loxodonta africana*) and asiatic elephant (*Elephas*  
18 *maximus*). *Cytogenet. Cell Genet.* 93, 249–252. 10.1159/000056992.
- 19 56. Hungerford, D.A., Chandra, H.S., Snyder, R.L., and Ulmer, J.F.A. (1966). Chromosomes of  
20 three elephants, two Asian (*Elephas maximus*) and one African (*Loxodonta africana*).  
21 *Cytogenetics* 5, 243–246.
- 22 57. Palkopoulou, E., Lipson, M., Mallick, S., Nielsen, S., Rohland, N., Baleka, S., Karpinski, E.,  
23 Ivancevic, A.M., To, T.H., Daniel Kortschak, R., et al. (2018). A comprehensive genomic  
24 history of extinct and living elephants. *Proc. Natl. Acad. Sci. U. S. A.* 115, E2566–E2574.  
25 10.1073/pnas.1720554115.
- 26 58. Kim, J., Farré, M., Auviel, L., Capitanu, B., Larkin, D.M., Ma, J., and Lewin, H.A. (2017).  
27 Reconstruction and evolutionary history of eutherian chromosomes. *Proc. Natl. Acad. Sci. U. S.*  
28 *A.* 114, E5379–E5388. 10.1073/pnas.1702012114.
- 29 59. Mitelman, F., Mertens, F., and Johanson, B. (1997). A breakpoint map of recurrent chromosomal  
30 rearrangements in human neoplasia. *Nat. Genet.* 15, 417–474. 10.1038/ng0497supp-417.
- 31 60. CytoSMART Technologies Inc Cytosmart cell confluence application.  
32 <https://cytosmart.com/applications/cell-culture/cell-proliferation>.
- 33 61. Supp, D.M., Hahn, J.M., Combs, K.A., McFarland, K.L., and Powell, H.M. (2022). Isolation  
34 and feeder-free primary culture of four cell types from a single human skin sample. *STAR*  
35 *Protoc.* 3, 101172. 10.1016/j.xpro.2022.101172.
- 36 62. Rodman, T.C., Flehinger, B.J., and Rohlf, F.J. (1980). Metaphase chromosome associations:  
37 Colcemid distorts the pattern. *Cytogenet. Genome Res.* 27, 98–110. 10.1159/000131471.